



Article

Recognition of Sedimentary Rock Occurrences in Satellite and Aerial Images of Other Worlds—Insights from Mars

Kenneth S. Edgett^{1,*} and Ranjan Sarkar²¹ Malin Space Science Systems, P.O. Box 910148, San Diego, CA 92191-0148, USA² Max Planck Institute for Solar System Research, Justus-von-Liebig-Weg 3, 37077 Göttingen, Germany; sarkarr@mps.mpg.de

* Correspondence: edgett@msss.com

Abstract: Sedimentary rocks provide records of past surface and subsurface processes and environments. The first step in the study of the sedimentary rock record of another world is to learn to recognize their occurrences in images from instruments aboard orbiting, flyby, or aerial platforms. For two decades, Mars has been known to have sedimentary rocks; however, planet-wide identification is incomplete. Global coverage at 0.25–6 m/pixel, and observations from the Curiosity rover in Gale crater, expand the ability to recognize Martian sedimentary rocks. No longer limited to cases that are light-toned, lightly cratered, and stratified—or mimic original depositional setting (e.g., lithified deltas)—Martian sedimentary rocks include dark-toned examples, as well as rocks that are erosion-resistant enough to retain small craters as well as do lava flows. Breakdown of conglomerates, breccias, and even some mudstones, can produce a pebbly regolith that imparts a “smooth” appearance in satellite and aerial images. Context is important; sedimentary rocks remain challenging to distinguish from primary igneous rocks in some cases. Detection of ultramafic, mafic, or andesitic compositions do not dictate that a rock is igneous, and clast genesis should be considered separately from the depositional record. Mars likely has much more sedimentary rock than previously recognized.

Keywords: MARS sedimentary rock; early Mars; Mars volcanism; extraterrestrial sediment; spacecraft image interpretation; satellite image interpretation; aerial image interpretation; rover image interpretation; sandstone landforms; conglomerate landforms



Citation: Edgett, K.S.; Sarkar, R. Recognition of Sedimentary Rock Occurrences in Satellite and Aerial Images of Other Worlds—Insights from Mars. *Remote Sens.* **2021**, *13*, 4296. <https://doi.org/10.3390/rs13214296>

Academic Editor: Louis Scuderi

Received: 30 September 2021

Accepted: 24 October 2021

Published: 26 October 2021

Publisher's Note: MDPI stays neutral with regard to jurisdictional claims in published maps and institutional affiliations.



Copyright: © 2021 by the authors. Licensee MDPI, Basel, Switzerland. This article is an open access article distributed under the terms and conditions of the Creative Commons Attribution (CC BY) license (<https://creativecommons.org/licenses/by/4.0/>).

1. Introduction

Sedimentary rocks are records of past surface and subsurface (diagenetic) environments that capture information about the nature and actions of fluids and the histories of associated tectonic, magmatic, and impact events. The foundational steps in the study of the sedimentary rock record of other worlds are to use images acquired by instruments onboard flyby, orbiting, airborne, ascending, or descending platforms to:

1. Learn to recognize sedimentary rock occurrences; and
2. Identify where they outcrop at the planet's (or moon's) surface.

These steps can then lead to detailed studies using existing data, e.g., [1–32], or to target new data collections, or to develop new spacecraft and instrumentation, to obtain additional observations.

This contribution is about learning to recognize sedimentary rock occurrences—for Mars—largely using visible wavelength, reflected light images, to identify sub-meter- to decameter-scale sedimentary structures and other signs that a given geological material, exposed at the planet's surface, is sedimentary rock. Identification of sedimentary rocks on worlds other than Mars likely requires remote sensing methods that differ from those employed for Mars; for example, finding a sedimentary rock record on Venus is a high scientific priority [33–35] that will likely require use of new imaging radar systems and

near-infrared airborne or descent cameras [36]. A search for sedimentary rocks on Titan, a world with present-day aeolian, fluvial, and lacustrine processes [37–40], might also require imaging radar systems and cameras on airborne, descending, and landed platforms such as the planned Dragonfly rotorcraft mission [41].

Sedimentary rocks were speculated to occur on Mars for decades [42–46], although some wondered whether the necessary diagenetic processes had ever been operative [47]. The first unambiguous evidence [48] that Mars has sedimentary rocks came in 1999 [49] from 1.4–4.5 m/pixel images obtained by a (then) new instrument orbiting the planet, the narrow angle camera of the Mars Global Surveyor (MGS) Mars Orbiter Camera system (MOC-NA) [50]. These early MOC-NA observations were soon followed by recognition of lithified landforms that resemble an aeolian dune field (Figure 1a) [51,52] and a river delta (Figure 1b) [53]. While some rocks at the Sojourner rover field site seen in 1997 were speculated to be conglomerates [54,55], the ultimate confirmation that sedimentary rocks occur on Mars came from images of the sandstones of the Burns formation examined using the Opportunity rover in 2004 in Meridiani Planum (Figure 1f) [56,57].

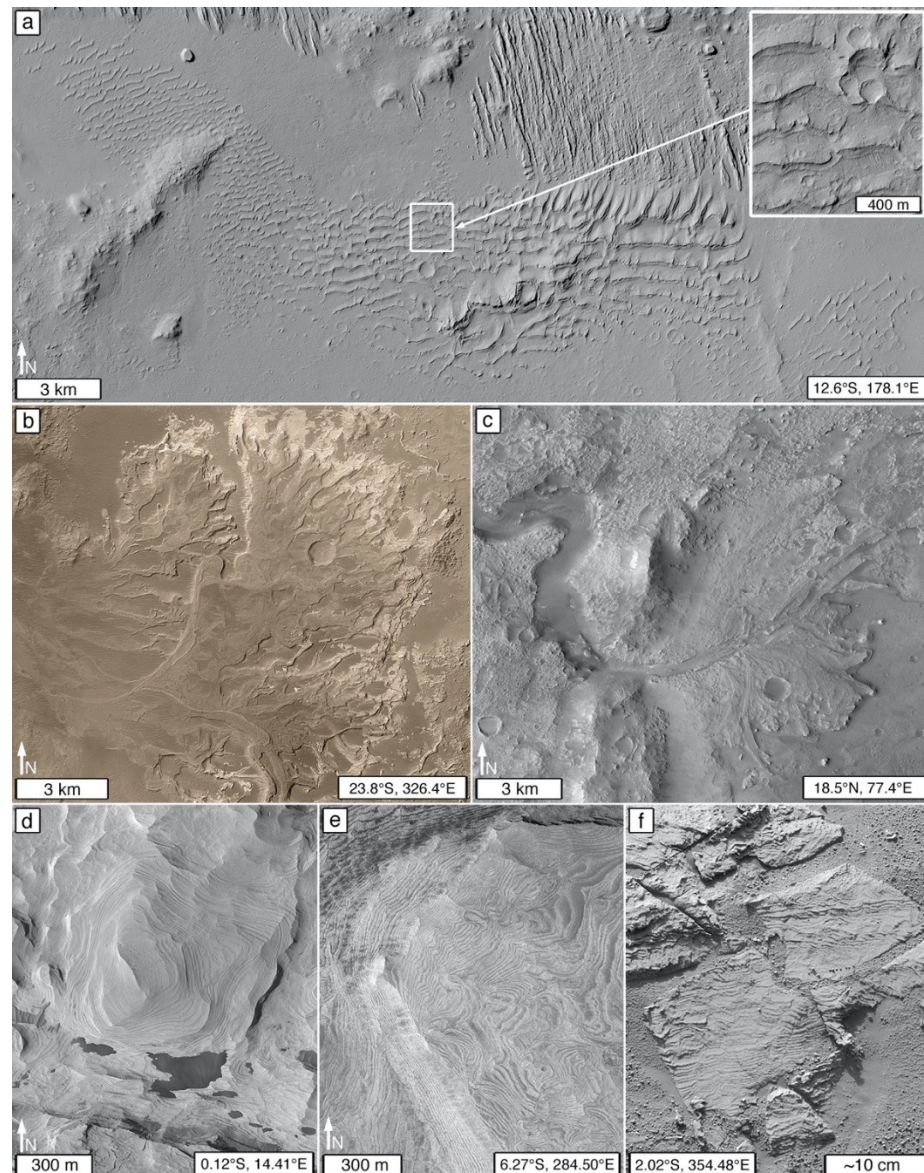


Figure 1. Example of Martian sedimentary rock occurrences known before Curiosity landed in 2012.

(a) Cratered, lithified aeolian dune field near the Apollinaris Sulci. The white box shows the location of the inset; the inset highlights the cratered nature of the dune field; HiRISE PSP_010453_1675 and CTX B02_010453_1675_XN_12S182W, J04_046452_1689_XN_11S181W, J20_052557_1688_XI_11S182 -W. (b) Lithified Eberswalde crater delta; MOC-NA mosaic from NASA/JPL-Caltech/Malin Space Science Systems. (c) Lithified deltaic sediment in western Jezero crater; CTX P03_002387_1-987_XI_18N282W. (d) Light-toned, un-cratered, stratified rock exposed in a crater in northwest Schiaparelli basin; HiRISE PSP_002930_1800. (e) Light-toned, stratified rock in west Candor Chasma; HiRISE ESP_056707_1735. (f) Light-toned sandstone of the Burns formation explored via the Opportunity rover; Olympia outcrop, target Overgaard [58]; MER Sol 695 left Pancam product 1p189898150rad64kcp2435l7c1. The center latitude and longitude of each panel is indicated (e.g., 28.3° S, 326.4° E); this practice is also applied to subsequent figures.

The sedimentary rock record of Mars is important to deciphering the planet's past. Without sustained, mobile-lid (plate) tectonics [59], the upper Martian crust might have retained much of its earliest sedimentary record [60]. Of course, some early sedimentary rocks would have been subjected to subsequent weathering, erosion, and recycling [61]. With strata time-equivalent to Earth's Hadean and early Archean eons—older than the oldest sedimentary and metasedimentary rocks on our planet [62,63]—the Martian archive presents opportunities to learn, by analog, about the kinds of environments that might have existed on Hadean Earth, Eoarchean Earth, or similar extrasolar worlds cf. [64]. If Mars never had life, then its sedimentary record also offers an opportunity to examine the products of deposition, diagenesis, weathering, and erosion—on a rocky planet with a silicate crust—in the absence of biological influence. In addition, Martian sedimentary strata might include records of local, to solar-system-wide, astronomical events [65,66], potentially correlative across multiple worlds.

This contribution is a guide to a daunting and unfinished task, the recognition of Martian sedimentary rock occurrences in images acquired by cameras aboard aerial (ascending, descending, or airborne platforms) and satellite (orbiting or flyby spacecraft orbiting another body or leaving the solar system) platforms that are, or were previously, operating (or someday will operate) at Mars. The observations, concepts, and ideas presented here are also applicable to future Mars landing site selection and robotic and human crew exploration planning efforts that make use of orbiter, aerial, or long-distance views from landed cameras. We use the term *occurrences* because *outcrop* inadequately limits identification; some examples can be recognized even though they are not strictly outcropping because they are partly (or mostly) covered with aeolian sand or dust [12,67,68].

Our work was highly informed by key observations made over the last decade using images obtained by cameras aboard the Mars Science Laboratory (MSL) Curiosity rover and the 99.97% (as of 1 January 2021) coverage of the planet achieved at ~6 m/pixel by the Mars Reconnaissance Orbiter (MRO) Context Camera (CTX). Tens of thousands of higher-spatial resolution orbiter images in the 0.25–6 m/pixel range, of select areas around the planet, also inform the results presented here.

Our overarching theme is that identification of sedimentary rocks on Mars is not limited to exposures that have geomorphic expressions that mimic their original depositional setting (Figure 1a–c), nor limited to stratified exposures of light tone that have poor impact crater retention (Figure 1d,e), nor is identification of sedimentary rock occurrences always easy. Contrary to understanding a decade ago [48,69], some sedimentary rocks are dark-toned (Figure 2), retain craters as well as do lava flows (Figure 3), and have mafic to felsic compositions [70–73] that, if observed remotely, could be misinterpreted as signals of igneous rock. One of the key challenges lies in the distinction of sedimentary from igneous rocks, including lava and tuff. This concern applies whether one is examining images acquired by orbiting cameras, airborne cameras, or even images obtained by rover cameras that view rock surfaces at scales of 16–32 μm per pixel (e.g., Figure 4).

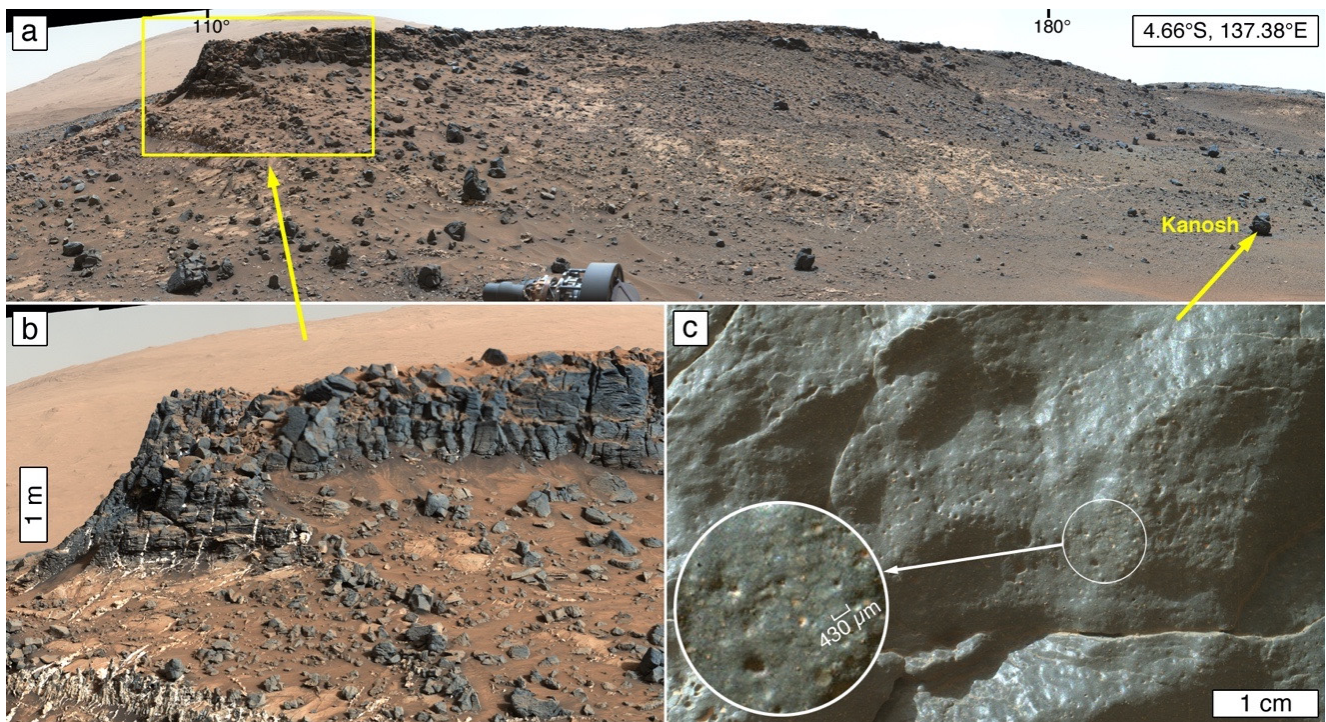


Figure 2. Example of dark-toned sedimentary rock occurrence on Mars. (a) View showing the dark gray Salsberry Peak sandstone that caps a mesa above the Pahrump Hills outcrop in Gale crater; MSL Sol 931 Mastcam-34 mosaic (sequence 004094); azimuths 110° and 180° indicated; see (b) for escarpment scale. (b) A closer look at the dark gray Salsberry Peak sandstone, overlying lighter-toned mudstones of the Murray formation. White materials are calcium-sulfate-bearing veins [74]; MSL Sol 939 Mastcam-100 mosaic (sequence 004119). (c) Portion of small boulder named, Kanosh, derived from the Salsberry Peak sandstone; inset shows the medium sand-sized grains that compose the rock; MSL MAHLI focus merge product 0942MH0001630000303666R00.

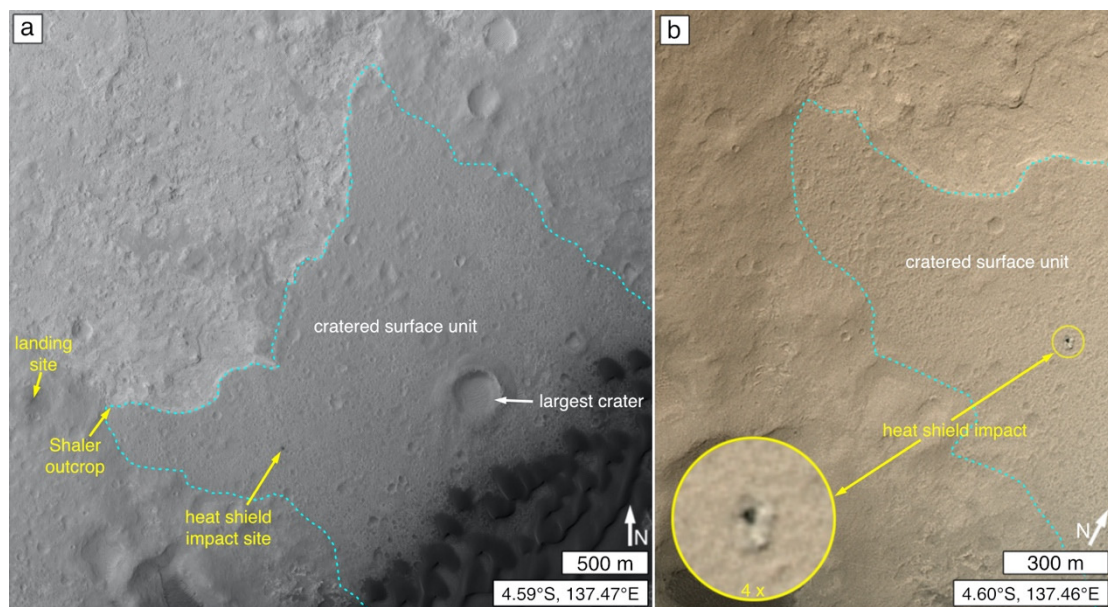


Figure 3. Cont.

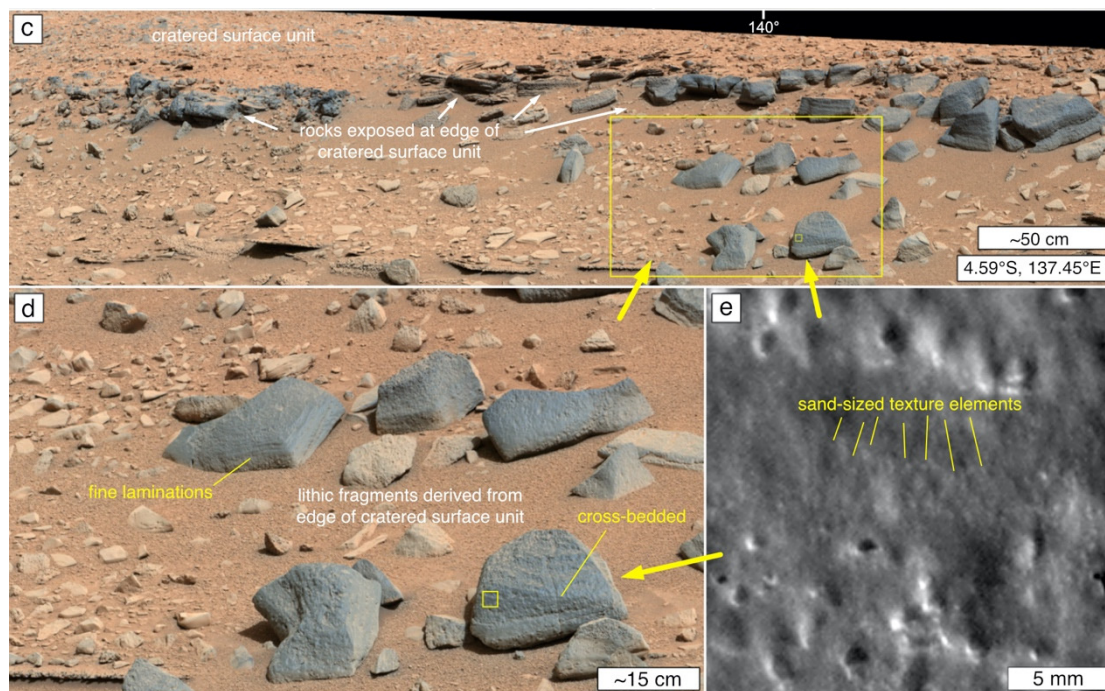


Figure 3. Example of an erosion-resistant (impact crater-retaining) sandstone. (a) Context view of “cratered surface unit” [75,76] in Gale crater near the Curiosity rover landing site. The northern edge of the unit was investigated at the Shaler outcrop [77,78]; HiRISE ESP_028335_1755. (b) Curiosity’s heat shield impacted the cratered surface unit, raising dust (inset) when it did; MSL Sol 0 MARDI 0000MD0000000000100352C00. (c) North edge of the cratered surface unit at the Shaler outcrop. The rocks are dark gray and laminated; large yellow box indicates location of (d); small yellow box indicates the location of (e); MSL Sol 315 Mastcam-100 mosaic (sequence 001291); azimuth 140° indicated. (d) Detailed view of a portion of the mosaic in (c), showing cobbles derived from the dark-gray, erosion-resistant rock that forms the bedrock of the cratered surface unit. Note that the rocks are laminated and cross-bedded. Yellow box indicates the location of (e). (e) Close-up view of a portion of the cobble named Mary River. Sunlit from the upper right; the rock surface exhibits millimeter-scale pits and medium- to coarse-sand-sized textural elements indicative of sand grains in the rock; MSL Sol 316 RMI cr_425563399prc_f0060704ccam0431611.

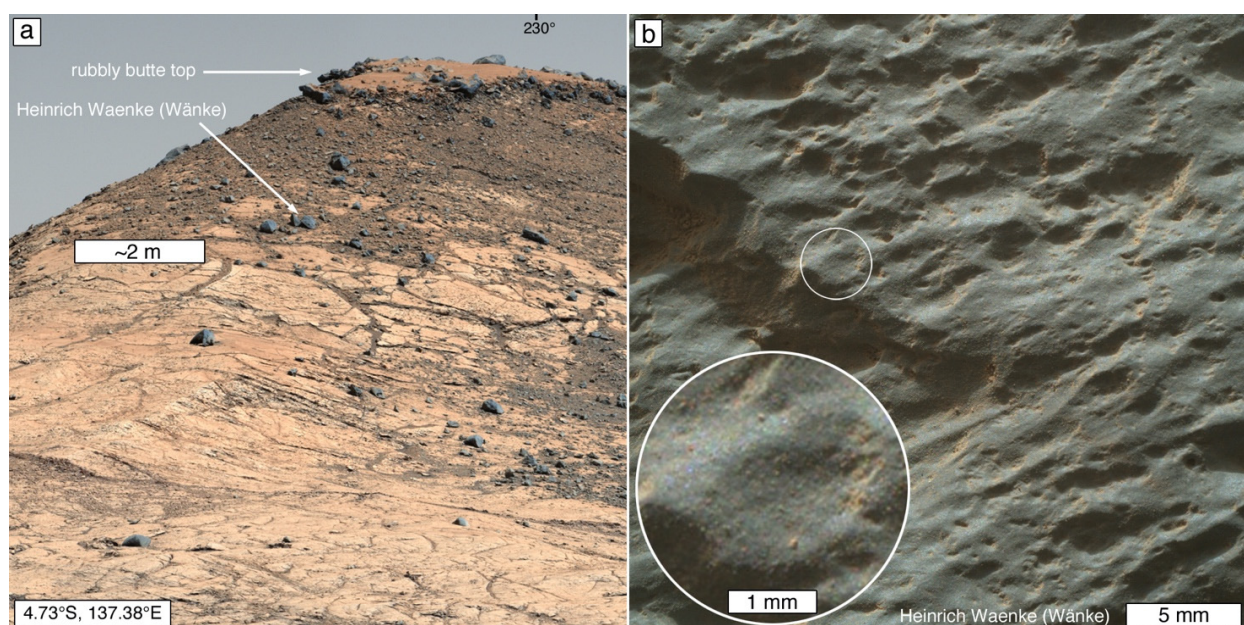


Figure 4. Identification of sedimentary rocks can be challenging, even when the images are acquired by a rover camera

at 16–32 $\mu\text{m}/\text{pixel}$. (a) This example considers a rock target named Heinrich Waenke (Wänke). It is a cobble accessed by Curiosity's MAHLI on Sol 2640. The cobble was derived from the rubble that caps Western Butte in Gale crater. Whether the rubble is mass movement debris or a broken-down cap rock is not certain. The rover could not drive to the top of the butte; thus, the Heinrich Waenke target was examined to determine rock type; MSL Sol 2616 Mastcam-100 mosaic (sequence 013743); azimuth 230° indicated. (b) A color, $23.0 \pm 0.3 \mu\text{m}/\text{pixel}$ image shows a dark gray rock with some areas covered by small patches of dust. The inset shows that the rock has $\sim 70\text{--}90 \mu\text{m}$ -scale features of differing size and color (plus orange/tan, adhering aeolian dust). These features could indicate very fine sand-sized sand grains, tephra, or (less likely) a crystalline texture (e.g., basalt). The problem is, the grains (if that is what the $70\text{--}90 \mu\text{m}$ -scale features are) are so fine, and the rock apparently so uniformly fine-grained, that no one will ever be certain whether the rock is sedimentary or igneous. In context with all of the other rocks explored in Gale crater e.g., [79–81], it is most likely (but inconclusively) sedimentary. MSL MAHLI focus merge product 2643MH0004580001001010R00.

In addition to serving as a guide to Martian sedimentary rock identification, this contribution is also an invitation to more deeply explore the vast data sets acquired from Mars over the last >55 years to look beyond the easy and the obvious. For example, are there sedimentary rocks—including those of dark tone and strong resistance to erosion—exposed in the walls of the Valles Marineris? What percentage of the yardang-forming and non-yardang-forming members and facies of the Medusae Fossae Formation [82] are sedimentary rocks rather than tuffs? How much of the upper crust of the Martian heavily cratered terrain is sedimentary, and are there sedimentary rocks beneath the Martian northern plains?

2. Materials and Methods

Pre-dating the 2021 arrival of (and, thus, not including results from) the Perseverance [83] and Zhurong [84] rovers, and the Ingenuity helicopter [85], the observations and ideas presented here come from more than two decades (February 1998–January 2021) of image acquisition planning, targeting, and examination of visible wavelength, reflected-light images obtained by cameras aboard Mars orbiters, descending platforms, and rovers. The data we used are described in the Data Availability Statement. Our data analysis focused on commonly used aerial, satellite, and remotely operated vehicle image interpretation approaches and skills, e.g., [86–88].

Most of the tens of thousands of satellite images examined were acquired by the MGS MOC-NA (1.4–12 m/pixel) [50,89], MRO CTX ($\sim 6 \text{ m}/\text{pixel}$ [90]), and MRO High Resolution Imaging Science Experiment (HiRISE; 25–60 cm/pixel [91]) cameras. Prioritized, hypothesis-driven acquisition of the data [50] was strongly informed after 2001 by the geomorphic expressions and thermophysical contrasts of rock and regolith revealed by the $\sim 100 \text{ m}/\text{pixel}$ images from the Mars Odyssey (ODY) Thermal Infrared Imaging System infrared subsystem (THEMIS-IR [92]) and, after 2006, also by the growing $6 \text{ m}/\text{pixel}$ coverage of Mars by CTX. High spatial resolution images from the Tianwen-1 High Resolution Imaging Camera (HiRIC [93]), and the ExoMars Trace Gas Orbiter (TGO) Colour and Stereo Surface Imaging System (CaSSIS [94]), were not examined for this study, but their data are relevant to application of the ideas presented here because these cameras provide images at scales that fall within the 0.25 to 6.0 m/pixel range bracketed by HiRISE and CTX.

Images from the cameras onboard the Curiosity rover, operative in Gale crater [95], were also vital and examined as the data were received on Earth. These include images obtained during the August 2012 landing by the Mars Descent Imager (MARDI [96]); images and mosaics acquired by the Navigation and Hazard cameras (Navcams, Hazcams [97]), Mast cameras (Mastcams [96]), and Remote Micro Imager (RMI [98]) on the rover's remote sensing mast [99]; as well as the Mars Hand Lens Imager (MAHLI [100]) on the turret at the end of Curiosity's robotic arm [101]. The rover's mobility system [102] was used to move the cameras to different localities in Gale crater. Images from the Panoramic camera (Pancam [103]), Microscopic Imager (MI [104]), and Descent Image Motion Estimation System (DIMES [105]), onboard the Mars Exploration Rover (MER), Opportunity—which operated in Meridiani Planum (2004–2018 [106])—also informed the results presented here.

3. Results

Identification of sedimentary rock occurrences on Mars can be challenging. This is true even when considering 16–32 $\mu\text{m}/\text{pixel}$ images of Martian rocks obtained by rover cameras (Figure 4). First, there is the likelihood that colleagues will disagree on interpretation, typically because they have not first agreed on the nature of the observables. This type of disagreement can occur even on Earth when a group of geologists of differing backgrounds and experience are together, examining an outcrop in the field. On Mars, no one is “in the field” and so the discussion is reliant on remotely gathered data. This section describes features that are sought to make the case that a given geological feature is an occurrence of sedimentary rock.

Sedimentary rock outcrop and landform erosional expressions are a function of rock physical properties and the processes and chemistries that have acted upon the rocks to modify them over time [107–109]. Important attributes include depositional texture (e.g., grain size, packing), depositional structure (e.g., bedding), diagenetic features at all scales (e.g., differential cementation, fractures, veins, concretions, etc.), and depositional, basin-scale facies configurations (e.g., interfingering of sandstones and mudstones; transgressive and regressive relations in subaqueous sediments). Deformational structure can also be helpful for sedimentary rock occurrence identification in some cases (e.g., jointed or polygonal fracture patterns).

Identification is aided by standard photointerpretation methods, particularly through the “recognition elements” of Ray [86]: tone (and color, where available), texture (frequency of tonal change as a function of image scale), pattern, shape, size, relation of a feature to associated features, and combinations of these. Solar illumination conditions and seasonal frost patterns are also important to consider when examining aerial and satellite images of Mars. The phase angle can have a profound impact on the visibility of landforms and the perception of tone and color.

Sedimentary rock occurrence identification also benefits from familiarity developed from field experience on Earth, robotic (rover) field experience on Mars, photographic guidebooks, e.g., [110,111], and illustrations of Earth’s sedimentary rock landforms [107,109,112–114]. For example, systematic, parallel, or subparallel alternations in tone [115]—characteristic of layered rock outcrops bearing distinct stratal horizons—provide approximate knowledge of the stratigraphic locations of depositional surfaces [116,117].

3.1. Signs That a Geological Material Is Rock

Identification of sedimentary rock occurrences in satellite and aerial images of Mars begins with determination of whether an observed feature is, or has the properties of, an exposure of rock. Rock is a consolidated (lithified) geological material that, on Mars, is distinguished from ice on the same basis that whole worlds are classified as rocky or icy. Rocky worlds are dominated by silicates and metals [118]; ices (e.g., H_2O , CO_2 , CH_4) dominate the crust and regolith of colder worlds [118]. Thus, while Mars has H_2O and CO_2 ices [119,120]—and these can cement sediment and regolith at high latitudes [121–123] and form ephemeral boulders during mass movement events [124]—ices and ice-cemented sediments on Mars are not generally considered to be rock.

Rock is created through lithification. On rocky worlds, it is produced by freezing of melt (magma, lava, pyroclasts, impact melt), welding of pyroclasts, sintering of clasts via impact-cratering-induced shock metamorphism [125], formation of chemical sediments, or diagenesis of sediment and primary volcanoclastic deposits. Clastic diagenesis can involve cementation, compaction, and cementation, or compaction without cementation [126]. Chemical sediments can also be subjected to diagenesis, including recrystallization. Lithification of clastic sediment can occur in both surface/near-surface, e.g., [127–129], and sub-surface environments, e.g., [126,130]. Clastic lithification is distinguished from induration because the latter refers to a broader range of phenomena. Induration includes lithification through sediment diagenesis and welding of tephra, but also refers to case hardening of weathered rock surfaces and thermal alteration of sediment or primary volcanoclastics in contact with lava or magma [131].

Recognition that a material is rock in high spatial resolution (e.g., centimeters to several meters per pixel) satellite or aerial images of Mars can be challenging, and the observables are not always fool proof. For example, even on Earth there remains a lack of consensus as to whether cemented, Quaternary loess (aeolian silt) should be considered to be rock [132]. Dry playa muds present another example; some playa surfaces can be so hard as to permit landing an aircraft or spacecraft on them [133]; such a material—if present on Mars and hardened at the surface/atmosphere interface—could be indistinguishable from bedrock. However, there are several observables that can be sought to help make an interpretation that a material is rock or—like dried playa muds—has properties similar to rock: boulder production; preservation of steep slopes; distinct contrasts in tone or color between strata; sharp expressions of faults, fractures, or joints; resistance to the impact of saltating grains; the presence of yardangs or other aeolian erosional forms; or the presence of an overlying material determined to be rock. These observables do not all have to be evident to make the case that a material is rock. In addition, they might not always be diagnostic.

3.1.1. Boulder and Megaclast Production

Clast production and release can occur as a unit of rock breaks down at a planet's surface. *Clast release* is the liberation of particles (grains or concretions) already present in a rock, whereas *clast production* refers to the breakdown sensu [134,135] of rock into smaller fragments. On Mars, boulders and megaclasts are typically produced when an impact cratering event fragments rock (Figure 5a), when rock is weathered and eroded from steep slopes, or when plateau-, mesa-, or butte-capping rocks break up as the landforms decay (Figure 5b,c). Boulders in crater ejecta are a good sign that the impacted material is rock, although boulders present in an impacted, unconsolidated deposit can also be released by such an event. Lava flows and sedimentary rock outcrops, alike, can exhibit signs of boulder production. Polygonal fracture patterns in rock can also lead to boulder-sized fragment production when fracture-bounded slabs are dislodged and displaced from their original outcrop position (Figure 5d).

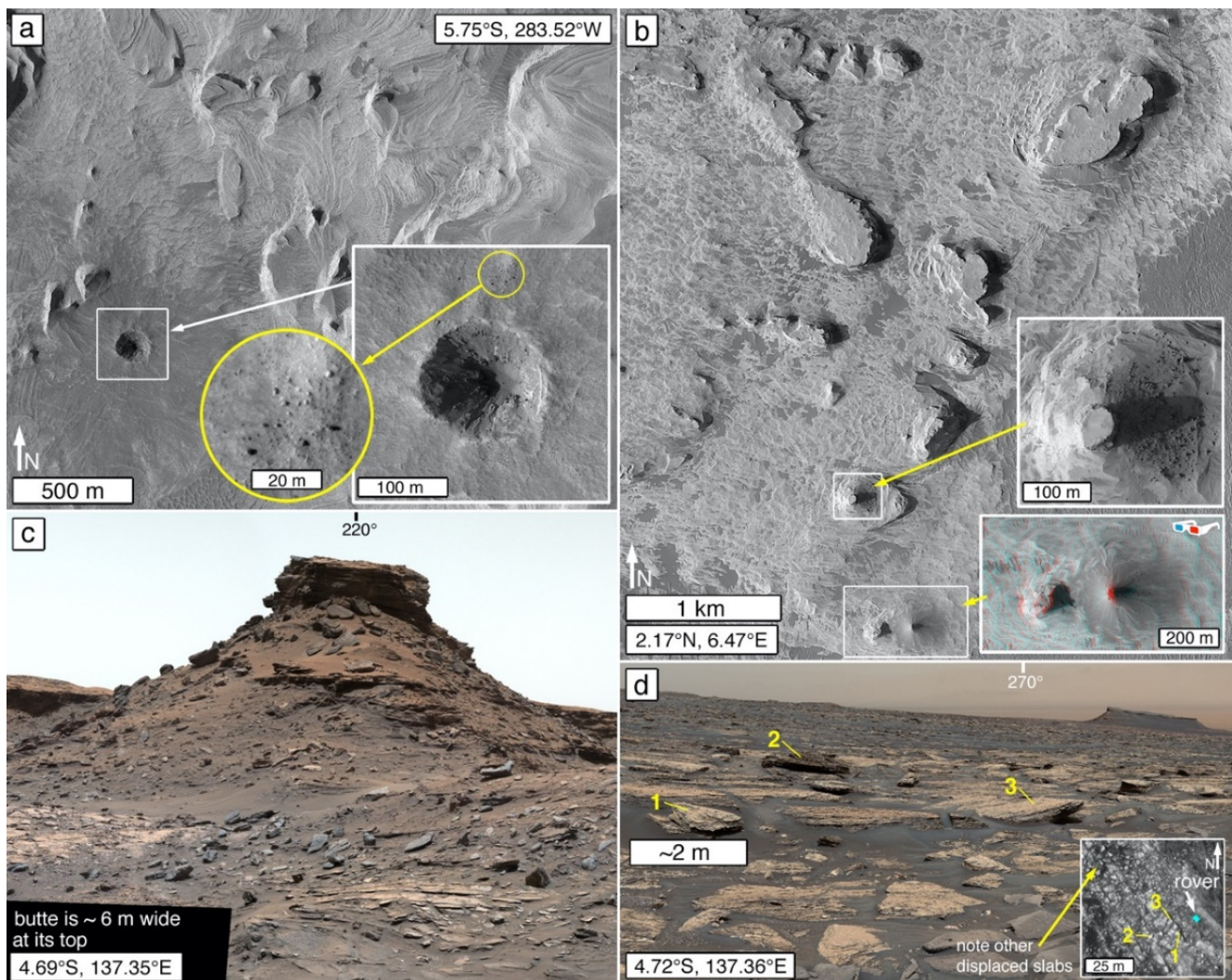


Figure 5. Example boulders produced from the breakdown of—and examples of mesas, buttes, and pinnacles formed of—Martian sedimentary rock. (a) Boulders produced by an impact cratering event in light-toned sedimentary rock in west Candor Chasma; inset in white box shows boulders in proximal ejecta; inset in yellow circle shows close-up view of some of the ejected boulders; HiRISE PSP_002841_1740. (b) Mesas, buttes, and pinnacle (stereopair anaglyph inset) formed in sedimentary rock in northeastern Sinus Meridiani. Butte in upper inset shows boulders produced and shed from the butte capping rock; HiRISE ESP_064616_1820; anaglyph ESP_064616_1820 and ESP_064761_1820. (c) Butte in the Murray buttes region of Gale crater showing boulder- and cobble-sized sandstone [136] fragments shed as the capping rock breaks down; MSL Sol 1432 Mastcam-34 mosaic (sequence 007075); azimuth 220° indicated. (d) Creation of boulder-sized rock fragments (examples labelled 1, 2, 3) from dislodgment and displacement of polygonally fractured slabs of Martian mudstone in the Murray formation, Gale crater. Inset shows view from MRO HiRISE (ESP_064519_1750); MSL Sol 1688 Mastcam-34 mosaic (sequence 008784); azimuth 270° indicated.

Of course, how long a produced boulder or megaclast may persist in the landscape—before being broken down to finer particles that are transported away—will depend upon the rock physical properties and the processes acting on that rock. A boulder produced from an erosionally-recessive rock, for example, will not persist as long as a boulder produced from an erosionally-resistant rock, as evident in the comparison of the landscapes at the Opportunity and Spirit rover sites in Meridiani Planum (sandstone bedrock) and Gusev crater (basalt lava bedrock) [137].

3.1.2. Retention of Steep Slopes

The ability of a geological material to hold a steep slope that exceeds the angle of repose—such as an escarpment, caldera wall, impact crater wall, or canyon wall—is a key indicator that a geological material is likely rock [12,49,138]. Slip faces of whole aeolian sand dunes that have become lithified [51,52,139] can also exceed the angle of repose [139,140]. Among Martian rock outcrops, escarpment-bounded landforms include plateaus, mesas, buttes, and pinnacles (Figure 5b; see definitions of [108]). Overhangs developed above recesses in escarpments also signal the presence of rock and can be rendered visible in satellite or aerial images by their shadows or via off-nadir views (Figure 6a).

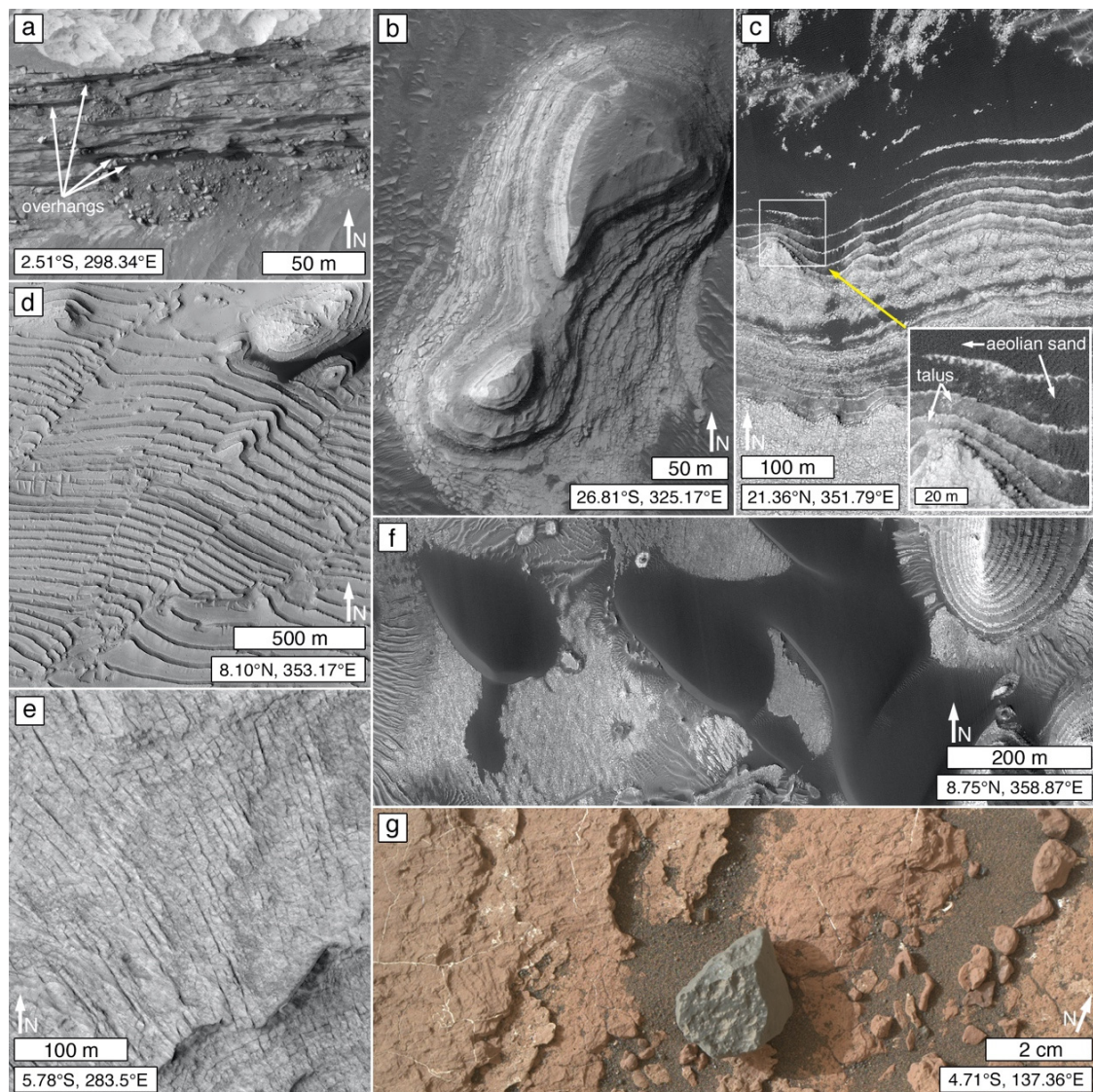


Figure 6. Example features that assist identification of rock outcrops on Mars. (a) Stratified rock with overhangs and rock fragment talus below; Juventae Chasma; HiRISE PSP_007561_1775. (b) Stratification identified by sharp contrasts between alternating strata or stratal packages; southern Holden crater; HiRISE ESP_019322_1530. (c) Stratification appearance enhanced by presence of modern sediment accumulations (aeolian sand; talus shed from rock slopes); Becquerel crater; HiRISE ESP_045140_2015. (d) Faulted rock; Danielson crater; HiRISE PSP_002733_1880. (e) Jointed rock; west Candor Chasma; HiRISE PSP_002841_1740. (f) Rock substrate across which aeolian sand has recently saltated; crater in western Arabia Terra; HiRISE ESP_066067_1890. (g) Close-up view of rock surfaces (reddish Murray formation [141] mudstone and a dark gray “float” rock) cleaned of aeolian dust by saltating sand; Gale crater, about 12 m north of Nathan Bridges dune [142]; MAHLI image 1600MH0001900010601863C00.

3.1.3. Distinct Contrast between Strata

Sharp contrasts in tone or color exhibited by, or a lack of blur between, adjacent strata or stratal packages exposed on a slope are good signals that rock is present (Figure 6b) [49]. One caution is that apparent sharp tonal contrasts between strata can, in some cases, instead be an indicator of modern sediment (aeolian sands; talus) deposited on rock outcrop benches separating strata of similar tone (Figure 6c) [24,25].

3.1.4. Sharp Expressions of Faults, Fractures, and Joints

Sharply distinguished faults and offsets along faults (Figure 6d) [49], as well as fractures and joints (Figure 6e) [8,25,143–145], are good indicators of the presence of rock. However, like the aforementioned uncertainty regarding cemented loess [132], the presence of fractures might not always indicate a lithified material.

3.1.5. Resistance to the Impact of Saltating Sands

Wind-mobilized sand is active on Mars in the modern environment [146,147]. Aeolian interdune substrates and dune transport corridors free of aeolian dust and sand accumulations can be good signs of rock exposures on Mars [49]. Saltating sand grains bounce off of hard surfaces [148], such as a bedrock exposure, limiting the accumulation of aeolian dust and sand. Figure 6f shows an example observed using an orbiting camera, and Figure 6g shows an example viewed from the ground in Gale crater.

3.1.6. Kharafish (Wind Erosion Forms)

Signaling the presence of rock—or at least indurated material—*kharafish* is an Egyptian term that encompasses the full range of aeolian erosional forms [149], from kilometer-scale mega-yardangs [150], to centimeter-scale ridges and grooves [151] (p. 68), and millimeter-scale flutes [152]. Yardang-scale kharafish (Figure 7a) occurs in a variety of forms that go beyond the classical inverted boat hull shape [153,154], including meter- to kilometer-scale scour-remnants that develop in the lee of knobs (Figure 7b) of greater erosion resistance [155] (p. 38). Yardangs form in a variety of lithologies on Earth, including carbonates, tuffs, and clastic sediment [156–161]; unusual examples include yardangs formed in weathered basalt [157] and weathered gneiss [155,162]. The term, kharafish, might extend to the “knapped” (Figure 7c) [24,25] erosional expression common to some Martian sedimentary rock outcrops, although the exact origins of these surfaces needs further study. Field studies, e.g., [153,157,163,164] indicate that the morphologies of yardangs and other kharafish are related to material properties such as texture (e.g., grain size), depositional structure (e.g., bedding), and deformational structure (e.g., joints, faults, folds). In addition, wind erosion shapes rock according to its physical properties, such that erosion-resistant heterogeneities in the rock may form protrusive elements (Figure 7d) [165].

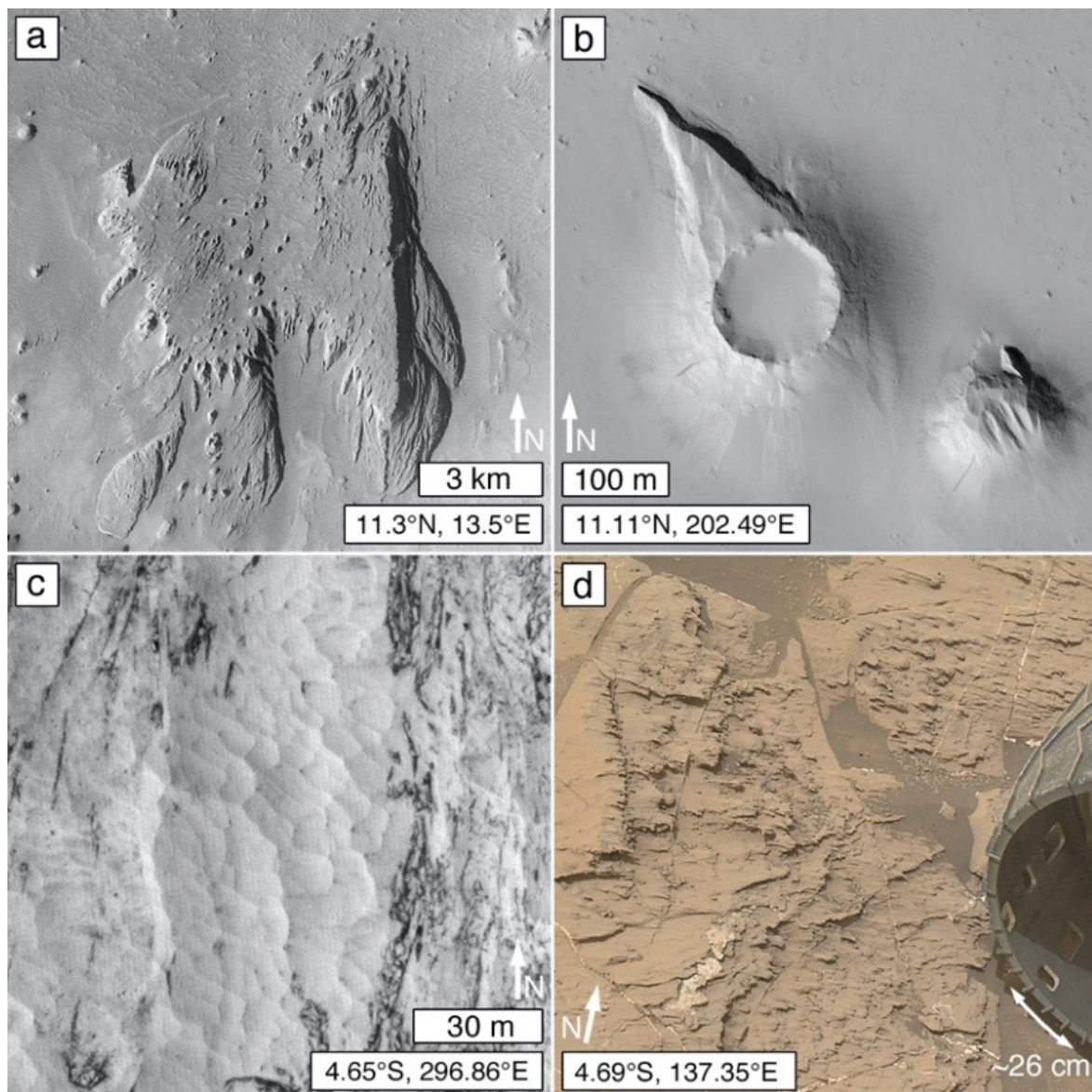


Figure 7. Example Martian wind erosion forms (kharafish) viewed at different scales. (a) Yardangs carved into in a plateau of stratified rock (e.g., see HiRISE PSP_006187_1915) in a crater in western Arabia Terra; CTX B04_011395_1915_XN_11N346W. (b) Large “wind tail” formed in rock in the lee of an exhumed impact crater in southern Amazonis Planitia; HiRISE ESP_066983_1910. (c) “Knapped” surface texture in light-toned rock in Juventae Chasma; HiRISE PSP_004291_1755. (d) Centimeter- and millimeter-scale wind tails and stalks [166], or dedos [167], in mudstone in Gale crater; MAHLI image 1463MH0003900010503794E01.

3.1.7. Emergence from Beneath a Body of Rock

Another sign that a material is rock is its partial exposure from beneath an overlying material that is determined to be rock based on any of the above observables. Figure 8a shows a case in northern Meridiani Planum in which an impact crater ejecta deposit is partly exhumed from beneath light-toned, sedimentary rock [168]. Because the stratigraphically higher light-toned material in Figure 8a has been lithified, the clastic impact ejecta beneath that rock must also have been subjected to diagenesis and lithification, not unlike examples of lithified impact ejecta on Earth e.g., [169,170]. The other examples in Figure 8 illustrate cases of fluvial and alluvial sedimentary forms (see Sections 3.5.2 and 3.5.3) emergent from beneath rock or remnants of rock. An exception occurs in cases of lava flow superposition on unconsolidated regolith, sediment e.g., [171], or tephra, provided that the underlying

material has not subsequently become lithified through diagenesis. It should also be noted that some sediments emergent from beneath units of rock could be much more poorly lithified than their overburden, such as much of the Fontainebleau Grés (Sandstone) in France, which is overlain by limestones [172–175].

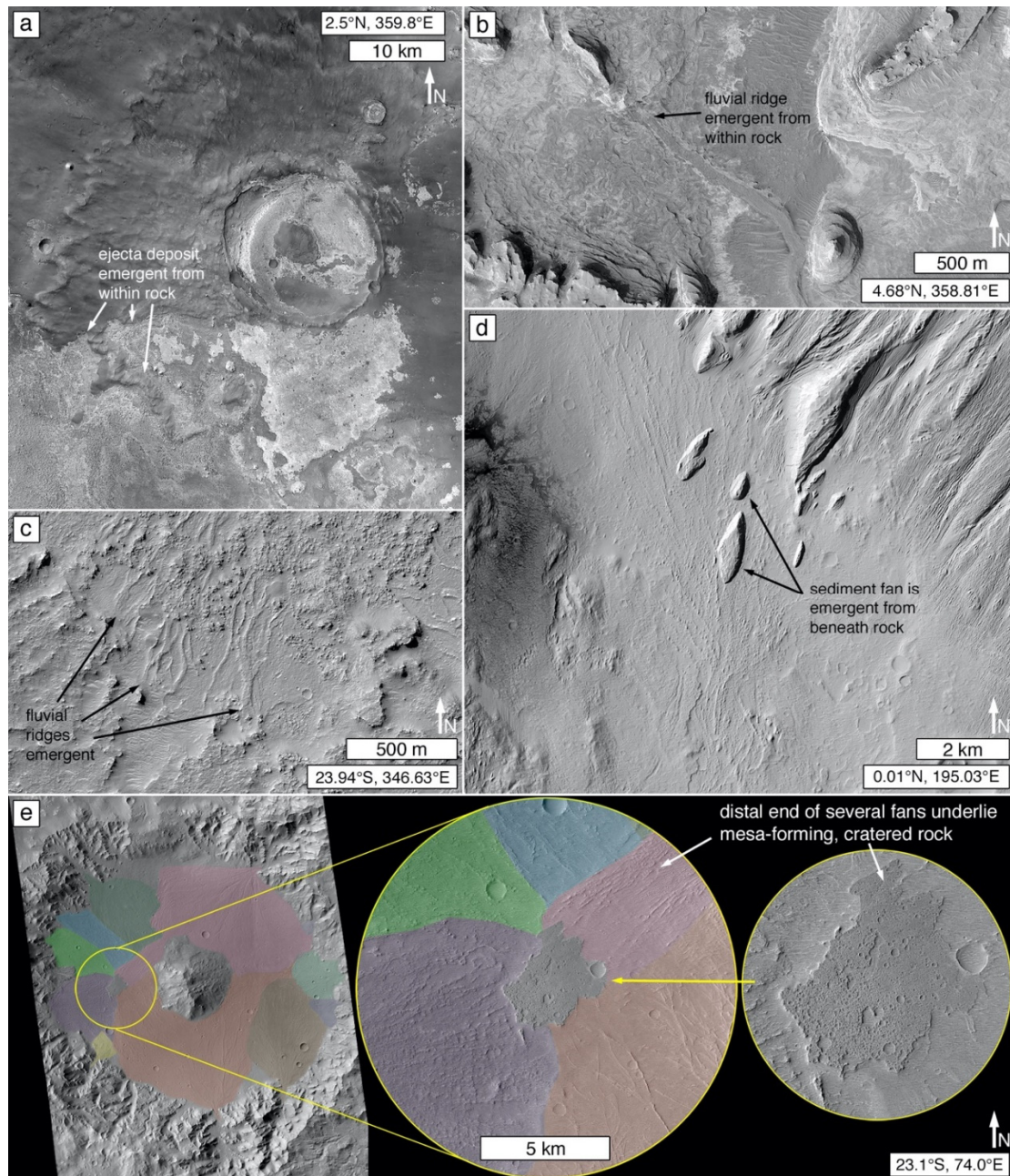


Figure 8. Examples of material emergent from beneath units of rock. (a) Impact crater ejecta deposit in northern Sinus Meridiani; CTX T01_000886_1819_XN_01N000W, P03_002113_1825_XI_02N000W, B05_011501_1820_XI_02N359W. (b) Emergence of a ‘fluvial ridge’ [176,177] from within light-toned sedimentary rock in northern Sinus Meridiani; HiRISE PSP_004091_1845. (c) Emergence of fluvial ridges from within rock in a crater in northern Noachis Terra; HiRISE ESP_044059_1560. (d) Emergence of sedimentary fan material in southern Nicholson crater from beneath yardang-forming rock; CTX F01_035994_1802_XN_00N165W. (e) Fans (each one colored) in a crater in Tyrrhena Terra emergent from beneath a mesa-forming, heavily cratered rock unit; left: CTX P03_002084_1567_XI_23S285W, P03_002295_1568_XI_23S286-W, B17_016417_1568_XI_23S285W; middle and right: CTX P03_002295_1568_XI_23S286W.

3.2. Stratification

Commonly expressed in landscapes and rock outcrops as a product of differential resistance to erosion, stratification is “fundamental to” [86] (p. 16) the recognition of sedimentary rock occurrences in satellite and aerial images [86,115–117]. Sedimentary strata are time-ordered records of change (i.e., geological history) and their three-dimensional configurations provide information about sediment transport and depositional conditions. Of course, strata are not unique to sedimentary rocks—unconsolidated sediment, primary volcanoclastic deposits, e.g., [178], accumulations of lava, e.g., [179], the perennial Martian polar caps [121,180,181], and even the igneous rocks and impactogenic regoliths of the Moon, e.g., [182–184], can all exhibit stratification.

MOC-NA and HiRISE images emphasized the ubiquity of stratified materials—sedimentary, igneous, and otherwise—exposed at the Martian surface [48,115,185,186]. In such images, stratification is identified through “the presence of alternations in brightness”, particularly those that are “laterally traceable for ~10 m or more”, or the observation of “distinct shadowed, shelf-like topographic breaks in slope” [115] (p. 17). Images of higher than HiRISE (~25 cm/pixel) spatial resolution can reveal stratification at finer scales, both in terms of lateral extent and layer thickness [21,187]. The finest strata on Mars—laminae undetectable using orbiter imaging systems sent to Mars thus far—display sub-millimeter thicknesses [188–190].

Satellite and aerial images of Martian sedimentary rock outcrops exhibit stratification through landform expression, stratal patterns, and the revelation—by erosional exposure—of major unconformities that reveal paleo-surfaces. Considerable information about the materials can be interpreted from images of Martian sedimentary strata, including (but not limited to) studies that address depositional settings and conditions, e.g., [1,2,5,17,27,191], depositional and deformational structure, e.g., [2,4,8,25], environmental controls on repeated (cyclic, rhythmic, periodic) stratification e.g., [16,48,192], and stratigraphic correlation across distance, e.g., [12,19,28].

3.2.1. Expressions of Stratification

Where large enough to spatially resolve in a given satellite or aerial image, strata exposed on Martian rock outcrop slopes are expressed as terraces or cliff-bench forms, alternating bands of differing color or tone, or through the presence of gaps that parallel or separate strata (Figure 9). Gaps, narrow relative to the scale of the outcrop (Figure 9d), can result from the presence of erosionally-recessed layers or from fractures or joints (fractures of regular spacing) that parallel the bedding. Fractures or joints (as well as bedding plane separations) can result from stress relief caused by overburden removal, e.g., [193] or by undermining. Gaps can also be apparent features, not true gaps, created at erosionally recessed partings on rock slopes, e.g., [194] (pp. 208–209); a parting is a thin stratum or group of strata consisting of a lithology that differs from the thicker, main lithology above and below it [195]. Gaps will be apparent on a rock face if a parting has recessed far enough back that it cannot be seen in available images.

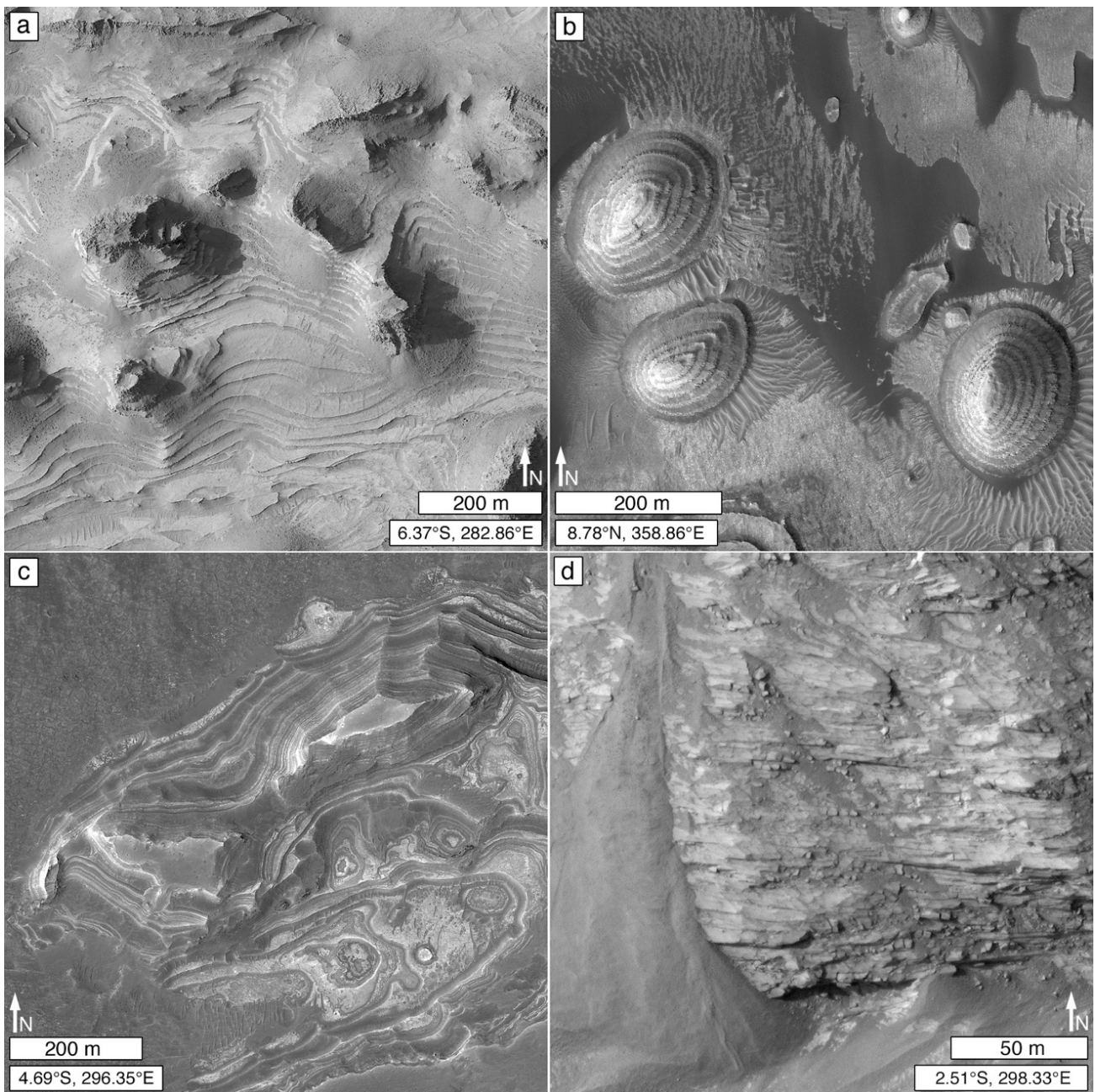


Figure 9. Examples of stratified Martian sedimentary rock outcrop expressions. (a) Cliff-bench outcrop in southwest Candor Chasma; HiRISE PSP_002340_1735. (b) Stair-stepped variant of cliff-bench expression (with cliffs and benches also partly covered with talus) in a crater in western Arabia Terra; HiRISE ESP_066067_1890. (c) Banded layered rock exposure on plateau above southwestern Juventae Chasma; HiRISE PSP_003579_1755. (d) Relatively narrow gaps between strata or stratal packages exposed in Juventae Chasma; HiRISE PSP_007561_1775.

Cliff-bench, stair-stepped, and terraced landform expressions are common, although not universal, among Martian sedimentary rock occurrences (Figure 9a,b). Cliff-bench forms consist of prominent stacks of layered rock exhibiting vertical (cliff) and horizontal (bench) elements. Stair-stepped occurrences are similar, but the vertical height of each cliff, and the width of each bench, are similar and repeated (or nearly so), like a staircase. Terraced hillslopes [109] are another variant in which benches form narrow terraces, cliffs are absent, and slopes may approach that of the angle of repose. The cliffs in cliff-bench sedimentary rock landforms are usually not actually vertical, and the pattern can be one of thin, erosion-recessive and thicker, erosion-resistant couplets [17]. A thin, recessive layer

need not always be present; differences in resistance to weathering and erosion resulting from differences between the top and bottom of a given stratum or stratal package (e.g., particle size, sorting, cementation, and/or composition [196]) could also contribute to the patterns observed.

Banding can indicate stratification, and is expressed in orbiter or aerial images of Mars as alternations of strata or stratal packages that exhibit differing color or tone (Figure 9c). Color or tone differences can result from intrinsic tonal or color properties of the rock, or from textures (e.g., rough vs. smooth) that exist on the rock surface (or alluvium accumulated on the rock surface) at a scale below the spatial resolution of the image (see Section 3.3). Banding can also result from accumulation of rock breakdown debris, wind-blown sand, or windblown dust on benches or terraces on slopes cutting across stratified rock (Figure 6c). Finally, banding might, in some cases, be reflective of stratigraphic properties but is actually a product of diagenesis or weathering. The Burns formation exposure in Endurance crater examined via Opportunity provided an example of diagenetic banding [57]. According to Young et al. [107] (p. 12), outcrops of the Glass Hill Sandstone of the Bungle Bungle range in the Australian Kimberley provide an example on Earth of banding that is only skin-deep. There, colorful bands exhibited by towering sandstone cliffs are caused by weathering and microbial activity acting on minor stratigraphic variations in porosity and clay content.

3.2.2. Patterns of Stratification

Exposures of stratified sediment can exhibit stratal patterns [197] that aid the identification of sedimentary rock and are useful for interpreting depositional settings and conditions [14]. Patterns include the nature of stratum and stratal package thickness, the three-dimensional shape of a stratum or stratal package (e.g., lens, wedge, etc.), repetitious stratification, and sedimentary structures large enough to observe in aerial and satellite images, such as meter- to decameter-scale cross stratification.

In their initial survey of sedimentary rocks in early MOC-NA images, Malin and Edgett [49] described units of thin, thick, and massive stratal packages. “Thin” packages were said to be a few meters to ~200 m thick and contain “one to hundreds” of thinner beds; “thick” packages were described as being ~200–2000 m thick and also contain thinner layers “Massive” packages were a few hundreds of meters to a few kilometers thick and exhibit poor to zero evidence of stratification within them. In describing a stratified rock occurrence observed in a satellite or aerial image, terms such as *thin* and *thick* should be accompanied by quantitative definitions [14,198]. *Massive*, too, is a problematic term—although it remains in use, even for Martian sediments e.g., [23,31,49]—because it has nothing to do with mass; an alternative term is *structureless* [197]. In this case, *structureless* refers to depositional rather than deformational structure [197]. The *structureless* descriptor should be applied relative to observation scale (e.g., the rock unit exhibits no depositional structure observable at an image scale of ~25 cm/pixel). Some of the rock units explored at the Opportunity and Curiosity rover sites can appear to be (or are nearly) *structureless* when observed in HiRISE images, but exhibit considerable sedimentary structure (e.g., fine laminae, cross bedding) when viewed at higher spatial resolution using rover cameras (Figure 10).

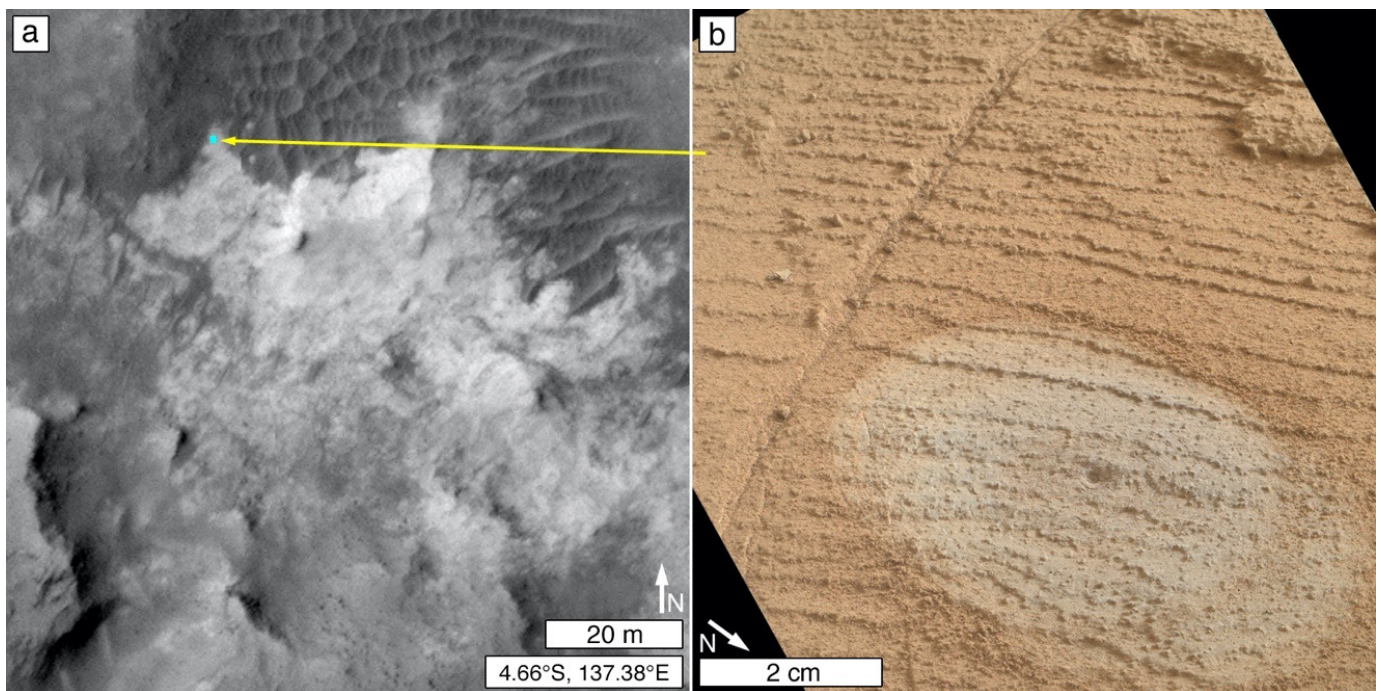


Figure 10. Some Martian sedimentary rock outcrops appear “massive” or “structureless” at the scale of HiRISE 0.25 m/pixel images, but are indeed stratified at millimeter to centimeter scales. (a) Light-toned area at the center is the Pahrump Hills outcrop explored via the Curiosity rover [189,199]; HiRISE PSP_009294_1750. (b) Oblique MAHLI view (receding away from the viewer) of fine, sub-millimeter-thickness strata at the Pelona target (blue box in (a)). Note light gray surface brushed by Curiosity’s dust removal tool [200]; MAHLI focus merge product 0806MH0004420000300703R00.

Stratification patterns include those that repeat and those that provide information about depositional forms and conditions (e.g., lenses, channel fills, cross stratification). Repeated patterns include repetition of stratum (or stratal package) thickness, rock properties (as expressed in the landscape by erosion), or the patterning within one stratal package as compared to the next. Repetition (Figure 9a) might be related to reoccurring, periodic, or quasi-periodic climate patterns [16,192]. In clastic rocks, repeated strata also imply that sediment supplies of similar or equivalent particle size, composition, and source are available through each period or cycle. Although spectacular in appearance [16,69,192], repeated (or cyclic) stratal patterns are, apparently [14,48], uncommon on Mars relative to the overall abundance of sedimentary rock occurrences identified (up to the year ~2012) in 0.25–6.0 m/pixel orbiter images.

Cross-stratification and other sedimentation patterns are sometimes evident—albeit very difficult to discern in many cases—in satellite or aerial images of well-exposed sedimentary rocks on Mars. Grotzinger and Milliken [48], for example, noted an outcrop that cut through a feature that they interpreted as a small, filled, buried impact structure. Dromart et al. [2] described a complex suite of stratal patterns in Melas Chasma—a stratal architecture—interpreted to include subaqueous clinoforms and channel fill sediments (Figure 11a). Meter- to decameter-scale cross stratification, interpreted to be aeolian, is seen in a variety of settings on Mars, including several locations in Juventae Chasma (e.g., Figure 11b) [25], and stratal packages exposed in Aeolis Mons in Gale crater [22,191,201]. An important caveat applies here; Fedo et al. [202] noted that, based on an experience with mudstones explored via Curiosity in Gale crater, some apparent cross-bedding patterns might—upon closer inspection—turn out to be a fracture (or fracture and vein) pattern, and determining this might be impossible using orbiter or aerial images.

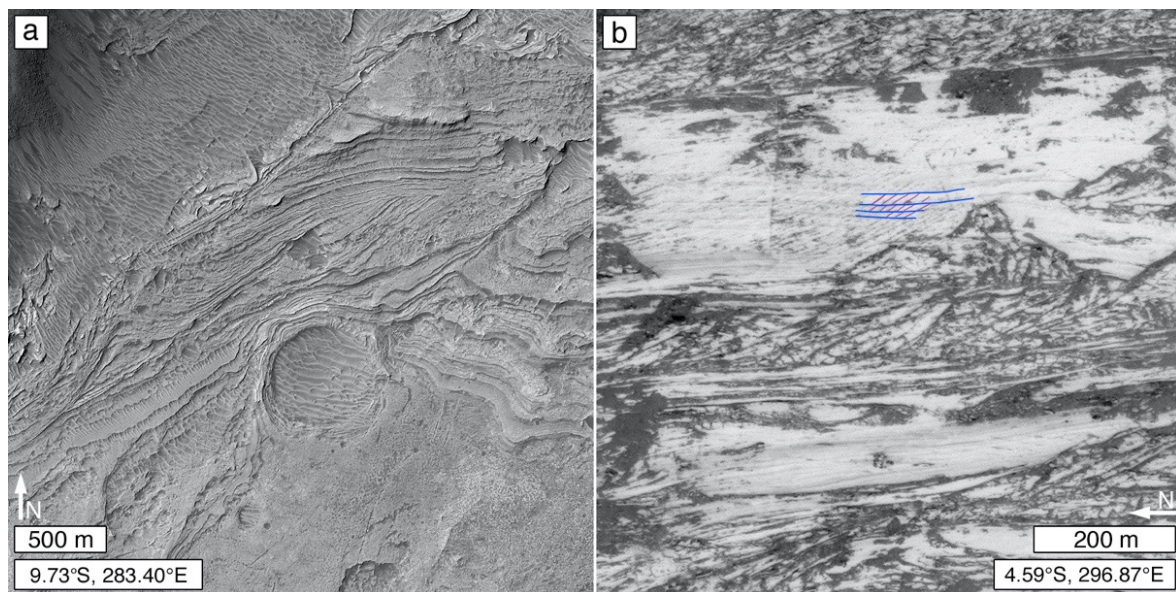


Figure 11. Example stratal architectures viewed in orbiter images of Mars. (a) Cross-cutting beds in southern Melas Chasma described by Dromart et al. [2]; HiRISE PSP_007878_1700. (b) Candidate aeolian cross-stratification in “feature A” (or “mound A”) in southwestern Juventae Chasma, reported by Sarkar et al. [25]; note that some cases of apparent cross-stratification could actually be poorly resolved fracture (or fracture and vein) patterns [202]; HiRISE PSP_004291_1755.

Another important challenge to interpretation of sedimentary rocks observed on Mars was explored by Day and Catling [30]. That is, some *known* Martian aeolian sandstones do not exhibit cross-bedding patterns that are large enough to be observed in the presently highest spatial resolution orbiter images (i.e., HiRISE), particularly the Burns formation in Meridiani Planum [57,203,204], and the Stimson formation in Gale crater [136,188].

3.2.3. Unconformities

Unconformities in sedimentary rock sections indicate episodes during which sediments were not deposited and erosion occurred [205]. Previously eroded surfaces, emergent from beneath sedimentary strata, provide the most obvious examples of unconformities that can be recognized in satellite and aerial images of Mars. Unconformities in stratal sections that expose older, partly exhumed terrain include the cratered surface identified by Malin and Edgett [49] about a quarter of the way up the north slope of Aeolis Mons in Gale crater (Figure 12a), and the partly-exhumed surfaces in Figure 8. Unconformities can also be identified in places where a younger stratal package overlies older strata in a cross-cutting relation; examples occur in Terby crater [see 11], Melas Chasma (Figure 11a) [2], and Galle crater (Figure 12b) [206].

3.3. Tone and Color

3.3.1. Tone

Global, visible wavelength image coverage of Mars at the highest spatial resolution currently available (6 m/pixel), is grayscale. Acquired by the panchromatic MRO CTX, these grayscale images provide the foundational basis for planet-wide identification of actual and candidate sedimentary rock occurrences. They also provide vital context for the higher spatial resolution views obtained by other orbiter cameras such as MOC-NA, HiRISE, HiRIC, and CaSSIS, as well as aerial imaging. While some of these higher spatial resolution cameras provided color views of Martian sedimentary rock outcrops, the entire planet has not yet been imaged, in color, at high spatial resolution (e.g., 0.25–6 m/pixel). Thus, tone is presently more valuable, globally, for identification, description, and inter-regional comparison of sedimentary rock occurrences. Tone is a qualitative proxy for

albedo that is usually discussed in a relative sense, i.e., whether a feature is lighter or darker than adjacent or nearby features in an image or image mosaic.

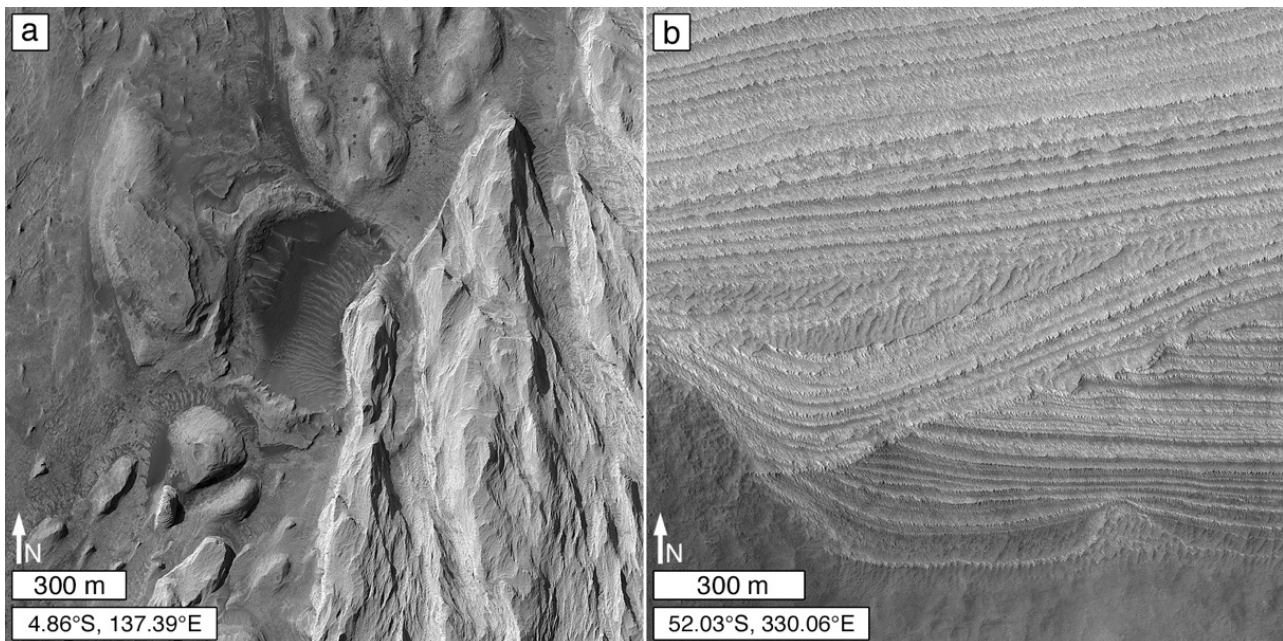


Figure 12. Example unconformities in the Martian sedimentary record as viewed from orbit. (a) Some erosional unconformities can be identified where an impact-cratered paleo-surface is in a state of partial exposure from beneath younger rock. Here, an eroded impact structure is emergent from beneath light-toned rock [49]; Aeolis Mons, Gale crater; HiRISE PSP_009294_1750. (b) Unconformities between stratal packages in a mound of sedimentary rock in southern Galle crater [50,206]; HiRISE PSP_003855_1275.

Many of the early identifications of sedimentary rock occurrences on Mars noted their light tone (Figure 1d,e and Figure 6f) [48,49]. In addition, the sandstones of the Burns formation at the Opportunity rover site were also light-toned (Figure 1f) [56,57]. However, sedimentary rocks of dark tone and “intermediate” tone (between light and dark) were also known [49], but considered less common.

Observations made at the Curiosity, Opportunity, and Spirit field sites have underscored a few important points regarding the tones of sedimentary rock occurrences observable in satellite and aerial images. First, the observed tone can be an intrinsic property of the rock, such as the observation that the sandstones at Meridiani Planum are light-toned (Figure 1f). Second, there is the possibility that tone can be an intrinsic property not of the rock but of a surface coating or weathering rind [207–209]. Third, and more importantly, the observed tone might be an extrinsic signal of a combination (in various proportions) of rock surface texture and aeolian dust or sand accumulation (Figure 13). Surface roughness at scales smaller than a given satellite or aerial image pixel can cause a rock surface to appear darker than the intrinsic rock tone because of self-shadowing. In contrast, accumulation of light-toned aeolian dust can make the rock appear to be lighter than its intrinsic tone (Figure 13a,b) [210] (p. 6). Martian aeolian sand is largely dark-toned [211], and saltating sand will generally bounce off of rock surfaces [148]; however, sand grains can accumulate in pits and fractures that are too small to observe in remotely-acquired images (Figure 13c,d) and, thus, can impart an apparent darker tone. It is also important to note that where an entire region is coated with dust, the apparent (extrinsic) tone of a given rock unit will be indistinguishable from the surroundings (e.g., lithified dune field near the Apollinaris Sulci, Figure 1a).

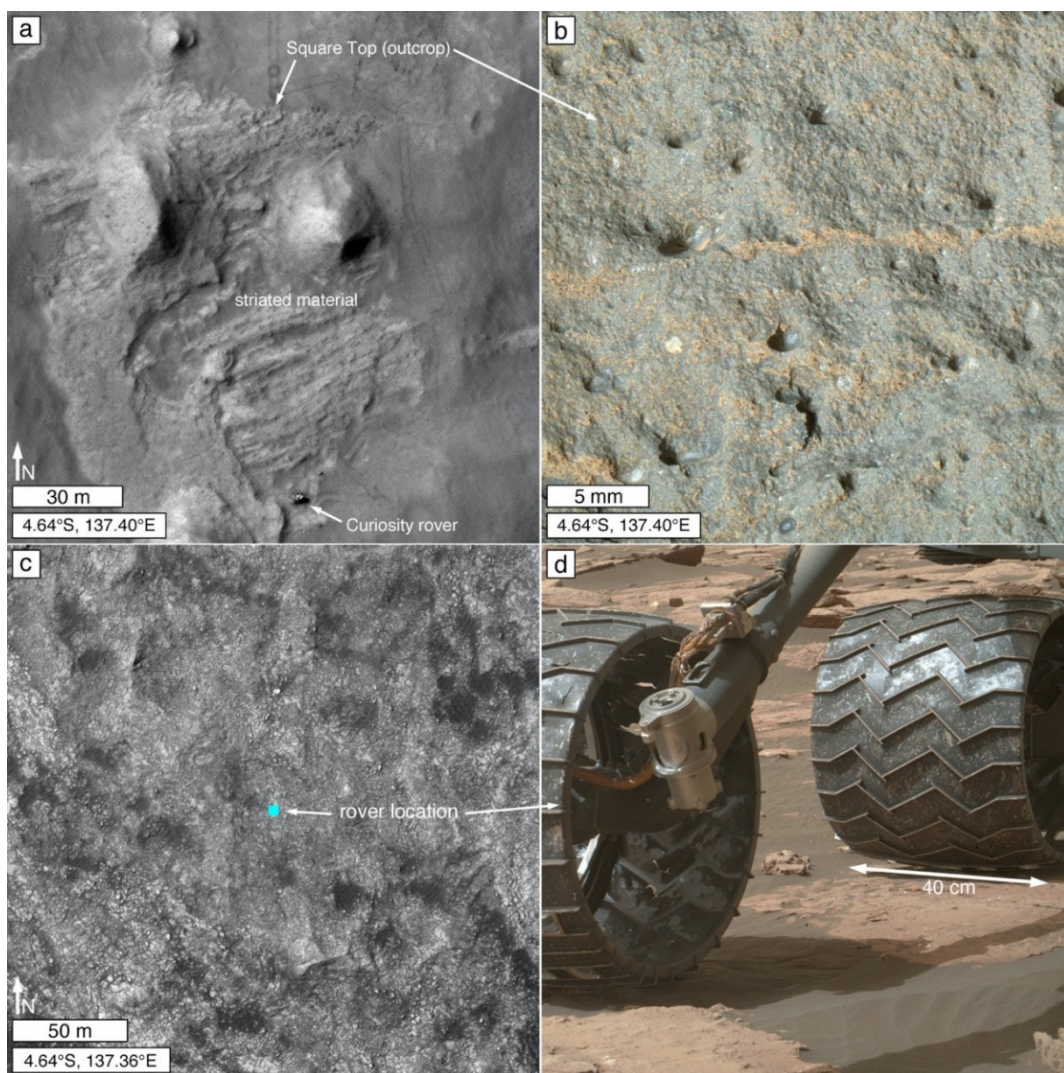


Figure 13. Tone apparent in satellite or aerial images is, in some cases, a function of the presence of surface roughness, aeolian sand, or dust cover, or both. (a) Orbiter image of Curiosity’s Kimberley field site in Gale crater; the striated rock that occurs between the rover and Square Top is light-toned relative to its surroundings; HiRISE ESP_036128_1755. (b) The light-toned, striated rock was examined on a vertically-oriented surface at Square Top and found to consist of dark-toned (gray) rock; orange-brown materials are adhering aeolian dust; MAHLI focus merge product 0586MH0003680000202975R00; sunlight from the right/upper right. (c) Light-toned rock can appear to be darker in tone, than it actually is, where the surface is rough (at sub-pixel scale), or where dark-toned aeolian sand is present in patches on the rock surface, or both; this view provides context for (d); HiRISE PSP_009650_1755. (d) A view from the ground at the location in (c), showing intermediate-toned, reddish-gray mudstone outcrops overlain by patches of dark, gray aeolian sand; MAHLI rover wheel inspection image 1512MH0002610010600069E01.

3.3.2. Color

Rock color is like tone. It can be an intrinsic property or it can be (literally) a reflection of sub-pixel scale roughness, superimposed aeolian sediment, or a combination of these. Color is also challenging to establish—what is the “true color” of something? If you have a lawn of green grass, how does that green look to your eye in sunlight? On a cloudy day? In the shadow of a tree? In twilight? Do your eyes perceive green the same way as another person’s eyes? In some cases, satellite and aerial imaging systems use cameras that attempt to capture color close to that which the typical human eye sees (e.g., Bayer pattern microfilters [212]), or they use cameras that capture images at wavelengths not visible to the human eye (e.g., MRO HiRISE near-infrared band [91]).

A key observation from the Curiosity rover mission in Gale crater is that Martian sedimentary rocks exhibit a variety of colors, as evident in Bayer pattern color interpolated images of bare rock surfaces acquired by the MAHLI (e.g., Figure 14). Examples from Curiosity include conglomerates, sandstones, and mudstones of various shades of gray, from nearly black to nearly white; mudstones that are reddish-brown, yellowish brown, or purplish-gray; and vein-forming minerals that are white and various shades of gray (Figure 14). The colors (excluding white) generally result from varied amounts of oxidized versus reduced iron-bearing minerals (e.g., hematite vs. magnetite [213,214]).

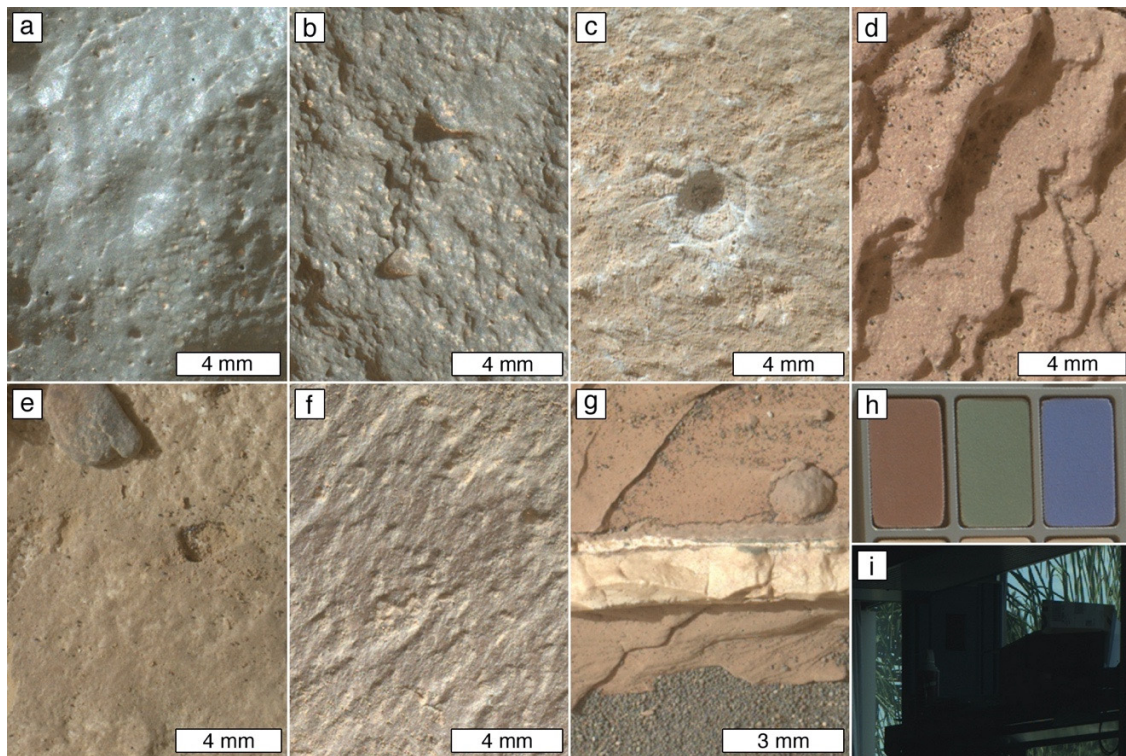


Figure 14. Example qualitative look at Martian sedimentary rock colors as recorded by Curiosity’s MAHLI red-green-blue Bayer pattern color detector in sunlight. (a) Dark gray sandstone; target Devil’s Punchbowl, 0942MH0001630000303666-R00. (b) Gray sandstone; target Rensselaer, Cooperstown field site, 0442MH000163-0000200183R00. (c) Light gray mudstone (tan material is aeolian dust) revealed by dust removal tool [200], which scratched a hole at the center; target Buckskin, 1057MH0002270000400369R00. (d) Reddish mudstone, laminae expressed as stair-steps; target Folly Island, 1518MH0001700000600213R00. (e) Yellowish mudstone; target Pulpit Ledge, 1702MH0001710000604328R00. (f) Purplish/yellowish mudstone; target Marimba; 1418MH0001530000503178R00. (g) White (calcium sulfate) vein in reddish mudstone with gray aeolian sand; target Burnt Coat, 1783MH0007060010700661C00. (h) Red, green, and blue swatches on the MAHLI calibration target [100], as imaged on Mars; 1696MH0003740010604177C00. (i) Blue sky and green palm fronds viewed through a window on Earth by MAHLI during testing on 19 September 2008; CAL_MH0809780140001207B00. No processing has been applied to alter the color or dynamic range of the original images; the calibration target and sky/palm images qualitatively demonstrate the fidelity of MAHLI’s ability to record visible wavelength color.

3.4. Rock Breakdown and Resistance to Erosion

Landforms and landscapes are temporary, even on the ancient surface of Mars [215] (p. 45). Their configurations result from the competition between the processes and rates at which new rocks are formed, or become exposed at the surface, versus the processes and rates at which rocks disaggregate and the fragments and dissolved ions are transported and deposited elsewhere. On modern and geologically recent Mars, lateral erosion (e.g., undermining, scarp retreat, rock falls, wind abrasion) has been proceeding at a higher rate than vertical erosion (lowering of surfaces); this is evident, for example, in the pace

of erosional exposure of rock in Gale crater [216]. Vertical erosion rates may slow as lags develop or erosion-resistant strata become exposed.

Subtle and not-so-subtle differences in rock properties can make a big difference in landscape configuration. In sedimentary rock exposures, these result from differences in lithology, including differing intraformational depositional or diagenetic facies [107]. For example, consider the impact on the landscape of the Petrified Forest National Park in Arizona, USA, of intraformational sandstones and conglomerates in the otherwise mudstone-dominated Chinle formation e.g., [217]. Such erosion-resistant rocks, part of the same formation as the very colorful and much more erodible mudstones [217], led to the creation of plateaus and hills that are capped by sandstones and conglomerates or mantled by—or formerly mantled by—their broken-down debris. Variability in intraformational diagenetic facies in the Murray formation, a largely mudstone-bearing rock unit in Gale crater, provides examples of diagenetic contributions (e.g., variable cementation) to landscape configuration, including Vera Rubin ridge [218,219].

Breakdown (or weathering or decay) [134,135,220], and erosion, of Martian sedimentary rock imparts signals of rock properties into the landscape that can be observed in images acquired by orbiting and aerial instrumentation. Some of these signals are interpretable as rudimentary information about sedimentary rock texture or structure. Others—such as impact crater retention and formation of escarpments—provide information that can be interpreted in terms of relative rock hardness. Resistance to breakdown and erosion can also be a function of the nature of overlying, unconsolidated debris, including lags deposits and aeolian bedforms that protect the bedrock from erosion.

3.4.1. Small Impact Crater Retention

The contribution of impact cratering to Martian rock breakdown and redistributive transport of the resulting debris should not be underestimated [137,221,222]. In this context, small (sub-kilometer diameter) impact crater retention refers to the opposite—the presence and abundance of impact structures, at the Martian surface, as a signal of rock physical properties. In particular, it refers to the erodibility of the rock in geologically recent and modern times, rather than the application of impact crater size-frequency distributions for absolute or relative age dating of geological materials.

Figure 15a illustrates the concept using an example of a lava flow located west of Meridiani Planum that superposes its surrounding terrain. In this case, the flow is younger than the materials it embays, but it retains many more small impact structures per unit area than does the older, surrounding terrain. Figure 15b, showing lavas that embay yardang-forming material in Galdakao crater, provides a similar illustration; in this case, the one large impact structure in the yardang-forming material underscores the greater crater retention age sensu [223] of these rocks, but the relative abundance of very small craters on the lava surface illustrate the point that the lavas are more resistant to erosion and, thus, retain small craters better than the yardang-forming material. Of course, it should be noted that not all lavas are heavily peppered with small impact craters. Figure 15c shows an example in Elysium Planitia that has a young crater retention age, attributed to the youth of these lavas. Vaucher et al. [224] estimated these lavas might be only 2.8 ± 0.5 million years old.

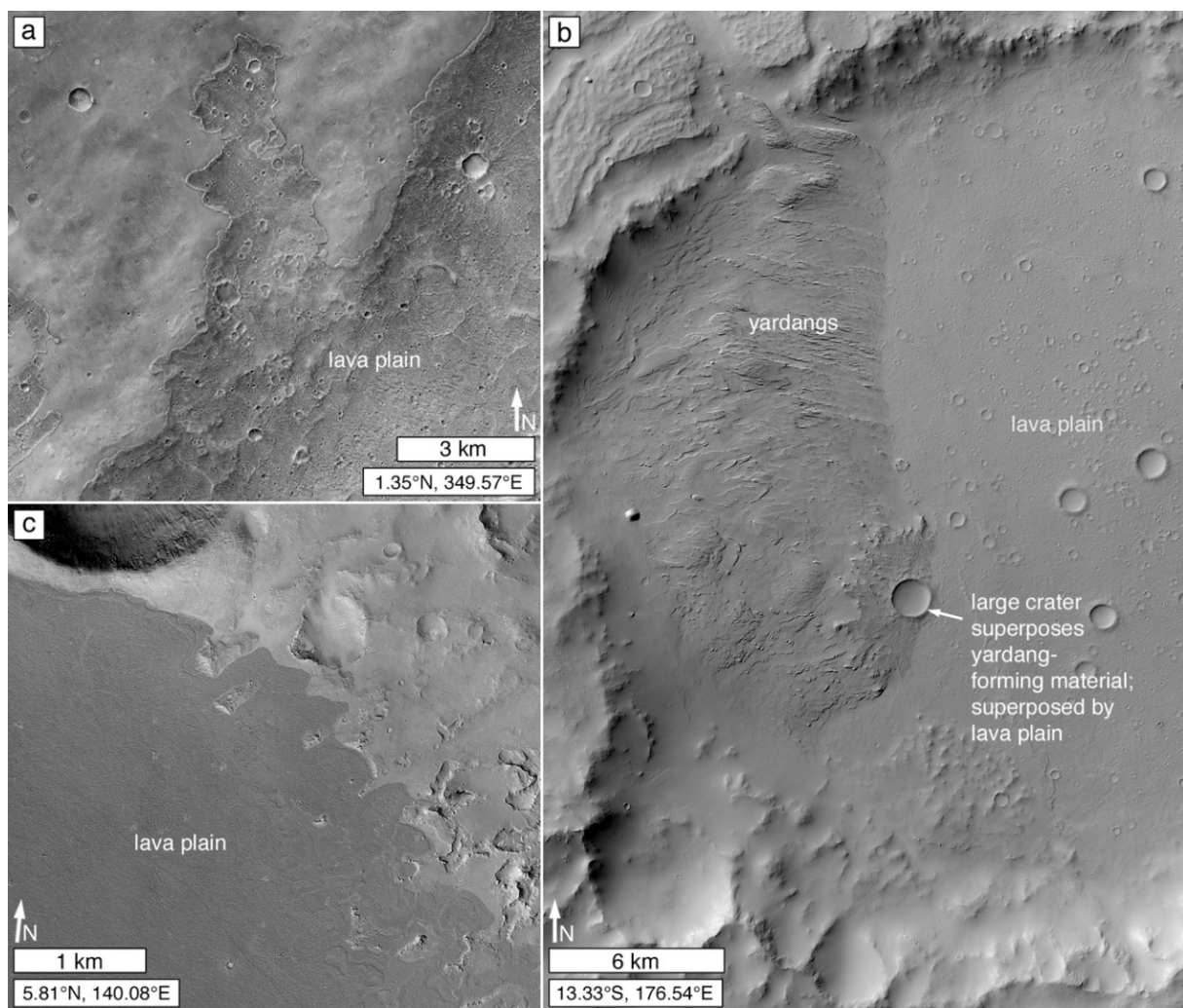


Figure 15. Retention of small impact craters on lava flow surfaces. (a) Dark-toned lava plain (right/bottom) retains more small craters than the older terrain (left/top) that it embays; CTX P15_006834_1793_XN_00S010W. (b) Lava plain (right) in Galdakao crater embays older yardang-forming rock (left). The yardang-forming material retains fewer impact structures than the lava surface, but the large crater that superposes the yardang-forming material is also embayed by the lava plain and indicates the greater age of the yardang-forming material; CTX P18_008172_1668_XI_13S183W. (c) Not all Martian lava plains are so heavily cratered as the examples in (a,b); younger lavas, such as this example in Elysium Planitia, have fewer craters because of their relative youth [224]; MOC-NA M07-00444 and S11-00617.

Until Curiosity's exploration in Gale crater was well underway, it had seemed that the majority of Martian sedimentary rock occurrences have very few superimposed impact craters [48,49,69,90,115,225]. This lack of craters was considered to be a signal of the erodibility of these rocks which, in turn, was seen to be an indicator that they consist of materials that are readily released by weathering and removed by erosion (e.g., clasts of sand size and smaller). In contrast, surfaces heavily peppered with sub-kilometer-diameter impact craters seemed to provide a good signal for distinguishing lava plains in cases for which no vents, edifices, flow fronts, pressure ridges, or other geomorphic evidence of volcanism are present [226]. However, there was a mystery. Among the very first sedimentary rocks identified on Mars—in MOC-NA images in 1999—were those of a lithified aeolian dune field in the Apollinaris Sulci region (Figure 1a) [51,52]. The lithified dune field is dotted by many small impact craters. One and two decades ago, the retention of small craters in a material that is best interpreted as sandstone seemed strange relative to the majority of known sedimentary rock occurrences [226].

The crater-retaining, lithified dune field (Figure 1a) was a signal that, perhaps, not all Martian sedimentary rock occurrences are so easily eroded. However, recognition that this observation is not unusual did not come until the early years of the Curiosity mission. During Curiosity's descent to the floor of Gale crater in 2012, its MARDI recorded an image of the impact of the MSL heat shield on a surface that retains many sub-kilometer-diameter impact structures (Figure 3b). For months thereafter, the science team considered it possible that this crater-retaining bedrock surface (literally called a "cratered surface unit" [75,76]) might be lava, with the largest crater on its surface (Figure 3a) a possible maar. Indeed, many other cratered surfaces, elsewhere in northern Gale crater, were also considered to be candidate lava surfaces [76]. Ultimately, Curiosity was driven close to the northern edge of the cratered surface unit that was impacted by the heat shield (Figure 3c) and its Mastcam and ChemCam RMI images (e.g., Figure 3d,e) showed that the rock is sandstone [77,78].

Thus, a picture began to emerge, that some Martian sedimentary rocks are sufficiently resistant to erosion that they retain (at least, qualitatively) sub-kilometer-diameter impact craters as well as or nearly as well as do Martian lava flows and plains [227]. Continued investigation via Curiosity has shown that while well-cemented [228] sandstones and conglomerates retain small impact craters [229], so, too, can some mudstones. This is particularly evident on Vera Rubin ridge (Figure 16). Diagenesis caused—in a manner that cuts across stratigraphic boundaries [190]—this particular part of the Murray formation to be more erosion-resistant than other parts [190,218]. While most of the Murray formation consists of recessive mudstones [81], Vera Rubin ridge is a topographic high and retains more craters per unit surface area than typical Murray formation exposures [230].

The number of small (sub-kilometer diameter) impact craters and remnant impact structures retained by a given surface (of a given surface area) on Mars is the integrated product of:

1. The total period (which can include multiple episodes of burial and exhumation) during which the surface was exposed to the atmosphere through which impactors penetrate to reach it;
2. The impact cratering rate and variability of that rate—owing to changes in atmospheric density, impactor supply, and astrodynamical availability of impactors—during the period(s) of exposure;
3. The formation of secondary impact craters and proximity to the primary impact site; and
4. The rate and variability of the rate at which impact structures are removed by erosion, including destruction by subsequent impact events.

The removal of small impact structures is, at least in part, a function of rock physical properties—erosion-resistant rocks can retain many small craters [137]. The Curiosity rover mission has shown that such erosion-resistant rocks can include mudstones (Figure 16), conglomerates, and, especially, well-cemented sandstones (Figure 3).

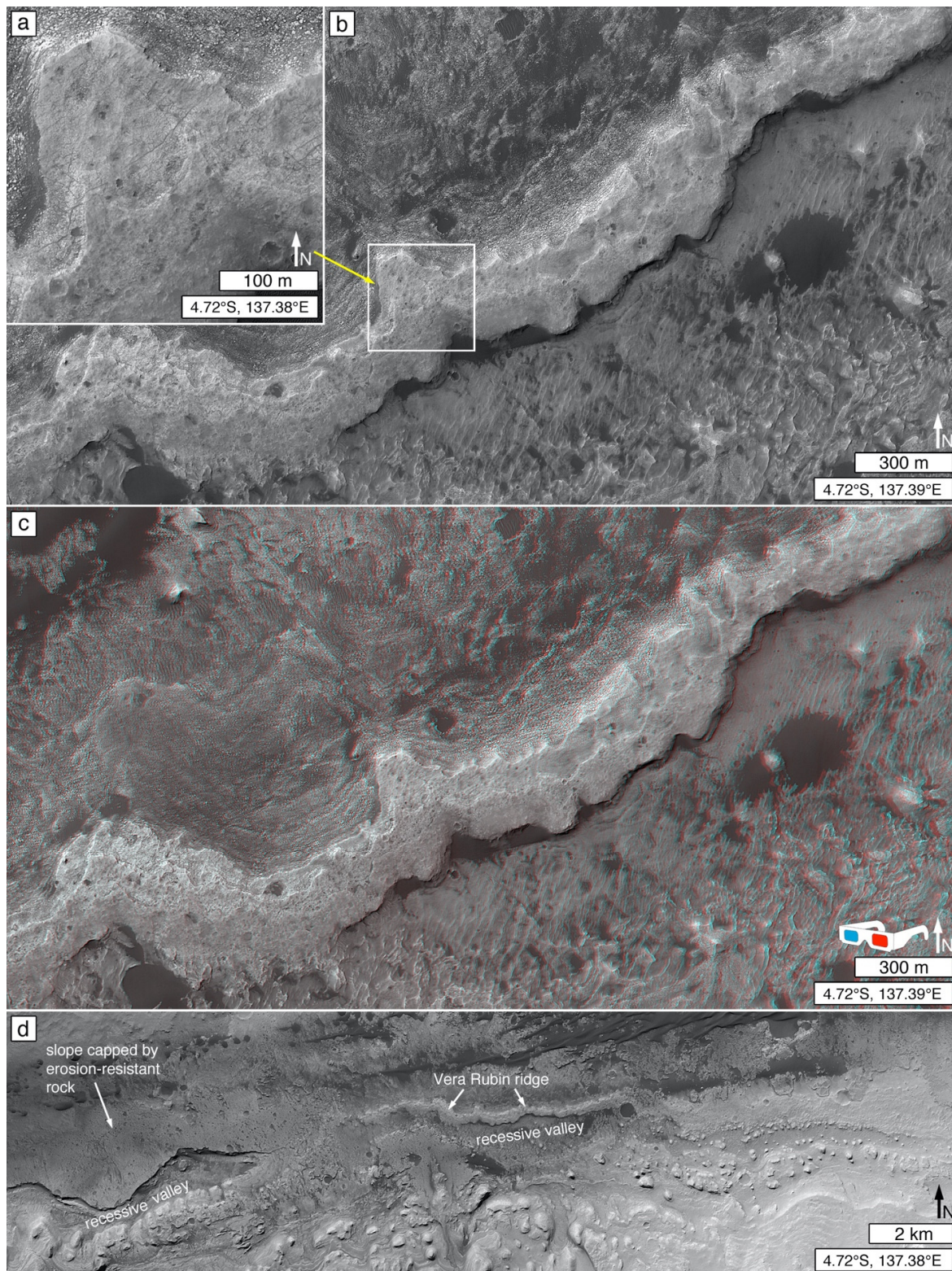


Figure 16. Erosion-resistant mudstone of the Vera Rubin ridge [219] in Gale crater. (a) The ridge retains more impact structures than is typical for other mudstone outcrops explored in Gale crater [230]; HiRISE PSP_009294_1750. (b) Context for ((a)); box on the ridge top; HiRISE PSP_009294_1750. (c) Stereopair anaglyph view of Vera Rubin ridge, emphasizing its erosion resistance; HiRISE PSP_009149_1750, PSP_009294_1750. (d) Context view of Vera Rubin ridge relative to the recessive valley to its immediate south and the recessive valley and erosion-resistant slope to the west; CTX P21_009294_1752_XI_04S222W.

3.4.2. Boulder Production and Retention

Retention of boulders, cobbles, and megaclasts [231] produced from rock breakdown is analogous to impact crater retention; rocks more resistant to erosion produce megaclasts, boulders, and cobbles that are retained longer because they are more resistant to post-production disaggregation and removal of the resultant fines (and vice versa). Boulders, cobbles, and megaclasts can be produced from sedimentary rock by impact events (Figure 5a), fracturing followed by dislodgement and displacement (e.g., mass movement; rock fall) at retreating escarpments (Figure 5b,c) and crater walls, or from fracturing followed by slower dislodgement and displacement processes (Figure 5d).

In MOC-NA images acquired through the middle months of the year 2000, boulders associated with sedimentary rock occurrences were not seen [49]. This observation was considered to be an indicator that the rocks are composed of fine-grained clasts such as clay, silt, and sand [49]. However, this notion changed dramatically once the MOC-NA was operated in cPROTO (compensated Pitch and Roll Targeted Observation) mode for higher spatial resolution views [50]. MOC-NA cPROTO images showed boulders shed from sedimentary rock escarpments in, for example, northern Sinus Meridiani and western Candor Chasma [168,232]. Subsequent imaging by MRO HiRISE and rover cameras has, of course, also shown boulders produced from Martian sedimentary rock (Figure 5). Still, of course, a lack of retained boulders is, in some cases, interpretable as a signal that a rock poorly resists erosion, and that any boulders produced are soon reduced to particle sizes small enough to be removed by wind [49,233].

3.4.3. Friability

Contrary to common usage of the term in Mars geoscience [72,225,234–237], the friability of a rock cannot be detected using satellite or aerial images. The geological term, *friable*, refers to rock that crumbles or sheds small fragments (such as sand grains) as a result of rubbing by human touch. No geomorphic observations can be said to indicate friability, although, in the Mars context, poor impact crater retention and kharafish landforms such as yardangs have been invoked as evidence of friability. Where no human hand (or robotic touch of similar pressure) has rubbed the rock, friability cannot be determined. Further, friability is not an indicator of rock hardness or resistance to erosion. For example, Young [238] described friable, yet steep-sloped (in some places, vertical), sandstone outcrops in the Bungle Bungle range of the Kimberley of Australia. In this case, a lack of intergranular cement makes the rock friable, but compaction and interlocking grains make the rock resist erosion [238].

3.4.4. Escarpments and Scarp Retreat

Slopes cut through sedimentary rock strata on Mars can take a variety of forms that reflect (1) local- to deposit-scale (or basin-scale) physical properties related to depositional and diagenetic texture and structure; (2) the landscape-shaping processes that have acted upon the outcrop, including (but not limited to) impact crater formation, faulting, mass movement, fluvial erosion, and aeolian erosion; and (3) the nature of subsequent slope-modifying processes and their relation to the time elapsed since the slope was initially formed. Differential erosion of stratified rock units of differing physical properties can be expressed in landscapes in the form of escarpments and scarp retreat (Figure 5b), leading to formation of the canonical progression of landforms from plateau to mesa to butte to pinnacle and hill [108,112,239]. Lateral erosion in rocks of differing properties may lead to undermining, collapse, disaggregation, and dispersal of erosion-resistant lithologies that overlie those of poorer resistance. Where rock is fractured and groundwater is present, it can lead to dissolution and weathering of the rock even before it is exposed at the planetary surface [108,240]. Where the rock is fractured, water, or ice tables are lowered or not present at all, and the environment is subject to aeolian processes, deflation and abrasion by saltating grains can contribute to scarp retreat and shallow basin formation [241,242].

As noted previously, rover observations made in Gale crater suggest that lateral scarp retreat rates via aeolian processes dominate over vertical erosion rates [216]. Plateaus, mesas, and buttes are generally topped by a capping rock unit that is more resistant to erosion than the rock beneath it. Observations from Gale crater demonstrate that such erosion-resistant rocks can be sedimentary (e.g., the sandstones capping the Emerson plateau and Murray buttes [136,188]). Such capping rocks can be intraformational, such as the sandstones and conglomerates of the Chinle Formation on Earth, noted above [217], or they can consist of a drastically differing lithology (e.g., lava overlying sedimentary rock). In any case, they can be either conformable or unconformable with subjacent strata; an example of the latter is the Salsberry Peak sandstone (Figure 2), which is part of the Pahrump Hills member of the Murray formation in Gale crater [74,80], and examples of the latter include the Stimson formation rocks that overlie the Murray formation also in Gale crater (Figure 17) [136,145,188].

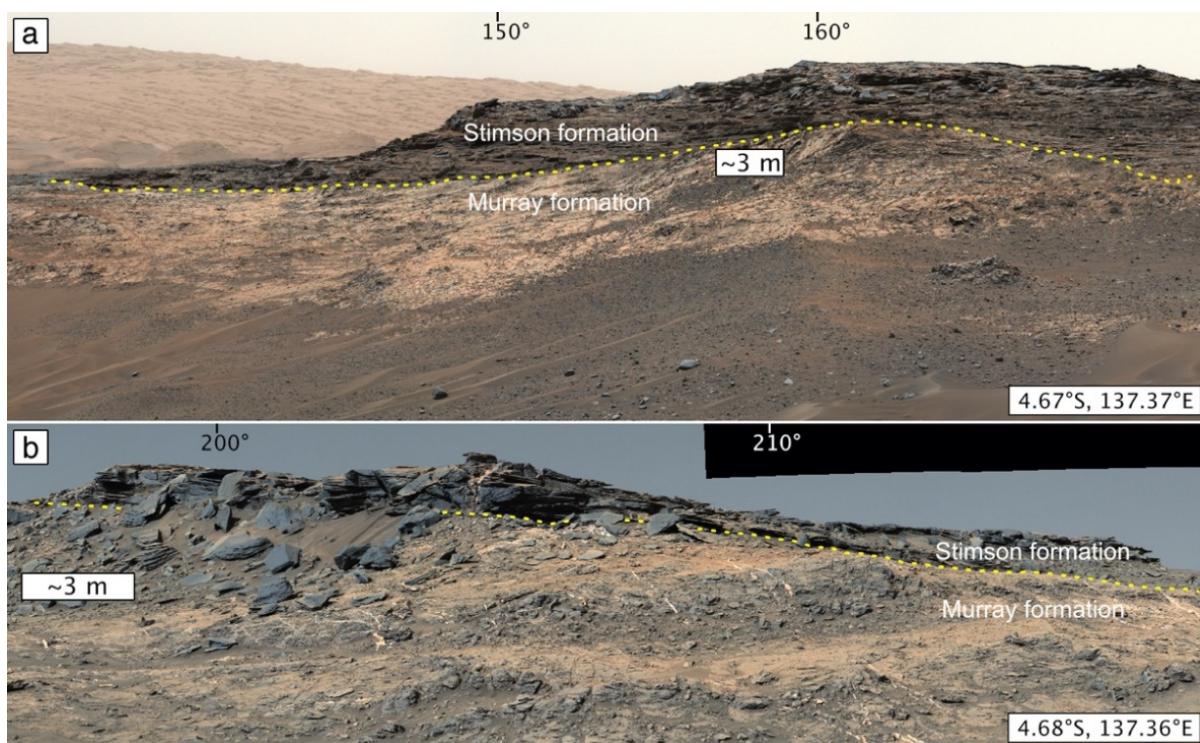


Figure 17. Example Stimson formation outcrops. The erosion-resistant Stimson formation sandstones form buttes, mesas, and plateaus that overlie Murray formation mudstones along an erosional unconformity that mimics the paleo-slope on which the Stimson sands were deposited [136,188,243]. (a) The Stimson/Murray contact on the east side of Emerson plateau; MSL Sol 981 Mastcam-24 mosaic (sequence 004333); azimuths 150° and 160° indicated. (b) The Stimson/Murray contact on the east side of Naukluft plateau; MSL Sol 1272 Mastcam-100 mosaic (sequence 005949); azimuths 200° and 210° are indicated.

3.4.5. Dispersal of Liberated Clasts or Rock Fragments in the Landscape

As clastic rocks break down, produced lithic fragments and liberated clasts are released into the landscape. In the case of sand-, silt-, and clay-sized particles, they are likely to be subject to mobilization and transport by wind. Distinguishing such materials and linking them directly to their source outcrop in satellite and aerial images is generally quite difficult. It would be ideal to be able to say that a given rock is a sandstone because a satellite image reveals it to be the source of liberated sand that has moved downwind from the outcrop. While this is usually not possible, Chojnacki et al. [244] demonstrated that a combination of satellite image and multispectral remote sensing analysis provided a reasonable indicator that some of the sulfate mineral-bearing sedimentary rocks in the Valles Marineris have

been shedding sand-sized material (whether produced fragments or liberated clasts cannot be known from the data) that is contributed locally to aeolian sand dunes.

Larger liberated or produced clasts—boulders, cobbles, and pebbles—are generally likely to remain near their source until they breakdown to finer particles and are removed by wind (exceptions can include ballistic transport by impact events and transport by fluvial action earlier in Martian history). The boulder-sized rock fragments referred to in Section 3.4.2 and Figure 5 provide an example, as do the pebbles liberated from and lying on the ground next to conglomerate outcrops in Gale crater (Figure 18a) [245], and pebbles produced from the breakdown of Jura member (of the Murray formation) mudstones, also in Gale crater (Figure 18b,c) [246].

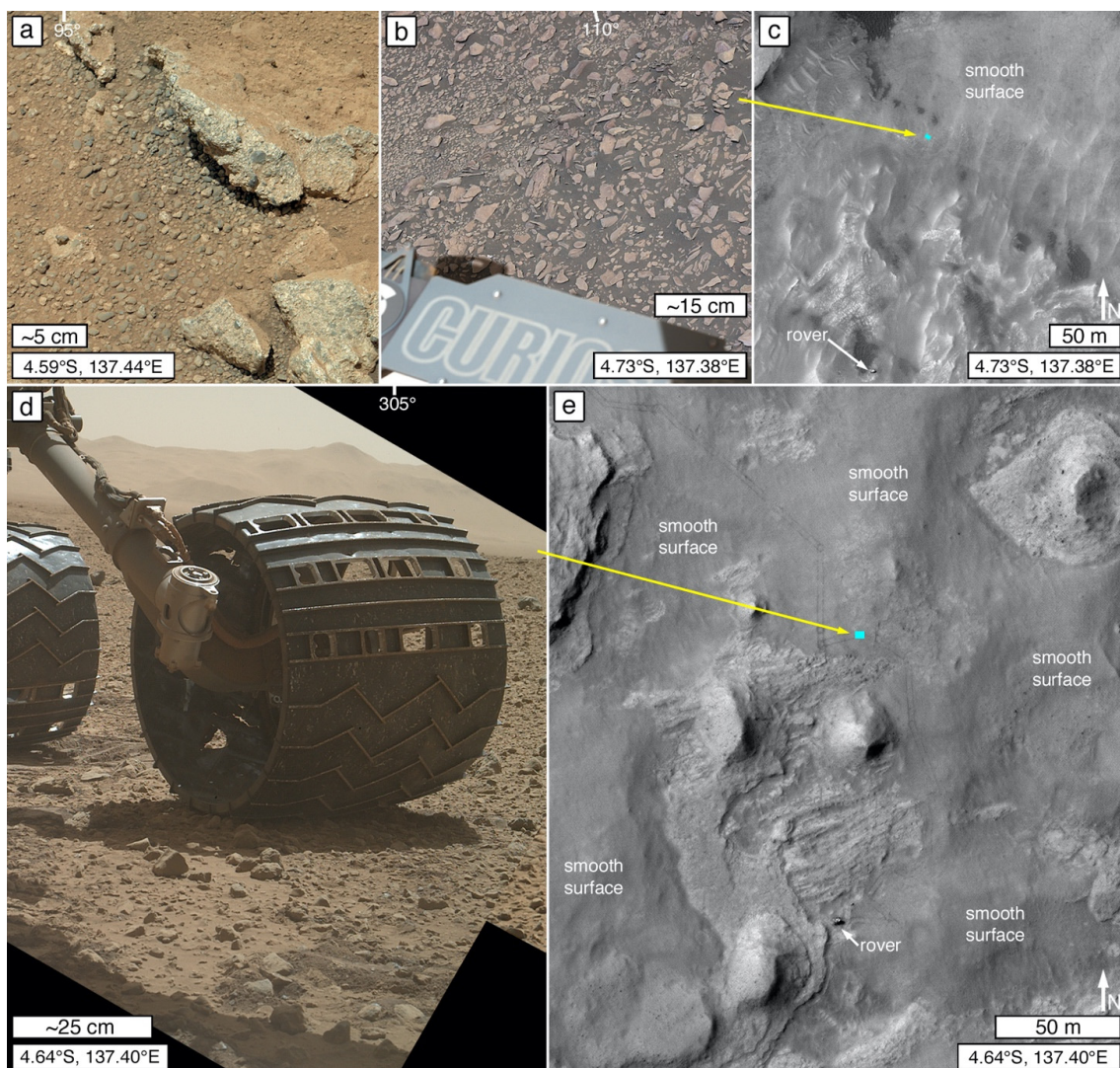


Figure 18. Pebbles liberated or produced from bedrock can form a pebbly regolith that translates to an apparent “smooth” surface at orbiter image scales (e.g., 25 cm/pixel HiRISE). (a) Example of pebbles liberated from conglomerate bedrock near Bradbury Landing, Gale crater; MSL Sol 27 Mastcam-100 mosaic of 0027MR0001290000100750E01 and 0027MR000-1290050100755E01. (b) Angular pebbles locally produced from breakdown of Jura member mudstone [190] in Glen Torridon, Gale Crater; MSL Sol 2432 Mastcam-34 mosaic (sequence 012875). (c) Orbiter view of the area in (b) shows that the pebbly regolith is expressed as a smooth surface in 25 cm/pixel images; blue rectangle indicates rover position at the time the view in (b) was acquired; HiRISE ESP_060840_1750. (d) Pebbly regolith produced by liberation of pebbles from a conglomerate bedrock (Point Coulomb member [247]) at the Kimberley site, Gale crater; mosaic of MAHLI wheel inspection images 0587MH0002640000203006E01 and 0587MH0002620000203007E01. (e) Orbiter view of the Kimberley site shows that the pebbly regolith is expressed as a smooth, surface; blue rectangle indicates rover position at the time the view in (d) was acquired; HiRISE ESP_036128_1755.

3.4.6. Burial or Lag Protection

Liberation or production of pebbles from rock breakdown can accumulate and form a pebbly regolith or an aeolian lag [248] that further enhances resistance to vertical erosion of underlying rock. A pebbly regolith or lag can appear to be smooth and featureless at image pixel scales that exceed the size of the pebbles. This is true whether the source of the pebbles is liberation from a conglomerate or breccia (Figure 18a) or breakdown of a finer-grained rock, such as mudstone (Figure 18b). An example of this occurs at the Kimberley field site visited by the Curiosity rover, where the Point Coulomb member of the Kimberley formation [247], a conglomerate bedrock, is overlain by a regolith lag of liberated pebbles (Figure 18d) that give the terrain a smooth appearance in HiRISE 0.25 m/pixel images (Figure 18e). At meter to decameter scales, of course, the rock is not smooth but hummocky, reflecting prior erosion of the conglomerate. In addition to lags, aeolian sand accumulations (i.e., dunes and dune fields) can also bury and protect underlying rock from vertical erosion, at least as long as the sand remains in place.

3.5. Depositional Setting Mimicry

Some sedimentary rock exposures are readily identified on Mars because their geomorphic expression in the modern landscape mimics their original depositional setting or deposit morphology (e.g., Figure 1a–c). Such landforms exhibit properties that indicate they are rock (Section 3.1). This mimicry is a product of the combined attributes of deposit-scale depositional structures, sedimentary facies, and the impact of diagenesis as a function of differing compaction, paleo-porosity, and paleo-permeability.

3.5.1. Bedforms

Lithified bedforms expressed in the modern Martian landscape include those that resemble whole, intact aeolian dunes and dune fields in Melas Chasma (Figure 19a) [50,139,249] and near the yardangs of the Apollinaris Sulci (Figure 1a) [51,140,185]. Preservation of intact dunes and dune fields requires a process or processes that allow the material to become rock, while not disrupting the original dune morphology. On Earth, such preservation sometimes occurs through inundation by lava [171,250]. As no lavas are apparent at the Melas Chasma and Apollinaris Sulci locations, the possibilities for preservation of these dune forms include rapid burial by aeolian dust or tephra to a depth at which the wind could no longer access and mobilize the sand, or through stabilization of the dunes (e.g., wetting, freezing, cementation), followed by—or not—slower, gentle air-fall deposition of dust or fine tephra over some period of time.

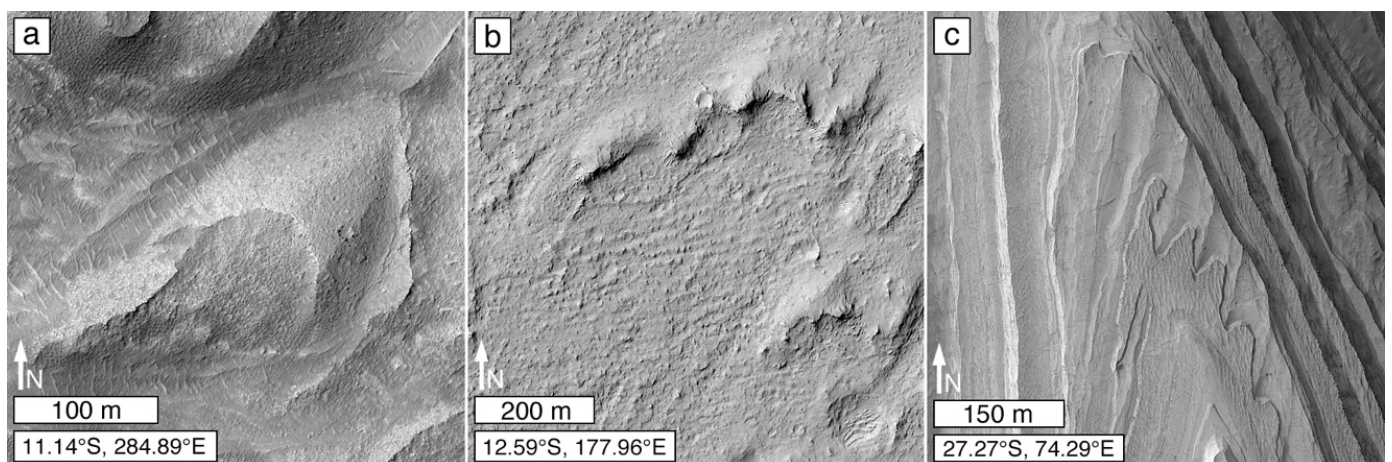


Figure 19. Cont.

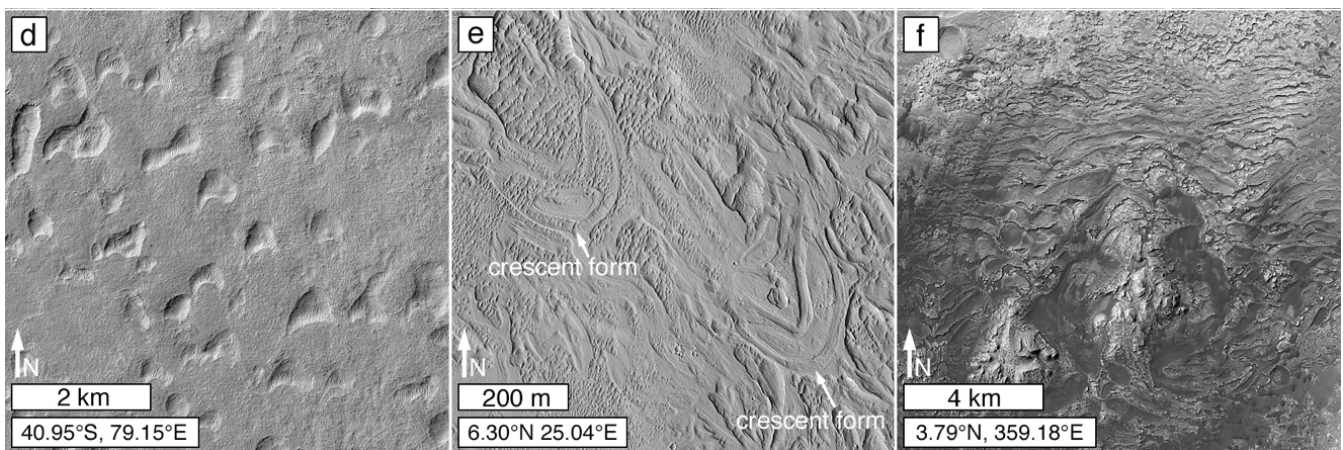


Figure 19. Depositional mimicry—lithified bedforms. (a) Cratered, lithified aeolian dune in south Melas Chasma [139]; HiRISE PSP_007522_1685. (b) Cratered, lithified, discontinuous subparallel ridges in lithified dune field near Apollinaris Sulci; in context, the ridges are interpreted as candidate, fossil transverse aeolian ridges (TARs); HiRISE PSP_007460_1675. (c) Large (90 m wavelength) bedforms preserved in stratified rock in Terby crater [50]; HiRISE PSP_001596_1525. (d) Barchan-dune-shaped pits (sunlight illuminates the scene from upper left) in eastern Hellas Planitia; “ghost dunes” of Day and Catling [251]; CTX P19_008558_1398_XI_40S281W. (e) Example crescent forms, interpreted as lithified remains of two barchan dunes, in Barth crater [27]. (f) Dune-like forms (with regards to morphology, scale, and intracrater setting) in rock, partially exhumed from beneath a dark-toned mantling unit, in a crater in southwestern Arabia Terra; CTX D21_035566_1822_XN_02N000W.

Features interpreted by some investigators to be smaller, lithified aeolian bedforms, such as “transverse aeolian ridges” [252,253], have also been identified (Figure 19b) [191]. Additionally, a rock stratum (or stratal package)—emergent from beneath subsequent strata—in Terby crater exhibits large “ripples” of wavelengths of ~90 m, crest-to-crest (Figure 19c). Whether these bedforms were deposited subaerially or subaqueously is unresolved [50].

The subject of Martian bedform preservation observable at satellite and aerial photograph scales intersects with preservation of the opposite—spaces left behind by the removal of a bedform. Day and Catling [251] described barchan dune-shaped depressions in Hellas Planitia (Figure 19d) and Noctis Labyrinthus that they termed “ghost dunes” and interpreted as dune casts (alternatively, they can be called molds because they have negative relief). Formation of such ghost dune hollows required deposition of interdune material that surrounded each dune, followed by erosion that removed mobile sand. Based on an Earth analog in Idaho [254], some amount of aeolian sand is thought to have remained in the Martian ghost dune hollows and could provide a sandstone or meta-sandstone record for future exploration [251]. Day et al. [27] described a different situation, in which similar-oriented, lithified, transverse and crescentic forms in and near Barth crater are the preserved remnants of former aeolian dunes (Figure 19e). Additional dune-like lithic forms are seen in Figure 19b.

Transverse ridge patterns preserved in Martian rock can be signs of former bedforms (Figure 19b)—or they can be faux signals of depositional setting mimicry. There are two varieties of concern. One is a ridge pattern called “periodic bedrock ridges” [255], and the other is a pattern of regularly spaced, low ridges and shallow troughs called “washboard” [201]. Periodic bedrock ridges exhibit patterns similar to aeolian bedforms but are created by the combination of (1) substrate protection from aeolian erosion beneath megaripples or transverse aeolian ridges; (2) aeolian erosion of the substrate between the bedforms; and (3) the eventual removal of the bedforms to reveal ridges of substrate material (e.g., rock) that had been protected beneath them [255,256].

The other transverse ridge and trough pattern, sometimes referred to as a “washboard” texture [191,201,257], is a geomorphic expression observed on rock surfaces as a series of regularly spaced troughs and ridges of decameter-scale wavelength and meter- to

decameter-scale amplitude (Figure 20). They are common in Gale crater [191,201] but also occur in other low latitude regions of Mars [257]. Some of the rocks in Gale crater that exhibit a washboard pattern have been explored using the Curiosity rover and are found to be aeolian sandstones [188]. However, no linkage between aeolian sedimentary structure (Figure 20d) and the washboard pattern was found [188]. A concern regarding washboard patterns in Gale crater is whether they are an erosional expression of aeolian sedimentary structures or of differential erosion of fractured (jointed) rock. To date, this concern is unaddressed and it is possible that some washboard patterns do reflect aeolian depositional architectures, while others reflect deformational and diagenetic events that occurred during or after lithification.

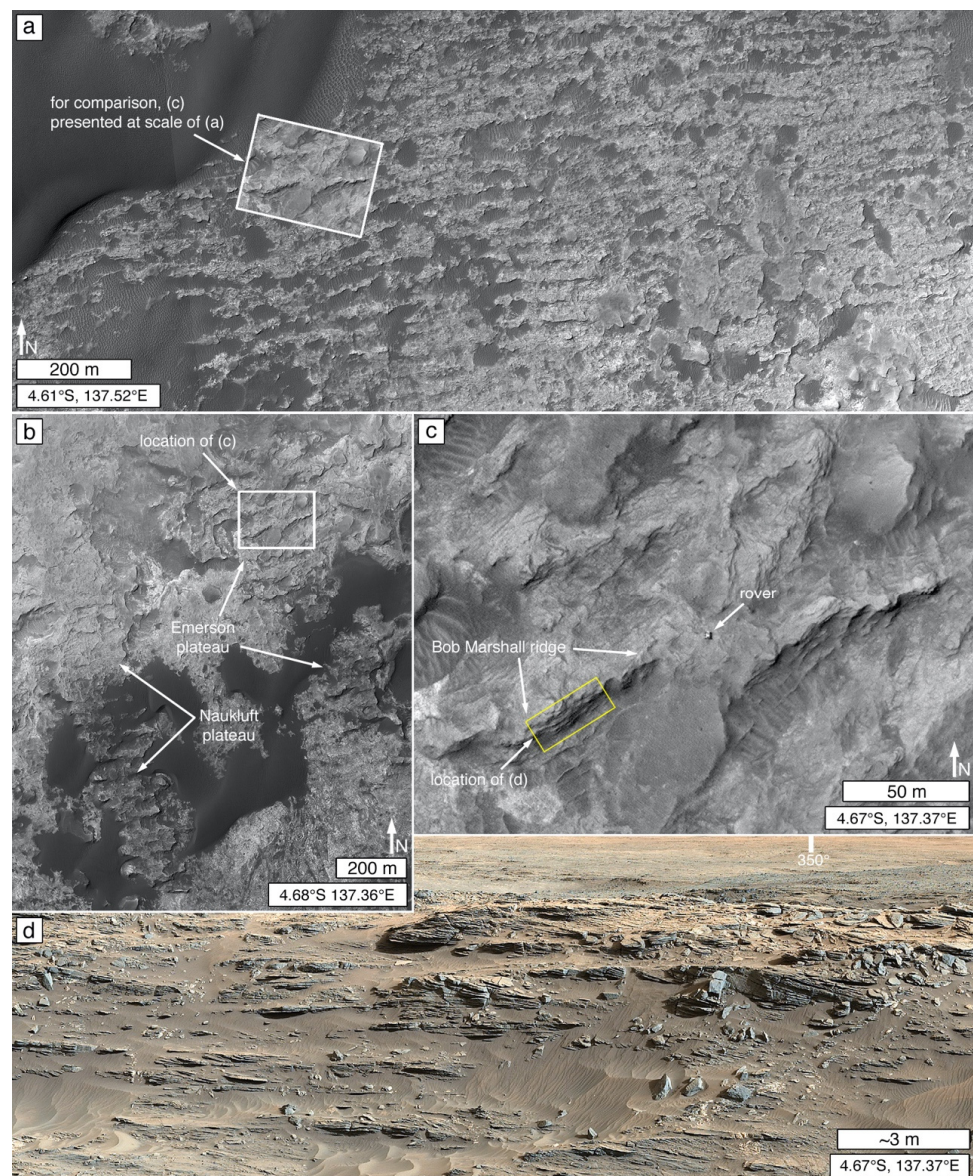


Figure 20. “Washboard” [201] rock outcrop surface relief patterns. (a) Typical washboard expression on the lower north-northeast slope of Aeolis Mons, Gale crater; HiRISE PSP_009505_1755. (b) Washboard-patterned surfaces of the Stimson formation exposed on Naukluft and Emerson plateaus, which Curiosity drove across in 2015–2016; HiRISE ESP_042-682_1755. (c) View of example washboard ridges and troughs explored via Curiosity on Emerson Plateau; HiRISE ESP_042682_1755, acquired 4 September 2015. (d) View of aeolian sandstone strata exposed on Bob Marshall ridge, Emerson Plateau, Gale crater; MSL Sol 1100, Mastcam-34 mosaic (sequence 004872); azimuth 350° indicated.

3.5.2. Deltas and Alluvial Fans

Perhaps the most broadly recognized examples of depositional setting mimicry are the deltaic landforms in Eberswalde and Jezero craters (Figure 1b,c) [53,258]. Many other similar, sediment distributive landforms are evident on Mars in the form of both deltas and fans [13,19,259–262]. In some cases, the colleagues who investigated these did not address whether the materials are lithified, but some percentage of them most certainly are. For example, Figure 8d,e shows sedimentary fans that are emergent from beneath younger rock; an observation that implies that these examples are lithified. Figure 21 shows additional examples, including a boulder-producing fan crosscut by a graben.

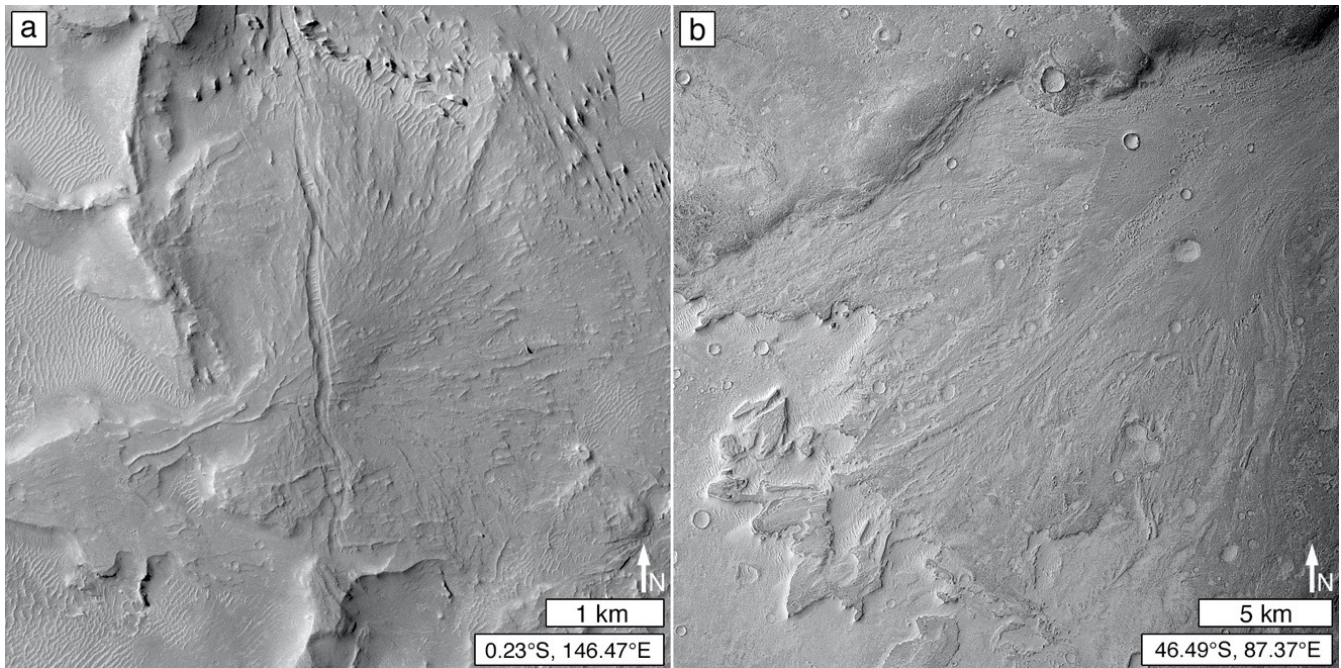


Figure 21. Depositional setting mimicry—sediment fans. (a) Example in western Gunjur crater; crosscut by a graben, the escarpments attest to the competence of the deposit; CTX P21_009109_1797_XN_00S213W. (b) Example in south-eastern Hellas Planitia; the fan terminus is bounded by escarpments and distal remnants form mesas and buttes; CTX K20_061053_1332_XI_46S272W.

3.5.3. River and Stream Sediment

The initial recognition of the lithified delta in Eberswalde crater included the observation of ridges that resemble former stream courses [53,263]. Similar landforms had been identified on Mars at a few locations before that time [264,265], and these were reminiscent of networked, inverted fluvial forms previously identified on Earth [266,267]. Colloquially referred to as “inverted channels” or “sinuous ridges” [201,235,268–271], in more recent years, the term “fluvial ridge” has been devised [176,177], especially because not all cases are a product of landscape inversion [13]. However, none of these terms adequately describes the landform [177], as some ridges are not sinuous and the other terms imply knowledge of process (inversion of topography) or material (fluvial sediment).

Ridges (and networks of ridges) that record the locations of former stream courses are quite common on Mars [26,177,272,273]. Figure 22a–d shows examples. On Earth, analogous ridges usually do not consist of 100% fluvial sediment [177]. In some cases, the bulk of the material might be an erosion-resistant igneous rock (e.g., lava) that filled the channel or valley of a former stream course. In other cases, much of the ridge volume might be occupied by rock that originally occurred beneath the stream (e.g., “ghost channels” of Clarke et al. [274]). Thus, a ridge that marks a former stream course might or might not indicate the presence of sedimentary rock.

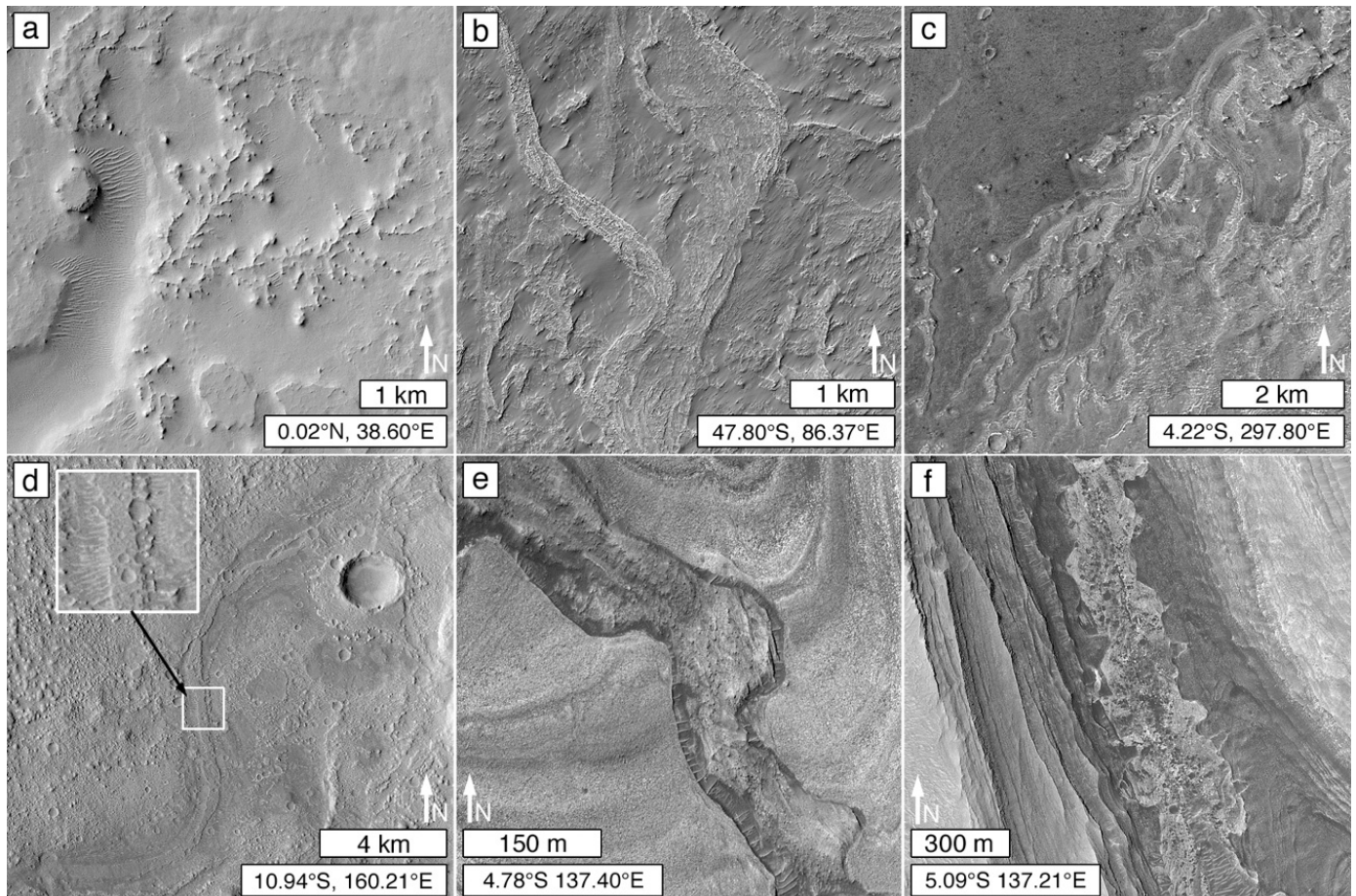


Figure 22. Depositional setting mimicry—fluvial forms. (a) Fine, contributory fluvial ridges at the southeastern head of Naktong Vallis in Arabia Terra; CTX F19_043068_1800_XI_00N321W. (b) Fluvial ridges in southeastern Hellas Planitia [177]; HiRISE ESP_032293_1320. (c) Fluvial ridge network on plateau immediately west of Juventae Chasma [50,268]; CTX N13_067415_1758_XN_04S063W. (d) Fluvial ridge in northern Terra Cimmeria, CTX G14_023798_1696_XN_10S199W. (e) Channel-fill sediment preserved in Gediz Vallis on northern Aeolis Mons in Gale crater [49]; HiRISE PSP_009149_1750. (f) Channel-fill sediment preserved in Sakara Vallis on western Aeolis Mons; HiRISE PSP_006855_1750.

Most Martian ridges that mark former stream courses are candidates for the presence of preserved fluvial sediment. Preservation of fluvial sediment in ridge form on Earth generally follows one of four pathways [177]:

1. The sediment and/or channel-adjacent alluvium become cemented in the surface/near-subsurface environment and becomes a ridge when adjacent, unconsolidated or poorly-cemented alluvium is eroded away;
2. The sediment is preserved beneath lava or tuff that filled the channel or valley;
3. The sediment becomes lithified by deep burial diagenesis (compaction, cementation) and then returns to the surface (tectonism, erosion) and is subjected to differential erosion and exposure; or The sediment is never lithified, and coarse fluvial sediment grains (boulders, cobbles, pebbles) are left behind as an aeolian lag to protect the material from further removal.

Cementation in the surface/near-subsurface environment, also known as early diagenesis or eogenesis [126], typically involves formation of a 'crete (silcrete, gypcrete, calcrete, etc.), at least on Earth [177].

While ridges—marking the locations of former stream courses—composed of lava are common on Earth [177], very few examples have been (thus far) been identified on Mars [275]. The proportion of the abundant fluvial ridges on Mars [26,177,273] that are the products of deep burial sediment diagenesis, surface/near-surface cementation, or aeolian lag development is not known. A few cases on Mars provide definitive examples of fluvial ridges that are emergent from beneath younger rock (Figure 8b,c). An initial remote sensing study of the thermophysical properties of 20 such ridges suggested that those examined are more likely composed of lithified material than unconsolidated sediment protected by a lag [276].

Mars orbiter imaging has also shown that not all stream channel depositional setting mimicry takes the form of a ridge. The inner channels of Gediz Vallis and Sakarya Vallis, two canyons that cut the stratified Aeolis Mons in Gale crater, contain sediment—interpreted to be lithified [20,49,201]—still located within the original channels (Figure 22e,f).

3.5.4. Lakes and Ponds

No specific attribute(s), such as water surface area or depth, distinguish lakes from ponds. Indeed, “it is difficult to specify an upper size limit to what is called a pond and when it should be called a shallow lake” [277] (p. 716). On Earth, ponds are more common than lakes [278] and are generally regarded as “small” water bodies [279,280] that lie along a continuum between megalakes [281] and bodies of surface area $\leq 100 \text{ m}^2$ [282,283]. Similar to ponds, pools are distinguished from ponds because they dry out at episodic (“regularly, yearly or every few years,” [277] (p. 716)) intervals [284].

Just as Mars has ridges that mimic stream courses and provide records of past fluvial sediment transport and depositional settings, so too, can some raised landforms (e.g., mesas, hills, mounds) reflect the former presence of a small lake, pond, or pool. The least ambiguous examples (Figure 23) occur as local topographic highs at a terminus of a ridge or ridges that record a former stream course. As with fluvial ridges, the proportion of the volume of these landforms that consists of aqueously deposited sediment is currently unknown, as is the pathway (surface/near-surface cementation, lava, deep burial diagenesis, and aeolian lag formation) by which any given example followed before attaining its present configuration in the Martian landscape. Analogs to these Martian examples do exist on Earth [285–289]. They do not always mimic the original lake or pond shape, but some examples do [290,291].

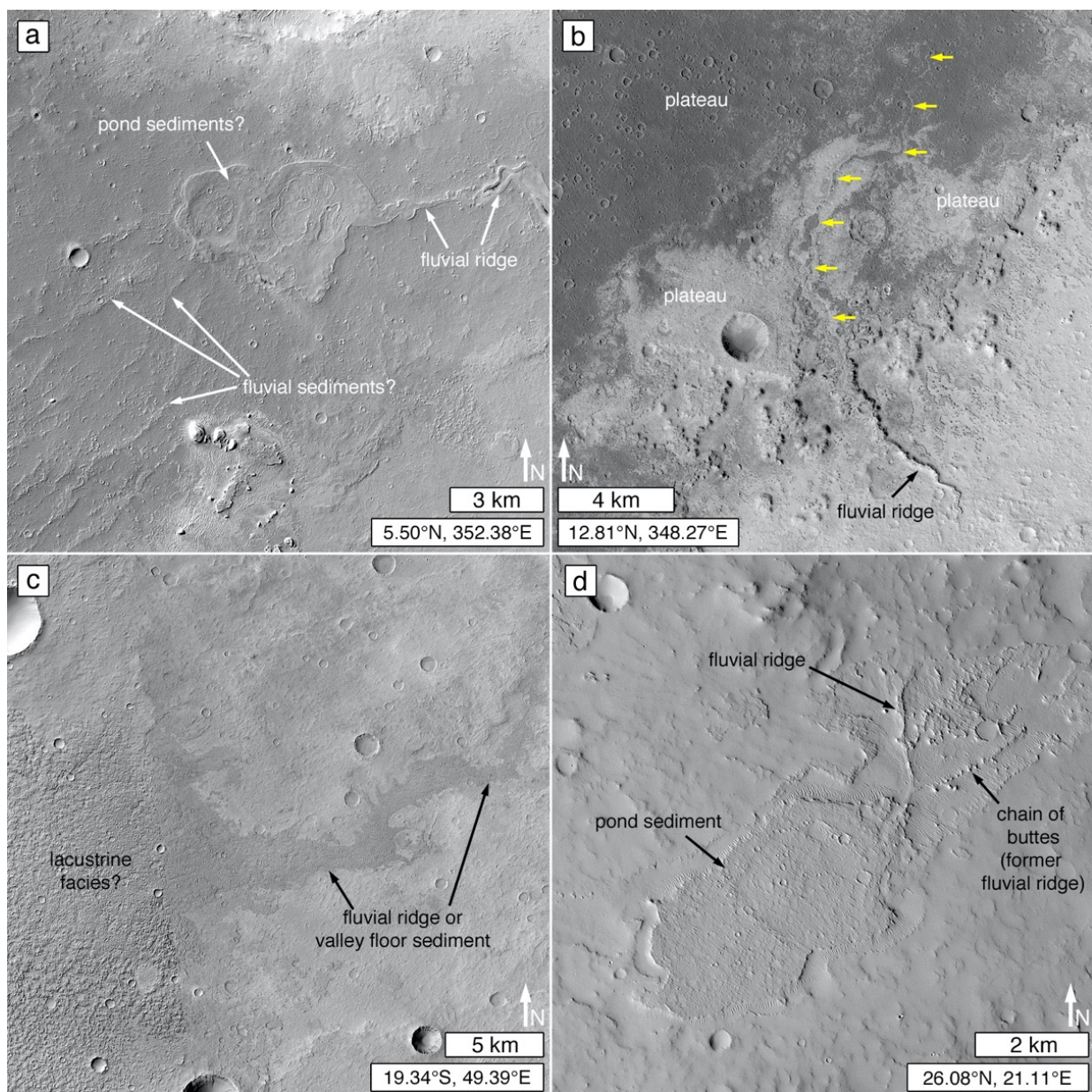


Figure 23. Depositional setting mimicry—candidate pond or lake sediments associated with fluvial ridges. (a) Convergence of fluvial ridge forms on a small area, ~6 km wide; candidate small lake or pond sediment facies [292]; western Arabia Terra; sunlight from the upper left; CTX J19_052300_1855_XN_05N007W. (b) Convergence of a fluvial ridge and its northward trace (yellow arrows) with plateau-forming rock; southwestern Arabia Terra; CTX N12_067004_1928_XN_12N011W. (c) Intersection of narrow, dark-toned plateau (former valley floor/fluvial sediment?) with eroded basin floor material to the west (left) in eastern Terra Sabaea; mosaic of CTX K23_062228_1603_XI_19S311W and K06_055555_1593_XN_20S310W; caution, note sharper contrast west (left) of the mosaic seam. (d) Convergence of ridges (former streams) with a small, crater-retentive plateau in north central Arabia Terra; CTX F05_037820_2056_X-I_25N338W.

3.5.5. Impact Crater Ejecta

Impact ejecta deposits consist of (1) material violently released from a given crater and (2) materials eroded from the substrate beneath the ejecta during emplacement [221,293]. Rock formed from impact melt can be locally present in an ejecta deposit [294], and some of the ejected rock fragments are shock-metamorphosed [295]. The bulk of an ejecta deposit, however, is essentially a clastic sediment (breccia) that can, like any other sediment, undergo diagenesis and lithification [169,170,296,297].

Some proximal impact crater ejecta deposits on Mars have been buried (or partly buried) and then partly exhumed from beneath sedimentary rock (e.g., Figure 8a). Their present-day geomorphic form mimics the original ejecta deposit but, because the material has been excavated from beneath subsequently emplaced rock, the ejecta deposit must be inferred to have been lithified.

3.5.6. Mass Movement Deposits

Like any other sediment, landslide deposits [298] can be subjected to burial and diagenesis or surface/near-surface diagenesis without burial. For example, in carbonate-clast-rich cases on Earth, near-surface diagenesis can (in some cases) cement and lithify the brecciated debris [299]. Lithified landslide deposits can mimic their original depositional form if they are exhumed, partly exhumed, or—like the aforementioned carbonate examples [299]—became lithified without burial. We have not yet definitively identified an example of a lithified landslide deposit on Mars, but Figure 24 shows a good candidate that is emergent from beneath subsequently-deposited, erosion-resistant (small impact crater-retaining), sedimentary fans that might also be lithified.

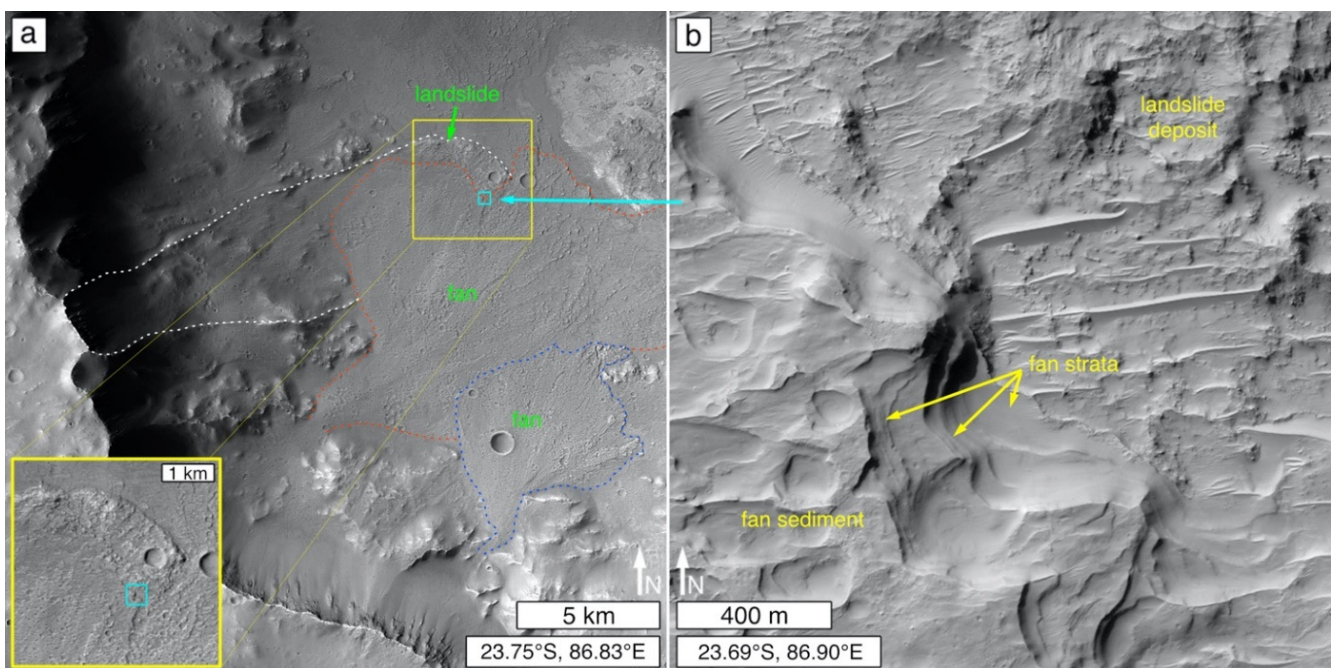


Figure 24. Depositional setting mimicry—candidate lithified landslide deposit. (a) Context showing landslide deposit emergent from beneath sedimentary fans; inset (lower left) shows some details of the contact between the landslide and fan materials; CTX mosaic of F05_037831_1559_XN_24S273W and J03_045928_1562_XI_23S273W. (b) Contact between fan (left/bottom) and landslide (right/top) sediments; fan sediments are stratified, retain eroded impact structures, and hold cliffs; the landslide materials are emergent from beneath the fan sediments; HiRISE ESP_062108_1560.

3.6. Distinction of Igneous from Sedimentary Rock

Distinction of igneous from sedimentary rock is one of the most challenging and vital concerns with regard to deciphering the geological history of Mars. Doing so is not always easy, whether using hand-lens-scale images from a rover (e.g., Figure 4), or using satellite and aerial images from Mars. Of course, some cases are not difficult at all; for example, there is little question that Olympus Mons is a volcanic edifice [300], and that repeated strata of repeated thickness and physical properties argue for environmental influences on deposition (i.e., sedimentation) [16,49]. However, with: (1) the recognition of erosion-resistant, dark-toned, mafic sedimentary rocks at the Curiosity field site [70,71,77,188]; (2) pre-Curiosity-landing speculation that some of the upper stratal packages of Aeolis Mons (the 5-km-high mountain in Gale crater) consist of Medusae Fossae Formation mate-

rial [301,302], considered by some colleagues to be tuffs [303–305]; and (3) pre-Perseverance-landing uncertainty, as to whether the bedrock at or near the surface of the floor of Jezero crater would be igneous or sedimentary [31,306]. The concern about distinguishing igneous from sedimentary rocks has become more acute and has real-world consequences, such as landing site selection.

The main concerns for discrimination between igneous and sedimentary rocks center on the diagnostic value (or not) of columnar jointing, wrinkle ridges, boulder production and retention, lobate rock unit margins, the nature and patterning of stratified outcrops, the challenge to distinguish tuffs, and, most importantly, rock outcrop context. In addition to these, first, we briefly depart from the imaging theme to discuss remote spectroscopic detection of rock composition. In particular, while some sedimentary rock occurrences might be dominated by infrared spectral signatures indicative of sulfates, clay minerals, hematite, chlorides, or carbonates, e.g., [29,307–310], others have compositions similar or equivalent to igneous or impact melt rocks and, therefore, can potentially be misinterpreted.

3.6.1. Remote Sensing of Composition

By itself, information regarding rock composition determined using satellite or aerial remote sensing instruments does not permit distinction between igneous (or impact melt) and sedimentary rock on Mars. Most important to this point is the detection by near- or thermal-infrared remote sensing of igneous rock-forming minerals (e.g., olivine, pyroxene, plagioclase), or a spectrum interpretable as an igneous rock type (e.g., basalt, andesite). Observations made using the instruments onboard Curiosity in Gale crater have, for example, shown that Martian sandstones can be basaltic [71,73,77], and even mudstones can contain considerable, detrital feldspar and pyroxene [141,214]—and, in some cases, olivine [311]. The investigations using orbiter observations of intercrater “bedrock plains” described by Rogers et al. [72] and Cowart et al. [312], and the studies of intracrater dark-toned pyroxene- and olivine-bearing rock and light-toned, feldspar-bearing rock by Irwin et al. [23], underscore the points that sedimentary rocks with igneous rock-like compositions are present on Mars, may be identifiable via satellite or aerial remote sensing, and might even be common.

Ultimately, compositional information (e.g., interpreted from infrared spectra) is informative of composition but it does not, alone, inform us of the genesis of a given rock unit. Indeed, Rogers et al. [72], Cowart et al. [312], and Irwin et al. [23] relied on geomorphic observables to make their interpretations. Such observables included poor retention of small impact craters (indicative of poor erosion resistance), kharafish (aeolian erosion forms, carved into the rock, at a variety of scales), paucity of regolith (indicative of aeolian removal of sand-size and finer rock breakdown debris), a presence of aeolian lags (e.g., small bedforms) and, in some cases, association with fluvially-incised valleys or the inverted forms of former fluvial systems [23,72,312]. A lack of volcanic features such as flows, vents, and edifices was also an important factor in their interpretations [23,72,312].

3.6.2. Columnar Jointing

One possible discriminator between igneous and sedimentary rock observable in satellite and aerial images of Mars is columnar jointing. Columnar jointed rocks definitively occur on Mars [144]. In fact, columnar jointing provides excellent—but not entirely conclusive—evidence for magmatism. On Earth, they are most common in lavas e.g., [179,313] and shallow igneous intrusive bodies like the Devil’s Tower volcanic plug in Wyoming, USA [314]. They also occur in some impact melt sheets [315] and welded [316] and non-welded [317] tuffs. Although unusual, examples of columnar joints also occur in metasedimentary rocks such as thermally altered chalk [318], paleosols baked beneath lava flows [318], and, especially, contact-metamorphosed sandstones [319–323]. Thus, although an excellent signal of magmatic activity, the context of columnar jointed rocks on Mars should be considered to evaluate whether they formed in igneous rock, impact melt, or in contact-metamorphosed sedimentary rock.

3.6.3. Wrinkle Ridges

During the first several decades of spacecraft exploration of Mars, wrinkle ridges were considered a reasonably good signal of the presence of a lava plain [324–326]. In some research products, the presence of a wrinkle ridge in a Mariner 9 or Viking orbiter image was the only evidence available to interpret a given inter- or intra-crater plain as volcanic [327–329]. However, others cautioned that wrinkle ridges might not be diagnostic of lava plains [330,331] and that Earth analogs include examples occurring in sedimentary rock [331,332].

The term, wrinkle ridge (e.g., Figure 25a), refers to a landform assemblage that generally consists, in cross-section, of a narrow ridge superimposed on a broader arch [332]. They typically range from linear to arcuate as measured along their axes. Their name comes from the viewer impression that near-surface bedrock has been wrinkled or buckled. They can also be called maria ridges, or mare-type ridges, because they were first known from telescopic investigations of the lunar maria [333]. Wrinkle ridges are surface expressions of compressional deformation—thrust faulting and/or folding [334,335]—in competent (typically, erosion-resistant) rock. It is because of their similarity to the wrinkled ridges of the volcanic lunar maria, that some early Mars investigators took their presence to be a good sign of a lava plain.

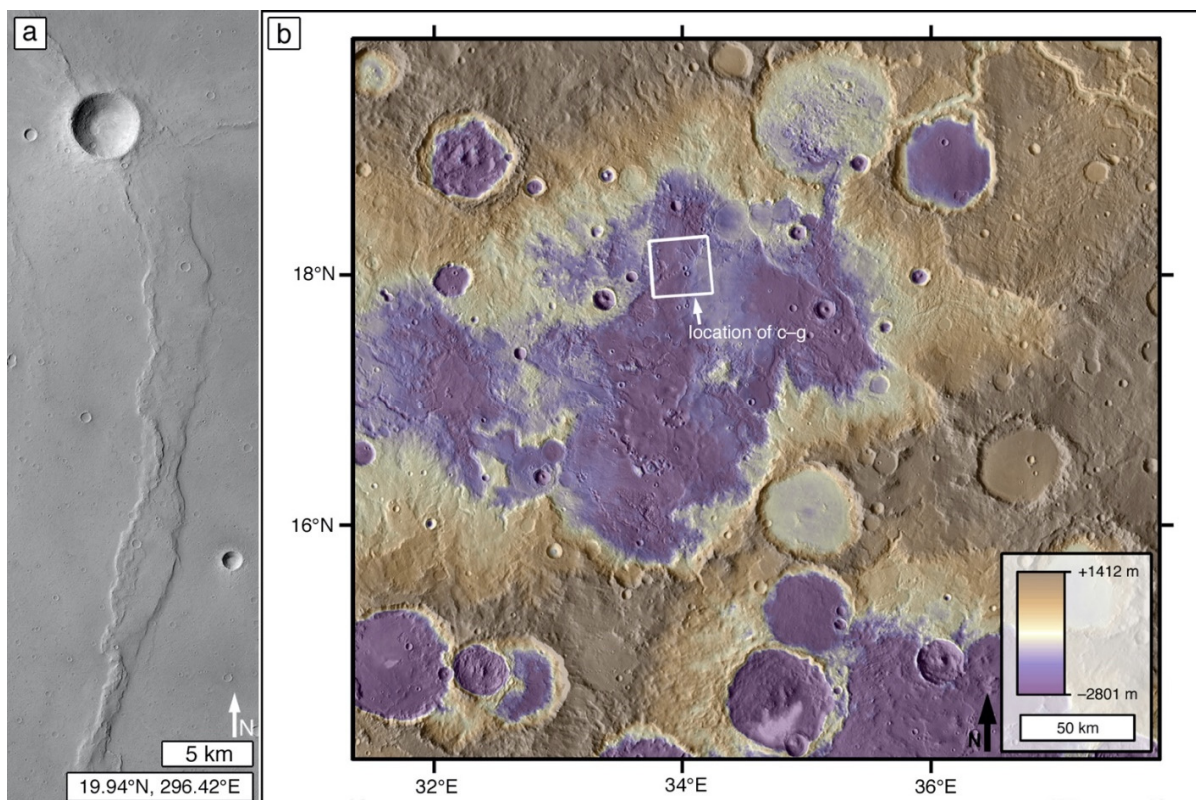


Figure 25. Cont.

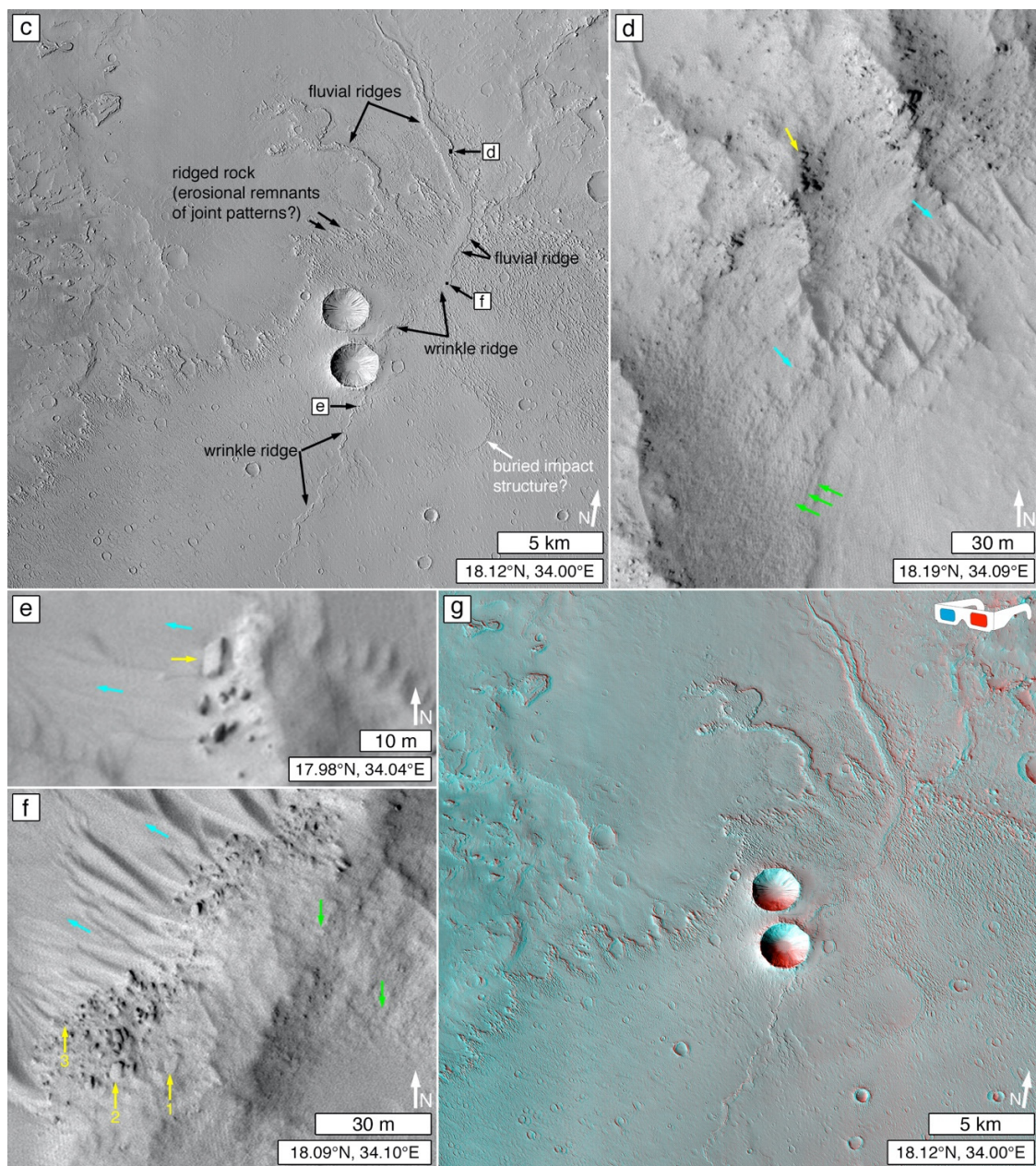


Figure 25. Wrinkle ridges. (a) Typical wrinkle ridge in northern Lunae Planum, commonly interpreted as a lava plain; CTX K23_062522_2007_XI_20N063W. (b) Context for wrinkle ridge in candidate sedimentary rock in an intercrater basin in central Arabia Terra; white box shows location of (c) through (g); presented on the next page; daytime THEMIS-IR base map [336] combined with the topographic product of Ferguson et al. [337]. (c) Wrinkle ridge (indicated) in candidate, small crater-retentive, sedimentary rock associated with several fluvial ridges (indicated); locations of (d–f) are indicated; CTX K17_059947_1972_XI_17N325W. (d) Boulder and megaclast production and stratification in a fluvial ridge north of the basin; slope direction indicated by blue arrows; dust- and debris-covered cliff-bench strata are evident (green arrows), as are angular rock slabs slightly displaced (yellow arrow) from the outcrop; HiRISE ESP_059314_1985. (e) Boulder and megaclast production at wrinkle ridge crest; the presence of a rhombohedral rock slab (yellow arrow) is suggestive of fractured sedimentary rock rather than lava; blue arrows indicate down-slope direction to the west of the ridge crest; HiRISE ESP_069404_1980. (f) Boulder and megaclast production at wrinkle ridge crest; a progression from (1) an intact (or nearly intact) rock slab, to (2) a dislodged, slightly displaced rock slab eroding from the outcrop, to (3) smaller boulders as slabs breakdown over time and distance from the source; green arrows indicate example dust-covered, in place, polygonal fracture-outlined rock slabs; blue arrows indicate down-slope direction to the west of the ridge crest; HiRISE ESP_059314_1985. (g) Stereo pair anaglyph of the same area as shown in (c); CTX K17_059947_1972_XI_17N325W and N11_066567_1972_XN_17N325W.

In recent decades, there has been occasional acknowledgement that Martian wrinkle ridges are not definitive signals of lava plains [186,338,339], and that they can be expressed in competent, erosion-resistant, sedimentary rock. However, they have not been described to occur in the major light-toned layered rock outcrops on Mars, such as Meridiani Planum e.g., [168,340] and the Valles Marineris interior layered materials e.g., [4,8,24]. Figure 25b–g presents a candidate example of a wrinkle-ridged sedimentary rock occurrence in an intercrater basin in Arabia Terra. No known volcanic (e.g., vents, flows) or intrusive (e.g., dikes, plugs) landforms occur in the region. In Figure 25c,g, wrinkle-ridged basin floor material is expressed as erosion-resistant bedrock (bounded by escarpments) that exhibit areas of differing erosional expression (e.g., some surfaces with many parallel ridges, some without). Two ~80–600 m-wide ridges intersect the intra-basin plain and can be traced laterally for about 8–9 km, outward, and then they merge with the plain. These ridges (or, based on Zaki et al. [177], some percentage of their interior materials) are interpreted as occurrences of fluvial sediment; their intersection with the plain is suggestive that the basin floor material consists of fluvial and lacustrine sediment. As shown in Figure 25d–f, the rock exposed on the steeper slopes of the wrinkle ridge, and on the larger fluvial ridge, has been breaking down, producing rhombohedral rock slabs (perhaps by undermining of a recessive rock layer). Boulders are less angular and more reduced in size the further they occur down the slope, away from the ridge from which they came. These observations regarding the setting and rock breakdown features on the wrinkle ridge and fluvial ridge slopes are suggestive that the material deformed by the wrinkle ridge is sedimentary rock rather than lava.

3.6.4. Boulder Production and Retention

When Martian sedimentary rock occurrences were first described in 2000 by Malin and Edgett [49], the MOC-NA images available, at the time, had insufficient spatial resolution to detect boulders produced by the breakdown of the sedimentary rocks that they identified. Such images did, however, show boulders produced at escarpments cut through igneous rock [185,341]. Thus, it seemed possible, for a few years, that boulder production and retention observations provide helpful information to distinguish sedimentary from, at least, competent igneous rocks such as basaltic lavas. However, today, we know that Martian sedimentary rocks produce boulders, and that some of these rocks are competent enough to retain those boulders over some time period (Figure 5). Boulders produced from the breakdown of sedimentary rocks only became apparent in satellite images with the advent, in 2003, of higher spatial resolution via the MOC-NA cPROTO technique [50,232] and the start of the MRO HiRISE imaging campaign in October 2006, e.g., [10,11,15,21,25,210,342]. Today we know that Mars has sedimentary rocks that are so competent that they retain many small impact craters, and produce and retain boulders, as well as do (or similar to) Martian lavas (Sections 3.4.1 and 3.4.2). The opposite is also likely true—that clastic rocks that poorly retain boulders produced from them (e.g., via impact cratering) could be sedimentary or they could be non-welded tuffs.

Thus, boulder production and retention are important observations to be made regarding rock physical properties, but an abundance of (or lack thereof) produced and retained boulders (or megaclasts, for that matter) is not a signal, by itself, for distinction of sedimentary from igneous rock. However, there is a possibility, yet unexplored, that boulders produced from lava might be larger or more abundant than those produced from competent sedimentary rocks; this notion comes from the fact that abundant, large boulders and megaclasts were indeed observable in volcanic regions of Mars at the lower spatial resolutions available in early MOC-NA images [185,341].

3.6.5. Lobate (or Arcuate) Rock Unit Margins

Lobate (or arcuate) margins of an erosion-resistant, planar to sub-planar bedrock unit are sometimes considered to be evidence for lava e.g., [343]. This interpretation is sometimes correct e.g., [343], but lobate margins, alone, are imperfect observables for the

distinction of lava from sediment. Some of the erosion-resistant rock units in northern Gale crater provide illustrative examples (Figures 3 and 26). Only one of these was investigated using the Curiosity rover (Figure 3). The other example (Figure 26) was too far away from the planned and executed rover traverse (Figure 26a). Before Curiosity landed, it would have been reasonable to interpret these crater-retaining, lobate-margined rock units as lavas. The example in Figure 3, addressed in Section 3.4.1, was investigated using the rover and turned out to be mafic sandstone [77,78]. The example in Figure 26 (see west side of Figure 26c) is partly confined to a low area within an impact structure. Extending Curiosity rover observations via HiRISE images into the nearby terrain not visited by the rover, Jacob [76] proposed that the topographically-confined example in Figure 26c,d could be either a lava flow or record the emplacement of clastic sediment via low-energy transport. Given the close proximity to the Peace Vallis fan (Figure 26a) [344]; the conglomerates, sandstones, and mudstones examined by Curiosity [79]; and the recognition that some sedimentary rocks can be resistant enough to erosion as to retain boulders and many small impact craters (Sections 3.4.1 and 3.4.2), the sedimentary interpretation seems more likely. If it were lava, other geomorphic evidence for flow might be expected (e.g., pressure ridges; nearby vents). Such features—that help distinguish lava—might not always be present at a given location on Mars; it depends, too, on the erosional state (including damage by impact cratering) of the material.

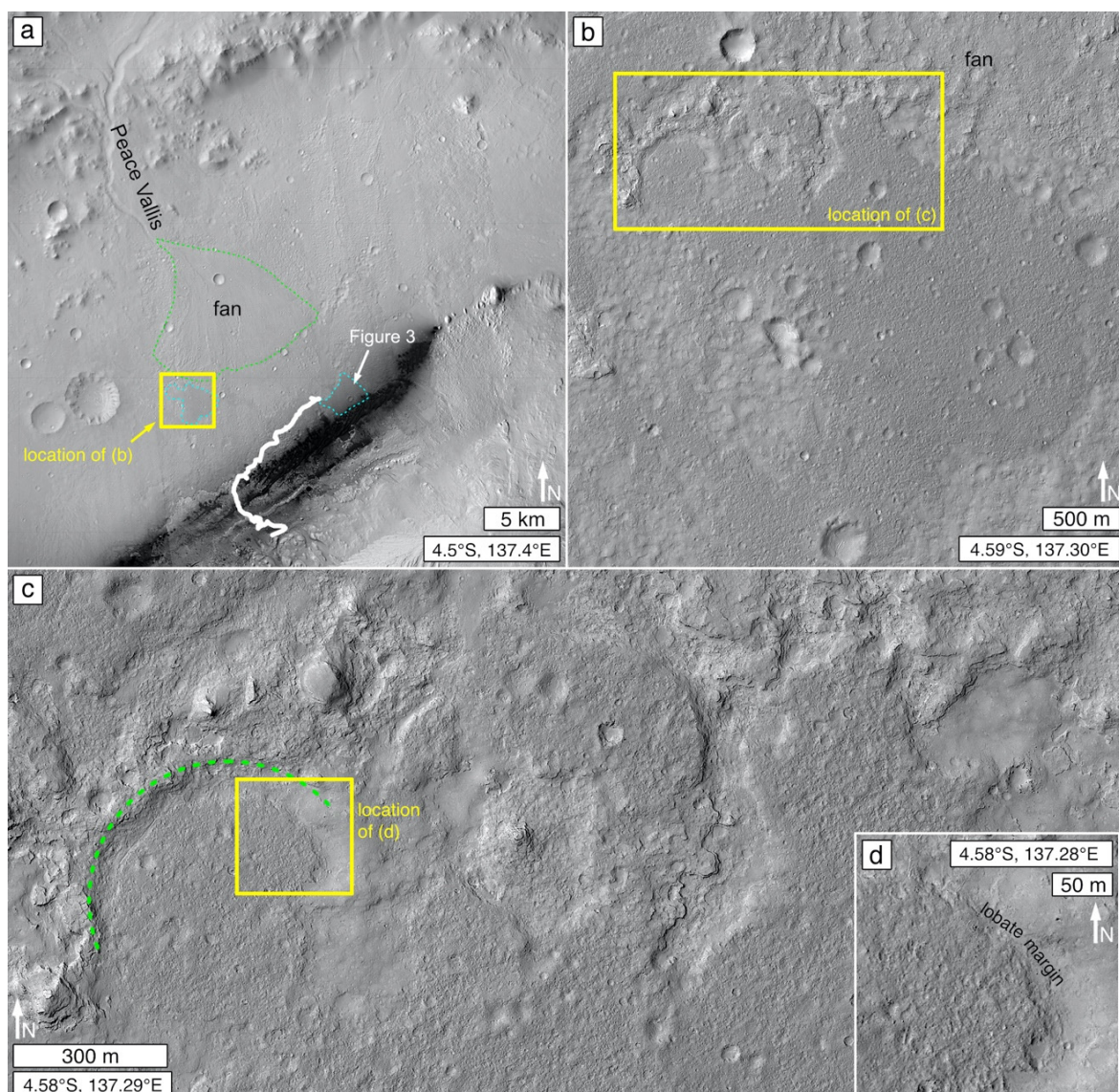


Figure 26. Lobate rock unit margins—example in northern Gale crater. (a) Context for the views in (b–d) relative to

the Curiosity rover traverse (white trace), the Peace Vallis sedimentary fan (green annotations), and the similar cratered, erosion-resistant rock unit illustrated in Figure 3; HiRISE image mosaic from Calef and Parker [345]. (b) A heavily cratered, somewhat dark-toned, erosion-resistant rock unit forms plain just south of the southwest edge of the Peace Vallis fan; its margins are lobate; HiRISE PSP_009650_1755. (c) Closer view of the erosion-resistant rock unit, showing the lobate nature of its margins and a relation to partial filling of an eroded impact structure (left; green dashed arc) per Jacob [76] (p. 63); HiRISE PSP_009650_1755. (d) Expanded view of the lobate margin in the impact structure; HiRISE PSP_009650_1755.

3.6.6. Stratified Outcrops

Another challenge to the distinction between igneous and sedimentary rocks in satellite and aerial images of Mars centers on stratification, particularly for cases in which the only exposure of the rock is in troughs and escarpments or crater walls and central uplifts. While sediments exhibit stratification, so too can accumulations of tuff and lava [178,179], even on the Moon [182,346]. However—given current knowledge that Martian sedimentary rocks can be dark-toned, erosion-resistant, and even have mafic compositions e.g., [71]—visual similarity [347] between layered rock outcrops on Mars and stratified volcanic rocks on Earth or the Moon, is insufficient information to declare a Martian case to be igneous.

Törmänen et al. [348] explored this concern by comparing layers exposed in escarpments cut through definitively volcanic rock (i.e., exposed on volcanoes) versus layers in examples of sedimentary rock on Mars. They examined only a limited set of examples, however. They noted that lava emplacement is generally episodic, local, and confined to volcanic regions (i.e., in which vents, edifices, and flows are common). Their survey suggested that stratified escarpments in igneous rock (generally, lava; they did not address tuff) tend to be very similar to each other from place to place, with slopes exhibiting spur-and-gully morphologies in their upper (approximately) one-third, and talus deposits covering their lower two-thirds. Figure 27a shows an example similar to what they [348] found, except that the proportion of stratified to talus-covered slopes is ~25% to ~75%. They found that layers, in lava accumulations, are best exposed in the spurs, and appear “very rough” and “highly serrated” (Figure 27b). Layered lavas were also described as “highly disrupted and consist of rounded and plate-like blocks” of meters to tens of meters size (e.g., Figure 27d). Over short distances (meters to kilometers), the layering in stratified lavas can have variable thickness and can be non-parallel. Törmänen et al. [348] did not comment on the fact that finding good slope exposures of definitive igneous rock is actually challenging to accomplish; for example, in Tharsis and Elysium, slopes are commonly mantled with sufficient debris, and aeolian sediment, that the rocks are obscured. We also note that a spur-and-gully morphology is not always observed in volcanic rock exposures (Figure 27c), and that much work remains to be done to consider how such exposures compare with sedimentary rocks on similar slopes that have undergone similar erosional processes.

The limited examples of sedimentary rock exposures examined by Törmänen et al. [348] suggested that sedimentary rocks are more likely, than igneous, to exhibit rhythmic layering, cliff-and-bench slope expressions, “smooth” and “gently winding” slopes, and lack talus deposits of comparable extent to those observed at volcanic sites, such as in Figure 27. Regarding rhythmic layering, Annex and Lewis [28] similarly emphasized that packages of repeated stratal patterns, or repeated thickness and physical properties (i.e., rhythmic or cyclic strata), are more likely to be sedimentary than to be tuffs because “volcanic events are stochastic and generally not forced by orbital variation or other cyclic drivers”.

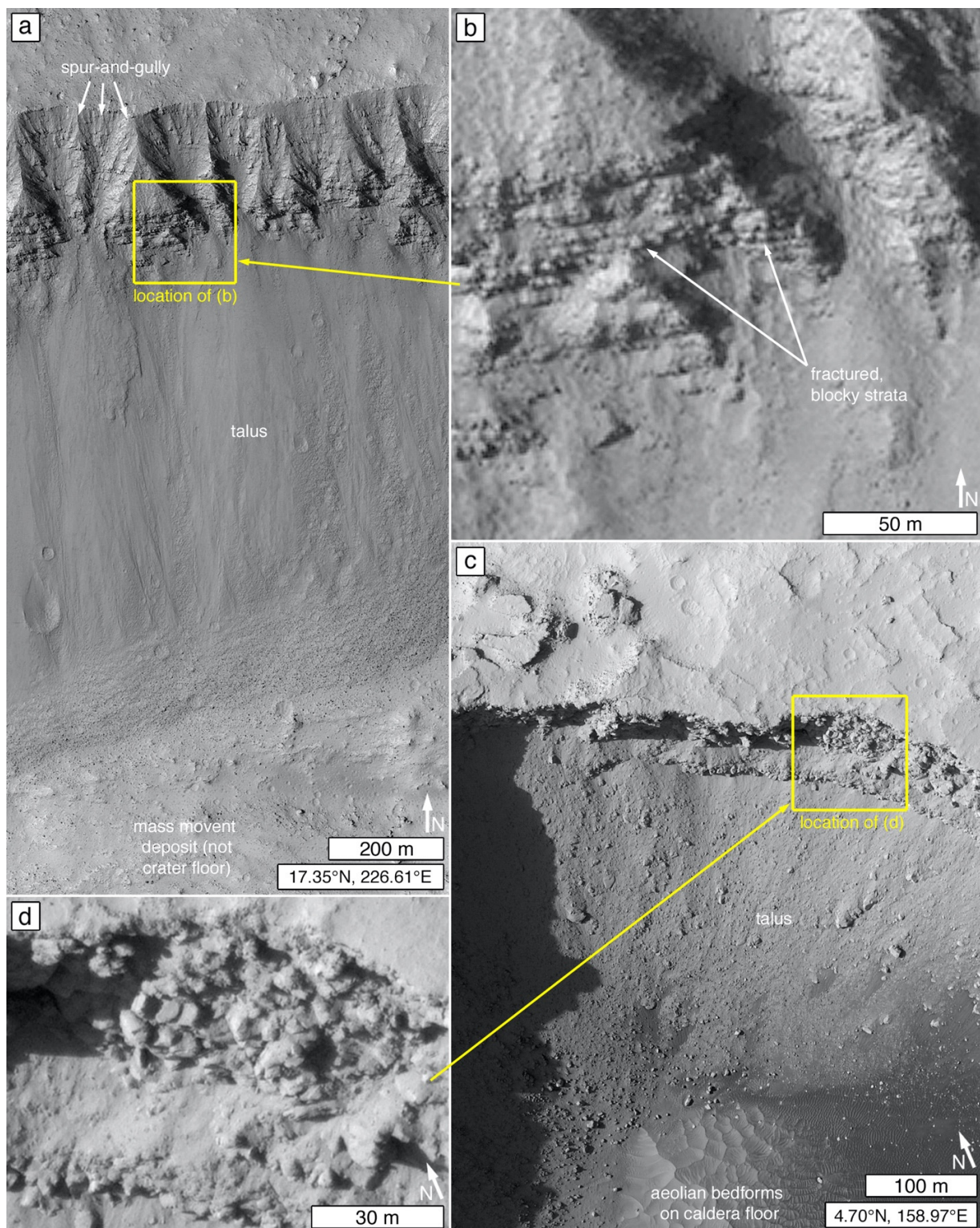


Figure 27. Examples of stratified rock outcrop expressions in definitively igneous rock. (a) North wall, modified by gravity-driven erosion (mass movement), of Pangboche crater high on the south slope of the volcano, Olympus Mons. The uppermost portion of the wall exhibits spur-and-gully erosion, while the majority of the slopes are hidden by talus; HiRISE PSP_001643_1975. (b) Close-up view of stratification in north wall of Pangboche crater; not the jointed, blocky erosional expression as strata breakdown in place; HiRISE PSP_001643_1975. (c) Northeast wall of a caldera on a small Cerberus Tholi shield volcano, showing modestly stratified rock in the upper wall and talus covering much of the lower wall; spur-and-gully erosion is not evident in this case; HiRISE ESP_017706_1845. (d) Close-up view of the rock exposed in the shield volcano caldera wall; it is breaking-down, in place, into large blocks and slabs; HiRISE ESP_017706_1845.

It is important to understand that tuffs, sediments, and regolith can become interbedded with lavas, and that these clastic materials may not be distinguishable on the basis of composition (e.g., presence of olivine, pyroxene, plagioclase) or tone (e.g., dark gray sandstone versus dark gray tuff versus dark gray lava). Beyer and McEwen [349] considered MOC-NA images of stratified rock exposed in the walls of Coprates Chasma, and identified an interbedding of apparent “strong” (erosion-resistant) and “weak” (erosion-recessive) layers (Figure 28). The erosion-resistant strata were seen as boulder producers and interpreted as likely being lava. The more recessive strata were considered more likely to consist of tuff, sediment, paleoregolith, thin lava flows, or some combination of these. The weaker layers were found to be more abundant, occurring in packages that are hundreds of meters thick, interbedded with resistant layers that have (or occur in packages of) tens of meters thickness. Given the current understanding from Gale crater that some sedimentary rocks can form very competent layers (Figure 3), including plateau-capping rocks (Figures 2, 5c and 17) [136,188], it now seems possible that even the “strong” layers investigated by Beyer and McEwen [349] could just as easily be sedimentary, as igneous.

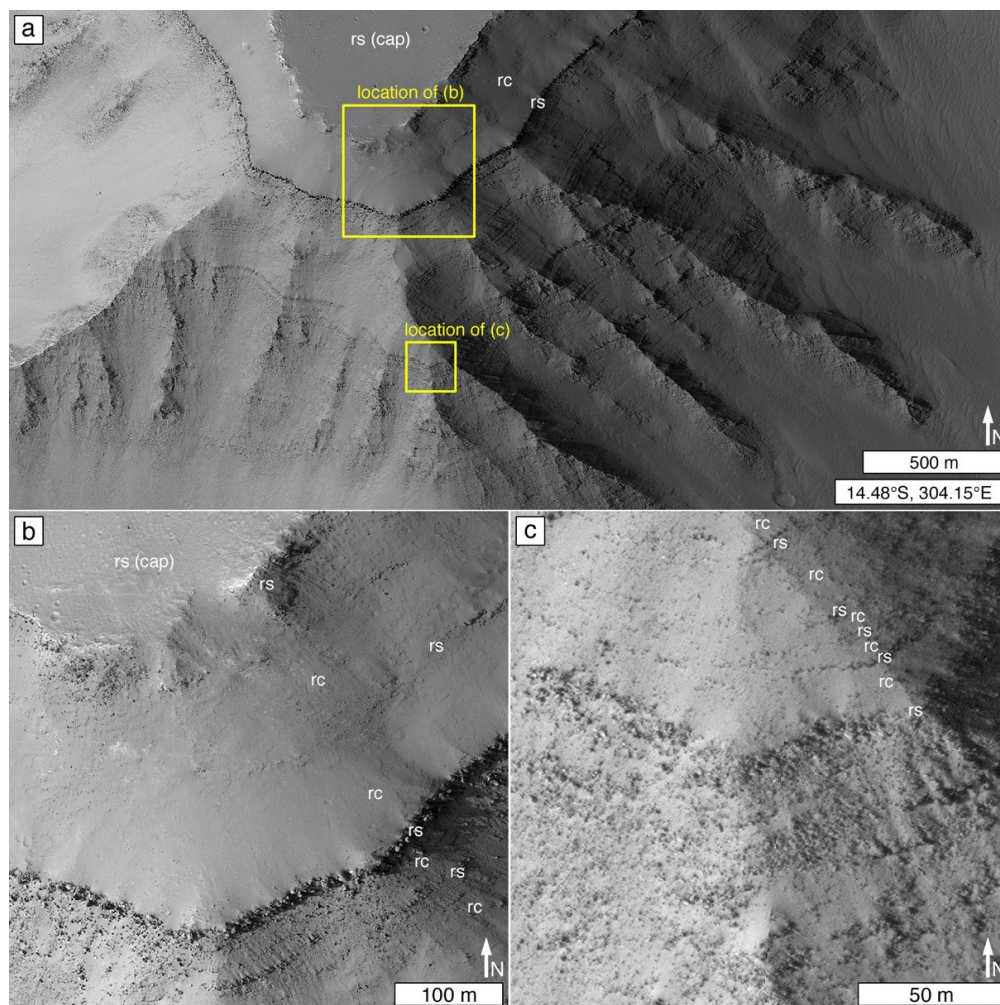


Figure 28. Successive packages of erosion-resistant (rs) and erosion-recessive (rc) strata near the top of a mesa in the Nectaris Montes in Coprates Chasma, Valles Marineris. (a) Context view showing recessive and resistant strata, as well as the locations of (b,c); this same location was previously studied by Malin et al. [341] and Beyer and McEwen [349], using MOC-NA images, before HiRISE reached Mars; HiRISE PSP_003104_1655. (b) Close-up view with example recessive and resistant stratal packages indicated. Some of the “smooth” material could be rock or could be rock covered by a mantle of gravel, aeolian dust, or both; HiRISE PSP_003104_1655. (c) Another close-up view with example recessive and resistant stratal packages indicated; HiRISE PSP_003104_1655. Note that, as spatial resolution increases from (a–c), strata actually become more challenging to identify and slopes appear to have more boulder debris upon them.

3.6.7. Distinction of Tuffs

Tuffs present a special challenge to the distinction of sedimentary from igneous rocks in satellite and aerial images of Mars. Here, we use the terms *volcaniclastic* and *tuff* in the sense proposed by White and Houghton [350], which focuses on clast genesis, a departure from earlier perspectives [351–353], which included epiclasts created by weathering of volcanic rocks (and contrasted with the term, plutonoclast e.g., [354,355], for grains created from intrusive rocks). The term, volcaniclastic, now applies only to particulate material produced by or resulting from volcanic eruptions [350,356]. Primary volcaniclastic deposits can include coexistent, co-located facies of reprocessed material—i.e., volcaniclasts deposited by a non-volcanic process such as wind or wave action that occurred simultaneously with an eruptive event [357]. In contrast, secondary volcaniclastic deposits are, essentially, sediments [350]. These sediments form from reworking of unconsolidated primary volcaniclastic deposits after some period of storage [350]; they are not considered igneous and are classified using the same terminology as other clastic sediments and sedimentary rocks [350]. Further complicating the matter is the fact that primary tephra deposits can undergo diagenesis including, compaction and cementation e.g., [358–360], just like sediment.

Observations made on the Martian surface at the Spirit field site in Gusev crater, and the Opportunity site in Meridiani Planum, illustrate the challenges of distinguishing tuffs from sediments. At these locations, the effort to discriminate sedimentary rock from tuff relied on rover cameras, rather than aerial and satellite images, yet, whether all examples identified and discussed are actually tuffs remains uncertain. The very best case that Martian tuffs exist comes from the Home Plate plateau in Gusev crater [361,362], but even the strata exposed at Home Plate might include a volume of sand-sized clasts that were reworked by wind to form a sediment [362]. Home Plate was considered to be a tuff, in part, because of an apparent bomb and bomb sag [361], although the “bomb” is only ~4 cm across. Vesicular stones identified at the Spirit site were called scoriaceous but were generally considered to be impact-produced fragments of vesicular basalt, rather than products of explosive volcanism [363]. Other clastic rocks observed in Gusev, composed of sand-size and smaller particles, drape over paleo-landform surfaces on Husband Hill [187,364]. Similar clastic rocks occur in Meridiani Planum on the ridges of the west side of the Endeavour impact structure [365,366]. Spirit and Opportunity team members interpreted these rocks as either airfall volcaniclastics or airfall impactites; but they could not distinguish between these hypotheses [187,367–370]. Given the challenges for the distinction of primary volcaniclastic deposits at the ground level, even using 31 μm /pixel images [368,370], trying to distinguish them in satellite and aerial data should be expected to be even more difficult.

Explosive volcanism is thought to have been common on Mars because degassing of volatile-bearing magma during ascent to the planet’s low-pressure atmosphere should be quite vigorous [371]. However, primary volcaniclastic deposits and tuffs are very difficult to identify using remote observations of Mars [372]. Those that have been identified are not all universally agreed upon, but one thing they have in common is proximity to an eruptive vent; this is the case whether considering the proposed very youthful tephra deposits among the Cerberus Fossae [373], the thermophysical observations considered suggestive of tephra on volcanoes such as Alba Mons [374] and Tyrrhena Patera [375], or individual cones or rings bearing a summit depression [376–379].

Some investigators have considered, too, the possibility that fine, Martian tephra has been deposited far from a source vent following aeolian suspension [234,236,380]. The most prominent and persistent interpretation of such materials is that of the yardang-forming rocks of the Medusae Fossae Formation [303,305,380–382], which we discuss in Section 4.2.3.

One of the more informative candidate identifications of tuff on Mars, made using orbiter data, comes from Kremer et al. [237] and Mandon et al. [383]. Kremer et al. [237] provided a good model as to how to attempt distinction between airfall tuff, pyroclastic flows, lava flows, and sedimentary rock. Both investigation teams studied stratified, olivine-bearing (some of which is also carbonate-bearing) rock exposures located along the western and southwestern margins of the ancient Isidis impact basin. The airfall tuff interpretation is based on several attributes of the material: (1) It is said to consist of rock of nearly uniform thickness that drapes over preceding topography (Figure 29) of relief, in some places, exceeding 100 m. (2) Layers within the material (where identifiable) exhibit parallelism that also conforms to the superposed paleo-topography (Figure 29). (3) The material is interpreted to be clastic, largely because of evidence for erodibility in the form of yardangs, poor impact crater retention, and a model-dependent, infrared observation-based, estimate of olivine grain sizes of ~1 mm [384]. (4) It exhibits no deformational features—at HiRISE 0.25 m/pixel scale—that would indicate flow (e.g., pressure ridges). (5) It occurs over a great areal extent, appears to have a uniform composition over that extent, and retains the above characteristics over its extent. Finally, (6) it occurs within a regional volcanic context, in this case the circum-Isidis extensional faults that were conduits for Syrtis Major volcanism [385]. The combination features—especially the large areal extent, draping relations, association with a region of known volcanism, and evidence that the material is likely clastic—make these olivine-bearing rocks a strong, although not conclusive, candidate for Martian tuffs.

The apparent overall deposit thickness, the repeated thickness of individual strata (or stratal packages), and the uniform erosional expression of these strata in the example in Figure 29, however, could also be interpreted as signs of sediment draped over the paleo-topography. Although the mafic or ultramafic composition and draping of paleo-topography make the materials in the Nili Fossae region described by Kremer et al. [237] an attractive candidate tuff, we note that Stimson formation outcrops in Gale crater (e.g., Figures 17 and 20b–d) exhibit near-uniform thickness, near-uniform basaltic composition, and drape across hundreds of meters of topography [243], yet are cross-bedded aeolian sandstones [136,188]. The cross-bedding is not observable in HiRISE images, and Day and Catling [251] provided a reminder that we should not expect aeolian cross-bedding to always be visible at the highest spatial scale obtainable by HiRISE. Where the Stimson formation and the rocks described by Kremer et al. [237] differ, besides the details of their composition, is that the Stimson formation rocks do not occur over a large, regional extent, and do not occur within a volcanic (or plausibly volcanic) context.

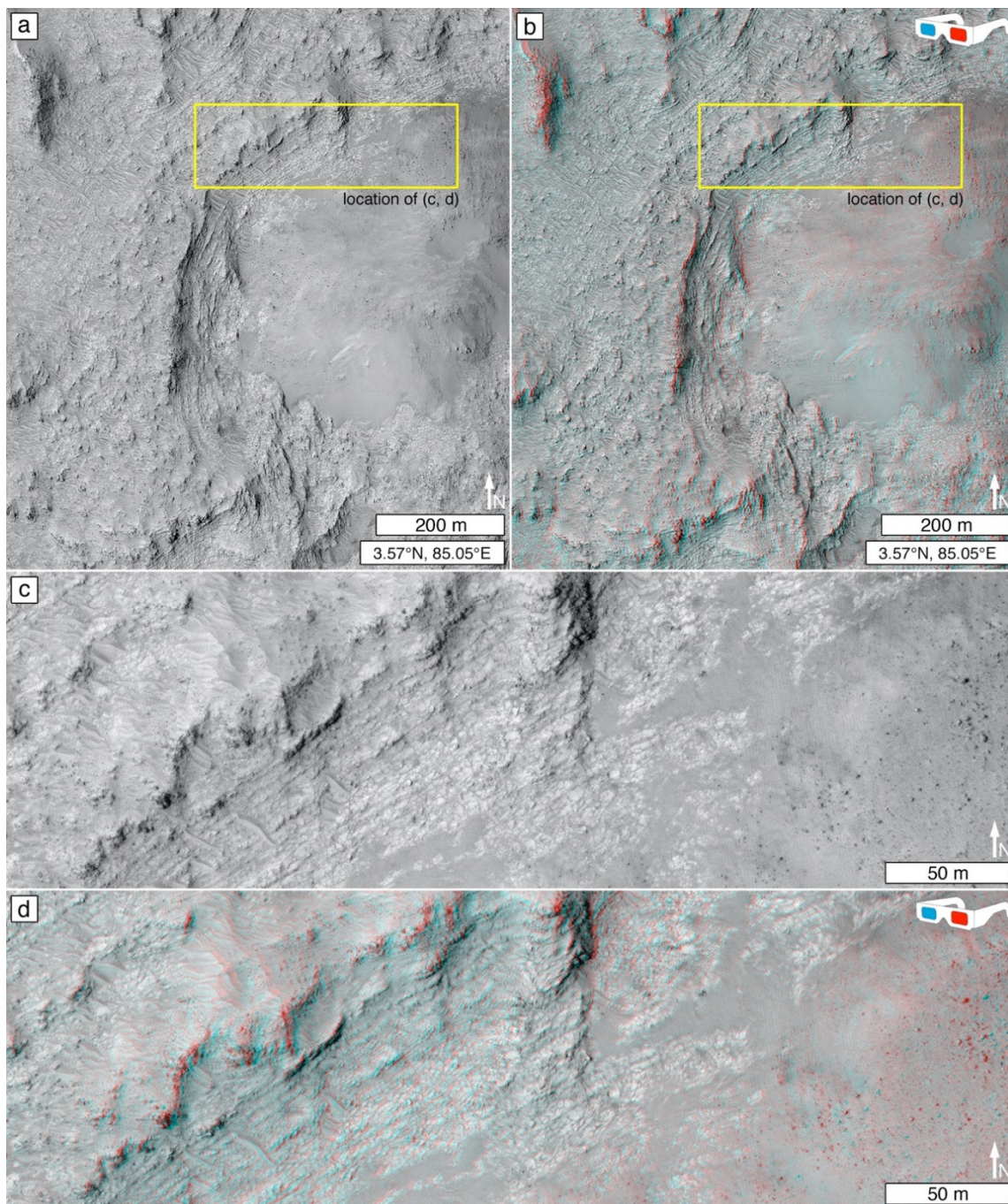


Figure 29. Example of stratified, paleo-topography-draping rock interpreted by Kremer et al. [237] to be part of a regional tuff deposit. This example is in the northern Libya Montes, north of Hashir crater, at the location of “Figure DR5” in the supporting online file of Kremer et al. [237]. (a) Light-toned, stratified rock surrounds and dips away from a relatively smooth-surfaced hill of intermediate tone; the hill is emergent from beneath the superposed, draping strata; HiRISE ESP_016034_1835. (b) For a three-dimensional perspective, this is a stereopair anaglyph of the same scene; HiRISE ESP_016034_1835 and ESP_017089_1835; (c,d) show a close-up view of a portion of the scene.

3.6.8. Importance of Context

Ultimately, what matters most for distinction between sedimentary and igneous rocks on Mars is context [115,186,312,386]. For example, pyroclastic deposits generally thin with distance from their source vents, and flows (whether lava or pyroclastic) move downslope from a vent or fissure. The presence of flows is not always diagnostic of volcanism; they could be mudflows [387] and might even be mudflows that came from a vent [388].

Another form of context is the regional setting. A flow within an impact crater, Isil, in the region of circum-Hellas basin volcanism [385] is more likely to be a lava flow (Figure 30a) than is a flow that is far from a known volcanic center, such as the proposed debris flows associated with the impact event that formed Hale crater (Figure 30b) [389].

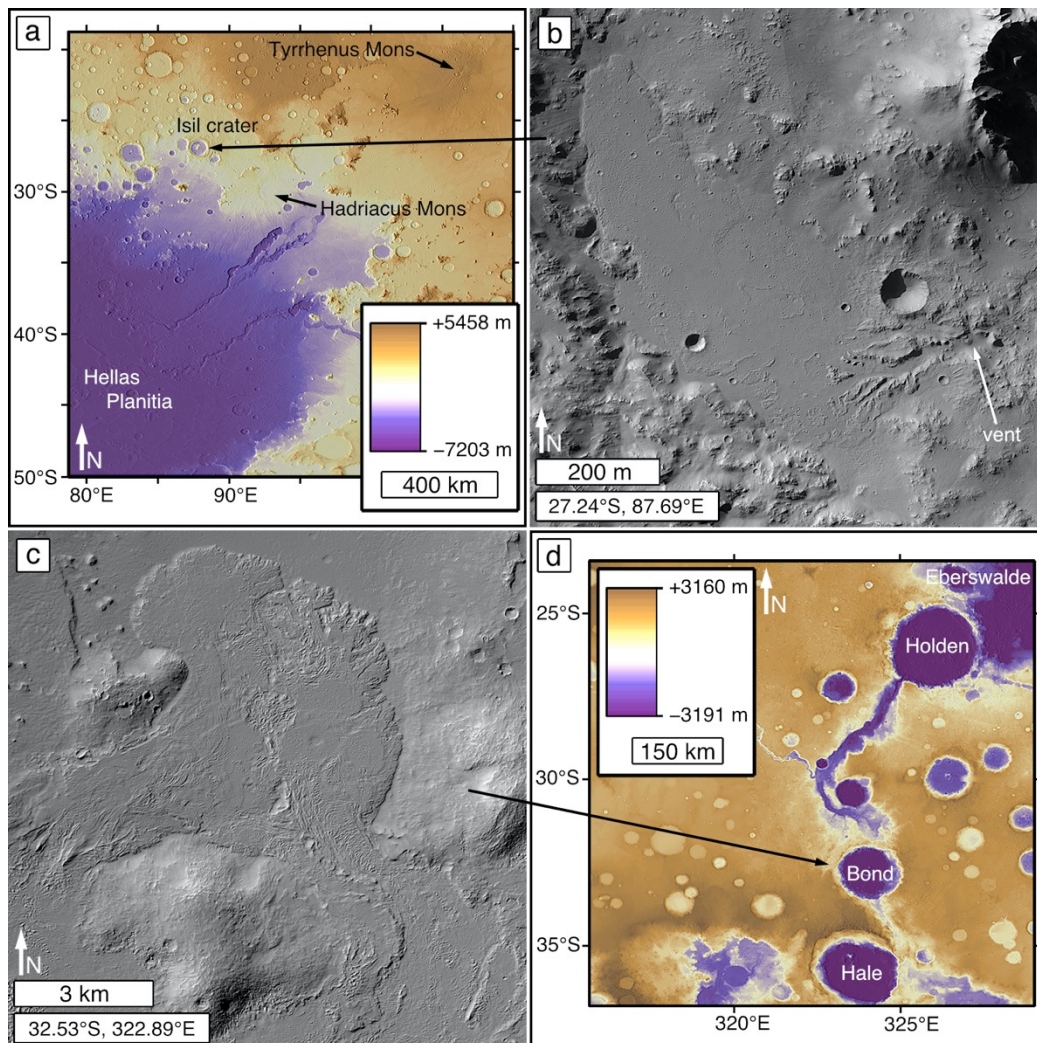


Figure 30. Importance of volcanic versus non-volcanic context; a lava flow and a debris flow. (a) Isil crater is located in the vicinity of Tyrrhenus Mons and Hadriacus Mons, volcanoes associated with faulting related to the Hellas basin impact structure; topographic product of Ferguson et al. [337]. (b) Given the context, the singular flow located in southwestern Isil crater is interpreted to most likely be a lava flow; mosaic of CTX P22_009797_1527_XN_27S272W and B20_017300_1528_XN_27S272W. (c) Flows located west of Bond crater (d) do not occur in a volcanic region; they are interpreted as debris flows [389] associated with other flow and outflow features interpreted to have been a direct result of the impact event that created the relatively youthful Hale crater [389]. (d) Context for the flows near Bond crater in (c); topographic product of Ferguson et al. [337].

Unknown is whether Mars has very ancient igneous landforms that are not recognized because they were completely buried, or were so battered by impact cratering, or so eroded in the early Martian climate, as to have retained no characteristics recognizable in satellite and aerial images of the planet's surface. Known Martian igneous rocks are most commonly associated with evidence for magma conduits to the surface—for example, the edifices in Tharsis and Elysium [300], the extensional faults of the Cerberus Fossae and Tempe Terra regions [224,390,391], and impact-induced conduits such as those that are semi-circumferential to the Hellas and Isidis basins [385,392]. Commonly acknowledged volcanic landforms are largely confined to specific regions, such as Tharsis, Amazonis,

Elysium, Syria/Sinai, Solis Planum, and the circum-Isidis and circum-Hellas regions. Other volcanoes might exist outside these regions; Xiao et al. [393] inventoried 75 landforms in the heavily cratered terrain of Mars that various investigators have interpreted as possible ancient volcanoes, but whether they actually are volcanoes is less certain. Interpretation of stratified rocks in or very near these regions should trigger caution as to whether the materials in question are igneous or sedimentary. Of course, the two rock types can coexist—for example, consider the conduits, edifices, and flows of the San Francisco volcanic field in northern Arizona, USA, which were cut through and superimposed upon Colorado Plateau sedimentary rocks [394].

Context is relatively easy to discern in regions of Mars where volcanic landforms are indisputably present. One seeks vents, edifices, and flows that emanated from them. One also seeks firm evidence of excavated dikes, sills, and plugs, e.g., [395]. However, it is important to recognize that dark-toned (or dust-covered), erosion-resistant material exposed at the present-day surface of an intercrater plain or a partly-filled impact structure—where no unambiguous flow or vent morphologies are present—is not necessarily volcanic, even if it has infrared spectra interpretable as mafic, and even if it is deformed by a wrinkle ridge.

3.7. Deformation

Deformation of rock is a product of stress, a force applied per unit area. Strain is the change in size, shape, or volume of the rock that results from stress. As stress and strain increase, deformation goes from elastic to ductile until the rock breaks (fractures). Evidence of deformation of Martian bedrock visible at satellite and aerial image scales includes folds, fractures, and faults. Joints are fractures at which displacement parallel to the surface of the rupture is imperceptible. Joint sets consist of multiple parallel, evenly spaced joints, and joint systems consist of intersecting joint sets. Mars exhibits abundant examples of bedrock deformation at sub-millimeter to multi-kilometer scales, e.g., [8,25,145,332,335,396–406]. These deformations are products of crustal tectonism, impact cratering, and smaller, more localized stressors such as thermal cycling, overburden removal, hydraulic fracturing, and gravity (e.g., fracturing of undermined rock, leading toward mass movement).

Faults, fractures, joint systems, deformation bands, and possibly folds have been observed in satellite images of Martian materials interpreted to be sedimentary rocks, e.g., [3,4,8,25,145,332,397,399–401,406–410]. The concern, here, is whether any deformational forms are diagnostic signals—or at least encouraging signs—of sedimentary rock. Section 3.6.2 considered columnar jointing, which usually provides a strong signal of magmatism and a likely (but not unique) signal that a rock is igneous. Section 3.6.3 considered “wrinkle ridges,” which have sometimes been cited as the only evidence for interpreting that a given rock occurrence is igneous [326,329].

Regarding the use of deformation features for the distinction of sedimentary rock occurrences on Mars, two observations, in particular, stand out. These are not diagnostic, but can be considered helpful. These are the presence of polygonally fractured rock for which the polygons exhibit similar sizes and patterns as known examples of sedimentary rock examined at rover field sites; and the presence of convoluted structures interpretable as post-deposition, soft sediment deformation. In the latter, deformation occurs before lithification.

3.7.1. Polygonal Fracture Patterns

Polygonal fracture patterns visible in orbiter images of Mars are not unique to sedimentary rocks and can occur in other materials including igneous rocks (Figure 31a) and middle- and high-latitude ice-rich regolith (Figure 31b), e.g., [411–413]. Polygonal fracture patterns occur at a wide range of scales, from centimeters to kilometers, and can form through a variety of processes. Relevant scales, materials, and processes are reviewed elsewhere [403,404,414].

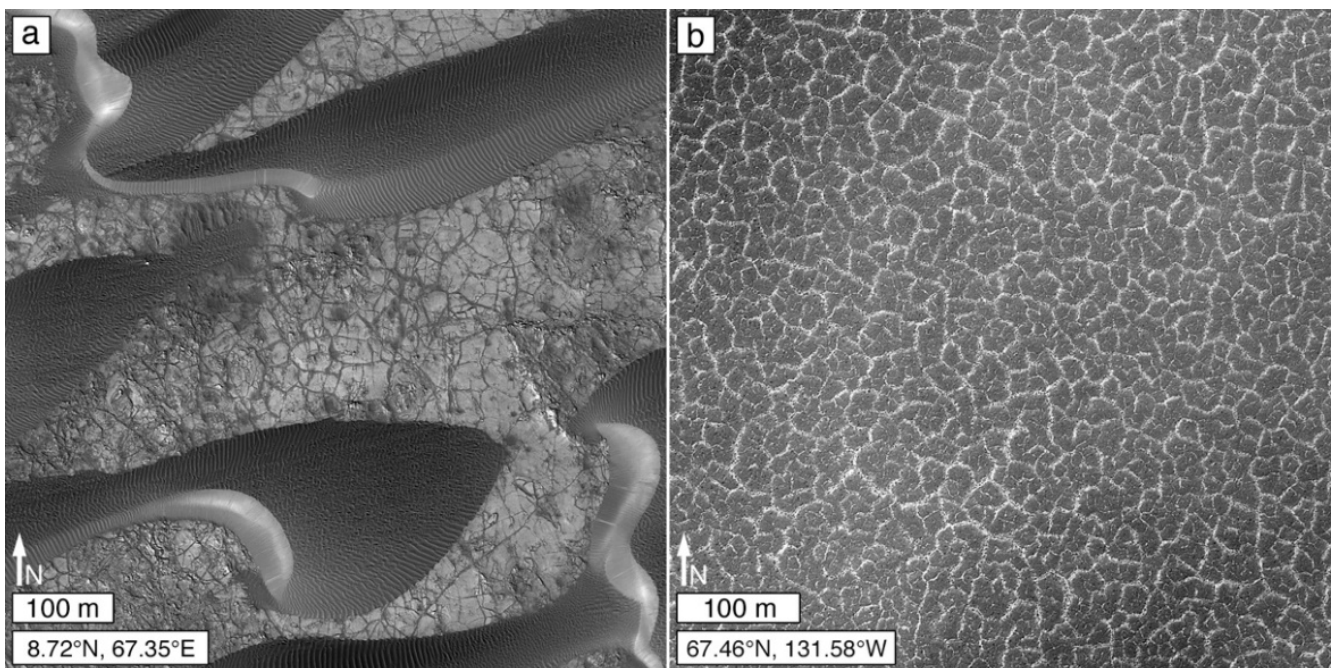


Figure 31. Examples of polygonal fracture patterns in materials that are not considered to be sedimentary rock. (a) Polygonally-fractured bedrock exposed between aeolian dunes in the Nili Patera caldera in Syrtis Major; given the context, the rock is broadly interpreted as igneous; HiRISE ESP_049093_1890. (b) Northern plains polygonal-patterned ground, visibility of troughs enhanced by remnant seasonal frost; viewed through thin haze in northern spring; HiRISE PSP_007448_2475; L_s 37.9°.

Joint systems, also not unique to sedimentary rock occurrences e.g., [158,179,415], create some of the variety of polygonal fracture patterns observed in some sedimentary rocks on Mars (e.g., Figure 6e) [25]. In some cases, such as in Gale crater, polygonally-fractured rocks can become dislodged and displaced, forming boulders or megaclasts that either remain close to where they were produced (e.g., Figure 5d), or can move downslope if a slope is available.

Here we focus on one key aspect of polygonally fractured sedimentary rock. That is, for locations on Mars where the rock is known to be sedimentary—or a very well-reasoned case can be made that it is sedimentary—finding a similar polygonal fracture pattern at another location on Mars might be a signal that the other locality has rocks of similar physical properties as those of the known (or well-reasoned) sedimentary rock case. For example, Figure 32 shows that the pattern and scale of polygonal fractures in rock exposed in northern Gale crater is similar to the pattern and scale of polygons in the Vistula Valles region, south of Chryse Planitia. The polygonally fractured rocks in Gale crater (Figure 32b) were not visited by the Curiosity rover, but a well-reasoned (albeit inconclusive) inference is that the material is sandstone [404]. This interpretation is based on similarity to sandstones that the rover did visit—at its Yellowknife Bay field site [79]—and based on a facies model that the rocks are coeval with the deposition of Peace Vallis fan (Figure 26a) sediments [344]. The inference, here, is that the fractured rocks at Vistula Valles could also be sandstones or, at least, they may be clastic rocks of similar mechanical properties.

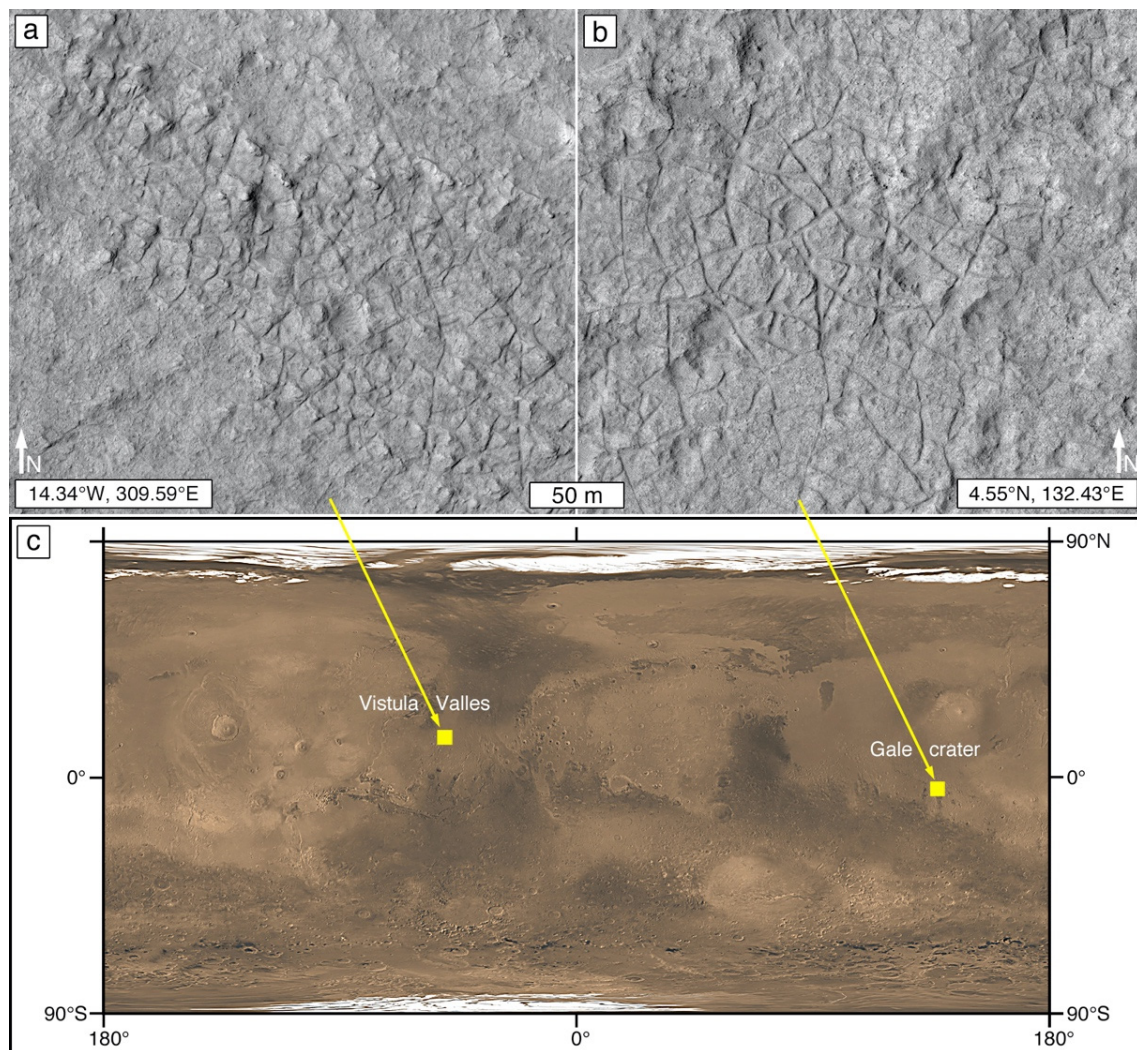


Figure 32. Similar polygonal fracture patterns, sizes, and erosional expressions of rock exposed half a world away might indicate rocks of similar physical properties. (a) Example from Vistula Valles; HiRISE ESP_035304_1950. (b) Example from Aeolis Palus in northern Gale crater, proposed to be sandstone based on similarities to rock encountered by the Curiosity rover; HiRISE ESP_028335_1755. (c) Map of Mars showing the locations of the examples at Vistula Valles and Gale crater; map created from MGS MOC wide angle geodesy campaign images [416].

3.7.2. Soft Sediment Deformation

Soft sediment deformation cannot actually be used to identify an occurrence of sedimentary rock, because doing so entails circular reasoning. However, deformation can occur in sediments after deposition—before lithification—and, where present, can (at least) be used to strengthen the case that a material is sedimentary. Soft sediment deformation usually occurs during and soon after deposition (i.e., syndepositional) while sediments are loosely packed and have plenty of intergranular fluids. Hence, some of the most common environments for these structures are deep water basins under the influence of tidal currents, river deltas, and shallow seas affected by storm currents [417]. The most common trigger for deformation is seismicity (including those induced by impact events); however, other triggering mechanisms are known, such as sediment loading, salt tectonics, submarine mass movement, tsunamis, storm waves, tidal activity, and karst dissolution and collapse [417]. Moreover, there are at least 120 different types of soft sediment deformation forms described on Earth, of which some of the common are convolute bedding, slump folds, flame structures, dish-and-pillar structures, load casts, and clastic injections [417].

As might be expected on a world that has a record of aqueous sedimentation, millimeter- to decimeter-scale soft sediment deformation examples have been interpreted to occur in rocks outcropping at the Opportunity [57,418] and Curiosity [419] rover sites. More surprising is the fact that much larger examples are considered to be visible in orbiter images, particularly in the Valles Marineris [407,420] and Capen [7], Terby [421] craters. Further, the prospect that mud volcanism may have occurred on Mars [422] underscores the likelihood that clastic, soft sediment deformation has occurred [423].

3.8. Sedimentary Rock Landforms

Recognition of sedimentary rock occurrences—and even identification of rock type—would be greatly assisted by a thorough understanding of the landforms that exposed, eroded Martian sedimentary rocks produce. Over the last few decades, studies of “sandstone landforms” and “sandstone landscapes” on Earth have proliferated [107,113,424–427], and the concepts have been extended to “conglomerate landforms” [109], as well. In addition, Danxia landforms in China include both sandstone and conglomerate variants [114]. These publications make the point that sedimentary rock types, when exposed at a planet’s surface, can exhibit common erosional expressions that relate to the physical properties and deformational states of rock at scales ranging from microscopic to entire depositional basins.

The recognition and study of Martian sedimentary rock landforms is in its infancy. The Martian landscape exhibits a wide variety of sedimentary rock landforms and erosional expressions for which rock type is currently unknown. Shaping sedimentary rock landforms on Mars is more than a matter of aeolian erosion in the modern, hyperarid, setting. Many of the landforms were initially shaped more than two or three billion years ago, when groundwater and surface runoff were more common—the fluvial canyons cut into the sedimentary rocks of Aeolis Mons in Gale crater [20,201,428] provide examples.

Connecting sedimentary rock landform expression to rock type on Mars is presently an imperfect prospect because not very many differing examples have been examined in field settings (i.e., rover missions). As illustrated in Section 3.5, some sedimentary rock landforms mimic their original clastic depositional setting. In some cases of depositional setting mimicry, rock type can be interpreted—or, at least, speculated upon—based on knowledge of Earth analog facies. For example, the lithified dune field near the Apollinaris Sulci (Figure 1a) is interpreted as sandstone [52], and the detailed geomorphology of the Eberswalde delta (Figure 1b) [1,15] can be used to infer which facies might contain conglomerates versus sandstones versus mudstones [429]. Here, we consider what is presently known about landforms created in clastic sedimentary rocks and chemical sediments (to the extent that they might exist on Mars).

3.8.1. Sandstone Landforms

We begin with sandstone landforms because they are the most well-studied cases on Earth. Sandstone exposures on our planet form a wide range of visually spectacular landscape features [107,112–114,427], including arches [430]. Counterparts of similar geomorphic expression have generally not yet been identified on Mars, but Martian sandstone outcrops do exhibit a range of morphologies, and it is likely that many candidate sandstones are yet to be identified. As shown in Section 3.5.1, depositional setting mimicry in the form of whole, lithified aeolian dunes [51,52,139,140,249], and “ghost dunes” [251], are excellent starting points, but such outcrop expressions are rare. Slightly less rare are bedrock outcrops that exhibit a “washboard” erosional pattern (Figure 20; Section 3.5.1). However, whether washboard patterns always indicate aeolian sandstone, or whether some cases result from deformational structure (e.g., fracture patterns), is not yet fully known (Section 3.5.1).

Most of the sandstones encountered by Curiosity in Gale crater are dark gray, well-cemented, and erosion-resistant (Figures 2, 5c and 17). A few of them, however, are recessive—these include sandstones beneath an overhang at the Cooperstown outcrop

(Figure 33a,b) [21,431]; dipping beds between prominent, erosion-resistant strata (Figure 13b) in rock interpreted to be deltaic clinoforms at the Kimberley field site (Figure 33c,d) [80]; and an occurrence of reddish, very fine-grained sandstone bedded with mudstones the Karasburg member of the Murray formation (Figure 33e,f). The clinoform [80] bedding is prominently seen as a “striated unit” [80,247] in HiRISE images of the Kimberley field site in Gale crater (Figures 13a and 18e).

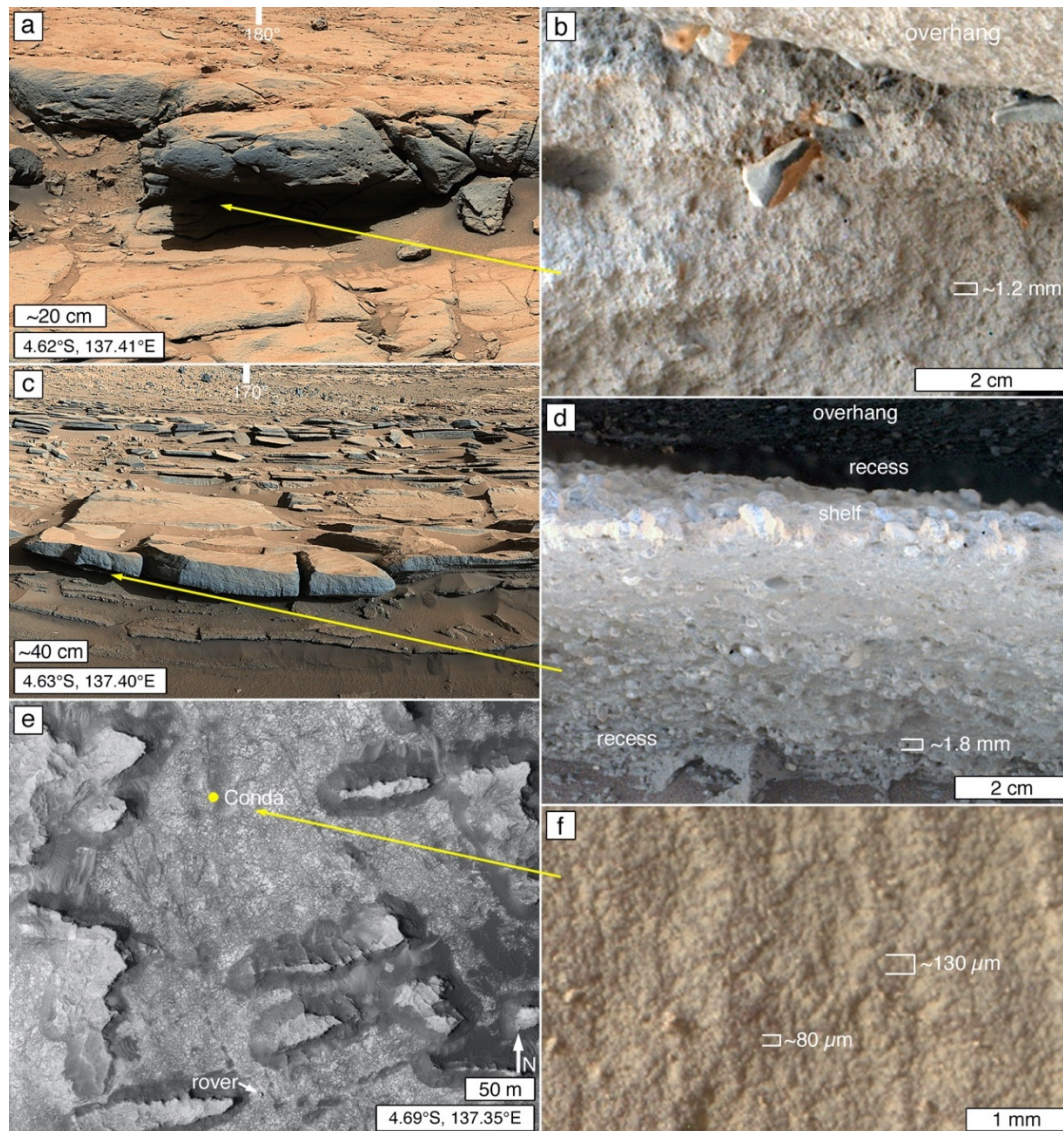


Figure 33. Examples of erosion-recessive sandstones identified in Gale crater. (a) A dark gray sandstone shelf at the Cooperstown field site (Figure 14b) overhangs a recessive sandstone; Sol 440 Mastcam-100 mosaic (sequence 001795); azimuth 180° indicated. (b) The recessive sandstone at Cooperstown consists of coarse and very coarse sand with scattered granules; MAHLI focus merge product 0443MH0003290000200193R00. (c) Clinoforms dipping southward at Square Top (Kimberley field site; Figure 13a,b and Figure 18d) exhibit alternating erosion-resistant and erosion-recessive strata; Sol 580 Mastcam-34 mosaic (sequence 002407); azimuth 170° indicated. (d) The recessive sandstones at Square Top consist of very coarse sand and granules; MAHLI focus merge product 0585MH0003660000202479R00. (e) Recessive sandstones at Conda occur amid the erosion-resistant Murray buttes [136], along with mudstone strata of the Murray formation [81]; note Curiosity rover for scale; HiRISE ESP_047416_1755, acquired 07 September 2016. (f) The sandstone at Conda consists of very fine sand; MAHLI 1436MH0004190010503512C00.

The dark gray, erosion-resistant aeolian sandstones of the Stimson formation in Gale crater are expressed as plateau, mesa, and butte-capping rocks (Figures 5c, 17 and 20)

[136,145,188,432]. They are underlain by recessive rocks, largely mudstones [80,81] of the Murray formation. Among the Murray buttes (e.g., Figure 5c), the sandstones occupy the bulk of each butte's volume [136]. In addition to their capping rock expression, Stimson formation outcrops also exhibit washboard-patterned surfaces of alternating, parallel ridges, and swales (Figure 20). Other erosion-resistant sandstones in Gale form cratered plains (Figure 3), benches that overhang recessive rocks (Figure 33a), or decimeter- to meter-scale escarpments.

Another sandstone visited by a Mars rover, Opportunity, is the Burns formation in Meridiani Planum [57,58,203,204,418]. These largely aeolian and wet interdune facies sandstones form the light-toned bedrock beneath a regolith of dark gray, aeolian bedforms [67]. The plains-forming sandstone is considerably more erodible than the lavas explored by Spirit at Gusev crater [137], and the dark gray, erosion-resistant sandstones in Gale crater. The full lateral extent of the Burns formation is not known; however, rocks of similar properties extend across the Meridiani region [168,340,433] and are exposed in northern Meridiani as mesas, buttes, and pinnacles (Figure 5b).

Other sandstone landform configurations likely occur on Mars. Meter-scale cross-bedding observed in mountainside outcrops of the sulfate-bearing rock unit in Aeolis Mons, Gale crater, have been interpreted to indicate that some this material is aeolian sandstone [191,434]; and two additional (non-sulfate-bearing) meter-scale cross-bedded stratal packages that occur higher in Aeolis Mons stratigraphy have also been interpreted as aeolian sandstones [22,201,435]. Similar meter-scale cross-bedding features occur in three of the four light-toned, sulfate-bearing, layered rock exposures (two of which are mounds) in Juventae Chasma [25]. These features, too, are suggestive of aeolian sandstones [25]. Yardang-forming rock on Mars might also include sandstones, but these do not form exclusively in sandstones on Earth [107,156]. Polygonal fracture patterns can occur in some Martian sandstones but can be absent from others.

3.8.2. Conglomerate Landforms

Migoñ [109] recently summarized current knowledge of conglomerate landforms on Earth. Perspectives on Martian conglomerate landforms is limited. Some of the depositional setting mimicry cases, such as alluvial fans and deltas, likely include conglomerates (Sections 3.5.2 and 3.5.3). Presently, the most extensive experience with in-place Martian conglomerate comes from the Curiosity site in Gale crater. When the rover landed, its terminal descent engines (Figure 34a) exposed conglomerate bedrock (Figure 34b) [245,436]. As viewed in MARDI descent images and HiRISE orbiter images (Figure 34c,d), the terrain on which Curiosity landed was described as having relief elements that are "rugged" and "hummocky" [79]. This terrain retains impact structures (Figure 34d), but not with the abundance of the neighboring, cratered sandstone that Curiosity's heat shield impacted (Figures 3 and 34d). Prior to landing, no one had experience that could have been used to predict that these observations were a sign of a conglomeratic bedrock. In general, the conglomerate where Curiosity landed is modestly erosion-resistant and pebbles, liberated from the rock, litter the ground (Figure 18a). As described in Section 3.4.6, another example of conglomerate landform configuration in Gale comes from the Kimberley field site, where terrain formed from a conglomeratic bedrock simply appears "smooth" and "hummocky" in HiRISE 0.25 m/pixel images (Figure 18d,e).

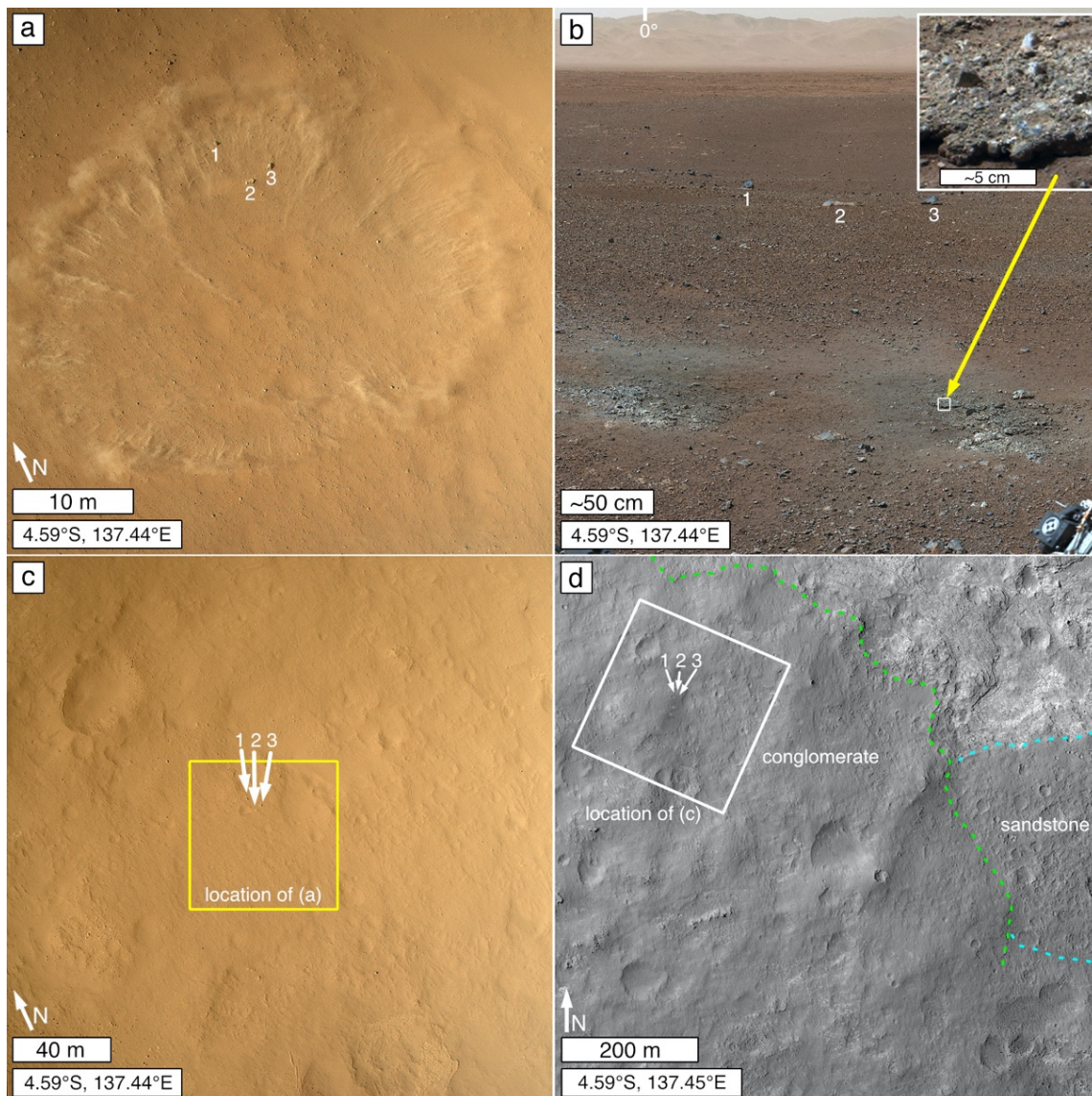


Figure 34. Conglomerate landscape as viewed by Curiosity from and above its Bradbury Landing field site. (a) Aerial image acquired during descent; engine impingement removed dust to expose the conglomerate bedrock seen in (b); for spatial reference, boulders labeled 1, 2, and 3 are identified in (a–d); MARDI 0000MD0000000000100526C00. (b) The view, looking north, at Bradbury Landing, with two patches of gray conglomerate at the Goulburn outcrop (see inset) exposed by the descent engines; note thin, pebbly regolith; Sol 3 Mastcam-34 mosaic (sequence 000007), azimuth 0° indicated; inset Sol 13 Mastcam-100 0013MR0000120070100046E01. (c) Aerial view of Bradbury Landing from a higher altitude, note “smooth” appearance of terrain mantled by thin, pebbly regolith; note impact crater retention; location of (a) is indicated; MARDI 0000MD0000000000100501C00. (d) Satellite view of Bradbury Landing; note “smooth” and “hummocky” nature of the conglomerate landscape and the difference in impact crater retention between it and the cratered sandstone (Figure 3) at the lower right; HiRISE ESP_034572_1755, acquired 11 December 2013.

3.8.3. Finestone Landforms

Finestones are clastic rocks that consist largely of grains smaller than sand size. The term is not used on Earth, but is preferred here to discuss rocks that encompass a range of clastic sedimentary rock types that consist of particles finer than sand: siltstones, mudstones (also known as shales), loessites, and duststones. Finestone is also a term that could be applied to very fine to extremely fine tuffs, where they cannot be distinguished from their sedimentary counterparts.

The terms siltstone, mudstone, loessite, and duststone are applicable to cases for which data are available to unambiguously determine the depositional conditions of the sediment. For example, to call a rock a mudstone requires knowledge—from sedimentary structures, facies, context, etc.—that the clasts were wet (i.e., mud) at the time of deposition. Identification of loessites requires knowledge that the materials consist of silt-sized grains deposited by wind [437,438]. The presence of loess or loessite does not require that the silt was produced by glacial processes [439], nor that they are composed of quartz. Duststone is a term coined specifically for Mars by Bridges and Muhs [440] that refers to knowledge that the material was deposited by settling out of suspension from the Martian atmosphere. Duststone is a term less restrictive than loessite with regard to particle size distribution, as long as the particles are generally of sizes transported in suspension in the Martian atmosphere. Particles that can travel in long-term aerial suspension [441] on Mars generally consist of silt- and clay-sized particles [442]. No loessite or duststone has been definitively identified at a rover field site on Mars.

A minor finestone facies was observed in the Burns formation at Meridiani Planum [443]. However, most of what is known about finestone landforms comes from examination of the mudstones of the >350-m-thick Murray formation in Gale crater [79,80,189,190,405]. In the highest spatial resolution satellite and aerial images acquired to date, layering in the Murray formation is not readily apparent (Figure 10a). Images acquired from the ground, however, show that the rocks are finely laminated at sub-millimeter to millimeter scales (Figure 10b,c). Polygonal fracturing and local displacement of fractured blocks—visible in HiRISE 0.25 m/pixel images—are common in some parts of the Murray formation (Figures 5d and 33e). Aeolian erosional forms (kharafish) are generally not evident in the existing satellite and aerial image data set, but millimeter- and centimeter-scale forms caused by aeolian abrasion are common in rover camera views [165,444]. One possible exception regarding aeolian erosion at scales visible in satellite images is a suite of parallel ridges interpreted as periodic bedrock ridges [445], which would have formed in Murray formation rocks as saltating grains abraded inter-bedform substrates between former (now gone) aeolian megaripples [255,256].

Murray formation finestones generally have a recessive erosional expression [80,446]. Areas with abundant, erosion-resistant veins can locally increase resistance to erosion and influence outcrop appearance. Although generally recessive, finestones, such as the Murray formation, can occur in positive-relief landforms in cases where an erosion-resistant cap rock has broken down and its debris removed at a pace that exceeded that of the gradation of the finestone beneath it. Further, the Vera Rubin ridge literally stands out as an exception to the recessive nature of the Murray formation (Figure 16). The rocks exposed on Vera Rubin ridge experienced diagenetic changes that differ from most of the other Murray formation mudstones; these changes might have rendered the rock more resistant to erosion [190,218,219,447]. Alternatively, Vera Rubin ridge was previously protected from erosion by a capping rock or coarse debris; this possibility is suggested by the fact that a similar ridge, capped by an erosion-resistant material, occurs west of Vera Rubin ridge (Figure 16d). It is actually possible that both things are true; that the ridge was protected from erosion by a previous capping material and its resistance to erosion was enhanced by late diagenetic alterations that occurred beneath, or at the interface with, this capping material. Surfaces that appear to be “smooth” in HiRISE 0.25 m/pixel images occur in the recessive Glen Torridon valley immediately south of Vera Rubin ridge; rover images show

(Figure 18b,c) that this smooth appearance results from a regolith that consists of abundant, pebble-sized mudstone fragments produced by the breakdown of the local bedrock [246].

3.8.4. Chemical Sediment Landforms

Earth has landforms and landscapes influenced by differential erosion of chemical sediment occurrences—and clastic materials cemented by chemical sediments—that formed in surface/near-surface environments in contact with meteoric waters [129]. For example, duricrusts can resist erosion and help leave former streams and ponds standing as inverted topography [177,448]. Whether similar chemical sediments occur on Mars is uncertain, but appears to be likely. The sulfate-bearing sandstones of the Burns formation [57] of Meridiani Planum were, for example, interpreted to consist (at least in part) of sand-sized aggregates of sulfate-bearing muds (containing detrital silicates) formed in ancient, evaporative playa settings [449]. In addition, an apparently stratified, clast-bearing, calcium sulfate pebble was found in a conglomerate boulder at the Curiosity rover site [61]. It was tentatively interpreted as a chemical sediment rock fragment [61]. However, the stratal package that the fragment came from is unknown.

Beyond the Burns formation in Meridiani Planum, and that one, mysterious pebble—and its less-well observed counterparts in the same boulder [61]—in Gale crater, the next best candidates for chemical sediments on Mars occur at the locations identified, using satellite-borne near-infrared or thermal-infrared remote sensing instruments, as having chlorides [310,450,451] or carbonates [29,384,452,453] present. It is unclear whether remote detections of sulfate-bearing rocks, beyond Meridiani Planum, are necessarily indicative of chemical sediments (e.g., evaporites) or diagenetic fluids.

Bridges et al. [454] provided a recent review regarding Martian carbonates. In general, most occurrences are not considered to be sediments [384,452,453,455], but might result from various rock alteration pathways (e.g., weathering, diagenesis, hydrothermal, serpentinization), particularly involving alteration of olivine. “Comanche Class” rocks studied using the Spirit rover in Gusev crater were interpreted as clastic [370] and to contain Mg-Fe carbonates [455]. These carbonates might have formed under hydrothermal conditions [455] or precipitated among silicate clasts in a lacustrine setting [369]. A promising candidate carbonate sedimentary rock occurrence lies at the crater wall/floor interface in western Jezero crater [29]. These Jezero crater examples occur in close proximity to fluvial and lacustrine landforms, including a remnant delta at the terminus of Neretva Vallis [29]. These carbonate-bearing rocks—whether a sediment or not—exhibit low surface relief, are light-toned, fractured, retain some (but not abundant) impact structures, and are described as having “blocky,” and “ridge-forming” morphologies (Figure 35a) [29,31]. Such descriptions are not likely diagnostic of carbonate chemical sediments; appropriate near- or thermal-infrared spectroscopy remains highly recommended to make such detections.

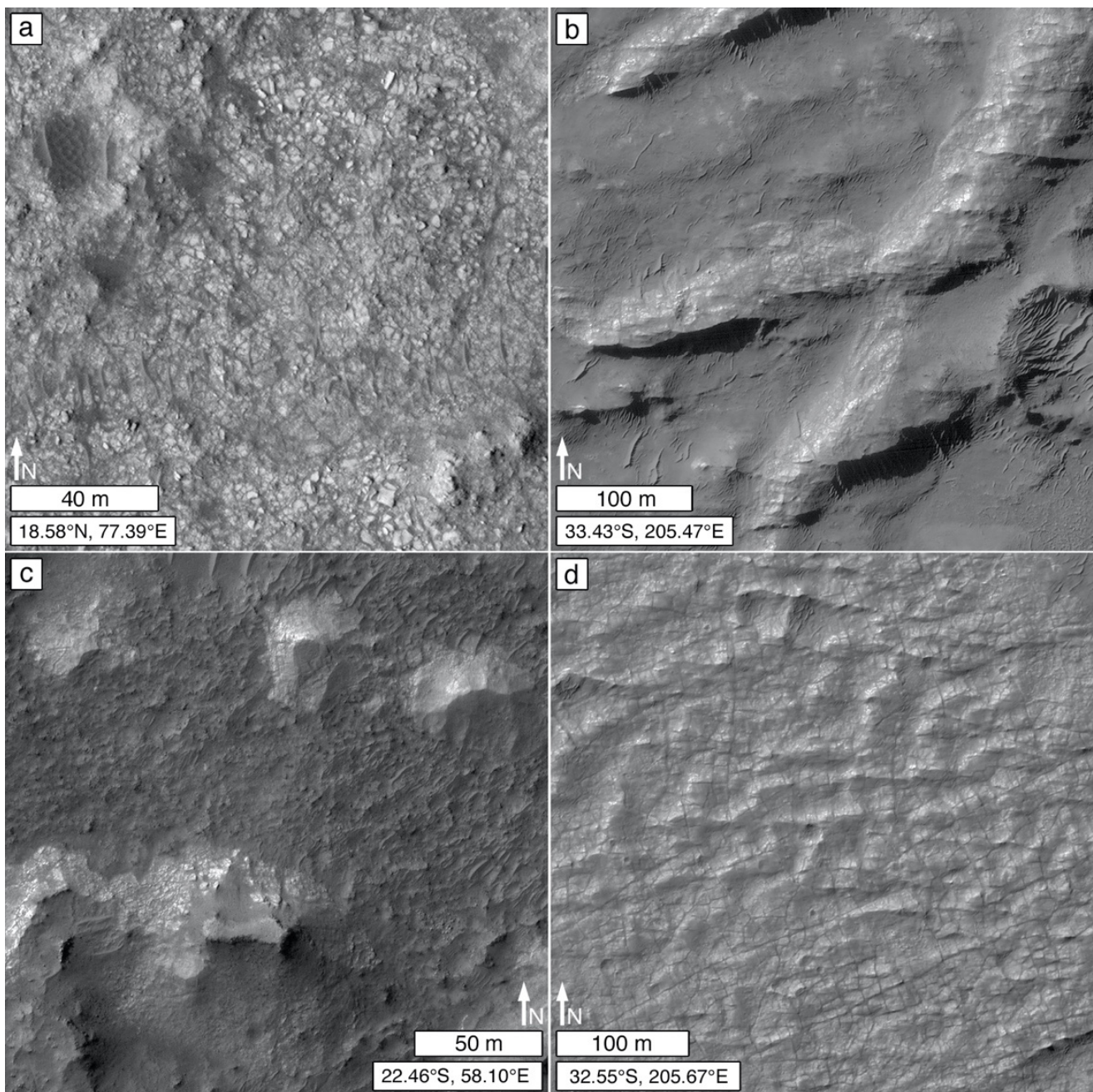


Figure 35. Example landforms associated with proposed carbonate and chloride-bearing sediments. (a) Terrain (resembling outcrops of Murray formation mudstone in Gale crater; e.g., Figures 5d and 33e) described by Horgan et al. [29] as an erosional expression of candidate lacustrine carbonate in western Jezero crater; HiRISE PSP_002387_1985. (b) Fluvial ridges marking the location of former stream courses [450]; although mantled with a dark-toned material, the light-toned rock exposed in the ridges was proposed by Osterloo et al. [450] to be chloride-bearing sediment; HiRISE PSP_009318_1465. (c) Buttes and erosional-remnant hills composed of light-toned material (proposed chloride-bearing sediment [450]) capped by a darker-toned, more erosion-resistant rock; HiRISE PSP_007649_1575. (d) Light-toned, ridged rock exposure, with polygonal, open-fractures, in material proposed to be chloride-bearing sediment [450]; HiRISE ESP_045383_1470.

The first satellite-based chloride salt detections resulted from observation by the ODY THEMIS-IR, a multispectral thermal infrared imaging instrument that images Mars at ~100 m/pixel [310]. Additional detections have been made using the near-infrared hyperspectral capabilities of the ~18 m/pixel MRO Compact Reconnaissance Imaging Spectrometer for Mars (CRISM) instrument [451,456]. Hundreds of locales have been identified [450]. They generally occur throughout the heavily cratered terrain in local

topographic lows with areal extents ranging 0.33 to 1300 km² [450]. In some cases, channels or fluvial ridges (inverted channels) converge on the low area [450,456–458], and in some of these cases, chlorides are detected in the channels or on the ridges [450]. The chlorides occur in association with silicic mineral fines (primary rock-forming minerals and/or clay minerals [310,450,459,460]). Colleagues have argued for and against the ideas that these chloride deposits record ancient groundwater upwellings, playas, or deeper lakes that lasted decades or more [310,450,456–461]; the convergence of fluvial channels and ridges at some of these locations argues strongly that some of them, at least, resulted from runoff of surface water (brines).

As with carbonates, we recommend that satellite or aerial near- or thermal-infrared spectroscopy is best employed to detect chloride sites. However, because there are hundreds of them, we can comment on some of their geomorphic elements in the context of chemical sediment landforms. As noted, they usually occur in localized topographic lows in inter- and intracrater settings in the Martian heavily cratered terrain [450]. The chloride occurrences are usually light-toned rocks; Figure 35b–d shows some of the variety of geomorphic expressions of chloride-bearing materials identified on Mars. Some occurrences are found in channel bottoms or compose sinuous ridges (Figure 35b) interpreted as topographically inverted channels [310,450]. Some occurrences include small buttes or hills capped by a more erosion-resistant material (Figure 35c) [450,456] some surfaces are ridged (Figure 35d) [450]; and some are emergent from beneath other rock strata (Figure 35c) [450]. Whether the materials are internally stratified (as best as can be determined in 0.25–6 m/pixel satellite images) has rarely been noted. About 75% of the occurrences are fractured meaning that about 25% are not [450]. Those that are fractured typically display intersecting, open (or aeolian sand- or regolith-filled) fractures that break-up the outcrop into polygonal patterns (Figure 35d) [450,459,461]. However, some polygonal patterns result from erosion-resistant ridges, rather than open fractures [450,459,461]. Polygonal patterns have received considerable attention with regard to interpretations of the desiccation of lake muds or playas [450,459,461], although little or no comparison with the plethora of other polygonally fractured sedimentary rock occurrences on Mars have been made.

4. Discussion

As the preceding section emphasizes, distinction of sedimentary rock occurrences in satellite and aerial images of Mars can be easy, in some cases, and very challenging in others. Presently unrecognized occurrences most certainly exist. In this section, we explore two remaining concerns: (1) the depth of burial at which Martian clastic sediment becomes rock, and (2) the global distribution of Martian sedimentary rocks. Both of these matters are unresolved and important to discuss because they point the way toward future work.

4.1. *Clastic Sediment Diagenesis and Depth at which Sediment Becomes Rock*

The settings in which clastic sediment lithification occur are very important to deciphering the geological history of Mars. Was a given sediment buried, compacted, cemented, and later returned to the surface as rock, or was it cemented in the surface/near-subsurface environment and never deeply buried? For example, was the delta in Eberswalde crater (Figure 1b) deeply (hundreds of meters to kilometers) buried and then exhumed? How deep was it buried? How much overburden had to be removed before the deltaic form was visible? Where did the overburden go? Alternatively, was the Eberswalde delta never buried, or only buried to a shallow depth, with its clasts cemented in the presence of meteoric waters by materials analogous to Earth's ferricretes, silcrettes, gypcretes, and calcrettes?

4.1.1. Perspectives on Burial Diagenesis from Gale Crater

The Salsberry Peak sandstone is a dark gray, erosion-resistant, plateau-forming rock (Figure 2) that occurs within the Pahrump Hills member of the Murray forma-

tion [74,80,189]. The Pahrump Hills member outcrops on the lower north flank of Aeolis Mons, the 5-km-high mountain in Gale crater. A boulder produced by breakdown of the Salsberry Peak sandstone was accessible to the Curiosity rover (Figure 2). Named Kanosh, MAHLI images of the boulder surface (Figure 2c) show 130–500 μm -sized sand grains that were cut across by either the fracturing that produced the boulder, aeolian abrasion, or both. The sandstone is very well-cemented; pits occur where grains were removed during diagenesis or weathering, but intergranular pore space is not visible. Rocks coeval with this sandstone, and the other sandstones and mudstones of the Pahrump Hills member [80,189] project southward into lower Aeolis Mons. Above these rocks lies ~ 4.5 km of additional strata. Thus, the sediments of very well-cemented Salsberry Peak sandstone, and the Pahrump Hills mudstones, are known to have been buried to at least ~ 4.5 km depth.

In contrast, a stratal package of boulder-producing layered rock occurs at the summit of Aeolis Mons (Figure 36), ~ 4.5 km above the Salsberry Peak sandstone [16,48]. These rocks are exposed at an elevation ~ 2.2 km above the crater's north rim, and lie ~ 800 m below the highest elevation on its south rim (Figure 36a). Because the layered materials at the summit of Aeolis Mons are lithified, does that mean that they were also, like the Salsberry Peak sandstone, once buried at several kilometers' depth, so as to become lithified? Knowing whether rocks exposed at the summit of Aeolis Mons in Gale crater were once at some depth below ground would have profound implications for the geological and hydrological history of the region, particularly if all of Gale crater—and the areas around it—were mostly buried.

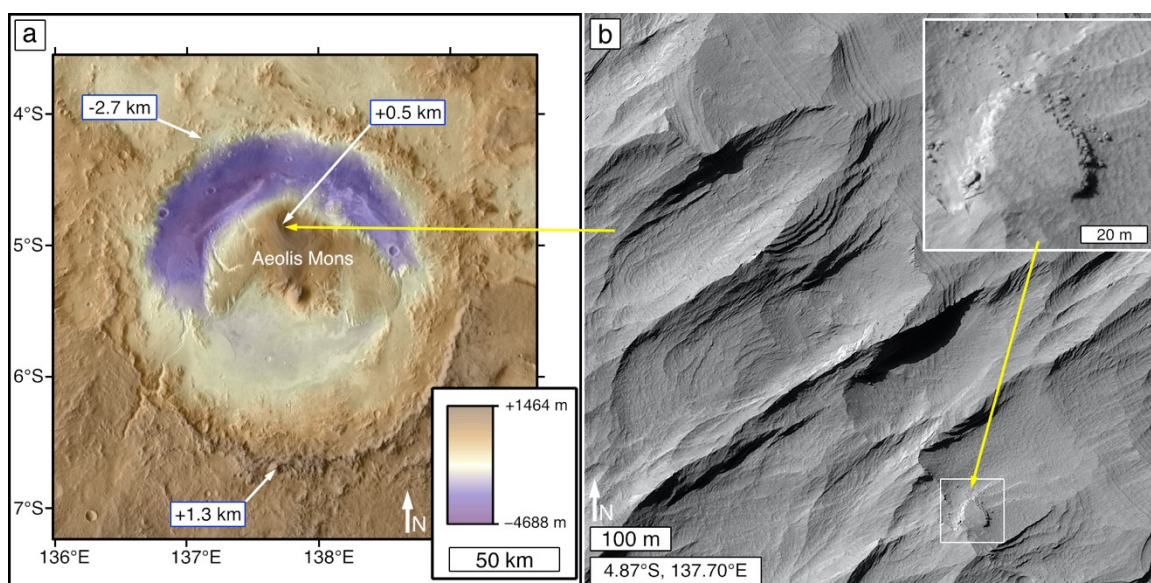


Figure 36. Stratified rock at the top of Aeolis Mons in Gale crater produces boulders as it erodes. (a) Context topographic map of Gale crater and Aeolis Mons, showing location of (b) at the summit; note the key elevations, with a low of -2.7 km on the northwest crater rim, $+1.3$ km on the south rim, and $+0.5$ km—higher than the north rim—higher than the north rim—at the mountain summit; daytime THEMIS-IR mosaic [336] combined with the Ferguson et al. [337] topographic product. (b) Stratified rocks—expressed in cliff-bench form and likely coated by aeolian dust—at the summit of Aeolis Mons; inset shows rock fractures and dislodgement that produced boulders as escarpments retreat; HiRISE PSP_009927_1750.

4.1.2. Burial and the Transition of Clastic Sediment to Rock

The scientific literature on clastic sediment diagenesis on Earth is vast, in part because of the value of this information (particularly regarding porosity and permeability) to the exploration for oil and gas e.g., [126,462–465]. Less common, however, are observations that show the transition of sediment to rock as a function of depth and diagenetic conditions. One such example comes from a submarine setting captured in a 1927-m-long core extracted off the east coast of South Island, New Zealand [466]. It showed fine-grained siliciclastic

and calcareous marine sediments transitioning from uncompacted sediment to rock. In the first ~50 m below the ocean floor, the sediment only exhibited signs of early diagenesis. As depth increased, a transition occurred between ~50 and ~350 m toward sediment compaction. Compacted sediments began to appear at 347 m depth; porosity loss due to compaction became more pronounced below 1300 m, and stylolites (jagged pressure solution features; see example in Figure 37) began to appear around 1600 m depth [466]. Of course, in detail, burial diagenesis involves more than just the pressures imposed by burial. Studies of the sediments deposited in the Gulf of Mexico, for example, provide insight into the complexities regarding the roles of pressure, temperature (which increases with depth), fluid chemistry, and the porosity and permeability of layered sediment of varied compositions and particles sizes, e.g., [130,467].

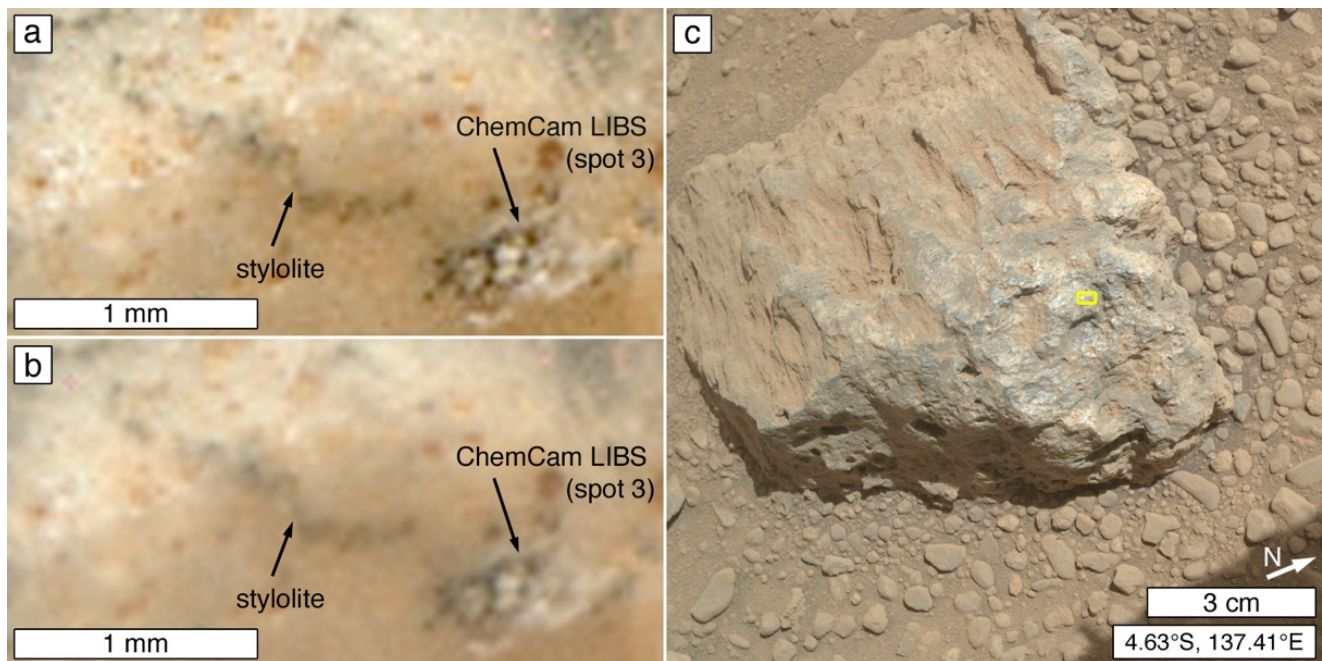


Figure 37. Example of a stylolite (pressure solution feature) observed on Mars. (a) Sharpened view of a stylolite exposed on a white rock surface near a pit created by Curiosity’s ChemCam Laser-Induced Breakdown Spectroscopy (LIBS) instrument [468]; MAHLI focus merge product 0512MH-0001630000200884R00. (b) Unsharpened view; in both cases (a,b) the figure is an expansion from the original image size. (c) Context; yellow box indicates location of (a,b); this MSL Sol 512 target, named Clinton, is a stone encountered along Curiosity’s drive toward Aeolis Mons. MAHLI image 0512MH0001900010200841C00. No other stylolite examples have been identified in MAHLI images (as of January 2021).

4.1.3. Forming Clastic Sedimentary Rock with Little or no Burial

While most clastic sedimentary rocks on Earth were formed during deep burial diagenesis, some were not. This is an important consideration for Mars. A key example to contrast with deep burial on Earth is the quartz beach and dune sands of the Oligocene Fontainebleau grés (sandstone) in France [172–175]. The sands are overlain by limestones and their maximum burial depth was ~100 m. Although emergent from beneath younger rock, most of the Fontainebleau sands are uncemented, except in very tightly-cemented lenses 2–8 m thick located at various levels and sites within the sand body [172–174]. These lenses are so well-cemented that they have sometimes been called quartzite [172]. These lenses do not result from the temperature and pressure effects of deep burial diagenesis but, instead, from silicification associated with the influences of climate, geomorphology (e.g., stream and pond locations), groundwater levels, and the geochemistry of meteoric fluids [172–174].

Other examples of earthy clastic sedimentary rocks that form or begin to form without deep burial diagenesis include aeolian beach sands cemented by carbonates in the subaerial,

littoral environment [469,470], aeolian gypsum sands that begin to cement in the presence of meteoric waters [128], and clastic sediments cemented by 'crete-forming (silcrete, ferricrete, calcrete, dolocrete, gypcrete) mineral or amorphous materials [129]. For example—and although further field investigations are needed to confirm many details—it appears that nearly 60% of the clastic sediments in Earth's known fluvial ridges (inverted channels) were cemented in surface and near-subsurface environments [177]. Chemical precipitate sediments (e.g., evaporites, tufa, and travertine)—which can, in some cases, contain clastic sediments—also form rock in surface and near-subsurface aqueous settings e.g., [471,472].

4.1.4. Martian Clastic Sedimentary Rock Formed under Conditions of Little to no Burial?

Until analyses from new and on-going exploration at the Perseverance and Zhurong rover sites are reported in the scientific literature, Mars offers at least one additional, important data point regarding sediment diagenesis and depth of burial, the Burns formation studied via the Opportunity rover in Meridiani Planum. There, the rover science team's interpretation was that sandstones of the Burns formation are largely aeolian dune sediments [57,203,204] with some water-lain (wet interdune) facies [57,58,418]. The wind-transported clasts were considered to be aggregates of basaltic, and perhaps clay-mineral-bearing [473], playa muds cemented by sulfates [449]. Subjected to multiple diagenetic episodes involving groundwater [57,449], the rocks might not have been buried more than ~80 m [474]. This depth assessment is based on the proposed erasure of Hesperian-aged impact craters [474]. Whether the Burns formation was more deeply buried at the time of lithification is not known, but the interpreted setting is consistent with the idea of a shallow or surface/near-surface diagenetic setting.

4.1.5. Clastic Sediment Diagenesis on Mars, Looking Forward

Martian clastic sediment diagenesis, the distinction of diagenetic from weathering influences on sediment composition, and the depths of burial involved, are at the frontier of Mars geoscience. To become lithified, clastic sediments must first be retained. Sediment deposited on a dry hilltop is less likely to be retained than sediment deposited in a wet basin setting. Earth instructs us, and—through Gale crater and Meridiani Planum—Mars has begun to inform us, that the planet likely has a continuum of clastic sediment burial depths and lithification conditions. We should not expect a single "depth of burial" that leads to clastic sediment lithification on Mars. A minimum depth of burial can be known for Martian sediments that are exposed on slopes for which overburden rock remains intact (e.g., the Salsberry Peak sandstone; Figure 2). However—and unlike the submarine core sample extracted near South Island, New Zealand [466]—these Martian burial depths do not tell us about the actual depth at which the sediment first became rock. In addition, identification of clastic sedimentary rocks lithified in the surface/near-subsurface environment—such as the nearly 60% of fluvial ridges on Earth [177]—will likely remain challenging for years to come, although colleagues are trying (and should continue to try) to identify such examples using relevant remote sensing techniques and understanding of Earth analogs [177,276].

4.2. Global Distribution of Martian Sedimentary Rocks

Early maps indicating where sedimentary rocks occur on Mars [48–50,115,475] have not been updated to reflect newer observations made over the last decade [476]. Indeed, based on the results presented here—and the general challenges of distinguishing sedimentary rocks from tuffs (Section 3.6.7) [72,312]—mapping the global distribution of sedimentary rocks exposed at the Martian surface is likely to be challenging and take many years to accomplish.

Here, we explore four key questions that, if addressed through new research, would greatly impact understanding of where Martian sedimentary rocks occur and the depth and breadth of the record of past environments available for study: (1) how much of the bedrock of the upper crust of Mars in its heavily cratered terrains consists of sedimentary rock? (2) Are there sedimentary rocks among the strata exposed in the walls of the Valles

Marineris? (3) What percentage of the rocks composing the Medusae Fossae Formation [82] consist of sedimentary versus igneous facies? (4) Are there sedimentary rocks beneath the northern lowland plains of Mars?

4.2.1. Sedimentary Rocks of the Martian Heavily Cratered Terrain?

Mariner 4, 6, and 7 Mars flyby images acquired in the 1960s showed that some fraction of the Martian surface is heavily cratered, like the moon, but (as compared with the moon) many of the impact craters were shallowed by material deposited in them and by widening of their walls and lowering of their rims by erosion [477,478]. Even back then, some impact structures appeared to contain fill materials that had been subsequently eroded [479] (p. 19).

The interface between the Martian surface and atmosphere on early Mars would have been a fragment production factory—impact cratering would create rock fragments and solidified melt droplets [294], volcanism would include volcaniclast production [480], and weathering processes would have broken down exposed rock surfaces, altered primary minerals, and carried ions away in solution [481]. Weathering would also have extended into the subsurface in the presence of groundwater, as occurs in cavernous and fractured rock (even siliciclastic rock [240,427]) on Earth. Once produced, the clasts of early Mars would have been subjected to (and, in some cases, sorted by) transport and deposition in aeolian, fluvial, lacustrine, mass movement, and perhaps glacial [233,482] environments. Impact craters, intercrater lows, and tectonically-formed depressions, would have served as depositional basins for these sediments [48,49,324,326].

Large portions of the bedrock of the Martian heavily cratered terrains are likely obscured by regolith, mantled by aeolian dust [483], mantled with presently or previously ice-bearing regolith or dust [484,485], or buried beneath south polar layered deposits and ices [121,486,487]. However, some regions do exhibit exposures of intercrater and intracrater rock [12,72,312,488–490]. Among these, and in particular, are portions of western, central, eastern, and northeastern Arabia Terra.

Arabia Terra is an important gift to Mars science. Despite considerable aeolian dust cover [68,483,491], the landscape is one that has been eroded in a manner that reveals the nature of the upper crust of the Martian heavily cratered terrain. Western Arabia Terra was so deeply eroded that it retains few valley networks [492] and impact structures once filled and buried have been excavated and returned to the surface [493]. Fluvial ridges, also known as inverted channels, are common across Arabia Terra [26,292], further attesting to the erosion of this landscape. Erosion throughout Arabia Terra has revealed the layered nature not only of materials deposited in impact structures [17,18,28,49,251,410,494], but also in the intervening, intercrater terrain [9,12,48,68,493,495–497]. Some percentage of the stratified rock that composes the upper Martian crust in Arabia Terra is sedimentary (Figure 19e, Figure 22a, Figure 23a,d, and Figure 25b–f) e.g., [12,26,27,292,493], although full understanding of the percentage awaits future study. In general—and modulated by proximity to volcanic regions [312]—the stratified inter- and intra-crater rocks of Arabia Terra could be representative (although specific lithologies may vary) of what lies beneath the surface in all of the other, less deeply eroded, heavily cratered terrains of Mars [185].

4.2.2. Sedimentary Rocks Exposed in the Walls of the Valles Marineris?

Stretching ~4160 km across the southern low-latitudes of Mars, the walls, intra-chasm ridges, and plateaus of the Valles Marineris, and associated Hebes and Juventae chasms, expose (laterally) more than 27,400 km of pre-chasm, Martian upper crust to depths that exceed more than 8 km, in places. The surrounding terrain includes wrinkle-ridged plains, lavas and volcanoes, impact craters, filled and partly filled impact structures, and heavily cratered terrain [327,498–502]. As implied by the very first geologic maps of the region [498,503], where the uplands surrounding the Valles Marineris are not heavily-cratered, the stratigraphy argues that ancient, heavily-cratered bedrock lies beneath the present surface and has been cut and exposed in the chasm walls.

Orbiter images of the walls of the Valles Marineris and associated chasms show that they are stratified [347,349,504]. This is known despite the fact that vast portions of the Valles Marineris walls are covered with material that obscures the bedrock. Some of this obscuration is talus, landslide debris [505], alluvial fans [506], aeolian bedforms, light-toned aeolian dust, and dark-toned mantling deposits of uncertain origin (tephra falls? aeolian silt and sand?). Some sections exhibit packages of erosion-resistant “strong” layers and erosion-recessive “weaker” layers (Figure 28) [349]. Some of the chasm walls at the east end of the Valles Marineris exhibit stratal packaging of layered rocks overlying dark-toned, poorly-layered or structureless (“massive”) boulder-producing materials, which, themselves, overlie lighter-toned, fractured, structureless rock of proposed magmatic origin [504]. These lower rocks are cut by mafic dikes [507,508] and the country rock adjacent to them has been subjected to visible alteration by contact metamorphism [507].

The layered rocks exposed in the Valles Marineris walls are mostly dark-toned and often interpreted as lavas, sometimes with a caveat that some amount of regolith, tephra, impact ejecta, and sediment could be interbedded with these materials [347,509]. Except where Valles Marineris walls intersect and cut through lava flows expressed at the present Martian surface, the case for lava deeper in chasm wall stratigraphy seems to have been a “looks like” argument—that some of the outcrop expressions resemble those of escarpments cut into flood basalt strata on Earth [510]. More evidence would be helpful. For example, a key signal of the likelihood of lava or intrusive magma is columnar jointing (Section 3.6.2). However, no columnar joints, or column-shaped boulders shed from columnar-jointed outcrops, have yet been identified in the strata of the Valles Marineris and associated chasms [24,502]. Of course, columnar joints too small to be identified in HiRISE 0.25 m/pixel images could be present, and candidate columnar jointing has been observed in some of the dikes exposed in the Valles Marineris [508]. Others have suggested that some of the layered rocks in the Valles Marineris might be crystallized, layered plutons [511], and still others suggest some of the “weaker” strata might be tuffs [480].

The distinction of stratified (and structureless at observable scales) sedimentary rocks from lavas, tuffs, sills, buried impact melt rocks, and paleosols (paleo-regoliths) exposed in the walls of the Valles Marineris is not easy and, thus, no examples of dark- or intermediate-toned sedimentary rock have yet been definitively identified [504]. Given the likelihood that, based on observations of Arabia Terra (Section 4.2.1), the sedimentary rocks may be common in the heavily cratered regions of Mars, and that the walls of the Valles Marineris (and associated chasms) had to have cut through heavily cratered terrain bedrock, it seems plausible that some of the rock exposed in the chasm walls has to be sedimentary. Observations from the Curiosity rover site in Gale crater show that sedimentary rocks exposed in the Valles Marineris walls need not be light-toned, can be dark-toned, can even be mafic, and can be sufficiently resistant to erosion so as to resemble the erosion resistance of lavas, sills, and impact melt rocks. In that case, both the “weak” and “strong” layers of Beyer and McEwen [349] have the potential to be sedimentary.

In addition to the darker-toned wall rocks, there is the question of whether light-toned, stratified rocks are exposed in various places in the walls of the Valles Marineris, and whether these are records of very ancient sediments (or tuffs) deposited before the chasms opened up, or deposited in the chasms after they opened up, or were deposited in precursor basins at various stages as the chasms slowly began to open. Based on a survey of the scientific literature, the latter hypothesis is generally favored [10,512–518]. However, some investigators have concluded that there do exist examples of light-toned rock—generally considered to be sedimentary, but could in some cases be tuffs—emergent from within Valles Marineris chasm wall strata [24,25,49,185,407,519,520]. The most frequently accepted occurrence is at “mound A” in southwestern Juventae Chasma (Figure 38a) [24,25,407,519,520]. Additional candidates have been identified in the ridge that separates north-central Candor Chasma from southwestern Ophir Chasma (Figure 38b–d) [49,185], a feature in Ganges Chasma called “Ganges 5” [342], a light-toned rock exposure called “feature D” in Juventae Chasma [24,25], occurrences in the lower walls of northwest Candor Chasma [519],

southern Melas Chasma [519], Hebes Chasma [519], southwestern Candor Chasma [185], the upper walls in a portion of Ganges Chasma [185], and on the Nectaris Montes in Coprates Chasma [185]. Light-toned, stratified rock in the Coprates Montes ridge in Coprates Chasma has been variously interpreted as an exposure of pre-chasm sedimentary rock [185] or as sediments deposited and lithified in a precursor depression that formed during a proposed multi-stage opening of Coprates Chasma [516]. A light-toned, wind-eroded, stratified rock occurrence “perched” [514] in an alcove above northwestern Coprates Chasma has also been variously interpreted as pre-chasm rock [185]—such as sediment filling a buried impact structure—or the eroded remnants of sediment deposited and lithified within a precursor depression during the period of the opening of the chasms [514,521]. In the former model, the alcove exists because of the pre-chasm presence of light-toned rock of relatively poor erosion resistance; as it was exposed by the extensional faulting and mass movement that opened the chasms, the more erosion-resistant overburden was undermined, broken-down, and removed by erosion, forming the alcove.

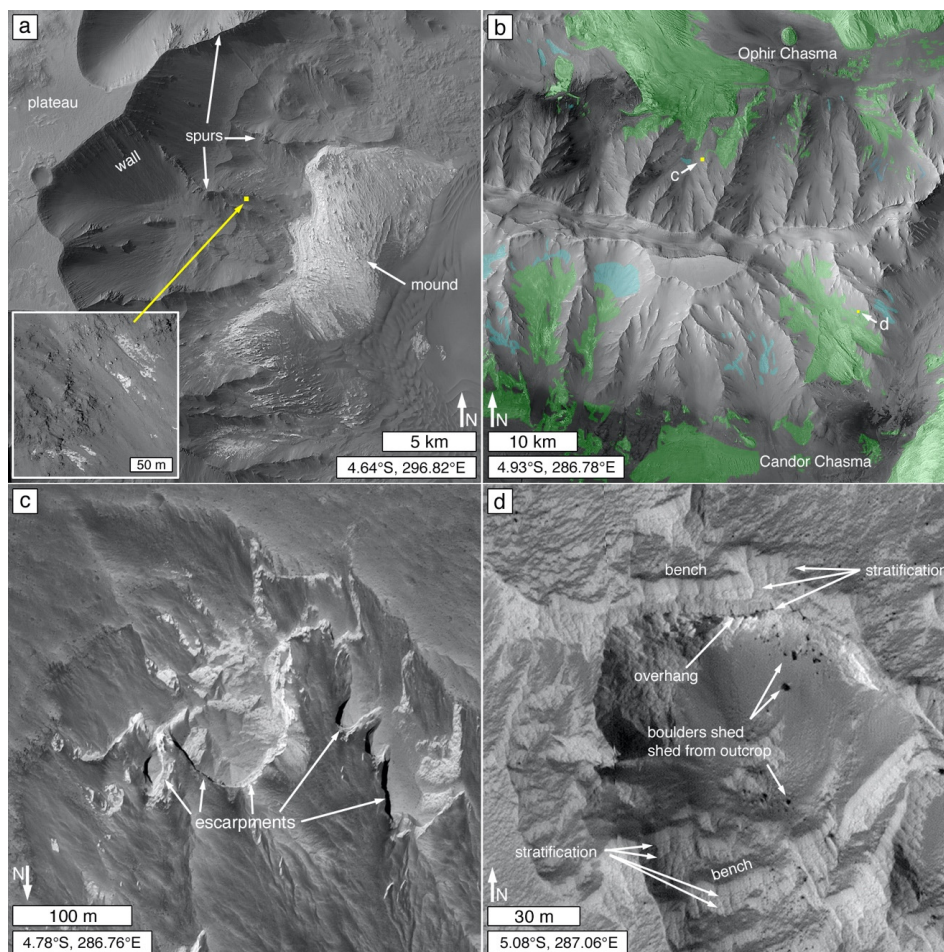


Figure 38. Example candidate cases of light-toned rock outcropping in Valles Marineris walls. (a) Example from southwestern Juventae Chasma; the light-toned mound is stratified rock that appears to be partially emergent from within wall rock spurs [24,25,407,519,520]; inset shows example (slope is toward lower right); CTX B20_017279_1751_XN_04S063W; inset is from HiRISE PSP_005557_1755. (b) The ridge (with an axial trough) that separates southwest Ophir Chasma from northern Candor Chasma contains various patches of light-toned rock [49,185]; sketched green pattern indicates light-toned rock; blue indicates candidate occurrences; the locations of (c,d) are indicated; mosaic of CTX P12_005676_1746_XI_05S073W, P13_006243_1746_XN_05S073W, P03_002208_1748_XN_05S072W. (c) Example light-toned, slope- and scarp-forming rock that outcrops from a spur in the wall of Ophir Chasma; downward slope is toward bottom; sunlight from the right; HiRISE ESP_033393_1750. (d) Example light-toned, stratified, wind-scoured rock that outcrops below a spur in the wall of north Candor Chasma; note overhang and tumbled-down boulders; HiRISE ESP_012018_1750.

There has been a general resistance to acceptance of evidence that light-toned, stratified rocks outcrop at some locations in the walls of the Valles Marineris. That resistance discourages investigation of this model and leads to a bias, which assumes that all such occurrences must be erosional remnants of sediment or tephra deposited in the chasms after they opened up, or during successive episodes of their opening and widening [10,498,499,512–518,522]. The resistance might stem, at least in part, from a misinterpretation of the Malin and Edgett [49] model, which viewed the rocks exposed in the Valles Marineris walls as heterolithic in both a lateral and vertical sense, reflective of the heterolithological appearance of the deeply-eroded terrains of western Arabia Terra [9,12,18,493]. Imagine, for a moment, what western Arabia Terra looked like before the deep erosion that erased some—and topographically inverted other—valley networks [292,492], and exhumed filled and buried impact structures [493]. Now, imagine using some earthmoving equipment to cut a several-kilometers wide and several-kilometers deep trench across that western Arabia paleo-landscape. What would be seen in the walls of that trench? Evident would be the same lateral and vertical lithological diversity, including dark- and light-toned strata of differing resistance to erosion, which we see exposed planimetrically in the region today. Now, imagine what lies buried beneath the terrain cut by the Valles Marineris. Should the walls of the Valles Marineris, and associated chasms, not also reveal a similar lithological diversity that includes rocks of differing tone and resistance to erosion, as well as various filled and buried impact structures and former intercrater terrain?

The question of Valles Marineris (and associated chasms) wall rock lithologies remains unresolved. Many excellent observations have been documented [24,324,347,349,396,502,504,505,507,519,523], but work remains to be done to decipher whether it is true that intrinsically-light-toned rocks of relatively poor erosion resistance are exposed in various patches and locations in these walls, whether “weak” or even “strong” stratal packages include sedimentary rocks, whether columnar joints (other than in magmatic dikes [508]) occur in any of the rocks, and whether filled and buried impact structures and filled, former valleys or channels can be identified in the rocks.

4.2.3. Sedimentary Rocks in the Medusae Fossae Formation?

Like the walls of the Valles Marineris, the Medusae Fossae Formation (Figure 39) presents additional challenges to identifying sedimentary rock occurrences on Mars [48], in part because of four decades of interpretation and assumption that the material is tuff [82,303]. The Medusae Fossae Formation is a suite of yardang-forming [524] and butte-, mesa-, and fractured-plateau-forming [305] rock units that occur in a discontinuous zone that stretches along the equator between western Tharsis and southern Elysium Planitia (Figure 39a) [82]. The rocks are stratigraphically younger than, and partly straddle [327,328], the Martian topographic dichotomy boundary [525]. Most of these rocks occur on the northern, lowland side of the boundary. Where they occur south of the boundary, they unconformably overlie bedrock previously heavily cratered and cut by fluvial valleys. Outlier remnants occur both north and south of the main bodies of the unit, suggesting that it was once more extensive [526,527]. In the northern lowlands, Medusae Fossae Formation rocks in some areas overlie, and in others are embayed (and buried) by, lava flows [224,303,528–531]. Fluvial sediment and sedimentary fan deposits, exhibiting depositional setting mimicry, occur in terrain adjacent to or emergent from beneath Medusae Fossae Formation rocks in the south-central (e.g., Figure 39d) [301] and western (e.g., Figure 39e), e.g., [13,19,532,533] parts of the region.

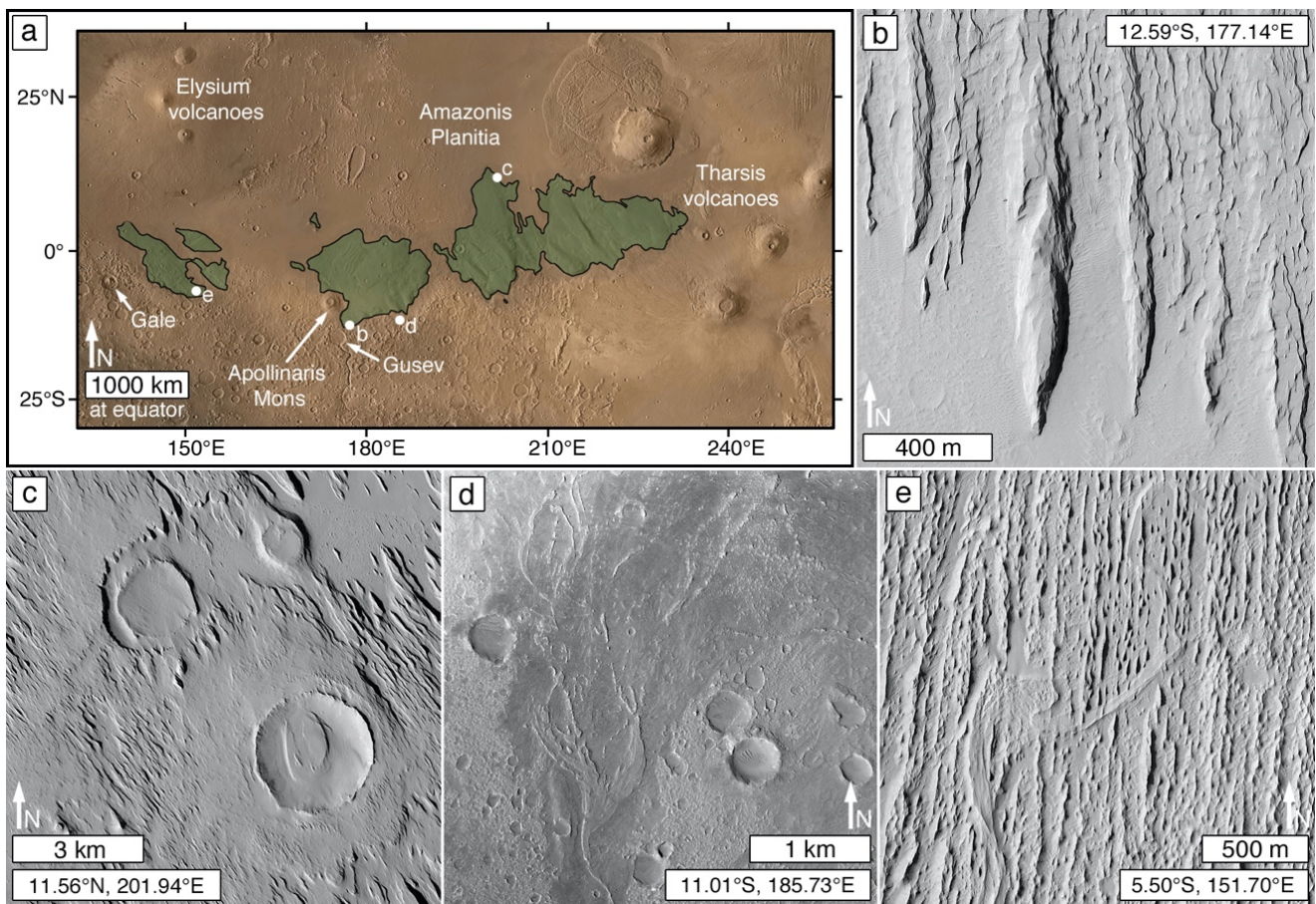


Figure 39. Medusae Fossae Formation extent and example features. (a) Map showing regional extent (in green) of the Medusae Fossae Formation based on Kerber and Head [528]; locations of (b–e) are indicated in white; MGS MOC wide angle geodesy campaign mosaic [416] overlain on shaded relief map created from MGS MOLA data [534]. (b) Example of typical Medusae Fossae Formation yardangs; HiRISE ESP_041929_1675. (c) Example of a typical attribute of the Medusae Fossae Formation, the burial, exhumation, and—in some cases—inversion (to form circular mesas) of impact structures; CTX J06_047018_1919_XI_11N158W. (d) One of several examples [301] of ridges composing a fluvial sedimentary fan exposed in the south-central Medusae Fossae Formation region. (e) One of many examples e.g., [13,19,270,532,535] of fluvial ridges among the yardangs of the western portion of the Medusae Fossae Formation.

In most areas, Medusae Fossae Formation rocks lie beneath a mantle of aeolian dust [483,536] and—in some areas—the rocks are covered by dust-coated or (less commonly) dust-free aeolian sand [528,537,538]. The materials retain some impact craters, but few enough that the rocks were considered for several decades to be Amazonian in age [301,327,328,539]. Later analyses, focused on impact crater counts and embayment or interbedding of Medusae Fossae Formation rocks with lavas, suggested that deposition might have begun during the Hesperian [302,528,540].

Because wind eroded some of the material to create yardangs (Figure 39b,c), and yardangs on Earth usually consist of clastic materials [156], Medusae Fossae Formation rocks have long been considered to be clastic [303,381]. The formation is not, however, monolithic [82]; in some analyses, these rocks have been subdivided into lower, middle, and upper stratigraphic members based on erosional expressions that are, reasonably, assumed to be connected to rock stratigraphic and physical properties [327,328]. High spatial resolution orbiter images show features that suggest these rocks can be further subdivided into more specific units and facies [304,305,528], including some that may be fluvial (e.g., Figure 39e) [13,19,70,235,541]. Whether the fluvial materials are properly part of the Medusae Fossae Formation, or a preceding formation, is debatable; certainly, some

of the fluvial sediments, expressed as ridges, might have become ridges before they were buried beneath yardang-forming material (Figure 39e).

A vital question regarding the Medusae Fossae Formation is whether it exhibits a lithological diversity commensurate with the observed geomorphic diversity [304,305], and whether some percentage of the materials are sedimentary rock [48]. A variety of interpretations for the origin of the materials have been proposed over the last > 4 decades, including pyroclastic flows (ignimbrites) [303,305,381], airfall tephra [304,381], aeolian sediment [328,542], marine-rafted pumice [543], marine carbonate platforms [544], and paleo-polar dust and ice mixtures [545].

Interpretations that the Medusae Fossae Formation consists of primary volcanics have generally dominated the discussion [82,303]. The proximity of the rocks to the volcanoes and lava flows of the Tharsis, Amazonis, Elysium, Apollinaris, and Cerberus Fossae regions provide the necessary volcanic context (Figure 39a). Further, models of possible tephra dispersal patterns [236,380] suggest that a relation between the volcanoes and the Medusae Fossae Formation is possible. However, the interpretation that the rocks consist of primary volcanoclastic material conflates two topics that should be considered separately: (1) the depositional processes and settings recorded by the rocks, and (2) the genesis of the clasts that compose the rocks. Interpretations regarding the relatively low density of the rocks [382,546,547] conflate a third topic: (3) the porosity of the rock, which is a product of the physical nature of the primary deposits and their diagenesis, including fracturing. Although the low density was interpreted by some [382,547] as an indicator of primary volcanics, density is not a signal of clast genesis.

As noted, the presence of yardangs in the Medusae Fossae Formation is a signal that the materials are likely clastic [381,524], but interpreting the material as clastic says nothing of clast genesis. Aeolis Mons (Mt. Sharp) in Gale crater illustrates the point. A few investigators have interpreted the yardang-forming rocks—and the other rock units exposed at and just below the mountain summit—to be erosional outliers of the Medusae Fossae Formation [301,302,527]. More recently, investigations of these rocks show that most of them, except the uppermost rock unit (Figure 36) [16,48], exhibit meter-scale cross bedding in rover and orbiter images, suggesting the materials were deposited as aeolian dunes [22,191,434,435]. Other depositional structures observed in some of these rocks might actually be fluvial [434]. Whether the yardang-forming rocks—and other rock units high in the stratigraphy on Aeolis Mons—are truly outliers of the Medusae Fossae Formation, or not, they certainly display depositional structures reflective of sedimentary environments and exhibit no evidence as to clast genesis or any relation to volcanism.

Unless the rocks reflective of fluvial sedimentation in the central and western areas of the Medusae Fossae Formation (e.g., Figure 39d,e) [13,19], and the upper stratigraphic units of Aeolis Mons in Gale crater, are part of the Medusae Fossae Formation, then no one has yet (or otherwise) performed the necessary, detailed analyses of depositional and deformational structures in the majority of the formation. Such studies are now possible with 100% orbiter image coverage at 0.25–6 m/pixel. If some rock units in the formation are ignimbrites [303] then such analyses would help pinpoint vent locations, a key concern regarding the ignimbrite hypothesis [548]. Such mapping would help discern the various depositional facies recorded in the Medusae Fossae Formation. In lieu of such detailed work, Figure 40 shows some features observed in various parts of the formation that appear to be depositional structures; these include an example of an erosional unconformity (Figure 40e). In the end, the degree to which the Medusae Fossae Formation includes sedimentary rocks, versus tuffs, remains to be deciphered, but it is possible that considerable amounts of sedimentary rocks are present.

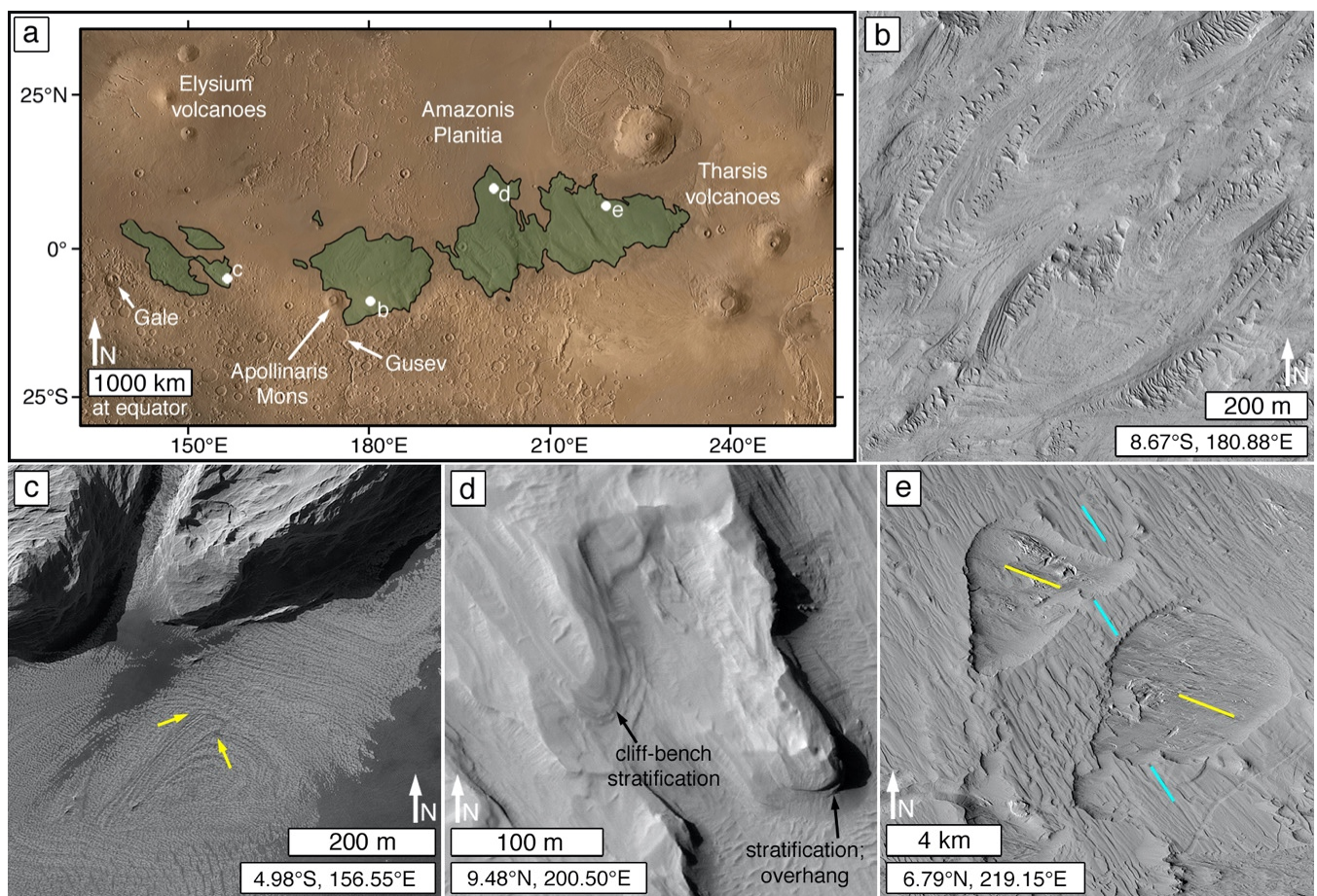


Figure 40. Example depositional structures in Medusae Fossae Formation materials. (a) Map showing location of (b–e) in the Medusae Fossae Formation (green); MGS MOC wide-angle geodesy campaign mosaic [416] overlain on shaded relief map created from MGS MOLA data [534]. (b) Example sharp, hairpin-curved cross-strata; compare with cross-strata described by Rubin and Carter [549] (pp. 60–62); HiRISE ESP_014079_1715. (c) Cross-strata (e.g., arrows) in rock unit beneath a prominent yardang-forming facies (top); HiRISE ESP_026409_1750. (d) Cliff-bench and overhanging erosional expressions of strata in yardang-forming rock; HiRISE ESP_045172_1895. (e) Yardangs exhibiting differing orientations occurring at different stratigraphic levels; these indicate an erosional unconformity, with the earlier (lower; yellow lines indicate orientation) yardang fleet having been buried by the material in which the younger ones (orientation indicated by blue lines) formed [550] (p. 354); CTX G05_020196_1868_XI_06N140W.

4.2.4. Sedimentary Rocks Beneath the Northern Plains?

Evidence for sedimentation in the northern lowlands of Mars—especially from the circum-Chryse outflow channels [500]—has been observed and discussed ever since receipt of images from the orbiter missions of the 1970s [551–554]. Whether the northern lowlands also served as an oceanic sedimentary basin has, likewise, been discussed and debated for several decades [555–559]. Landforms interpreted as mud volcanoes [422,423,560] attest to the possibility of fluid expulsion events over large areas of the proposed sedimentary deposits [561,562]; various flow-like forms and flow fronts suggest intrabasinal sediment transport [552,553,555,563]; and intersecting troughs forming “giant” polygon patterns are suggestive, to some, of compaction of fine-grained sediment resulting from loss of subsurface material such as water or ice [564,565].

The presence of sedimentary deposits in some (or all?) parts of the northern lowlands [566] leads to the question of whether sedimentary rocks are present beneath these landscapes. Burial diagenesis can involve compaction, alone, or compaction and cementation [126]. In addition, the other element of clastic sediment lithification—time—has been plenty; for example, several billion years have elapsed since the circum-Chryse outflow

channel sediments were deposited [566]. Salvatore and Christensen [562,567] proposed that fine-grained, light-toned, stratified sediments deposited in the Chryse and Acidalia basins by outflow channel flood events can be identified in the walls of many impact craters in the region. These layered materials exhibit depositional structures suggestive of sedimentation, such as lenses and pinch-outs, and infrared spectra suggest they contain hydrated minerals [562,567]. Geomorphic evidence for fluid expulsion associated with these sediments (e.g., giant polygons and proposed mud volcanoes [561,562]) strengthen the case that compacted sediments are present [567]. Elsewhere in the northern lowlands, Gross et al. [568] identified stratified rocks containing phyllosilicates, exposed in northern plains impact structures; these, they suggested, could be northern plains sediments or could be much older, sub-basin (e.g., buried, heavily cratered terrain) sediments.

As currently understood, we should expect sedimentary rocks to occur beneath the northern lowland plains of Mars, and Salvatore and Christensen [567] have identified excellent candidate examples. Exposures of northern plains sedimentary rocks are likely to be limited to impact structures, boulders and megaclasts in impact ejecta, and perhaps areas where regolith has been removed by aeolian or fluvial erosion, exposing bedrock, if such surfaces exist. There is also value in recalling the surprisingly “hard,” vesiculated, salt-bearing mudstones produced in near-vacuum conditions in a laboratory forty years ago [569]; these were considered among the various candidate explanations for the vesiculated rocks at the northern lowland Viking 2 lander site [570]. On today’s Mars, we also recognize that ice occurs beneath some of the northern lowland plains [571–573]. The role of ice in terms of contribution or inhibition of Martian sediment diagenesis is unknown.

4.2.5. Additional Challenges

Most recognized Martian sedimentary rock occurrences are found at equatorial to middle latitudes, but this might be a bias with regard to their visibility. There is no reason to expect, for example, that heavily cratered terrain at middle and high latitudes have fewer sedimentary rock occurrences. For instance, the bedrock beneath most of the troughs of the mid-latitude fretted terrain (sensu [398]) north of Arabia Terra is obscured by materials that have been variously interpreted as ice-bearing or as previously ice-bearing “lineated valley fill” e.g., [574–577], but there are areas in the Nilosyrtris Mensae fretted terrain in which such landforms are absent and stratified, likely sedimentary rocks, are observed (Figure 41a) [578]. Sedimentary rocks also occur in a similar setting, in the opposite hemisphere, among the mountains and valleys on the west side of the Argyre impact structure (Figure 41b).

Additional challenges to global identification (and mapping) of sedimentary rock occurrences at and very near the surface of Mars include: (1) middle and high latitude mantling deposits that obscure bedrock [484,485]; (2) the aforementioned blanket of aeolian dust over much of Arabia Terra [483,491]; (3) seasonal frost and the fogs and dust storms that accompany seasonal polar cap retreat and limit frost-free viewing opportunities during parts of late winter and spring at middle to high latitudes; and (4) low image contrast at 50° to 70° south latitude during frost-free periods, interpreted to be a result of dust coatings on surfaces, and subsequent vigorous, spaghetti-like streaking of these surfaces by dust devils, that challenge bedrock visibility and identification.

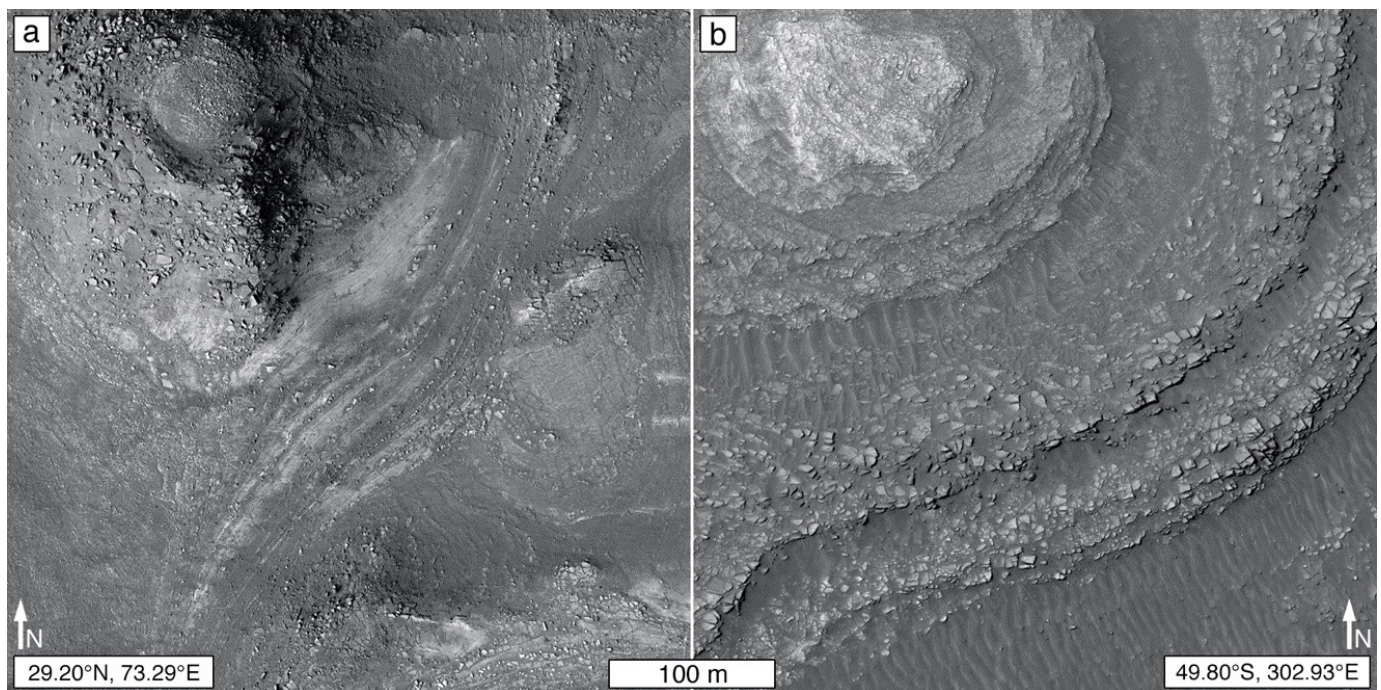


Figure 41. Stratified rock exposures—candidate sedimentary rocks—in middle (or near-middle) latitude regions where most bedrock is obscured by overburden. (a) Example in the Nilosyrtris Mensae region, where much of the bedrock is hidden by fretted terrain “aprons” and “lineated valley fill”; the circular feature at the top of the butte (upper left) might be an impact structure; fine stratification is evident in the lighter-toned area just north of the image center; HiRISE PSP_003231_2095. (b) Example in a valley between the mountains that bound the west side of Argyre Planitia; HiRISE ESP_021947_1300.

5. Concluding Statements

Geology is the pursuit in which all of the sciences meet to tell the history of worlds. It is also the pathway for identification and management of rock, mineral, and geochemical resources. Both of these notions apply to efforts to locate sedimentary rocks on Mars, Venus, Titan, and other bodies, now and in the future. Two decades after the seminal publication regarding the observation of sedimentary rocks on Mars [49], identification of occurrences exposed at the planet’s surface remains challenging and incomplete. In some cases, care must be taken to develop certainty that a feature observed is truly observed, and that one’s hidden assumptions are identified and addressed. Overreliance on previously published interpretations is rarely wise; one should continuously question one’s certitude, and investigators should clearly separate observations from interpretations (and label speculations as such).

We have been careful in this contribution to not use the words, *criteria*, and *criterion*, in the context of identifying Martian sedimentary rock occurrences. There is not—and should not be—a checklist of criteria that guarantee identification (indeed, use of a checklist would be an oversimplification). We hope that what we have done here is to provide some guidance and made it clear that the light-toned, stratified occurrences, the less-common intermediate-toned and “dark mesa-forming” materials [49], and the examples of depositional setting mimicry identified before 2012 [48,69], were a sub-set of a greater whole. We hope we have made it clear that:

1. Some Martian sedimentary rock occurrences have physical properties that permit them to resist erosion and retain small impact craters in a manner similar to lava plains;
2. Tone (e.g., light-toned rocks) can be a property intrinsic to the rock, intrinsic to a coating or weathering rind, or can be a function of rock surface roughness and aeolian

- sediment (light-toned, dust; dark-toned, sand) accumulation on its skyward-facing surface;
3. Pebble-sized clasts can be liberated from conglomerates and breccias, or produced from the breakdown of erosion-resistant, fine-grained rocks, and these pebbles can form lags that give the terrain a “smooth” appearance at image spatial resolutions of (at least) 0.25–6 m/pixel;
 4. Martian sedimentary rocks include examples that are dark-toned and have primary igneous rock compositions (e.g., containing glass, plagioclase, pyroxene, olivine), and remote detection of such rock compositions (e.g., basaltic) should not automatically be interpreted as tuffs or lavas; and
 5. Distinction of sedimentary from igneous rock is not always easy, even when viewed by landed payload cameras at sub-millimeter scales; for cases in which making the distinction is not possible, it is important to acknowledge the observational reason(s) as to why.

A key concern going forward is to separate questions of clast genesis from the processes of clast deposition and depositional setting. The > 4 decades of dialog regarding the Medusae Fossae Formation, for example, teaches us to worry less about clast genesis before being concerned with the geological record of depositional conditions. Over the 1979–1982 period, cases were made on the basis of erosional expression that the Medusae Fossae Formation rocks must be clastic. Most of the discussion, since then, focused on whether the large volume of clasts was produced by explosive volcanism. However, the proposed clasts cannot be seen without in situ investigation, and, thus, their genesis cannot actually be known. There is presently a higher value in encouraging renewed study of the large CTX, HiRISE, and CaSSIS data sets to consider (or reconsider) the depositional (and diagenetic, if present) structures in the Medusae Fossae Formation (e.g., Figure 40) and interpret the depositional facies present.

Although obscured by regolith, aeolian dust, or mid-latitude landforms and materials in some regions, sedimentary rocks might be quite common throughout the Martian heavily cratered terrain—in impact structures, in the spaces between them, and in buried examples of the same. Sedimentary rocks could also have formed from sediments deposited in the northern lowland plains of Mars. With impact events, volcanism, weathering, and erosion making the interface between the early Martian lithosphere, hydrosphere, cryosphere, and atmosphere a clast production factory, and with the wider variety of sedimentary rock landforms now recognized, it is reasonable to anticipate that the upper crust of Mars has a considerably more voluminous sedimentary rock record than previously realized. This record awaits further exploration.

Author Contributions: Conceptualization, K.S.E. and R.S.; methodology, K.S.E. and R.S.; formal analysis, K.S.E. and R.S.; investigation, K.S.E. and R.S.; writing—original draft preparation, K.S.E.; writing—review and editing, K.S.E. and R.S.; visualization, K.S.E. and R.S. All authors have read and agreed to the published version of the manuscript.

Funding: A portion of this research (~75%) was funded between 2012 and 2021 by subcontracts of NASA funds through the California Institute of Technology’s Jet Propulsion Laboratory to Malin Space Science Systems for mission operations and data analysis for the MRO CTX and MSL Mastcam, MAHLI, and MARDI investigations. The remaining portion was self-funded.

Data Availability Statement: Experiment Data Record (EDR) and, where useful, Reduced Data Record (RDR), NASA Mars orbiter and rover camera images used for this study are openly available in the NASA Planetary Data System (PDS; <https://pds.nasa.gov/>, accessed on 27 September 2021). These data include images from MGS MOC-NA (doi:10.17189/1520255), ODY THEMIS-IR (doi:10.17189/1520332), MER Pancam (doi:10.17189/1518988), MER MI (doi:10.17189/1519006), MRO CTX (doi:10.17189/1520266), MRO HiRISE (doi:10.17189/1520303), MSL MARDI (doi:10.17189/1520173), MSL Mastcam (doi:10.17189/1520190), MSL MAHLI (doi:10.17189/1520187; doi:10.17189/1520396), and MSL ChemCam RMI (doi:10.17189/1519494). Derived data products we used include an orthographic mosaic of the Curiosity site in Gale crater by Calef and Parker [345], a global mosaic

of MGS MOC wide angle geodesy campaign images [416]; a shaded relief map produced from the MGS MOLA global topography data set [534]; the global daytime THEMIS-IR map of Mars of Edwards et al. [336] (https://astrogeology.usgs.gov/search/map/Mars/Odyssey/THEMIS-IR-Mosaic-ASU/Mars_MO_THEMIS-IR-Day_mosaic_global_100m_v12; accessed on 27 September 2021), and the combined Mars Orbiter Laser Altimeter (MOLA) and High Resolution Stereo Camera (HRSC) topography product of Ferguson et al. [337].

Acknowledgments: We are grateful to the MRO HiRISE team for their public image target suggestion program, HiWISH, which allowed us to alert them to hundreds of targets observed in CTX images for which they then acquired HiRISE views that we used to address some of our hypotheses regarding candidate locations of sedimentary rock on Mars. We are also grateful to the thousands of personnel that built and operated the Mariner, Viking, MGS, ODY, MRO, and MSL missions, NASA's Deep Space Network, and NASA's Planetary Data System, for more than 55 years of amazing data collection, archiving, and analysis, all of which contributed to our ability to conduct this research. We thank the anonymous peer reviewers and the Academic Editor for their helpful comments and suggestions.

Conflicts of Interest: The authors declare no conflict of interest.

References

1. Wood, L.J. Quantitative geomorphology of the Mars Eberswalde delta. *Geol. Soc. Am. Bull.* **2006**, *118*, 557–566. [CrossRef]
2. Dromart, G.; Quantin, C.; Broucke, O. Stratigraphic architectures spotted in southern Melas Chasma, Valles Marineris, Mars. *Geology* **2007**, *35*, 363–366. [CrossRef]
3. Okubo, C.H.; Lewis, K.W.; McEwen, A.S.; Kirk, R.L. Relative age of interior layered deposits in southwest Candor Chasma based on high-resolution structural mapping. *J. Geophys. Res. Planets* **2008**, *113*, E12002:1–E12002:15. [CrossRef]
4. Fueten, F.; Stesky, R.; MacKinnon, P.; Hauber, E.; Zegers, T.; Gwinner, K.; Scholten, F.; Neukum, G. Stratigraphy and structure of interior layered deposits in west Candor Chasma, Mars, from High Resolution Stereo Camera (HRSC) stereo imagery and derived elevations. *J. Geophys. Res. Planets* **2008**, *113*, E10008:1–E10008:19. [CrossRef]
5. Metz, J.M.; Grotzinger, J.P.; Mohrig, D.; Milliken, R.; Prather, B.; Pirmez, C.; McEwen, A.S.; Weitz, C.M. Sublacustrine depositional fans in southwest Melas Chasma. *J. Geophys. Res. Planets* **2009**, *114*, E10002:1–E10002:17. [CrossRef]
6. Murchie, S.; Roach, L.; Seelos, F.; Milliken, R.; Mustard, J.; Arvidson, R.; Wiseman, S.; Lichtenberg, K.; Andrews-Hanna, J.; Bishop, J.; et al. Evidence for the origin of layered deposits in Candor Chasma, Mars, from mineral composition and hydrologic modeling. *J. Geophys. Res. Planets* **2009**, *114*, E00D05:1–E00D05:15. [CrossRef]
7. Okubo, C.H.; Schultz, R.A.; Chan, M.A.; Komatsu, G.; HiRISE Team. Deformation band clusters on Mars and implications for subsurface fluid flow. *Geol. Soc. Am. Bull.* **2009**, *121*, 474–482. [CrossRef]
8. Okubo, C.H. Structural geology of Amazonian-aged layered sedimentary deposits in southwest Candor Chasma, Mars. *Icarus* **2010**, *207*, 210–225. [CrossRef]
9. Loizeau, D.; Mangold, N.; Poulet, F.; Ansan, V.; Hauber, E.; Bibring, J.-P.; Gondet, B.; Langevin, Y.; Masson, P.; Neukum, G. Stratigraphy in the Mawrth Vallis region through OMEGA, HRSC color imagery and DTM. *Icarus* **2010**, *205*, 396–418. [CrossRef]
10. Sowe, M.; Jaumann, R.; Neukum, G. A comparative study of interior layered deposits on Mars. In *Martian Geomorphology*; Balme, M.R., Bargery, A.S., Gallagher, C.J., Gupta, S., Eds.; Geological Society of London Publications: London, UK, 2011; Volume 356, pp. 281–300. [CrossRef]
11. Ansan, V.; Loizeau, D.; Mangold, N.; Le Mouélic, S.; Carter, J.; Poulet, F.; Dromart, G.; Lucas, A.; Bibring, J.-P.; Gendrin, A.; et al. Stratigraphy, mineralogy, and origin of layered deposits inside Terby crater, Mars. *Icarus* **2011**, *211*, 273–304. [CrossRef]
12. Zabusky, K.; Andrews-Hanna, J.C.; Wiseman, S.M. Reconstructing the distribution and depositional history of the sedimentary deposits of Arabia Terra, Mars. *Icarus* **2012**, *220*, 311–330. [CrossRef]
13. DiBiase, R.A.; Limaye, A.B.; Scheingross, J.S.; Fischer, W.W.; Lamb, M.P. Deltaic deposits at Aeolis Dorsa: Sedimentary evidence for a standing body of water on the northern plains of Mars. *J. Geophys. Res. Planets* **2013**, *118*, 1284–1302. [CrossRef]
14. Stack, K.M.; Grotzinger, J.P.; Milliken, R.E. Bed thickness distributions on Mars: An orbital perspective. *J. Geophys. Res. Planets* **2013**, *118*, 1323–1349. [CrossRef]
15. Rice, M.S.; Bell, J.F., III; Gupta, S.; Warner, N.H.; Goddard, K.; Anderson, R.B. A detailed geologic characterization of Eberswalde crater, Mars. *Mars* **2013**, *8*, 15–57. Available online: <https://www.marsjournal.org/contents/2013/0002/> (accessed on 26 September 2021).
16. Lewis, K.W.; Aharonson, O. Occurrence and origin of rhythmic sedimentary rocks on Mars. *J. Geophys. Res. Planets* **2014**, *119*, 1432–1457. [CrossRef]
17. Cadieux, S.B.; Kah, L.C. To what extent can intracrater layered deposits that lack clear sedimentary textures be used to infer depositional environments? *Icarus* **2015**, *248*, 526–538. [CrossRef]
18. Pondrelli, M.; Rossi, A.P.; Le Deit, L.; Fueten, F.; van Gasselt, S.; Glamoclija, M.; Cavalazzi, B.; Hauber, E.; Franchi, F.; Pozzobon, R. Equatorial layered deposits in Arabia Terra, Mars: Facies and process variability. *Geol. Soc. Am. Bull.* **2015**, *127*, 1064–1089. [CrossRef]

19. Kite, E.S.; Howard, A.D.; Lucas, A.S.; Armstrong, J.C.; Aharonson, O.; Lamb, M.P. Stratigraphy of Aeolis Dorsa, Mars: Stratigraphic context of the great river deposits. *Icarus* **2015**, *253*, 223–242. [[CrossRef](#)]
20. Fraeman, A.A.; Ehlmann, B.L.; Arvidson, R.E.; Edwards, C.S.; Grotzinger, J.P.; Milliken, R.E.; Quinn, D.P.; Rice, M.S. The stratigraphy and evolution of lower Mount Sharp from spectral, morphological, and thermophysical orbital data sets. *J. Geophys. Res. Planets* **2016**, *121*, 1713–1736. [[CrossRef](#)]
21. Stack, K.M.; Edwards, C.S.; Grotzinger, J.P.; Gupta, S.; Sumner, D.Y.; Calef, F.J., III; Edgar, L.A.; Edgett, K.S.; Fraeman, A.A.; Jacob, S.R.; et al. Comparing orbiter and rover image-based mapping of an ancient sedimentary environment, Aeolis Palus, Gale crater, Mars. *Icarus* **2016**, *280*, 3–21. [[CrossRef](#)]
22. Anderson, R.B.; Edgar, L.A.; Rubin, D.M.; Lewis, K.W.; Newman, C. Complex bedding geometry in the upper portion of Aeolis Mons, Gale crater, Mars. *Icarus* **2018**, *314*, 246–264. [[CrossRef](#)]
23. Irwin, R.P., III; Wray, J.J.; Mest, S.C.; Maxwell, T.A. Wind-eroded crater floors and intercrater plains, Terra Sabaea, Mars. *J. Geophys. Res. Planets* **2018**, *123*, 445–467. [[CrossRef](#)]
24. Sarkar, R.; Edgett, K.S.; Singh, P.; Porwal, A. The light-toned stratified sedimentary rock exposures in western Juventae Chasma, Mars, in context. *Icarus* **2018**, *312*, 7–35. [[CrossRef](#)]
25. Sarkar, R.; Edgett, K.S.; Ghosh, D.; Porwal, A.; Singh, P. Tectonic evolution of Juventae Chasma, Mars, and the deformational and depositional structural attributes of the four major light-toned rock exposures therein. *Icarus* **2019**, *333*, 199–233. [[CrossRef](#)]
26. Davis, J.M.; Gupta, S.; Balme, M.; Grindrod, P.M.; Fawdon, P.; Dickeson, Z.I.; Williams, R.M.E. A diverse array of fluvial depositional systems in Arabia Terra: Evidence for mid-Noachian to early Hesperian rivers on Mars. *J. Geophys. Res. Planets* **2019**, *124*, 1913–1934. [[CrossRef](#)] [[PubMed](#)]
27. Day, M.; Edgett, K.S.; Stumbaugh, D. Ancient stratigraphy preserving a wet-to-dry, fluvio-lacustrine to aeolian transition near Barth crater, Arabia Terra, Mars. *J. Geophys. Res. Planets* **2019**, *124*, 3402–3421. [[CrossRef](#)]
28. Annex, A.M.; Lewis, K.W. Regional correlations in the layered deposits of Arabia Terra, Mars. *J. Geophys. Res. Planets* **2020**, *125*, e2019JE006188:1–e2019JE006188:14. [[CrossRef](#)]
29. Horgan, B.H.N.; Anderson, R.B.; Dromart, G.; Amador, E.S.; Rice, M.S. The mineral diversity of Jezero crater: Evidence for possible lacustrine carbonates on Mars. *Icarus* **2020**, *339*, 113526:1–113526:34. [[CrossRef](#)]
30. Day, M.D.; Catling, D.C. Potential aeolian deposition of intra-crater layering: A case study of Henry crater, Mars. *Geol. Soc. Am. Bull.* **2020**, *132*, 608–616. [[CrossRef](#)]
31. Stack, K.M.; Williams, N.R.; Calef, F., III; Sun, V.Z.; Williford, K.H.; Farley, K.A.; Eide, S.; Flannery, D.; Hughes, C.; Jacob, S.R.; et al. Photogeologic map of the Perseverance rover field site in Jezero crater constructed by the Mars 2020 Science Team. *Space Sci. Rev.* **2020**, *216*, 127:1–127:47. [[CrossRef](#)]
32. Quantin-Nataf, C.; Carter, J.; Mandon, L.; Thollot, P.; Balme, M.; Volat, M.; Pan, L.; Loizeau, D.; Millot, C.; Breton, S.; et al. Oxia Planum: The landing site for the ExoMars “Rosalind Franklin” rover mission: Geological context and prelanding interpretation. *Astrobiology* **2021**, *21*, 345–366. [[CrossRef](#)] [[PubMed](#)]
33. Florensky, C.P.; Basilevsky, A.T.; Kryuchkov, V.P.; Kusmin, R.O.; Nikolaeva, O.V.; Pronin, A.A.; Chernaya, I.M.; Tyufin, Y.S.; Selivanov, A.S.; Naraeva, M.K.; et al. Venera 13 and Venera 14: Sedimentary rocks on Venus? *Science* **1983**, *221*, 57–59. [[CrossRef](#)] [[PubMed](#)]
34. Way, M.J.; Del Genio, A.D.; Kiang, N.Y.; Sohl, L.E.; Grinspoon, D.H.; Aleinov, I.; Kelley, M.; Clune, T. Was Venus the first habitable world of our solar system? *Geophys. Res. Lett.* **2016**, *43*, 8376–8383. [[CrossRef](#)]
35. Byrne, P.K.; Ghail, R.C.; Gilmore, M.S.; Celâl Şengör, A.M.; Klimczak, C.; Senske, D.A.; Whitten, J.L.; Khawja, S.; Ernst, R.E.; Solomon, S.C. Venus tesserae feature layered, folded, and eroded rocks. *Geology* **2020**, *49*, 81–85. [[CrossRef](#)]
36. Garvin, J.; Arney, G.; Getty, S.; Johnson, N.; Kiefer, W.; Lorenz, R.; Ravine, M.; Malespin, C.; Webster, C.; Campbell, B.; et al. DAVINCI+: Deep Atmosphere of Venus Investigation of Noble gases, Chemistry & Imaging, plus. In Proceedings of the 51st Lunar and Planetary Science Conference, (Cancelled Meeting; COVID-19 Pandemic), Houston, TX, USA, 16–20 March 2020; Abstract Number 2599. Lunar and Planetary Institute: Houston, TX, USA, 2020. Available online: <https://www.hou.usra.edu/meetings/lpsc2020/pdf/2599.pdf> (accessed on 26 September 2021).
37. Lunine, J.I.; Lorenz, R.D. Rivers, lakes, dunes, and rain: Crustal processes in Titan’s methane cycle. *Annu. Rev. Earth Planet. Sci.* **2009**, *37*, 299–320. [[CrossRef](#)]
38. Barnes, J.W.; Lorenz, R.D.; Radebaugh, J.; Hayes, A.G.; Arnold, K.; Chandler, C. Production and global transport of Titan’s sand particles. *Planet. Sci.* **2015**, *4*, 1:1–1:19. [[CrossRef](#)]
39. Hayes, A.G. The lakes and seas of Titan. *Annu. Rev. Earth Planet. Sci.* **2016**, *44*, 57–83. [[CrossRef](#)]
40. Radebaugh, J.; Ventra, D.; Lorenz, R.D.; Farr, T.; Kirk, R.; Hayes, A.; Malaska, M.J.; Birch, S.; Liu, Z.Y.-C.; Lunine, J.; et al. Alluvial and fluvial fans on Saturn’s moon Titan reveal processes, materials and regional geology. In *Geology and Geomorphology of Alluvial and Fluvial Fans: Terrestrial and Planetary Perspectives*; Ventra, D., Clarke, L.E., Eds.; Geological Society Publication: London, UK, 2018; Volume 440, pp. 281–305. [[CrossRef](#)]
41. Barnes, J.W.; Turtle, E.P.; Trainer, M.G.; Lorenz, R.D.; MacKenzie, S.M.; Brinckerhoff, W.B.; Cable, M.L.; Ernst, C.M.; Freissinet, C.; Hand, K.P.; et al. Science goals and objectives for the Dragonfly Titan rotorcraft relocatable lander. *Planet. Sci. J.* **2021**, *2*, 130:1–130:18. [[CrossRef](#)]
42. Loomis, A.A. Some geologic problems of Mars. *Geol. Soc. Am. Bull.* **1965**, *76*, 1083–1104. [[CrossRef](#)]
43. McKay, C.P.; Nedell, S.S. Are there carbonate deposits in the Valles Marineris, Mars? *Icarus* **1988**, *73*, 142–148. [[CrossRef](#)]

44. Tanaka, T. Examination of Martian sedimentary rocks to understand possible paleo-ocean and its age. In *Workshop on Mars Sample Return Science*; Lunar and Planetary Institute Technical Report 88-07; Drake, M.J., Greeley, R., McKay, G.A., Blanchard, D.P., Carr, M.H., Gooding, J., McKay, C.P., Spudis, P.D., Squyres, S.W., Eds.; Lunar and Planetary Institute: Houston, TX, USA, 1988; p. 166. Available online: <https://hdl.handle.net/20.500.11753/940> (accessed on 26 September 2021).
45. Markun, C.D. Martian sediments and sedimentary rocks. In *Workshop on Mars Sample Return Science*; Lunar and Planetary Institute Technical Report 88-07; Drake, M.J., Greeley, R., McKay, G.A., Blanchard, D.P., Carr, M.H., Gooding, J., McKay, C.P., Spudis, P.D., Squyres, S.W., Eds.; Lunar and Planetary Institute: Houston, TX, USA, 1988; pp. 117–118. Available online: <https://hdl.handle.net/20.500.11753/940> (accessed on 26 September 2021).
46. Ashley, G.M.; Delaney, J.S. If a meteorite of Martian sandstone hit you on the head would you recognize it? In Proceedings of the 30th Lunar and Planetary Science Conference, Houston, TX, USA, 15–19 March 1999; Abstract Number 1273. Lunar and Planetary Institute: Houston, TX, USA, 1999. Available online: <https://hdl.handle.net/20.500.11753/1081> (accessed on 26 September 2021).
47. Lewis, A.S. The sedimentology of Mars: A review. *Vistas Astron.* **1984**, *27*, 25–53. [[CrossRef](#)]
48. Grotzinger, J.P.; Milliken, R.E. The sedimentary rock record of Mars: Distribution, origins, and global stratigraphy. In *Sedimentary Geology of Mars*; Grotzinger, J.P., Milliken, R.E., Eds.; SEPM: Tulsa, OK, USA, 2012; Volume 102, pp. 1–48, ISBN 978-156-576-313-5. [[CrossRef](#)]
49. Malin, M.C.; Edgett, K.S. Sedimentary rocks of early Mars. *Science* **2000**, *290*, 1927–1937. [[CrossRef](#)]
50. Malin, M.C.; Edgett, K.S.; Cantor, B.A.; Caplinger, M.A.; Danielson, G.E.; Jensen, E.H.; Ravine, M.A.; Sandoval, J.L.; Supulver, K.D. An overview of the 1985–2006 Mars Orbiter Camera science investigation. *Mars* **2010**, *5*, 1–60. [[CrossRef](#)]
51. Edgett, K.S.; Malin, M.C. New views of Mars eolian activity, materials, and surface properties: Three vignettes from the Mars Global Surveyor Mars Orbiter Camera. *J. Geophys. Res. Planets* **2000**, *105*, 1623–1650. [[CrossRef](#)]
52. Edgett, K.S.; Malin, M.C. Examples of Martian sandstone: Indurated, lithified, and cratered dunes in MGS MOC images. In Proceedings of the 31st Lunar and Planetary Science Conference, Houston, TX, USA, 13–17 March 2000; Abstract Number 1071. Lunar and Planetary Institute: Houston, TX, USA, 2000. Available online: <https://hdl.handle.net/20.500.11753/1082> (accessed on 26 September 2021).
53. Malin, M.C.; Edgett, K.S. Evidence for persistent flow and aqueous sedimentation on early Mars. *Science* **2003**, *302*, 1931–1934. [[CrossRef](#)]
54. Rover Team. Characterization of the Martian surface deposits by the Mars Pathfinder rover, Sojourner. *Science* **1997**, *278*, 1765–1768. [[CrossRef](#)]
55. Basilevsky, A.T.; Markiewicz, W.J.; Thomas, N.; Keller, H.U. Morphologies within and near the Rock Garden at the Mars Pathfinder landing site. *J. Geophys. Res. Planets* **1999**, *104*, 8617–8636. [[CrossRef](#)]
56. Squyres, S.W.; Arvidson, R.E.; Bell, J.F., III; Brückner, J.; Cabrol, N.A.; Calvin, W.; Carr, M.H.; Christensen, P.R.; Clark, B.C.; Crumpler, L.; et al. The Opportunity rover’s Athena science investigation at Meridiani Planum, Mars. *Science* **2004**, *306*, 1698–1703. [[CrossRef](#)]
57. Grotzinger, J.P.; Arvidson, R.E.; Bell, J.F., III; Calvin, W.; Clark, B.C.; Fike, D.A.; Golombek, M.; Greeley, R.; Haldemann, A.; Herkenhoff, K.E.; et al. Stratigraphy and sedimentology of a dry to wet eolian depositional system, Burns formation, Meridiani Planum, Mars. *Earth Planet. Sci. Lett.* **2005**, *240*, 11–72. [[CrossRef](#)]
58. Metz, J.M.; Grotzinger, J.P.; Rubin, D.M.; Lewis, K.W.; Squyres, S.W.; Bell, J.F., III. Sulfate-rich eolian and wet interdune deposits, Erebus crater, Meridiani Planum, Mars. *J. Sediment. Res.* **2009**, *79*, 247–264. [[CrossRef](#)]
59. Stern, R.J.; Gerya, T.; Tackley, P.J. Stagnant lid tectonics: Perspectives from silicate planets, dwarf planets, large moons, and large asteroids. *Geosci. Front.* **2018**, *9*, 103–119. [[CrossRef](#)]
60. Grotzinger, J.; Beaty, D.; Dromart, G.; Griffes, J.; Gupta, S.; Harris, P.; Hurowitz, J.; Kocurek, G.; McLennan, S.; Milliken, R.; et al. The sedimentary record of Mars. *Sediment. Rec.* **2011**, *9*, 4–8. [[CrossRef](#)]
61. Edgett, K.S.; Banham, S.G.; Bennett, K.A.; Edgar, L.A.; Edwards, C.S.; Fairén, A.G.; Fedo, C.M.; Fey, D.M.; Garvin, J.B.; Grotzinger, J.P.; et al. Extraformational sediment recycling on Mars. *Geosphere* **2020**, *16*, 1508–1537. [[CrossRef](#)] [[PubMed](#)]
62. Condie, K.C. Earth’s oldest rocks and minerals. In *Earth’s Oldest Rocks*; Van Kranendonk, M.J., Bennett, V., Hoffmann, J.E., Eds.; Elsevier: Amsterdam, The Netherlands, 2019; pp. 239–253, ISBN 978-044-463-901-1. [[CrossRef](#)]
63. Harrison, T.M. *Hadean Earth*; Springer Nature: Cham, Switzerland, 2020; ISBN 978-303-046-687-9. [[CrossRef](#)]
64. Arney, G.; Domagal-Goldman, S.D.; Meadows, V.S.; Wolf, E.T.; Schwieterman, E.; Charnay, B.; Claire, M.; Hébrard, E.; Trainer, M.G. The pale orange dot: The spectrum and habitability of hazy Archean Earth. *Astrobiology* **2016**, *16*, 873–899. [[CrossRef](#)]
65. Hesselbrock, A.J.; Minton, D.A. An ongoing satellite–ring cycle of Mars and the origins of Phobos and Deimos. *Nat. Geosci.* **2017**, *10*, 266–269. [[CrossRef](#)]
66. Spalding, C.; Fischer, W.W.; Laughlin, G. An orbital window into the ancient sun’s mass. *Astrophys. J. Lett.* **2018**, *689*, L19:1–L19:6. [[CrossRef](#)]
67. Sullivan, R.; Banfield, D.; Bell, J.F., III; Calvin, W.; Fike, D.; Golombek, M.; Greeley, R.; Grotzinger, J.; Herkenhoff, K.; Jerolmack, D.; et al. Aeolian processes at the Mars Exploration Rover Meridiani Planum landing site. *Nature* **2005**, *436*, 58–61. [[CrossRef](#)]
68. Ferguson, R.L.; Christensen, P.R. Formation and erosion of layered materials: Geologic and dust cycle history of eastern Arabia Terra, Mars. *J. Geophys. Res. Planets* **2008**, *113*, E12001:1–E12001:22. [[CrossRef](#)]

69. Beyer, R.A.; Stack, K.M.; Griffes, J.L.; Milliken, R.E.; Herkenhoff, K.E.; Byrne, S.; Holt, J.W.; Grotzinger, J.P. An atlas of Mars sedimentary rocks as seen by HIRISE. In *Sedimentary Geology of Mars*; Grotzinger, J.P., Milliken, R.E., Eds.; SEPM: Tulsa, OK, USA, 2012; Volume 102, pp. 49–95, ISBN 978-156-576-313-5. [[CrossRef](#)]
70. Treiman, A.H.; Bish, D.L.; Vaniman, D.T.; Chipera, S.J.; Blake, D.F.; Ming, D.W.; Morris, R.V.; Bristow, T.F.; Morrison, S.M.; Baker, M.B.; et al. Mineralogy, provenance, and diagenesis of a potassic basaltic sandstone on Mars: CheMin X-Ray diffraction of the Windjana sample (Kimberley area, Gale crater). *J. Geophys. Res. Planets* **2016**, *121*, 75–106. [[CrossRef](#)] [[PubMed](#)]
71. Yen, A.S.; Ming, D.W.; Vaniman, D.T.; Gellert, R.; Blake, D.F.; Morris, R.V.; Morrison, S.M.; Bristow, T.F.; Chipera, S.J.; Edgett, K.S.; et al. Multiple stages of aqueous alteration along fractures in mudstone and sandstone strata in Gale crater, Mars. *Earth Planet. Sci. Lett.* **2017**, *471*, 186–198. [[CrossRef](#)]
72. Rogers, A.D.; Warner, N.H.; Golombek, M.P.; Head, J.W., III; Cowart, J.C. Areal extent of surface bedrock exposures on Mars: Many are clastic rocks, not lavas. *Geophys. Res. Lett.* **2018**, *45*, 1767–1777. [[CrossRef](#)] [[PubMed](#)]
73. Bedford, C.C.; Schwenger, S.P.; Bridges, J.C.; Banham, S.; Wiens, R.C.; Gasnault, O.; Rampe, E.B.; Frydenvang, J.; Gasda, P.J. Geochemical variation in the Stimson formation of Gale crater: Provenance, mineral sorting, and a comparison with modern Martian dunes. *Icarus* **2020**, *341*, 113622:1–113622:22. [[CrossRef](#)]
74. Kronyak, R.E.; Kah, L.C.; Edgett, K.S.; VanBommel, S.J.; Thompson, L.M.; Wiens, R.C.; Sun, V.Z.; Nachon, M. Mineral-filled fractures as indicators of multigenerational fluid flow in the Pahrump Hills member of the Murray formation, Gale crater, Mars. *Earth Space Sci.* **2019**, *6*, 238–265. [[CrossRef](#)]
75. Calef, F.J., III; Dietrich, W.E.; Edgar, L.; Farmer, J.; Fraeman, A.; Grotzinger, J.; Palucis, M.C.; Parker, T.; Rice, M.; Rowland, S.; et al. Geologic mapping of the Mars Science Laboratory landing ellipse. In Proceedings of the 44th Lunar and Planetary Science Conference, The Woodlands, TX, USA, 18–22 March 2013; Abstract Number 2511. Lunar and Planetary Institute: Houston, TX, USA, 2013. Available online: <https://hdl.handle.net/20.500.11753/1139> (accessed on 26 September 2021).
76. Jacob, S.R. Characteristics and Origin of an Erosionally Resistant Unit in the Mars Science Laboratory Landing Ellipse (Gale crater, Mars), Based on Analyses of Surface Data and Orbital Images. Master's Thesis, University of Hawaii, Honolulu, HI, USA, 2015. Available online: <http://hdl.handle.net/10125/50930> (accessed on 26 September 2021).
77. Anderson, R.; Bridges, J.C.; Williams, A.; Edgar, L.; Ollila, A.; Williams, J.; Nachon, M.; Mangold, N.; Fisk, M.; Schieber, J.; et al. ChemCam results from the Shaler outcrop in Gale crater, Mars. *Icarus* **2015**, *249*, 2–21. [[CrossRef](#)]
78. Edgar, L.A.; Gupta, S.; Rubin, D.M.; Lewis, K.W.; Kocurek, G.A.; Anderson, R.B.; Bell, J.F., III; Dromart, G.; Edgett, K.S.; Grotzinger, J.P.; et al. Shaler: In situ analysis of a fluvial sedimentary deposit on Mars. *Sedimentology* **2018**, *65*, 96–122. [[CrossRef](#)]
79. Grotzinger, J.P.; Sumner, D.Y.; Kah, L.C.; Stack, K.; Gupta, S.; Edgar, L.; Rubin, D.; Lewis, K.; Schieber, J.; Mangold, N.; et al. A habitable fluvio-lacustrine environment at Yellowknife Bay, Gale crater, Mars. *Science* **2014**, *343*, 1242777:1–1242777:14. [[CrossRef](#)]
80. Grotzinger, J.P.; Gupta, S.; Malin, M.C.; Rubin, D.M.; Schieber, J.; Siebach, K.; Sumner, D.Y.; Stack, K.M.; Vasavada, A.R.; Arvidson, R.E.; et al. Deposition, exhumation, and paleoclimate of an ancient lake deposit, Gale crater, Mars. *Science* **2015**, *350*, aac7575:1–aac7575:12. [[CrossRef](#)] [[PubMed](#)]
81. Rivera-Hernández, F.; Sumner, D.Y.; Mangold, N.; Banham, S.G.; Edgett, K.S.; Fedo, C.M.; Gupta, S.; Gwizd, S.; Heydari, E.; Maurice, S.; et al. Grain size variations in the Murray formation: Stratigraphic evidence for changing depositional environments in Gale crater, Mars. *J. Geophys. Res. Planets* **2020**, *125*, e2019JE006230:1–e2019JE006230:18. [[CrossRef](#)]
82. Zimbelman, J.R.; Gregg, T.K.P.; Crown, D.A.; Mouginiis-Mark, P.J.; Barry, W.B. Medusae Fossae Formation and the northern lowlands. In *The Volcanoes of Mars*; Zimbelman, J.R., Crown, D.A., Mouginiis-Mark, P.J., Gregg, T.K.P., Eds.; Elsevier: Amsterdam, The Netherlands, 2021; pp. 138–160, ISBN 978-012-822-876-0. [[CrossRef](#)]
83. Farley, K.A.; Williford, K.H.; Stack, K.M.; Bhartia, R.; Chen, A.; de la Torre, M.; Hand, K.; Goreva, Y.; Herd, C.D.K.; Hueso, R.; et al. Mars 2020 mission overview. *Space Sci. Rev.* **2020**, *216*, 142:1–142:41. [[CrossRef](#)]
84. Li, C.; Zhang, R.; Yu, D.; Dong, G.; Liu, J.; Geng, Y.; Sun, Z.; Yan, W.; Ren, X.; Su, Y.; et al. China's Mars exploration mission and science investigation. *Space Sci. Rev.* **2021**, *217*, 57:1–57:24. [[CrossRef](#)]
85. Balaram, J.; Aung, M.; Golombek, M.P. The Ingenuity helicopter on the Perseverance rover. *Space Sci. Rev.* **2021**, *217*, 56:1–56:11. [[CrossRef](#)]
86. Ray, R.G. Aerial photographs in geologic interpretation and mapping. *U.S. Geol. Surv. Prof. Pap.* **1960**, 373. [[CrossRef](#)]
87. De Hon, R.A.; Barlow, N.G.; Reagan, M.K.; Bettis, E.A., III; Foster, C.T., Jr.; Gulick, V.C.; Crumpler, L.S.; Aubele, J.C.; Chapman, M.G.; Tanaka, K.L. Observation of the geology and geomorphology of the 1999 Marsokhod test site. *J. Geophys. Res. Planets* **2001**, *106*, 7665–7682. [[CrossRef](#)]
88. Fonstad, M.A.; Zettler-Mann, A. The camera and the geomorphologist. *Geomorphology* **2020**, *366*, 107181:1–107181:15. [[CrossRef](#)]
89. Malin, M.C.; Danielson, G.E.; Ingersoll, A.P.; Masursky, H.; Veverka, J.; Ravine, M.A.; Soulanille, T.A. The Mars Observer Camera. *J. Geophys. Res. Planets* **1992**, *97*, 7699–7718. [[CrossRef](#)]
90. Malin, M.C.; Bell, J.F., III; Cantor, B.A.; Caplinger, M.A.; Calvin, W.M.; Clancy, R.T.; Edgett, K.S.; Edwards, L.; Haberle, R.M.; James, P.B.; et al. Context Camera investigation on board the Mars Reconnaissance Orbiter. *J. Geophys. Res. Planets* **2007**, *112*, E05S04:1–E05S04:25. [[CrossRef](#)]
91. McEwen, A.S.; Eliason, E.M.; Bergstrom, J.W.; Bridges, N.T.; Hansen, C.J.; Delamere, W.A.; Grant, J.A.; Gulick, V.C.; Herkenhoff, K.E.; Keszthelyi, L.; et al. Mars Reconnaissance Orbiter's High Resolution Imaging Science Experiment (HiRISE). *J. Geophys. Res. Planets* **2007**, *112*, E05S02:1–E05S02:40. [[CrossRef](#)]

92. Christensen, P.R.; Jakosky, B.M.; Kieffer, H.H.; Malin, M.C.; McSween, H.Y., Jr.; Neelson, K.; Mehall, G.L.; Silverman, S.H.; Ferry, S.; Caplinger, M.; et al. The Thermal Emission Imaging System (THEMIS) for the Mars 2001 Odyssey Mission. *Space Sci. Rev.* **2004**, *110*, 85–130. [[CrossRef](#)]
93. Meng, Q.; Wang, D.; Wang, X.; Li, W.; Yang, X.; Yan, D.; Li, Y.; Cao, Z.; Ji, Q.; Sun, T.; et al. High Resolution Imaging Camera (HiRIC) on China's first Mars exploration Tianwen-1 mission. *Space Sci. Rev.* **2021**, *217*, 42:1–42:29. [[CrossRef](#)]
94. Thomas, N.; Cremonese, G.; Ziethe, R.; Gerber, M.; Brändli, M.; Bruno, G.; Erismann, M.; Gambicorti, L.; Gerber, T.; Ghose, K.; et al. The Colour and Stereo Surface Imaging System (CaSSIS) for the ExoMars Trace Gas Orbiter. *Space Sci. Rev.* **2017**, *212*, 1897–1944. [[CrossRef](#)]
95. Vasavada, A.R.; Grotzinger, J.P.; Arvidson, R.E.; Calef, F.J.; Crisp, J.A.; Gupta, S.; Hurowitz, J.; Mangold, N.; Maurice, S.; Schmidt, M.E.; et al. Overview of the Mars Science Laboratory mission: Bradbury Landing to Yellowknife Bay and beyond. *J. Geophys. Res. Planets* **2014**, *119*, 1134–1161. [[CrossRef](#)]
96. Malin, M.C.; Ravine, M.A.; Caplinger, M.A.; Ghaemi, F.T.; Schaffner, J.A.; Maki, J.N.; Bell, J.F., III; Cameron, J.F.; Dietrich, W.E.; Edgett, K.S.; et al. The Mars Science Laboratory (MSL) mast cameras and descent imager: Investigation and instrument descriptions. *Earth Space Sci.* **2017**, *4*, 506–539. [[CrossRef](#)] [[PubMed](#)]
97. Maki, J.; Thiessen, D.; Pourangi, A.; Kobzeff, P.; Litwin, T.; Scherr, L.; Elliott, S.; Dingizian, A.; Maimone, M. The Mars Science Laboratory engineering cameras. *Space Sci. Rev.* **2012**, *170*, 77–93. [[CrossRef](#)]
98. Le Mouélic, S.; Gasnault, O.; Herkenhoff, K.E.; Bridges, N.T.; Langevin, Y.; Mangold, N.; Maurice, S.; Wiens, R.C.; Pinet, P.; Newsom, H.E.; et al. The ChemCam Remote Micro-Imager at Gale crater: Review of the first year of operations on Mars. *Icarus* **2015**, *249*, 93–107. [[CrossRef](#)]
99. Warner, N.; Silverman, M.; Samuels, J.; DeFlores, L.; Sengstacken, A.; Maki, J.; Scodary, A.; Peters, S.; Litwin, T.; Metz, B. The Mars Science Laboratory Remote Sensing Mast. In Proceedings of the 2016 IEEE Aerospace Conference, Big Sky, MT, USA, 5–12 March 2016. [[CrossRef](#)]
100. Edgett, K.S.; Yingst, R.A.; Ravine, M.A.; Caplinger, M.A.; Maki, J.N.; Ghaemi, F.T.; Schaffner, J.A.; Bell, J.F., III; Edwards, L.J.; Herkenhoff, K.E.; et al. Curiosity's Mars Hand Lens Imager (MAHLI) investigation. *Space Sci. Rev.* **2012**, *170*, 259–317. [[CrossRef](#)]
101. Robinson, M.; Collins, C.; Leger, P.; Carsten, J.; Tompkins, V.; Hartman, F.; Yen, J. In-situ operations and planning for the Mars Science Laboratory robotic arm: The first 200 sols. In Proceedings of the 8th IEEE International Conference on System of Systems Engineering, Maui, HI, USA, 2–6 June 2013; pp. 153–158. [[CrossRef](#)]
102. Heverly, M.; Matthews, J.; Lin, J.; Fuller, D.; Maimone, M.; Beisiadecki, J.; Leichty, J. Traverse performance characterization of the Mars Science Laboratory rover. *J. Field Robot.* **2013**, *30*, 835–846. [[CrossRef](#)]
103. Bell, J.F., III; Squyres, S.W.; Herkenhoff, K.E.; Maki, J.N.; Arneson, H.M.; Brown, D.; Collins, S.A.; Dingizian, A.; Elliot, S.T.; Hagerott, E.C.; et al. Mars Exploration Rover Athena Panoramic Camera (Pancam) investigation. *J. Geophys. Res. Planets* **2003**, *108*, 8063:1–8063:30. [[CrossRef](#)]
104. Herkenhoff, K.E.; Squyres, S.W.; Bell, J.F., III; Maki, J.N.; Arneson, H.M.; Bertelsen, P.; Brown, D.I.; Collins, S.A.; Dingizian, A.; Elliott, S.T.; et al. Athena Microscopic Imager investigation. *J. Geophys. Res. Planets* **2003**, *108*, 8065:1–8065:23. [[CrossRef](#)]
105. Cheng, Y.; Johnson, A.; Matthies, L. MER-DIMES: A planetary landing application of computer vision. In Proceedings of the 2005 IEEE Computer Society Conference on Computer Vision and Pattern Recognition, San Diego, CA, USA, 20–25 June 2005; pp. 806–813. [[CrossRef](#)]
106. Callas, J.L.; Golombek, M.P.; Fraeman, A.A. *Mars Exploration Rover Opportunity End of Mission Report*; National Aeronautics and Space Administration, Jet Propulsion Laboratory, California Institute of Technology; JPL Publication: Pasadena, CA, USA, 2019; p. 56. Available online: <http://hdl.handle.net/2014/47103> (accessed on 26 September 2021).
107. Young, R.W.; Wray, R.A.L.; Young, A.R.M. *Sandstone Landforms*; Cambridge University Press: New York, NY, USA, 2009; ISBN 978-052-187-733-6.
108. Duszyński, F.; Migoń, P.; Strzelecki, M.C. Escarpment retreat in sedimentary tablelands and cuesta landscapes—Landforms, mechanisms and patterns. *Earth Sci. Rev.* **2019**, *196*, 102890:1–102890:42. [[CrossRef](#)]
109. Migoń, P. Geomorphology of conglomerate terrains—Global overview. *Earth Sci. Rev.* **2020**, *208*, 103302:1–103302:22. [[CrossRef](#)]
110. Stow, D.A.V. *Sedimentary Rocks in the Field: A Colour Guide*, 1st ed.; Manson: London, UK, 2005; ISBN 978-187-454-569-9.
111. Maley, T.S. *Field Geology Illustrated*, 2nd ed.; Mineral Land Publications: Boise, ID, USA, 2005; ISBN 978-094-094-905-8.
112. Mainguet, M. *Le Modelé des Grès: Problèmes Généraux*; Institute Géographique National: Paris, France, 1972; Volume 1–2.
113. Härtel, H.; Cílek, V.; Herben, T.; Jackson, A.; Williams, R. (Eds.) *Sandstone Landscapes*; Academia: Praha, Czech Republic, 2007; ISBN 978-802-001-577-8.
114. Peng, H. *China Danxia*; Springer: Singapore, 2020; ISBN 978-981-135-959-0. [[CrossRef](#)]
115. Stack, K.M. Global Distribution of Stratified Rocks on Mars. In Reconstructing Past Depositional and Diagenetic Processes through Quantitative Stratigraphic Analysis of the Martian Sedimentary Rock Record. Ph.D. Dissertation, California Institute of Technology, Pasadena, CA, USA, 2015; pp. 12–56. [[CrossRef](#)]
116. Sgavetti, M. Photostratigraphy of Ancient Turbidite Systems. In *Seismic Facies and Sedimentary Processes of Submarine Fans and Turbidite Systems*; Weimer, P., Link, M.H., Eds.; Springer: New York, NY, USA, 1991; pp. 107–125, ISBN 978-146-848-276-8. [[CrossRef](#)]
117. Sgavetti, M. Criteria for stratigraphic correlation using aerial photographs: Examples from the south-central Pyrenees. *Am. Assoc. Pet. Geol. Bull.* **1992**, *76*, 708–730. [[CrossRef](#)]

118. Lodders, K. Exoplanet chemistry. In *Formation and Evolution of Exoplanets*; Barnes, R., Ed.; Wiley-VCH: Weinheim, Germany, 2010; pp. 157–186, ISBN 978-352-762-976-3. [CrossRef]
119. Neugebauer, G.; Münch, G.; Kieffer, H.; Chase, S.C., Jr.; Miner, E. Mariner 1969 infrared radiometer results: Temperatures and thermal properties of the Martian surface. *Astron. J.* **1971**, *76*, 719–726. [CrossRef]
120. Kieffer, H.H.; Chase, S.C., Jr.; Martin, T.Z.; Miner, E.D.; Palluconi, F.D. Martian north polar summer temperatures: Dirty water ice. *Science* **1976**, *194*, 1341–1344. [CrossRef]
121. Cutts, J.A. Nature and origin of layered deposits of the Martian polar regions. *J. Geophys. Res.* **1973**, *78*, 4231–4249. [CrossRef]
122. Byrne, S.; Murray, B.C. North polar stratigraphy and the paleo-erg of Mars. *J. Geophys. Res. Planets* **2002**, *107*, 5044:1–5044:12. [CrossRef]
123. Smith, P.H.; Tamppari, L.K.; Arvidson, R.E.; Bass, D.; Blaney, D.; Boynton, W.V.; Carswell, A.; Catling, D.C.; Clark, B.C.; Duck, T.; et al. H₂O at the Phoenix landing site. *Science* **2009**, *325*, 58–61. [CrossRef] [PubMed]
124. Fanara, L.; Gwinner, K.; Hauber, E.; Oberst, J. Present-day erosion rate of north polar scarps on Mars due to active mass wasting. *Icarus* **2020**, *342*, 113434:1–113434:6. [CrossRef]
125. Spray, J.G. Lithification mechanisms for planetary regoliths: The glue that binds. *Annu. Rev. Earth Planet. Sci.* **2016**, *44*, 139–174. [CrossRef]
126. Worden, R.H.; Burley, S.D. Sandstone diagenesis: The evolution of sand to stone. In *Sandstone Diagenesis: Recent and Ancient*; International Association of Sedimentologists Reprint Series 4; Burley, S.D., Worden, R.H., Eds.; Blackwell: Oxford, UK, 2003; pp. 3–44, ISBN 978-144-430-445-9. [CrossRef]
127. Chafetz, H.S. Surface diagenesis of limestone. *J. Sediment. Petrol.* **1972**, *42*, 325–329. [CrossRef]
128. Schenk, C.J.; Fryberger, S.G. Early diagenesis of eolian dune and interdune sands at White Sands, New Mexico. *Sediment. Geol.* **1988**, *55*, 109–120. [CrossRef]
129. Nash, D.J.; McLaren, S.J. (Eds.) *Geochemical Sediments and Landscapes*; Wiley-Blackwell: Oxford, UK, 2007; ISBN 978-047-071-291-7. [CrossRef]
130. Land, L.S.; Milliken, K.L.; McBride, E.F. Diagenetic evolution of Cenozoic sandstones, Gulf of Mexico sedimentary basin. *Sediment. Geol.* **1987**, *50*, 195–225. [CrossRef]
131. Fairbridge, R.W. Induration. In *Geomorphology, Encyclopedia of Earth Science*; Springer: Berlin, Germany, 1968; ISBN 978-354-031-060-0. [CrossRef]
132. Sprafke, T.; Obrecht, I. Loess: Rock, sediment or soil—What is missing for its definition? *Quatern. Int.* **2016**, *399*, 198–207. [CrossRef]
133. Neal, J.T. Playas and military operations. In *Military Geology in War and Peace*; Underwood, J.R., Jr., Guth, P.L., Eds.; Geological Society of America Reviews in Engineering Geology, Geological Society of America: Boulder, CO, USA, 1998; Volume 13, pp. 165–172, ISBN 978-081-375-813-8. [CrossRef]
134. Bourke, M.C.; Viles, H.A. (Eds.) *A Photographic Atlas of Rock Breakdown Features in Geomorphic Environments*; Planetary Science Institute: Tucson, AZ, USA, 2007; ISBN 097-852-360-1.
135. Viles, H.; Messenzehl, K.; Mayaud, J.; Coombes, M.; Bourke, M. Stress histories control rock-breakdown trajectories in arid environments. *Geology* **2018**, *46*, 419–422. [CrossRef]
136. Banham, S.G.; Gupta, S.; Rubin, D.M.; Edgett, K.S.; Barnes, R.; Van Beek, J.; Watkins, J.A.; Edgar, L.A.; Fedo, C.M.; Williams, R.M.; et al. A rock record of complex aeolian bedforms in a Hesperian desert landscape: The Stimson formation as exposed in the Murray buttes, Gale crater, Mars. *J. Geophys. Res. Planets* **2021**, *126*, e2020JE006554:1–e2020JE006554:35. [CrossRef]
137. Grant, J.R.; Arvidson, R.E.; Crumpler, L.S.; Golombek, M.P.; Hahn, B.; Haldemann, A.F.C.; Li, R.; Soderblom, L.A.; Squyres, S.W.; Wright, S.P.; et al. Crater gradation in Gusev crater and Meridiani Planum, Mars. *J. Geophys. Res. Planets* **2006**, *111*, E02S08:1–E02S08:23. [CrossRef]
138. Zimbelman, J.R.; Craddock, R.P. An evaluation of probable bedrock exposure in the Sinus Meridiani region of the Martian highlands. In *Proceedings of Lunar and Planetary Science 21*; Sharpston, V.L., Ryder, G., Eds.; Lunar and Planetary Institute: Houston, TX, USA, 1991; pp. 645–655.
139. Chojnacki, M.; Fenton, L.K.; Weintraub, A.R.; Edgar, L.A.; Jodhpurkar, M.J.; Edwards, C.S. Ancient Martian aeolian sand dune deposits recorded in the stratigraphy of Valles Marineris and implications for past climates. *J. Geophys. Res. Planets* **2020**, *125*, e2020JE006510:1–e2020JE006510:24. [CrossRef]
140. Chojnacki, M.; Jodhpurkar, M.; Fenton, L.K.; Edgar, L.A.; Edwards, C.; Weintraub, A.R. Ancient paleo-erg deposits in Apollinaris Sulci—A record of aeolian system change and preservation. In *Proceedings of the 6th International Planetary Dunes Workshop, Virtual Meeting, 12–13 May 2020*; Abstract Number 3020. Lunar and Planetary Institute: Houston, TX, USA, 2020. Available online: <https://hdl.handle.net/20.500.11753/1763> (accessed on 26 September 2021).
141. Rampe, E.B.; Ming, D.W.; Blake, D.F.; Bristow, T.F.; Chipera, S.J.; Grotzinger, J.P.; Morris, R.V.; Morrison, S.M.; Vaniman, D.T.; Yen, A.S.; et al. Mineralogy of an ancient lacustrine mudstone succession from the Murray formation, Gale crater, Mars. *Earth Planet. Sci. Lett.* **2017**, *471*, 172–185. [CrossRef]
142. Lapotre, M.G.A.; Rampe, E.B. Curiosity’s investigation of the Bagnold dunes, Gale crater: Overview of the two-phase scientific campaign and introduction to the special collection. *Geophys. Res. Lett.* **2018**, *45*, 10200–10210. [CrossRef]
143. Okubo, C.H.; McEwen, A.S. Fracture-controlled paleo-fluid flow in Candor Chasma, Mars. *Science* **2007**, *315*, 983–985. [CrossRef]

144. Milazzo, M.P.; Keszthelyi, L.P.; Jaeger, W.L.; Rosiek, M.; Mattson, S.; Verba, C.; Beyer, R.A.; Geissler, P.E.; McEwen, A.S.; HiRISE Team. Discovery of columnar jointing on Mars. *Geology* **2009**, *37*, 171–174. [[CrossRef](#)]
145. Kronyak, R.E.; Kah, L.C.; Miklusicak, N.B.; Edgett, K.S.; Sun, V.Z.; Bryk, A.B.; Williams, R.M.E. Extensive polygonal fracture network in Siccar Point group strata: Fracture mechanisms and implications for fluid circulation in Gale crater, Mars. *J. Geophys. Res. Planets* **2019**, *124*, 2613–2634. [[CrossRef](#)]
146. Sullivan, R.; Arvidson, R.; Bell, J.F., III; Gellert, R.; Golombek, M.; Greeley, R.; Herkenhoff, K.; Johnson, J.; Thompson, S.; Whelley, P.; et al. Wind-driven particle mobility on Mars: Insights from Mars Exploration Rover observations at “El Dorado” and surroundings at Gusev crater. *J. Geophys. Res. Planets* **2008**, *113*, E06S07:1–E06S07:70. [[CrossRef](#)]
147. Baker, M.M.; Lapotre, M.G.A.; Minitti, M.E.; Newman, C.E.; Sullivan, R.; Weitz, C.M.; Rubin, D.A.; Vasavada, A.R.; Bridges, N.T.; Lewis, K.W. The Bagnold dunes in Southern Summer: Active sediment transport on Mars observed by the Curiosity rover. *Geophys. Res. Lett.* **2018**, *45*, 8853–8863. [[CrossRef](#)]
148. Bagnold, R.A. *The Physics of Blown Sand and Desert Dunes*; Methuen: London, UK, 1941; Re-printed Springer: Dordrecht, The Netherlands, 1973; pp. 25–35, ISBN 978-940-095-682-7. [[CrossRef](#)]
149. Embabi, N.S. The karstified carbonate platforms in the Western Desert. In *Landscapes and Landforms of Egypt*; Embabi, N.S., Ed.; Springer: Cham, Switzerland, 2018; pp. 85–104, ISBN 978-331-965-661-8. [[CrossRef](#)]
150. Goudie, A.S. Mega-yardangs: A global analysis. *Geogr. Compass* **2007**, *1*, 65–81. [[CrossRef](#)]
151. Edgell, H.S. *Arabian Deserts: Nature, Origin, and Evolution*; Springer: Dordrecht, The Netherlands, 2006; ISBN 978-140-203-970-6. [[CrossRef](#)]
152. Lancaster, N. Characteristics and occurrence of wind erosion features in the Namib Desert. *Earth Surf. Process. Landf.* **1984**, *9*, 469–479. [[CrossRef](#)]
153. Hamdan, M.A. Sedimentological characteristics and geomorphic evolution of the Holocene playa of Wadi el Obeiyid. In *From Lake to Sand: The Archaeology of Farafra Oasis, Western Desert, Egypt*; Barich, B.E., Lucarini, G., Hamdan, M.A., Hassan, F.A., Eds.; All’Insegna del Giglio: Firenze, Italy, 2014; pp. 81–100, ISBN 978-887-814-520-7.
154. Maghsoudi, M. Hydro-aeolian landforms. In *Desert Landscapes and Landforms of Iran*; Maghsoudi, M., Ed.; Springer Nature: Cham, Switzerland, 2021; pp. 87–98, ISBN 978-303-058-911-0. [[CrossRef](#)]
155. Corbett, I.B. The Sedimentology of Diamondiferous Deflation Deposits within the Sperrgebiet, Namibia. Ph.D. Dissertation, University of Cape Town, Cape Town, South Africa, 1989. Available online: <http://hdl.handle.net/11427/17696> (accessed on 26 September 2021).
156. McCauley, J.F.; Grolier, M.J.; Breed, C.S. Yardangs of Peru and other desert regions. *U.S. Geol. Surv. Interag. Rep. Astrogeol.* **1977**, *81*, 1–177.
157. Inbar, M.; Risso, C. Holocene yardangs in volcanic terrains in the southern Andes, Argentina. *Earth Surf. Process. Landf.* **2001**, *26*, 657–666. [[CrossRef](#)]
158. de Silva, S.L.; Bailey, J.E. Some unique surface patterns on ignimbrites on Earth: A “bird’s eye” view as a guide for planetary mappers. *J. Volcanol. Geotherm. Res.* **2017**, *342*, 47–60. [[CrossRef](#)]
159. Whitney, J.W.; Breit, G.N.; Buckingham, S.E.; Reynolds, R.L.; Bogle, R.C.; Luo, L.; Goldstein, H.L.; Vogel, J.M. Aeolian responses to climate variability during the past century on Mesquite Lake Playa, Mojave Desert. *Geomorphology* **2015**, *230*, 13–25. [[CrossRef](#)]
160. Hamdan, M.A.; Hassan, F.A. Quaternary of Egypt. In *The Geology of Egypt*; Hamimi, Z., El-Barkooky, A., Martínez Frías, J., Fritz, H., Abd El-Rahman, Y., Eds.; Springer: Cham, Switzerland, 2020; pp. 445–493, ISBN 978-303-015-265-9. [[CrossRef](#)]
161. Ding, Z.; Zhao, J.; Wang, J.; Lai, Z. Yardangs on Earth and implications to Mars: A review. *Geomorphology* **2020**, *364*, 107230:1–107230:15. [[CrossRef](#)]
162. Corbett, I.B. Sediment dynamics of the Namib aeolian erosion basin and the arid zone diamond placers of the northern Sperrgebiet, Namibia. In *Geological Processes and Stratigraphy of the Diamond Placers of the Northern Sperrgebiet*; Pickford, M., Ed.; Memoir of the Geological Survey of Namibia; Geological Survey of Namibia: Windhoek, Namibia, 2016; Volume 22, pp. 6–171.
163. Hu, C.; Chen, N.; Kapp, P.; Chen, J.; Xiao, A.; Zhao, Y. Yardang geometries in the Qaidam Basin and their controlling factors. *Geomorphology* **2017**, *299*, 142–151. [[CrossRef](#)]
164. Lin, Y.; Xu, L.; Mu, G. Differential erosion and the formation of layered yardangs in the Loulan region (Lop Nur), eastern Tarim Basin. *Aeolian Res.* **2018**, *30*, 41–47. [[CrossRef](#)]
165. Schieber, J.; Minitti, M.E.; Sullivan, R.; Edgett, K.S.; Malin, M.C.; Parker, T.; Calef, F. Engraved on the rocks—Aeolian abrasion of Martian mudstone exposures and their relationship to modern wind patterns in Gale Crater, Mars. *Depos. Rec.* **2020**, *6*, 625–647. [[CrossRef](#)]
166. Thomas, M.; Clarke, J.D.A.; Pain, C.F. Weathering, erosion, and landscape processes on Mars identified from recent rover imagery, and possible Earth analogs. *Aust. J. Earth Sci.* **2005**, *52*, 365–368. [[CrossRef](#)]
167. Laity, J.E. Wind erosion in drylands. In *Arid Zone Geomorphology: Process, Form and Change in Drylands*, 3rd ed.; Thomas, D.S.G., Ed.; Wiley-Blackwell: West Sussex, UK, 2011; pp. 539–568, ISBN 978-047-071-077-7. [[CrossRef](#)]
168. Edgett, K.S. The sedimentary rocks of Sinus Meridiani: Five key observations from data acquired by the Mars Global Surveyor and Mars Odyssey orbiters. *Mars* **2005**, *1*, 5–58. [[CrossRef](#)]
169. Ainsaar, L.; Suuroja, K.; Semidor, M. Long-term effect of the Kärddla crater (Hiiumaa, Estonia) on Late Ordovician carbonate sedimentation. *Deep Sea Res. Part II Top. Stud. Oceanogr.* **2002**, *49*, 1145–1155. [[CrossRef](#)]

170. Suuroja, S.; Suuroja, K. Kärđla impact (Hiiumaa Island, Estonia)—Ejecta blanket and environmental disturbances. In *Biological Processes Associated with Impact Events*; Cockell, C., Koeberl, C., Gilmour, I., Eds.; Springer: Berlin, Germany, 2006; pp. 309–333, ISBN 978-3-540-25736-3. [[CrossRef](#)]
171. Waichel, B.L.; Scherer, C.M.S.; Frank, H.T. Basaltic lava flows covering active aeolian dunes in the Paraná Basin in southern Brazil: Features and emplacement aspects. *J. Volcanol. Geotherm. Res.* **2008**, *171*, 59–72. [[CrossRef](#)]
172. Thiry, M.; Aryault, M.B.; Grisoni, J.-C. Groundwater silicification and leaching in sands: Example of the Fontainebleau sand (Oligocene) in the Paris Basin. *Geol. Soc. Am. Bull.* **1988**, *100*, 1283–1290. [[CrossRef](#)]
173. Thiry, M.; Maréchal, B. Development of tightly cemented sandstone lenses in uncemented sand: Example in the Fontainebleau Sand (Oligocene) in the Paris Basin. *J. Sed. Res.* **2001**, *71*, 473–483. [[CrossRef](#)]
174. Thiry, M.; Schmitt, J.-M.; Innocent, C.; Cojan, I. Sables et grès de Fontainebleau: Que reste-t-il des faciès sédimentaires initiaux? 14ème Congrès Français de Sédimentologie, Paris 2013, Trois excursions géologiques en région parisienne, Livre d’excursions. *Publ. Assoc. Sedimentol. Fr.* **2013**, *74*, 37–90.
175. Missenard, Y.; Parizot, O.; Barbarand, J. Age of the Fontainebleau sandstones: A tectonic point of view. *Bull. Soc. Géol. Fr.* **2017**, *188*, 28:1–28:14. [[CrossRef](#)]
176. Hayden, A.T.; Lamb, M.P. Fluvial sinuous ridges of the Morrison Formation, USA: Meandering, scarp retreat, and implications for Mars. *J. Geophys. Res.* **2020**, *125*, e2020JE006470:1–e2020JE006470:32. [[CrossRef](#)]
177. Zaki, A.S.; Pain, C.F.; Edgett, K.S.; Castellort, S. Global inventory of fluvial ridges on Earth and lessons applicable to Mars. *Earth Sci. Rev.* **2021**, *216*, 103561:1–103561:46. [[CrossRef](#)]
178. Branney, M.J.; Kokelaar, P. Pyroclastic density currents and the sedimentation of ignimbrites. *Geol. Soc. Lond. Mem.* **2002**, *27*, 1–143. [[CrossRef](#)]
179. Sheth, H. *A Photographic Atlas of Flood Basalt Volcanism*; Springer: Cham, Switzerland, 2018; ISBN 978-331-967-705-7T. [[CrossRef](#)]
180. Thomas, P.C.; Malin, M.C.; Edgett, K.S.; Carr, M.H.; Hartmann, W.K.; Ingersoll, A.P.; James, P.B.; Soderblom, L.A.; Veverka, J.; Sullivan, R. North-south geological differences between the residual polar caps on Mars. *Nature* **2000**, *404*, 161–164. [[CrossRef](#)]
181. Putzig, N.E.; Phillips, R.J.; Campbell, B.A.; Holt, J.W.; Plaut, J.J.; Carter, L.M.; Egan, A.F.; Bernardini, F.; Safaeinili, A.; Seug, R. Subsurface structure of Planum Boreum from Mars Reconnaissance Orbiter shallow radar soundings. *Icarus* **2009**, *204*, 443–457. [[CrossRef](#)]
182. Robinson, M.S.; Ashley, J.W.; Boyd, A.K.; Wagner, R.V.; Speyerer, E.J.; Hawke, B.R.; Hiesinger, H.; van der Bogert, C.H. Confirmation of sublunarean voids and thin layering in mare deposits. *Planet. Space Sci.* **2012**, *69*, 18–27. [[CrossRef](#)]
183. Stickle, A.M.; Patterson, G.W.; Cahill, J.T.S.; Bussey, D.B.J. Mini-RF and LROC observations of mare crater layering relationships. *Icarus* **2016**, *273*, 224–236. [[CrossRef](#)]
184. Fa, W.; Zhu, M.-H.; Liu, T.; Plescia, J.B. Regolith stratigraphy at the Chang’E-3 landing site as seen by lunar penetrating radar. *Geophys. Res. Lett.* **2015**, *42*, 10179–10187. [[CrossRef](#)]
185. Malin, M.C.; Edgett, K.S. Mars Global Surveyor Mars Orbiter Camera: Interplanetary cruise through primary mission. *J. Geophys. Res. Planets* **2001**, *106*, 23429–23570. [[CrossRef](#)]
186. Ivanov, M.A.; Abdrakhimov, A.M.; Guseva, E.N.; Kostama, V.P.; Raitala, J.; Kortenien, J.; Törmänen, T. Morphologic characteristics of volcanic and sedimentary sequences on Mars. *Sol. Syst. Res.* **2014**, *48*, 130–138. [[CrossRef](#)]
187. Crumpler, L.S.; Arvidson, R.E.; Squyres, S.W.; McCoy, T.; Yingst, A.; Ruff, S.; Farrand, W.; McSween, H.Y.; Powell, M.; Ming, D.W.; et al. Field reconnaissance geologic mapping of the Columbia Hills, Mars, based on Mars Exploration Rover Spirit and MRO HiRISE observations. *J. Geophys. Res. Planets* **2011**, *116*, E00F24:1–E00F24:55. [[CrossRef](#)]
188. Banham, S.G.; Gupta, S.; Rubin, D.M.; Watkins, J.A.; Sumner, D.Y.; Edgett, K.S.; Grotzinger, J.P.; Lewis, K.W.; Edgar, L.A.; Stack-Morgan, K.M.; et al. Ancient Martian aeolian processes and palaeomorphology reconstructed from the Stimson formation on the lower slope of Aeolis Mons, Gale crater, Mars. *Sedimentology* **2018**, *65*, 993–1042. [[CrossRef](#)]
189. Stack, K.M.; Grotzinger, J.P.; Lamb, M.P.; Gupta, S.; Rubin, D.M.; Kah, L.C.; Edgar, L.A.; Fey, D.M.; Hurowitz, J.A.; McBride, M.; et al. Evidence for plunging river plume deposits in the Pahrump Hills member of the Murray formation, Gale crater, Mars. *Sedimentology* **2019**, *66*, 1768–1802. [[CrossRef](#)]
190. Edgar, L.A.; Fedo, C.M.; Gupta, S.; Banham, S.; Fraeman, A.A.; Grotzinger, J.P.; Stack Morgan, K.; Stein, N.; Bennett, K.; Rivera-Hernández, F.; et al. A lacustrine paleoenvironment recorded at Vera Rubin ridge, Gale crater: Overview of the sedimentology and stratigraphy observed by the Mars Science Laboratory Curiosity rover. *J. Geophys. Res. Planets* **2020**, *125*, e2019JE006307:1–e2019JE006307:22. [[CrossRef](#)]
191. Milliken, R.E.; Ewing, R.C.; Fischer, W.W.; Hurowitz, J. Wind-blown sandstones cemented by sulfate and clay minerals in Gale crater, Mars. *Geophys. Res. Lett.* **2014**, *41*, 1149–1154. [[CrossRef](#)]
192. Lewis, K.W.; Aharonson, O.; Grotzinger, J.P.; Kirk, R.L.; McEwen, A.S.; Suer, T.-A. Quasi-periodic bedding in the sedimentary rock record of Mars. *Science* **2008**, *322*, 1532–1535. [[CrossRef](#)]
193. Meigs, L.C.; Beauheim, R.L. Characteristics of the Culebra. In *Interpretations of Tracer Tests Performed in the Culebra Dolomite at the Waste Isolation Pilot Plant Site*; Meigs, L.C., Beauheim, R.L., Jones, T.L., Eds.; Sandia National Laboratories Report SAND97-3109; Sandia National Laboratories: Albuquerque, NM, USA; Livermore, CA, USA, 2000; pp. 9–15. [[CrossRef](#)]
194. Howard, A.D.; Selby, M.J. Rock slopes. In *Geomorphology of Desert Environments*, 2nd ed.; Parsons, A.J., Abrahams, A.D., Eds.; Springer: Dordrecht, The Netherlands, 2009; pp. 189–232, ISBN 978-140-205-719-9. [[CrossRef](#)]
195. Payne, T.G. Stratigraphical analysis and environmental reconstruction. *Am. Assoc. Pet. Geol. Bull.* **1942**, *26*, 1697–1770. [[CrossRef](#)]

196. Mikulás, R. Microforms of the sandstone relief. In *Sandstone Landscapes*; Härtel, H., Cílek, V., Herben, T., Jackson, A., Williams, R., Eds.; Academia: Praha, Czech Republic, 2007; pp. 66–75, ISBN 978-802-001-577-8.
197. Jacka, A.D. The Environmental Significance of Stratification. Ph.D. Dissertation, Rice University, Houston, TX, USA, 1959. Available online: <https://hdl.handle.net/1911/18310> (accessed on 26 September 2021).
198. Kelley, V.C. Thickness of strata. *J. Sediment. Res.* **1956**, *26*, 289–300. [[CrossRef](#)]
199. Minitti, M.E.; Malin, M.C.; Van Beek, J.K.; Caplinger, M.C.; Maki, J.N.; Ravine, M.; Calef, F.J., III; Edgar, L.A.; Harker, D.; Herkenhoff, K.E.; et al. Distribution of primary and secondary features in the Pahrump Hills outcrop (Gale crater, Mars) as seen in a Mars Descent Imager (MARDI) “sidewalk” mosaic. *Icarus* **2019**, *328*, 193–209. [[CrossRef](#)]
200. Davis, K.; Herman, J.; Maksymuk, M.; Wilson, J.; Chu, P.; Burke, K.; Jandura, L.; Brown, K. Mars Science Laboratory dust removal tool. In Proceedings of the 41st Aerospace Mechanisms Symposium, Pasadena, CA, USA, 16–18 May 2012; pp. 279–292, NASA Conference Proceedings NASA/CP-2012-217653.
201. Anderson, R.B.; Bell, J.F., III. Geologic mapping and characterization of Gale crater and implications for its potential as a Mars Science Laboratory landing site. *Mars* **2010**, *5*, 76–128. [[CrossRef](#)]
202. Fedo, C.M.; Grotzinger, J.P.; Schieber, J.; Gupta, S.; House, C.H.; Edgett, K.S.; Siebach, K.L.; Fraeman, A.A.; Edgar, L.A.; Kronyak, R.E.; et al. Things are not always as they seem: Detangling intersecting planar and curvi-planar veins and fractures from primary bedding in the Vera Rubin Ridge member, Murray formation, Mars. Abstract Number 5-5. *Geol. Soc. Am. Abstr. Programs* **2018**, *50*. [[CrossRef](#)]
203. Hayes, A.G.; Grotzinger, J.P.; Edgar, L.A.; Squyres, S.W.; Watters, W.A.; Sohl-Dickstein, J. Reconstruction of eolian bed forms and paleocurrents from cross-bedded strata at Victoria crater, Meridiani Planum, Mars. *J. Geophys. Res. Planets* **2011**, *116*, E00F21:1–E00F21:17. [[CrossRef](#)]
204. Edgar, L.A.; Grotzinger, J.P.; Hayes, A.G.; Rubin, D.M.; Squyres, S.W.; Bell, J.F.; Herkenhoff, K.E. Stratigraphic architecture of bedrock reference section, Victoria crater, Meridiani Planum, Mars. In *Sedimentary Geology of Mars*; Grotzinger, J.P., Milliken, R.E., Eds.; SEPM Special Publication: Tulsa, OK, USA, 2012; Volume 102, pp. 195–209, ISBN 978-156-576-313-5. [[CrossRef](#)]
205. Miall, A.D. The valuation of unconformities. *Earth Sci. Rev.* **2016**, *163*, 22–71. [[CrossRef](#)]
206. Edgar, L.A. Recognition and Significance of Stratal Geometries and Unconformities in Martian Layered Deposits. In Identifying and Interpreting Stratification in Sedimentary Rocks on Mars: Insight from Rover and Orbital Observations and Terrestrial Field Analogs. Ph.D. Dissertation, California Institute of Technology, Pasadena, CA, USA, 2013; pp. 93–117. [[CrossRef](#)]
207. Haskin, L.A.; Wang, A.; Jolliff, B.L.; McSween, H.Y.; Clark, B.C.; Des Marais, D.J.; McLennan, S.M.; Tosca, N.J.; Hurowitz, J.A.; Farmer, J.D.; et al. Water alteration of rocks and soils on Mars at the Spirit rover site in Gusev crater. *Nature* **2005**, *436*, 66–69. [[CrossRef](#)] [[PubMed](#)]
208. Knoll, A.H.; Jolliff, B.L.; Farrand, W.H.; Bell, J.F., III; Clark, B.C.; Gellert, R.; Golombek, M.P.; Grotzinger, J.P.; Herkenhoff, K.E.; Johnson, J.R.; et al. Veneers, rinds, and fracture fills: Relatively late alteration of sedimentary rocks at Meridiani Planum, Mars. *J. Geophys. Res. Planets* **2008**, *113*, E06S16:1–E06S16:27. [[CrossRef](#)]
209. Mahaney, W.C.; Fairén, A.G.; Dohm, J.M.; Krinsley, D.H. Weathering rinds on clasts: Examples from Earth and Mars as short and long term recorders of paleoenvironment. *Planet. Space Sci.* **2012**, *73*, 243–253. [[CrossRef](#)]
210. Wiens, R.C.; Edgett, K.S.; Stack, K.M.; Dietrich, W.E.; Bryk, A.B.; Mangold, N.; Bedford, C.; Gasda, P.; Fairén, A.; Thompson, L.; et al. Origin and composition of three heterolithic boulder- and cobble-bearing deposits overlying the Murray and Stimson formations, Gale crater, Mars. *Icarus* **2020**, *350*, 113897:1–113897:38. [[CrossRef](#)]
211. Tirsch, D.; Jaumann, R.; Pacifici, A.; Poulet, F. Dark aeolian sediments in Martian craters: Composition and sources. *J. Geophys. Res. Planets* **2011**, *116*, E03002:1–E03002:25. [[CrossRef](#)]
212. Bayer, B.E. Color Imaging Array. U.S. Patent 39710065, 20 July 1976.
213. Hurowitz, J.A.; Grotzinger, J.P.; Fischer, W.W.; McLennan, S.M.; Milliken, R.E.; Stein, N.; Vasavada, A.R.; Blake, D.F.; Dehouck, E.; Eigenbrode, J.L.; et al. Redox stratification of an ancient lake in Gale crater, Mars. *Science* **2017**, *356*, eaah6849:10. [[CrossRef](#)]
214. Rampe, E.B.; Blake, D.F.; Bristow, T.F.; Ming, D.W.; Vaniman, D.T.; Morris, R.V.; Achilles, C.N.; Chipera, S.J.; Morrison, S.M.; Tue, V.M.; et al. Mineralogy and geochemistry of sedimentary rocks and eolian sediments in Gale crater, Mars: A review after six Earth years of exploration with Curiosity. *Geochemistry* **2020**, *80*, 125605:1–125605:31. [[CrossRef](#)]
215. Öpik, E.J. Dust and the planets. *Ir. Astron. J.* **1950**, *1*, 37–47.
216. Farley, K.A.; Malespin, C.; Mahaffy, P.; Grotzinger, J.P.; Vasconcelos, P.M.; Milliken, R.E.; Malin, M.; Edgett, K.S.; Pavlov, A.A.; Hurowitz, J.A.; et al. In situ radiometric and exposure age dating of the Martian surface. *Science* **2014**, *343*, 1247166:1–1247166:5. [[CrossRef](#)] [[PubMed](#)]
217. Martz, J.W.; Parker, W.G.; Skinner, L.; Raucci, J.J.; Umhoefer, P.; Blakey, R.C. Geologic Map of Petrified Forest National Park, Arizona. Arizona Geol. Survey Contributed Map 2012, CM-12-A, Scale 1:50,000. Available online: <https://hdl.handle.net/10150/630688> (accessed on 26 September 2021).
218. Bennett, K.A.; Rivera-Hernández, F.; Tinker, C.; Horgan, B.; Fey, D.M.; Edwards, C.; Edgar, L.A.; Kronyak, R.; Edgett, K.S.; Fraeman, A.; et al. Diagenesis revealed by fine-scale features at Vera Rubin ridge, Gale crater, Mars. *J. Geophys. Res. Planets* **2021**, *126*, e2019JE006311:1–e2019JE006311:24. [[CrossRef](#)]
219. Fraeman, A.A.; Edgar, L.A.; Rampe, E.B.; Thompson, L.M.; Frydenvang, J.; Fedo, C.M.; Catalano, J.G.; Dietrich, W.E.; Gabriel, T.S.J.; Vasavada, A.R.; et al. Evidence for a diagenetic origin of Vera Rubin ridge, Gale crater, Mars: Summary and synthesis of Curiosity’s exploration campaign. *J. Geophys. Res. Planets* **2020**, *125*, e2020JE006527:1–e2020JE006527:34. [[CrossRef](#)]

220. Hall, K.; Thorn, C.; Sumner, P. On the persistence of ‘weathering’. *Geomorphology* **2012**, *149–150*, 1–10. [[CrossRef](#)]
221. Oberbeck, V.R. The role of ballistic erosion and sedimentation in lunar stratigraphy. *Rev. Geophys.* **1975**, *13*, 337–362. [[CrossRef](#)]
222. McGlynn, I.O.; Fedo, C.M.; McSween, H.Y., Jr. Origin of basaltic soils at Gusev crater, Mars, by aeolian modification of impact-generated sediment. *J. Geophys. Res. Planets* **2011**, *116*, E00F22:1–E00F22:15. [[CrossRef](#)]
223. Hartmann, W.K. Martian cratering. *Icarus* **1966**, *5*, 565–576. [[CrossRef](#)]
224. Vaucher, J.; Baratoux, D.; Mangold, N.; Pinet, P.; Kurita, K.; Grégoire, M. The volcanic history of central Elysium Planitia: Implications for Martian magmatism. *Icarus* **2009**, *204*, 418–442. [[CrossRef](#)]
225. Grindrod, P.M.; Warner, N.H. Erosion rate and previous extent of interior layered deposits on Mars revealed by obstructed landslides. *Geology* **2014**, *42*, 795–798. [[CrossRef](#)]
226. Edgett, K.S. MRO CTX and MGS MOC observations regarding small impact craters and substrate resistance to erosion on Mars. In Proceedings of the 41st Astronomical Society Division for Planetary Sciences Meeting, Fajardo, PR, USA, 4–10 October 2009. Abstract Number 58.06.
227. Edgett, K.S.; Malin, M.C. Heavily-cratered sedimentary rock occurrences at the surface of Mars. Abstract Number 202-1. *Geol. Soc. Am. Abstr. Programs* **2014**, *46*, 496.
228. Siebach, K.L. Formation and Diagenesis of Sedimentary Rocks in Gale Crater, Mars. Ph.D. Dissertation, California Institute of Technology, Pasadena, CA, USA, 2016. [[CrossRef](#)]
229. Newsom, H.E.; Mangold, N.; Kah, L.C.; Williams, J.M.; Arvidson, R.E.; Stein, N.; Ollila, A.M.; Bridges, J.C.; Schwenzer, S.P.; King, P.L.; et al. Gale crater and impact processes—Curiosity’s first 364 Sols on Mars. *Icarus* **2015**, *249*, 108–128. [[CrossRef](#)]
230. Calef, F.J., III; Wellington, D.; Newsom, H.; Gabriel, T. Geology and origin of Taconite crater on the Vera Rubin ridge. In Proceedings of the 50th Lunar and Planetary Science Conference, The Woodlands, TX, USA, 18–22 March 2019; Abstract Number 1983. Lunar and Planetary Institute: Houston, TX, USA, 2019. Available online: <https://www.hou.usra.edu/meetings/lpsc2019/pdf/1983.pdf> (accessed on 26 September 2021).
231. Terry, J.P.; Goff, J. Megaclasts: Proposed revised nomenclature at the coarse end of the Udden-Wentworth grain-size scale for sedimentary particles. *J. Sediment. Res.* **2014**, *84*, 192–197. [[CrossRef](#)]
232. Malin, M.C.; Edgett, K.S. MGS MOC: First views of Mars at sub-meter resolution from orbit. In Proceedings of the 36th Lunar and Planetary Science Conference, League City, TX, USA, 14–18 March 2005; Abstract Number 1172. Lunar Planetary Institute Contribution 1234: Houston, TX, USA, 2005. Available online: <https://hdl.handle.net/20.500.11753/1088> (accessed on 26 September 2021).
233. Rodriguez, J.A.P.; Noe Dobrea, E.; Kargel, J.S.; Baker, V.R.; Crown, D.A.; Webster, K.D.; Berman, D.C.; Wilhelm, M.B.; Buckner, D. The oldest highlands of Mars may be massive dust fallout deposits. *Sci. Rep.* **2020**, *10*, 10347:1–10347:15. [[CrossRef](#)]
234. Hynes, B.M.; Phillips, R.J.; Arvidson, R.E. Explosive volcanism in the Tharsis region: Global evidence in the Martian geologic record. *J. Geophys. Res. Planets* **2003**, *108*, 5111:1–5111:16. [[CrossRef](#)]
235. Zimelman, J.R.; Griffin, L.J. HiRISE images of yardangs and sinuous ridges in the lower member of the Medusae Fossae Formation, Mars. *Icarus* **2010**, *205*, 198–210. [[CrossRef](#)]
236. Kerber, L.; Head, J.W.; Madeleine, J.-B.; Forget, F.; Wilson, L. The dispersal of pyroclasts from ancient explosive volcanoes on Mars: Implications for the friable layered deposits. *Icarus* **2012**, *219*, 358–381. [[CrossRef](#)]
237. Kremer, C.H.; Mustard, J.F.; Bramble, M.S. A widespread olivine-rich ash deposit on Mars. *Geology* **2019**, *47*, 677–681. [[CrossRef](#)]
238. Young, R.W. Sandstone landforms of the tropical East Kimberley region, Northwestern Australia. *J. Geol.* **1987**, *95*, 205–218. [[CrossRef](#)]
239. Howard, A.D.; Kochel, R.C. Introduction of cuesta landforms and sapping processes on the Colorado Plateau. In *Sapping Features of the Colorado Plateau*; Howard, A.D., Kochel, R.C., Holt, H.R., Eds.; NASA Special Publication SP-491; U.S. Government Printing Office; National Aeronautics and Space Administration: Washington, DC, USA, 1988; pp. 6–56.
240. Wray, R.A.L.; Sauro, F. An updated global review of solutional weathering processes and forms in quartz sandstones and quartzites. *Earth Sci. Rev.* **2017**, *171*, 520–557. [[CrossRef](#)]
241. Blackwelder, E. The lowering of playas by deflation. *Am. J. Sci.* **1931**, *221*, 140–144. [[CrossRef](#)]
242. Allison, I.S. Pluvial Fort Rock Lake, Lake County, Oregon. *State Or. Dep. Geol. Miner. Ind. Spec. Pap.* **1979**, *7*, 1–72. Available online: <https://digital.osl.state.or.us/islandora/object/osl:27065> (accessed on 26 September 2021).
243. Watkins, J.; Grotzinger, J.; Stein, N.; Banham, S.G.; Gupta, S.; Rubin, D.; Stack, K.M.; Edgett, K.S. Paleotopography of erosional unconformity, base of Stimson formation, Gale crater, Mars. In Proceedings of the 47th Lunar and Planetary Science Conference, The Woodlands, TX, USA, 21–25 March 2016; Abstract Number 2939. Lunar and Planetary Institute: Houston, TX, USA, 2016. Available online: <https://hdl.handle.net/20.500.11753/1142> (accessed on 26 September 2021).
244. Chojnacki, M.; Burr, D.M.; Moersch, J.E.; Wray, J.J. Valles Marineris dune sediment provenance and pathways. *Icarus* **2014**, *232*, 187–219. [[CrossRef](#)]
245. Williams, R.M.E.; Grotzinger, J.P.; Dietrich, W.E.; Gupta, S.; Sumner, D.Y.; Wiens, R.C.; Mangold, N.; Malin, M.C.; Edgett, K.S.; Maurice, S.; et al. Martian fluvial conglomerates at Gale crater. *Science* **2013**, *340*, 1068–1072. [[CrossRef](#)]
246. Khan, S.Y.; Stack, K.M.; Yingst, R.A. Characterization of clasts in the Glen Torridon region observed [*sic*] by the MSL Curiosity rover. In Proceedings of the 52nd Lunar and Planetary Science Conference, Virtual Meeting, 15–19 March 2021; Abstract Number 2649. Lunar and Planetary Institute: Houston, TX, USA, 2021. Available online: <https://www.hou.usra.edu/meetings/lpsc2021/pdf/2649.pdf> (accessed on 26 September 2021).

247. Rice, M.S.; Gupta, S.; Treiman, A.H.; Stack, K.M.; Calef, F.; Edgar, L.A.; Grotzinger, J.; Lanza, N.; Le Deit, L.; Lasue, J.; et al. Geologic overview of the Mars Science Laboratory rover mission at the Kimberley, Gale crater, Mars. *J. Geophys. Res. Planets* **2017**, *122*, 2–20. [[CrossRef](#)]
248. Dixon, J.C. Stone pavements, lag deposits, and contemporary landscape evolution. In *Dynamic Mars: Recent and Current Landscape Evolution of the Red Planet*; Soare, R.J., Conway, S.J., Clifford, S.M., Eds.; Elsevier: Amsterdam, The Netherlands, 2018; pp. 387–410, ISBN 978-012-813-018-6. [[CrossRef](#)]
249. Lorenz, R.D.; Zimbleman, J.R. Mars dunes. In *Dune Worlds: How Windblown Sand Shapes Planetary Landscapes*; Lorenz, R.D., Zimbleman, J.R., Eds.; Springer Praxis: Berlin, Germany, 2014; pp. 135–155, ISBN 978-354-089-725-5. [[CrossRef](#)]
250. Jerram, D.A.; Mountney, N.P.; Howell, J.A.; Long, D.; Stollhofen, H. Death of a sand sea: An active aeolian erg systematically buried by the Etendeka flood basalts of NW Namibia. *J. Geol. Soc. Lond.* **2000**, *154*, 513–516. [[CrossRef](#)]
251. Day, M.D.; Catling, D.C. Dune casts preserved by partial burial: The first identification of ghost dune pits on Mars. *J. Geophys. Res. Planets* **2018**, *123*, 1431–1448. [[CrossRef](#)]
252. Balme, M.; Berman, D.C.; Bourke, M.C.; Zimbleman, J.R. Transverse aeolian ridges (TARs) on Mars. *Geomorphology* **2008**, *101*, 703–720. [[CrossRef](#)]
253. Berman, D.C.; Balme, M.R.; Michalski, J.R.; Clark, S.C.; Joseph, E.C.S. High-resolution investigations of transverse aeolian ridges on Mars. *Icarus* **2018**, *312*, 247–266. [[CrossRef](#)]
254. Gaylord, D.R.; Rittenour, T.M.; Link, P.K.; Turrin, B.D.; Kuntz, M.A. Ghost-dune hollows of the eastern Snake River Plain, Idaho: Their genesis, evolution, and relevance to Martian ghost-dune pits. *Geology* **2021**, *49*, 899–904. [[CrossRef](#)]
255. Montgomery, D.R.; Bandfield, J.L.; Becker, S.K. Periodic bedrock ridges on Mars. *J. Geophys. Res. Planets* **2012**, *117*, E03005:12. [[CrossRef](#)]
256. Hugenholtz, C.H.; Barchyn, T.E.; Favaro, E.A. Formation of periodic bedrock ridges on Earth. *Aeolian Res.* **2015**, *18*, 135–144. [[CrossRef](#)]
257. Stumbaugh, D.L.; Day, M.D.; Dorn, T.C. Investigating an aeolian origin to washboard terrain on Mars. In Proceedings of the American Geophysical Union Fall Meeting 2018, Washington, DC, USA, 10–14 December 2018; Abstract Number EP51C-1833.
258. Fassett, C.I.; Head, J.W., III. Fluvial sedimentary deposits on Mars: Ancient deltas in a crater lake in the Nili Fossae region. *Geophys. Res. Lett.* **2005**, *32*, L14201:1–L14201:5. [[CrossRef](#)]
259. Moore, J.M.; Howard, A.D. Large alluvial fans on Mars. *J. Geophys. Res. Planets* **2005**, *110*, E04005:1–E04005:24. [[CrossRef](#)]
260. Kraal, E.R.; Asphaug, E.; Moore, J.M.; Howard, A.; Brecht, A. Catalogue of large alluvial fans in Martian impact craters. *Icarus* **2008**, *194*, 101–110. [[CrossRef](#)]
261. di Achille, G.; Hynek, B.M. Deltas and valley networks on Mars: Implications for a global hydrosphere. In *Lakes on Mars*; Cabrol, N.A., Grin, E.A., Eds.; Elsevier: Amsterdam, The Netherlands, 2010; pp. 223–248, ISBN 978-044-452-854-4. [[CrossRef](#)]
262. Wilson, S.A.; Morgan, A.M.; Howard, A.D.; Grant, J.A. The global distribution of craters with alluvial fans and deltas on Mars. *Geophys. Res. Lett.* **2021**, *48*, e2020GL091653:1–e2020GL091653:10. [[CrossRef](#)]
263. Moore, J.M.; Howard, A.D.; Dietrich, W.E.; Schenk, P.M. Martian layered fluvial deposits: Implications for Noachian climate scenarios. *Geophys. Res. Lett.* **2003**, *30*, 2292:1–2292:4. [[CrossRef](#)]
264. Grant, J.A.; Schultz, P.H. Gradational epochs on Mars: Evidence from west-northwest of Isidis basin and Electris. *Icarus* **1990**, *84*, 166–195. [[CrossRef](#)]
265. Crown, D.A.; Price, K.H.; Greeley, R. Geologic evolution of the east rim of the Hellas basin, Mars. *Icarus* **1992**, *100*, 1–25. [[CrossRef](#)]
266. Miller, R.P. Drainage lines in bas-relief. *J. Geol.* **1937**, *45*, 432–438. [[CrossRef](#)]
267. Maizels, J. Raised channels as indicators of palaeohydrologic change: A case study from Oman. *Palaeogeogr. Palaeoclimatol. Palaeoecol.* **1990**, *76*, 241–277. [[CrossRef](#)]
268. Weitz, C.M.; Milliken, R.E.; Grant, J.A.; McEwen, A.S.; Williams, R.M.E.; Bishop, J.L. Light-toned strata and inverted channels adjacent to Juventae and Ganges chasmata, Mars. *Geophys. Res. Lett.* **2008**, *35*, L19202:1–L19202:5. [[CrossRef](#)]
269. Williams, R.M.E.; Irwin, R.P., III; Zimbleman, J.R. Evaluation of paleohydrologic models for terrestrial inverted channels: Implications for application to Martian sinuous ridges. *Geomorphology* **2009**, *107*, 300–315. [[CrossRef](#)]
270. Burr, D.M.; Williams, R.M.E.; Wendell, K.D.; Chojnacki, M.; Emery, J.P. Inverted fluvial features in the Aeolis/Zephyria Plana region, Mars: Formation mechanism and initial paleodischarge estimates. *J. Geophys. Res. Planets* **2010**, *115*, E07011:1–E07011:20. [[CrossRef](#)]
271. Newsom, H.E.; Lanza, N.L.; Ollila, A.M.; Wiseman, S.M.; Roush, T.L.; Marzo, G.A.; Tornabene, L.L.; Okubo, C.H.; Osterloo, M.M.; Hamilton, V.E.; et al. Inverted channel deposits on the floor of Miyamoto crater, Mars. *Icarus* **2010**, *205*, 64–72. [[CrossRef](#)]
272. Pain, C.F.; Clarke, J.D.A.; Thomas, M. Inversion of relief on Mars. *Icarus* **2007**, *190*, 478–491. [[CrossRef](#)]
273. Dickson, J.L.; Lamb, M.P.; Williams, R.M.E.; Fischer, W.W. The global distribution of depositional rivers on early Mars. *Geology* **2021**, *49*, 504–509. [[CrossRef](#)]
274. Clarke, J.; Pain, C.F.; Rupert, S. Complex expressions of inverted and exhumed relief in central Utah, and some Martian counterparts. *Phys. Geogr.* **2020**. [[CrossRef](#)]
275. Zaki, A.S.; Pain, C.F.; Edgett, K.S.; Giegengack, R. Inverted stream channels in the Western Desert of Egypt: Synergistic remote, field observations and laboratory analysis on Earth with applications to Mars. *Icarus* **2018**, *309*, 105–124. [[CrossRef](#)]
276. Williams, R.M.E.; Moersch, J.E.; Ferguson, R.L. Thermophysical properties of Martian fluvial sinuous ridges: Inferences on “inverted channel” induration agent. *Earth Space Sci.* **2018**, *5*, 516–528. [[CrossRef](#)]

277. De Meester, L.; Declerck, S.; Stoks, R.; Louette, G.; Van De Muetter, F.; De Bie, T.; Michels, E.; Brendonck, L. Ponds and pools as model systems in conservation biology, ecology, and evolutionary biology. *Aquat. Conserv. Mar. Freshw. Ecosyst.* **2005**, *15*, 715–725. [CrossRef]
278. Bartout, P.; Touchart, L.; Terasmaa, J.; Choffel, Q.; Marzecova, A.; Koff, T.; Kapanen, G.; Qsair, Z.; Maleval, V.; Millot, C.; et al. A new approach to inventorying bodies of water, from local to global scale. *Erde* **2015**, *146*, 245–258. [CrossRef]
279. Downing, J.A. Emerging global role of small lakes and ponds: Little things mean a lot. *Limnetica* **2010**, *29*, 9–24. [CrossRef]
280. Terasmaa, J.; Bartout, P.; Marzecova, A.; Touchart, L.; Vandell, E.; Koff, T.; Choffel, Q.; Kapanen, G.; Maleval, V.; Vainu, M.; et al. A quantitative assessment of the contribution of small standing water bodies to the European waterscapes—Case of Estonia and France. *Heliyon* **2019**, *5*, e02482:1–e02482:8. [CrossRef]
281. Quade, J.; Dente, E.; Armon, M.; Ben Dor, Y.; Morin, E.; Adam, O.; Enzel, Y. Megalakes in the Sahara? A review. *Quat. Res.* **2018**, *90*, 253–275. [CrossRef]
282. Downing, J.A.; Prairie, Y.T.; Cole, J.J.; Duarte, C.M.; Tranvik, L.J.; Striegl, R.G.; McDowell, W.H.; Kortelainen, P.; Caraco, N.F.; Melack, J.M.; et al. The global abundance and size distribution of lakes, ponds, and impoundments. *Limnol. Oceanogr.* **2006**, *51*, 2388–2397. [CrossRef]
283. Søndergaard, M.; Jeppesen, E.; Jensen, J.P. Pond or lake: Does it make any difference? *Arch. Hydrobiol.* **2005**, *162*, 143–165. [CrossRef]
284. Keeley, J.E.; Zedler, P.H. Characterization and global distribution of vernal pools. In *Ecology, Conservation, and Management of Vernal Pool Ecosystems: Proceedings from a 1996 Conference*; Witham, C.W., Bauder, E.T., Belk, D., Ferren, W.R., Jr., Ornduff, R., Eds.; California Native Plant Society: Sacramento, CA, USA, 1998; pp. 1–14, ISBN 978-094-346-037-6.
285. Quirke, T.T. Geology of the Kildeer Mountains, Dunn County, North Dakota. Master's Thesis, University of North Dakota, Grand Forks, ND, USA, 1913. Available online: <https://commons.und.edu/theses/237> (accessed on 26 September 2021).
286. Wendorf, F. Members of the Combined Prehistoric Expedition. Late Pleistocene and Recent climatic changes in the Egyptian Sahara. *Geogr. J.* **1977**, *143*, 211–234. [CrossRef]
287. Twidale, C.R.; Milnes, A.R. Slope processes active late in arid scarp retreat. *Z. Geomorph.* **1983**, *27*, 343–361. [CrossRef]
288. Haynes, C.V., Jr.; Eyles, C.H.; Pavlish, L.A.; Ritchie, J.C.; Rybak, M. Holocene palaeoecology of the eastern Sahara. Selima Oasis. *Quat. Sci. Rev.* **1989**, *8*, 109–136. [CrossRef]
289. Verrecchia, E.P. Lacustrine and palustrine geochemical sediments. In *Geochemical Sediments and Landscapes*; Nash, D.J., McLaren, S.J., Eds.; Wiley-Blackwell: Oxford, UK, 2007; pp. 298–329, ISBN 978-047-071-291-7. [CrossRef]
290. Smith, R.M.H.; Mason, T.R. Sedimentary environments and trace fossils of Tertiary oasis deposits in the central Namib Desert, Namibia. *Palaios* **1998**, *13*, 547–599. [CrossRef]
291. Clarke, J.D.A.; McQuirk, S.; Pandey, S. Inverted dune swales, Hunder, Ladakh, India. *Phys. Geogr.* **2020**. [CrossRef]
292. Davis, J.M.; Balme, M.; Grindrod, P.M.; Williams, R.M.E.; Gupta, S. Extensive Noachian fluvial systems in Arabia Terra: Implications for early Martian climate. *Geology* **2016**, *44*, 847–850. [CrossRef]
293. Hörz, F. Ejecta of the Ries Crater, Germany. In *Geological Implications of Impacts of Large Asteroids and Comets on the Earth*; Silver, L.T., Schultz, P.H., Eds.; Geological Society of America: Boulder, CO, USA, 1982; Volume 190, pp. 39–55. [CrossRef]
294. Osinski, G.R.; Tornabene, L.L.; Grieve, R.A.F. Impact ejecta emplacement on terrestrial planets. *Earth Planet. Sci. Lett.* **2011**, *310*, 167–181. [CrossRef]
295. Stöffler, D.; Hamann, C.; Metzler, K. Shock metamorphism of planetary silicate rocks and sediments: Proposal for an updated classification system. *Meteorit. Planet. Sci.* **2017**, *53*, 5–49. [CrossRef]
296. Gurov, E.P.; Kelley, S.P.; Koeberl, C. Ejecta of the Boltys impact crater in the Ukrainian Shield. In *Impact Markers in the Stratigraphic Record*; Koeberl, C., Martínez-Ruiz, F.C., Eds.; Springer: Berlin, Germany, 2003; pp. 179–202, ISBN 978-364-255-463-6. [CrossRef]
297. Losiak, A.; Wild, E.M.; Geppert, W.D.; Huber, M.S.; Jöeleht, A.; Kriiska, A.; Kulkov, A.; Paavel, K.; Pirovic, I.; Plado, J.; et al. Dating a small impact crater: An age of Kaali crater (Estonia) based on charcoal emplaced within proximal ejecta. *Meteorit. Planet. Sci.* **2016**, *51*, 682–695. [CrossRef]
298. Pánek, T. Landslides and related sediments. In *Encyclopedia of Geology*, 2nd ed.; Alderton, D., Elias, S.A., Eds.; Academic: London, UK, 2021; pp. 708–728, ISBN 978-008-102-909-1. [CrossRef]
299. Sanders, D.; Ostermann, M.; Brandner, R.; Prager, C. Meteoric lithification of catastrophic rockslide deposits: Diagenesis and significance. *Sediment. Geol.* **2010**, *223*, 150–161. [CrossRef]
300. Carr, M.H. Volcanism on Mars. *J. Geophys. Res.* **1973**, *78*, 4049–4062. [CrossRef]
301. Scott, D.H.; Chapman, M.G. Geologic and Topographic Maps of the Elysium Paleolake Basin, Mars. U.S. Geological Survey Scientific Investigations Map 1995, I-2397, Scale 1:5,000,000. Available online: <https://pubs.er.usgs.gov/publication/i2397> (accessed on 26 September 2021). [CrossRef]
302. Zimbelman, J.R.; Scheidt, S.P. Hesperian age for western Medusae Fossae Formation, Mars. *Science* **2012**, *336*, 1683. [CrossRef]
303. Scott, D.H.; Tanaka, K.L. Ignimbrites of Amazonis Planitia region of Mars. *J. Geophys. Res. Solid Earth* **1982**, *87*, 1179–1190. [CrossRef]
304. Bradley, B.A.; Sakimoto, S.E.H.; Frey, H.; Zimbelman, J.R. Medusae Fossae Formation: New perspectives from Mars Global Surveyor. *J. Geophys. Res. Planets* **2002**, *107*, 5058:1–5058:17. [CrossRef]
305. Mandt, K.E.; de Silva, S.L.; Zimbelman, J.R.; Crown, D.A. Origin of the Medusae Fossae Formation, Mars: Insights from a synoptic approach. *J. Geophys. Res. Planets* **2008**, *113*, E12011:1–E12011:15. [CrossRef]

306. Schon, S.C.; Head, J.W.; Fassett, C.I. An overfilled lacustrine system and progradational delta in Jezero crater, Mars: Implications for Noachian climate. *Planet. Space Sci.* **2012**, *67*, 28–45. [CrossRef]
307. Christensen, P.R.; Bandfield, J.L.; Clark, R.N.; Edgett, K.S.; Hamilton, V.E.; Hoefen, T.; Kieffer, H.H.; Kuzmin, R.O.; Lane, M.D.; Malin, M.C.; et al. Detection of crystalline hematite mineralization on Mars by the Thermal Emission Spectrometer: Evidence for near-surface water. *J. Geophys. Res. Planets* **2000**, *105*, 9623–9642. [CrossRef]
308. Gendrin, A.; Mangold, N.; Bibring, J.-P.; Langevin, Y.; Gondet, B.; Poulet, F.; Bonello, G.; Quantin, C.; Mustard, J.; Arvidson, R.; et al. Sulfates in Martian layered terrains: The OMEGA/Mars Express view. *Science* **2005**, *307*, 1587–1591. [CrossRef]
309. Poulet, F.; Bibring, J.-P.; Mustard, J.F.; Gendrin, A.; Mangold, N.; Langevin, Y.; Arvidson, R.E.; Gondet, B.; Gomez, C.; OMEGA Team. Phyllosilicates on Mars and implications for early Martian climate. *Nature* **2005**, *438*, 623–627. [CrossRef]
310. Osterloo, M.M.; Hamilton, V.E.; Bandfield, J.L.; Glotch, T.D.; Baldridge, A.M.; Christensen, P.R.; Tornabene, L.L.; Anderson, F.S. Chloride-bearing materials in the southern highlands of Mars. *Science* **2008**, *319*, 1651–1654. [CrossRef] [PubMed]
311. Vaniman, D.T.; Bish, D.L.; Ming, D.W.; Bristow, T.F.; Morris, R.V.; Blake, D.F.; Chipera, S.J.; Morrison, S.M.; Treiman, A.H.; Rampe, E.B.; et al. Mineralogy of a mudstone at Yellowknife Bay, Gale crater, Mars. *Science* **2014**, *343*, 1243480:1–1243480:8. [CrossRef] [PubMed]
312. Cowart, J.C.; Rogers, A.D.; Edwards, C.S. Mapping and characterization of Martian intercrater bedrock plains: Insights into resurfacing processes in the Martian cratered highlands. *J. Geophys. Res. Planets* **2019**, *124*, 3181–3204. [CrossRef]
313. DeGraff, J.M.; Aydin, A. Surface morphology of columnar joints and its significance to mechanics and direction of joint growth. *Geol. Soc. Am. Bull.* **1987**, *99*, 605–617. [CrossRef]
314. Robinson, C.S. Geology of Devils Tower National Monument, Wyoming. *U.S. Geol. Surv. Bull.* **1956**, *1021-I*, 289–302. [CrossRef]
315. Osinski, G.R.; Grieve, R.A.F.; Bleacher, J.E.; Neish, C.D.; Pilles, E.A.; Tornabene, L.L. Igneous rocks formed by hypervelocity impact. *J. Volcanol. Geotherm. Res.* **2018**, *353*, 25–54. [CrossRef]
316. Lim, C.; Huh, M.; Yi, K.; Lee, C. Genesis of the columnar joints from welded tuff in Mount Mudeung National Geopark, Republic of Korea. *Earth Planets Space* **2015**, *67*, 152:1–152:19. [CrossRef]
317. Wright, H.M.N.; Lesti, C.; Cas, R.A.F.; Porreca, M.; Viramonte, J.G.; Folkes, C.B.; Giordano, G. Columnar jointing in vapor-phase-altered, non-welded Cerro Galán Ignimbrite, Paycuqui, Argentina. *Bull. Volcanol.* **2011**, *73*, 1567–1582. [CrossRef]
318. Weinberger, R.; Burg, A. Reappraising columnar joints in different rock types and settings. *J. Struct. Geol.* **2019**, *125*, 185–194. [CrossRef]
319. Haynes, C.V. The Darb El-Arba'in Desert: A product of Quaternary climatic change. In *Desert Landforms of Southwest Egypt: A Basis for Comparison with Mars*; El-Baz, F., Maxwell, T.A., Eds.; NASA Contractor Report, CR-3611; U.S. Government Printing Office: Washington, DC, USA, 1982; pp. 91–117.
320. Summer, N.S.; Ayalon, A. Dike intrusion into unconsolidated sandstone and the development of quartzite contact zones. *J. Struct. Geol.* **1995**, *17*, 997–1010. [CrossRef]
321. Young, G.M. Origin of enigmatic structures: Field and geochemical investigation of columnar joints in sandstones, Island of Bute, Scotland. *J. Geol.* **2008**, *116*, 527–536. [CrossRef]
322. Velázquez, V.F.; Giannini, P.C.F.; Riccomini, C.; Sallun, A.E.M.; Hachiro, J.; de Barros Gomes, C. Columnar joints in the Patiño Formation sandstones, Eastern Paraguay: A dynamic interaction between dyke intrusion, quartz dissolution and cooling-induced fractures. *Episodes* **2008**, *31*, 302–308. [CrossRef]
323. Čilek, V.; Adamovič, J.; Suková, L. Sandstone columns of the 3rd Nile Cataract (Nubia, Northern Sudan). *Z. Geomorphol. Suppl.* **2015**, *59*, 151–163. [CrossRef]
324. Malin, M.C. Nature and Origin of Intercrater Plains on Mars. In *Studies of the Surface Morphology of Mars*. Ph.D. Dissertation, California Institute of Technology, Pasadena, CA, USA, 1976; pp. 101–176. [CrossRef]
325. Greeley, R.; Spudis, P.D. Volcanism on Mars. *Rev. Geophys.* **1981**, *19*, 13–41. [CrossRef]
326. Goldspiel, J.M.; Squyres, S.W. Ancient aqueous sedimentation on Mars. *Icarus* **1991**, *89*, 392–410. [CrossRef]
327. Scott, D.H.; Tanaka, K.L. Geologic Map of the Western Equatorial Region of Mars. U.S. Geological Survey Miscellaneous Investigations Series Map 1986, 1802-A, Scale 1: 500,000. Available online: <https://pubs.er.usgs.gov/publication/i1802A> (accessed on 26 September 2021). [CrossRef]
328. Greeley, R.; Guest, J.E. Geologic Map of the Eastern Equatorial Region of Mars. U.S. Geological Survey Miscellaneous Investigations Series Map 1987, I-1802-B, Scale 1:5,000,000. Available online: <https://pubs.er.usgs.gov/publication/i1802B> (accessed on 26 September 2021). [CrossRef]
329. Greeley, R.; Schneid, B.D. Magma generation on Mars: Amounts, rates, and comparisons with Earth, Moon, and Venus. *Science* **1991**, *254*, 996–998. [CrossRef] [PubMed]
330. Wilhelms, D.E. Comparison of Martian and lunar geologic provinces. *J. Geophys. Res.* **1974**, *79*, 3933–3941. [CrossRef]
331. Plescia, J.B.; Golombek, M.P. Origin of planetary wrinkle ridges based on the study of terrestrial analogs. *Geol. Soc. Am. Bull.* **1986**, *97*, 1289–1299. [CrossRef]
332. Watters, T.R. Wrinkle ridge assemblages on the terrestrial planets. *J. Geophys. Res. Solid Earth* **1988**, *93*, 10236–10254. [CrossRef]
333. Quaife, W. Rilles, ridges, and domes—Clues to maria history. *Icarus* **1965**, *4*, 374–389. [CrossRef]
334. Mueller, K.; Golombek, M. Compressional structures on Mars. *Annu. Rev. Earth Planet. Sci.* **2004**, *32*, 435–464. [CrossRef]
335. Andrews-Hanna, J.C. The tectonic architecture of wrinkle ridges on Mars. *Icarus* **2020**, *351*, 113937:1–113937:19. [CrossRef]

336. Edwards, C.S.; Nowicki, K.J.; Christensen, P.R.; Hill, J.; Gorelick, N.; Murray, K. Mosaicking of global planetary image datasets: 1. Techniques and data processing for Thermal Emission Imaging System (THEMIS) multi-spectral data. *J. Geophys. Res. Planets* **2011**, *116*, E10008:1–E10008:21. [CrossRef]
337. Ferguson, R.L.; Hare, T.M.; Laura, J. HRSC and MOLA blended digital elevation model at 200 m, version 2. In *Astrogeology Planetary Data System Annex*; U.S. Geological Survey: Flagstaff, AZ, USA, 2018. Available online: http://bit.ly/HRSC_MOLA_Blend_v0 (accessed on 26 September 2021).
338. Craddock, R.A.; Greeley, R. Minimum estimates of the amount and timing of gases released into the Martian atmosphere from volcanic eruptions. *Icarus* **2009**, *204*, 512–526. [CrossRef]
339. Williams, D.A.; Greeley, R.; Manfredi, L.; Raitala, J.; Neukum, G.; HRSC Co-Investigator Team. The circum-Hellas volcanic province, Mars: Assessment of wrinkle-ridged plains. *Earth Planet. Sci. Lett.* **2010**, *294*, 492–505. [CrossRef]
340. Hynek, B.; Di Achille, G. Geologic Map of Meridiani Planum, Mars. U.S. Geological Survey Scientific Investigations Map 2017, 3356, Scale 1:2,000,000. Available online: <https://pubs.er.usgs.gov/publication/sim3356> (accessed on 26 September 2021). [CrossRef]
341. Malin, M.C.; Carr, M.H.; Danielson, G.E.; Davies, M.E.; Hartmann, W.K.; Ingersoll, A.P.; James, P.B.; Masursky, H.; McEwen, A.S.; Soderblom, L.A.; et al. Early views of the Martian surface from the Mars Orbiter Camera of Mars Global Surveyor. *Science* **1998**, *279*, 1681–1685. [CrossRef] [PubMed]
342. Sowe, M. Interior Layered Deposits in Chaotic Terrains on Mars. Ph.D. Dissertation, Freie Universität Berlin, Berlin, Germany, 2009. [CrossRef]
343. Martínez-Alonso, S.; Jakosky, B.M.; Mellon, M.T.; Putzig, N.E. A volcanic interpretation of Gusev Crater surface materials from thermophysical, spectral, and morphological evidence. *J. Geophys. Res. Planets* **2005**, *110*, E01003:1–E01003:20. [CrossRef]
344. Palucis, M.C.; Dietrich, W.E.; Hayes, A.G.; Williams, R.M.E.; Gupta, S.; Mangold, N.; Newsom, H.; Hardgrove, C.; Calef, F., III; Sumner, D.Y. The origin and evolution of the Peace Vallis fan system that drains to the Curiosity landing area, Gale crater, Mars. *J. Geophys. Res. Planets* **2014**, *119*, 705–728. [CrossRef]
345. Calef, F.J., III; Parker, T. *MSL Gale Merged Orthophoto Mosaic*; PDS Annex; U.S. Geological Survey: Flagstaff, AZ, USA, 2016. Available online: http://bit.ly/MSL_Basemap (accessed on 26 September 2021).
346. Scott, D.R.; Worden, A.M.; Irwin, J.B. Crew observations. In *Apollo 15 Preliminary Science Report*; NASA Special Publication SP-289; U.S. Government Printing Office; National Aeronautics and Space Administration: Washington, DC, USA, 1972; pp. 4-1–4-4.
347. McEwen, A.S.; Malin, M.C.; Carr, M.H.; Hartmann, W.K. Voluminous volcanism on early Mars revealed in Valles Marineris. *Nature* **1999**, *397*, 584–586. [CrossRef]
348. Törmänen, T.; Ivanov, M.; Raitala, J.; Korteniemi, J.; Kostama, V.-P. End-member morphologies of volcanic and sedimentary layered rocks on Mars from high-resolution images. In Proceedings of the 41st Lunar and Planetary Science Conference, Houston, TX, USA, 1–5 March 2010; Abstract Number 1310. Lunar and Planetary Institute: Houston, TX, USA, 2010. Available online: <https://hdl.handle.net/20.500.11753/1083> (accessed on 26 September 2021).
349. Beyer, R.A.; McEwen, A.S. Layering stratigraphy of eastern Coprates and northern Capri Chasmata, Mars. *Icarus* **2005**, *179*, 1–23. [CrossRef]
350. White, J.D.L.; Houghton, B.F. Primary volcanoclastic rocks. *Geology* **2006**, *34*, 677–680. [CrossRef]
351. Fisher, R.V. Rocks composed of volcanic fragments and their classifications. *Earth Sci. Rev.* **1966**, *1*, 287–298. [CrossRef]
352. Fisher, R.V.; Smith, G.A. Volcanism, tectonics, and sedimentation. In *Sedimentation in Volcanic Settings*; Fisher, R.V., Smith, G.A., Eds.; SEPM Special Publication: Tulsa, Ok, USA, 1991; Volume 45, pp. 1–5. [CrossRef]
353. Edgett, K.S.; Lancaster, N. Volcanoclastic aeolian dunes: Terrestrial examples and application to Martian sands. *J. Arid Environ.* **1993**, *25*, 271–297. [CrossRef]
354. Hessler, A.M.; Lowe, D.R. Initial generation of sand across climate zones of the Mojave, Sierra Nevada, and Klamath Batholiths in California, U.S.A. *Sediment. Geol.* **2017**, *348*, 37–50. [CrossRef]
355. Weltje, G.J.; Paredis, B.; Caracciolo, L.; Heins, W.A. Quantitative analysis of crystal-interface frequencies in granitoids: Implications for modelling of parent-rock texture and its influence on the properties of plutonic sands. *Sediment. Geol.* **2018**, *375*, 72–85. [CrossRef]
356. Manville, V.; Németh, K.; Kano, K. Source to sink: A review of three decades of progress in the understanding of volcanoclastic processes, deposits, and hazards. *Sediment. Geol.* **2009**, *220*, 136–161. [CrossRef]
357. Sohn, C.; Sohn, Y.K. Distinguishing between primary and secondary volcanoclastic deposits. *Sci. Rep.* **2019**, *9*, 12425:1–12425:7. [CrossRef]
358. Mahood, R.O. Petrology, Sedimentology, and Diagenesis of Volcanoclastics and Sandstones from Leg 63 of the Deep Sea Drilling Project, Baja California and Southern California Continental Borderland. Master's Thesis, Oregon State University, Corvallis, OR, USA, 1986.
359. Sheppard, R.A. Diagenetic alteration of basaltic tephra in lacustrine deposits, southwestern Idaho and southeastern Oregon. *U.S. Geol. Surv. Open File Rep.* **1996**, *96–697*, 1–25. [CrossRef]
360. Kutterolf, S.; Schacht, U.; Wehrmann, H.; Freundt, A.; Mörz, T. Onshore to offshore tephrostratigraphy and marine ash layer diagenesis. In *Central America: Geology, Resources and Hazards*; Bundschuh, J., Alvarado, G.E., Eds.; Taylor & Francis: London, UK, 2007; pp. 395–421, ISBN 978-042-907-437-0. [CrossRef]

361. Squyres, S.W.; Aharonson, O.; Clark, B.C.; Cohen, B.A.; Crumpler, L.; de Souza, P.A.; Farrand, W.H.; Gellert, R.; Grant, J.; Grotzinger, J.P.; et al. Pyroclastic activity at Home Plate in Gusev crater, Mars. *Science* **2007**, *316*, 738–742. [[CrossRef](#)]
362. Lewis, K.W.; Aharonson, O.; Grotzinger, J.P.; Squyres, S.W.; Bell, J.F., III; Crumpler, L.S.; Schmidt, M.E. Structure and stratigraphy of Home Plate from the Spirit Mars Exploration Rover. *J. Geophys. Res. Planets* **2008**, *113*, E12S36:1–E12S36:16. [[CrossRef](#)]
363. Yingst, R.A.; Crumpler, L.; Farrand, W.H.; Li, R.; Cabrol, N.A.; Neakrase, L.D. Morphology and texture of particles along the Spirit rover traverse from sol 450 to sol 745. *J. Geophys. Res. Planets* **2008**, *113*, E12S41:1–E12S41:17. [[CrossRef](#)]
364. McCoy, T.J.; Sims, M.; Schmidt, M.E.; Edwards, L.; Tornabene, L.L.; Crumpler, L.S.; Cohen, B.A.; Soderblom, L.A.; Blaney, D.L.; Squyres, S.W.; et al. Structure, stratigraphy, and origin of Husband Hill, Columbia Hills, Gusev crater, Mars. *J. Geophys. Res. Planets* **2008**, *113*, E06S03:1–E06S03:14. [[CrossRef](#)]
365. Crumpler, L.S.; Arvidson, R.E.; Bell, J.; Clark, B.C.; Cohen, B.A.; Farrand, W.H.; Gellert, R.; Golombek, M.; Grant, J.A.; Guinness, E.; et al. Context of ancient aqueous environments on Mars from in situ geologic mapping at Endeavour Crater. *J. Geophys. Res. Planets* **2015**, *120*, 538–569. [[CrossRef](#)]
366. Mittlefehldt, D.W.; Gellert, R.; VanBommel, S.; Ming, D.W.; Yen, A.S.; Clark, B.C.; Morris, R.V.; Schröder, C.; Crumpler, L.S.; Grant, J.A.; et al. Diverse lithologies and alteration events on the rim of Noachian-aged Endeavour crater, Meridiani Planum, Mars: In situ compositional evidence. *J. Geophys. Res. Planets* **2018**, *123*, 1255–1306. [[CrossRef](#)]
367. Squyres, S.W.; Arvidson, R.E.; Blaney, D.L.; Clark, B.C.; Crumpler, L.; Farrand, W.H.; Gorevan, S.; Herkenhoff, K.E.; Hurowitz, J.; Kusack, A.; et al. Rocks of the Columbia Hills. *J. Geophys. Res. Planets* **2006**, *111*, E02S11:1–E02S11:19. [[CrossRef](#)]
368. Herkenhoff, K.E.; Squyres, S.W.; Anderson, R.; Archinal, B.A.; Arvidson, R.E.; Barrett, J.M.; Becker, K.J.; Bell, J.F., III; Budney, C.; Cabrol, N.A.; et al. Overview of the Microscopic Imager investigation during Spirit’s first 450 sols in Gusev crater. *J. Geophys. Res. Planets* **2006**, *111*, E02S04:1–E02S04:30. [[CrossRef](#)]
369. Ruff, S.W.; Niles, P.B.; Alfano, F.; Clarke, A.B. Evidence for a Noachian-aged ephemeral lake in Gusev crater, Mars. *Geology* **2014**, *42*, 359–362. [[CrossRef](#)]
370. Herkenhoff, K.E.; Squyres, S.W.; Arvidson, R.E.; Cole, S.B.; Sullivan, R.; Yingst, A.; Cabrol, N.; Lee, E.M.; Richie, J.; Sucharski, B. Overview of Spirit Microscopic Imager results. *J. Geophys. Res. Planets* **2019**, *124*, 528–584. [[CrossRef](#)]
371. Wilson, L.; Head, J.W., III. Mars: Review and analysis of volcanic eruption theory and relationships to observed landforms. *Rev. Geophys.* **1994**, *32*, 221–263. [[CrossRef](#)]
372. Brož, P.; Bernhardt, H.; Conway, S.J.; Parekh, R. An overview of explosive volcanism on Mars. *J. Volcanol. Geotherm. Res.* **2021**, *409*, 107125:1–107125:26. [[CrossRef](#)]
373. Horvath, D.G.; Moitra, P.; Hamilton, C.W.; Craddock, R.A.; Andrews-Hanna, J.C. Evidence for geologically recent explosive volcanism in Elysium Planitia, Mars. *Icarus* **2021**, *365*, 114499:1–114499:14. [[CrossRef](#)]
374. Mouginiis-Mark, P.J.; Wilson, L.; Zimbleman, J.R. Polygenetic eruptions on Alba Patera, Mars. *Bull. Volcanol.* **1988**, *50*, 361–379. [[CrossRef](#)]
375. Greeley, R.; Crown, D.A. Volcanic geology of Tyrrhena Patera, Mars. *J. Geophys. Res. Solid Earth* **1990**, *95*, 7133–7145. [[CrossRef](#)]
376. Wood, C.A. Monogenetic volcanoes of the terrestrial planets. In *Tenth Lunar and Planetary Science Conference*; Geochim. Cosmochim. Acta Supplement 11; Pergamon Press: New York, NY, USA, 1979; pp. 2815–2840, ISBN 978-008-025-128-8.
377. Fagents, S.A.; Thordarson, T. Rootless volcanic cones in Iceland and on Mars. In *The Geology of Mars: Evidence from Earth-Based Analogs*; Chapman, M., Ed.; Cambridge University Press: Cambridge, UK, 2007; pp. 151–177, ISBN 978-052-183-292-2. [[CrossRef](#)]
378. Brož, P.; Hauber, E. A unique volcanic field in Tharsis, Mars: Pyroclastic cones as evidence for explosive eruptions. *Icarus* **2012**, *218*, 88–99. [[CrossRef](#)]
379. Brož, P.; Hauber, E. Hydrovolcanic tuff rings and cones as indicators for phreatomagmatic explosive eruptions on Mars. *J. Geophys. Res. Planets* **2013**, *118*, 1656–1675. [[CrossRef](#)]
380. Kerber, L.; Head, J.W.; Madeleine, J.-B.; Forget, F.; Wilson, L. The dispersal of pyroclasts from Apollinaris Patera, Mars: Implications for the origin of the Medusae Fossae Formation. *Icarus* **2011**, *216*, 212–220. [[CrossRef](#)]
381. Malin, M.C. Mars: Evidence of indurated deposits of fine materials. In *Proceedings of the Second International Colloquium on Mars*, Pasadena, CA, USA, 15–18 January 1979; p. 54, NASA Conference Publication 2072.
382. Ojha, L.; Lewis, K. The density of the Medusae Fossae Formation: Implications for its composition, origin, and importance in Martian history. *J. Geophys. Res. Planets* **2018**, *123*, 1368–1379. [[CrossRef](#)]
383. Mandon, L.; Quantin-Nataf, C.; Thollot, P.; Mangold, N.; Lozac’h, L.; Dromart, G.; Beck, P.; Dehouck, E.; Breton, S.; Millot, C.; et al. Refining the age, emplacement and alteration scenarios of the olivine-rich unit in the Nili Fossae region, Mars. *Icarus* **2020**, *336*, 113436:1–113436:17. [[CrossRef](#)]
384. Edwards, C.S.; Ehlmann, B.L. Carbon sequestration on Mars. *Geology* **2015**, *43*, 863–866. [[CrossRef](#)]
385. Wichman, R.W.; Schultz, P.H. Sequence and mechanisms of deformation around the Hellas and Isidis Impact basins on Mars. *J. Geophys. Res. Solid Earth* **1989**, *94*, 17333–17357. [[CrossRef](#)]
386. Caudill, C.M.; Tornabene, L.L.; McEwen, A.S.; Byrne, S.; Ojha, L.; Mattson, S. Layered megablocks in the central uplifts of impact craters. *Icarus* **2012**, *221*, 710–720. [[CrossRef](#)]
387. Williams, R.M.E.; Malin, M.C. Evidence for late stage fluvial activity in Kasei Valles, Mars. *J. Geophys. Res. Planets* **2004**, *109*, E06001:1–E06001:10. [[CrossRef](#)]
388. Wilson, L.; Mouginiis-Mark, P.J. Dynamics of a fluid flow on Mars: Lava or mud? *Icarus* **2014**, *233*, 268–280. [[CrossRef](#)]

389. Grant, J.A.; Wilson, S.A. The nature and emplacement of distal aqueous-rich ejecta deposits from Hale crater, Mars. *Meteorit. Planet. Sci.* **2017**, *53*, 839–856. [[CrossRef](#)]
390. Hodges, C.A.; Moore, H.J. Atlas of volcanic landforms on Mars. *U.S. Geol. Surv. Prof. Pap.* **1994**, *1534*, 1–194. [[CrossRef](#)]
391. Baratoux, D.; Pinet, P.; Toplis, M.J.; Mangold, N.; Greeley, R.; Baptista, A.R. Shape, rheology and emplacement times of small Martian shield volcanoes. *J. Volcanol. Geotherm. Res.* **2009**, *185*, 47–68. [[CrossRef](#)]
392. Schaber, G.G. Syrtis Major: A low-relief volcanic shield. *J. Geophys. Res. Solid Earth* **1982**, *87*, 9852–9866. [[CrossRef](#)]
393. Xiao, L.; Huang, J.; Christensen, P.R.; Greeley, R.; Williams, D.A.; Zhao, J.; He, Q. Ancient volcanism and its implication for thermal evolution of Mars. *Earth Planet. Sci. Lett.* **2012**, *323–324*, 9–18. [[CrossRef](#)]
394. Robinson, H.H. The San Franciscan volcanic field, Arizona. *U.S. Geol. Surv. Prof. Pap.* **1913**, *76*, 1–213. [[CrossRef](#)]
395. Lanz, J.K.; Wagner, R.; Wolf, U.; Kröcher, J.; Neukum, G. Rift zone volcanism and associated cinder cone field in Utopia Planitia, Mars. *J. Geophys. Res. Planets* **2010**, *115*, E12019:1–E12019:21. [[CrossRef](#)]
396. Sharp, R.P. Mars: Troughed terrain. *J. Geophys. Res.* **1973**, *78*, 4063–4072. [[CrossRef](#)]
397. Sharp, R.P. Mass movements on Mars. In *Geology, Seismicity, and Environmental Impact*; Moran, D.E., Slosson, J.E., Stone, R.O., Yelverton, C.A., Eds.; Association of Engineering Geologists Special Publication, University Publishers: Los Angeles, CA, USA, 1973; pp. 115–122.
398. Sharp, R.P. Mars: Fretted and chaotic terrains. *J. Geophys. Res.* **1973**, *78*, 4073–4083. [[CrossRef](#)]
399. Andrews-Hanna, J.C.; Zuber, M.T.; Hauck, S.A. Strike-slip faults on Mars: Observations and implications for global tectonics and geodynamics. *J. Geophys. Res. Planets* **2008**, *113*, E08002:1–E08002:19. [[CrossRef](#)]
400. Hauber, E.; Grott, M.; Kronberg, P. Martian rifts: Structural geology and geophysics. *Earth Planet. Sci. Lett.* **2010**, *294*, 393–410. [[CrossRef](#)]
401. Schultz, R.A.; Hauber, E.; Kattenhorn, S.A.; Okubo, C.H.; Watters, T.R. Interpretation and analysis of planetary structures. *J. Struct. Geol.* **2010**, *32*, 855–875. [[CrossRef](#)]
402. Andrews-Hanna, J.C. The formation of Valles Marineris: 1. Tectonic architecture and the relative roles of extension and subsidence. *J. Geophys. Res. Planets* **2012**, *117*, E03006:1–E03006:18. [[CrossRef](#)]
403. El-Maarry, M.R.; Watters, W.; McKeown, N.K.; Carter, J.; Noe Dobra, E.; Bishop, J.L.; Pommerol, A.; Thomas, N. Potential desiccation cracks on Mars: A synthesis from modeling, analogue-field studies, and global observations. *Icarus* **2014**, *241*, 248–268. [[CrossRef](#)]
404. Oehler, D.Z.; Mangold, N.; Hallet, B.; Fairén, A.G.; Le Deit, L.; Williams, A.J.; Sletten, R.S.; Martínez-Frías, J. Origin and significance of decameter-scale polygons in the lower Peace Vallis fan of Gale crater, Mars. *Icarus* **2016**, *277*, 56–72. [[CrossRef](#)]
405. Schieber, J.; Bish, D.; Coleman, M.; Reed, M.; Hausrath, E.M.; Cosgrove, J.; Gupta, S.; Miniti, M.E.; Edgett, K.S.; Malin, M. Encounters with an unearthy mudstone: Understanding the first mudstone found on Mars. *Sedimentology* **2017**, *64*, 311–358. [[CrossRef](#)]
406. Stein, N.; Grotzinger, J.P.; Schieber, J.; Mangold, N.; Hallet, B.; Newsom, H.; Stack, K.M.; Berger, J.A.; Thompson, L.; Siebach, K.L.; et al. Desiccation cracks provide evidence of lake drying on Mars, Sutton Island member, Murray formation, Gale Crater. *Geology* **2018**, *46*, 515–518. [[CrossRef](#)]
407. Metz, J.M.; Grotzinger, J.; Okubo, C.; Milliken, R. Thin-skinned deformation of sedimentary rocks in Valles Marineris, Mars. *J. Geophys. Res. Planets* **2010**, *115*, E11004:1–E11004:28. [[CrossRef](#)]
408. Birnie, C.; Fueten, F.; Stesky, R.; Hauber, E. Underlying structural control of small-scale faults and fractures in west Candor Chasma, Mars. *J. Geophys. Res. Planets* **2012**, *117*, E11001:1–E11001:20. [[CrossRef](#)]
409. Okubo, C.H.; Gauthier, T.A. Bedrock and Structural Geologic Maps of Eastern Candor Sulci, Western Ceti Mensa, and Southeastern Ceti Mensa, Candor Chasma, Valles Marineris Region of Mars. U.S. Geological Survey Scientific Investigations Map 2017, 3359, Scale 1:18,000. Available online: <https://pubs.er.usgs.gov/publication/sim3359> (accessed on 26 September 2021). [[CrossRef](#)]
410. Murana, A. Geology of Danielson crater, Mars. *J. Maps* **2018**, *14*, 161–172. [[CrossRef](#)]
411. El-Maarry, M.R.; Markiewicz, W.J.; Mellon, M.T.; Goetz, W.; Dohm, J.M.; Pack, A. Crater floor polygons: Desiccation patterns of ancient lakes on Mars? *J. Geophys. Res. Planets* **2010**, *115*, E10006:1–E10006:20. [[CrossRef](#)]
412. Fawdon, P.; Skok, J.R.; Balme, M.R.; Vye-Brown, C.L.; Rothery, D.A.; Jordan, C.J. The geological history of Nili Patera, Mars. *J. Geophys. Res. Planets* **2015**, *120*, 951–977. [[CrossRef](#)]
413. Eggers, G.L.; Wray, J.J.; Dufek, J. Compositional mapping of the Nili Patera feldspathic unit: Extent and implications for formation. *J. Geophys. Res. Planets* **2021**, *126*, e2020JE006383:1–e2020JE006383:17. [[CrossRef](#)]
414. Dang, Y.; Xiao, L.; Xu, Y. Polygons. In *Mars on Earth: A Study of the Qaidam Basin*; Xiao, L., Ed.; World Scientific: Singapore, 2021; Volume 5, pp. 199–248. [[CrossRef](#)]
415. Mazzoli, S.; Vitale, S.; Delmonaco, G.; Guerriero, V.; Margottini, C.; Spizzichino, D. ‘Diffuse faulting’ in the Machu Picchu granitoid pluton, eastern Cordillera, Peru. *J. Struct. Geol.* **2009**, *31*, 1395–1408. [[CrossRef](#)]
416. Caplinger, M.A.; Malin, M.C. Mars Orbiter Camera Geodesy Campaign. *J. Geophys. Res. Planets* **2001**, *106*, 23595–23606. [[CrossRef](#)]
417. Shanmugam, G. Global case studies of soft-sediment deformation structures (SSDs): Definitions, classifications, advances, origins, and problems. *J. Palaeogeogr.* **2017**, *6*, 251–320. [[CrossRef](#)]
418. Grotzinger, J.; Bell, J., III; Herkenhoff, K.; Johnson, J.; Knoll, A.; McCartney, E.; McLennan, S.; Metz, J.; Moore, J.; Squyres, S.; et al. Sedimentary textures formed by aqueous processes, Erebus crater, Meridiani Planum, Mars. *Geology* **2006**, *34*, 1085–1088. [[CrossRef](#)]

419. Rubin, D.M.; Fairén, A.G.; Martínez-Frías, J.; Frydenvang, J.; Gasnault, O.; Gelfenbaum, G.; Goetz, W.; Grotzinger, J.P.; Le Mouélic, S.; Mangold, N.; et al. Fluidized-sediment pipes in Gale crater, Mars, and possible Earth analogs. *Geology* **2017**, *45*, 7–10. [CrossRef]
420. Okubo, C.H. Bedrock Geologic and Structural Map through the Western Candor Colles Region of Mars. U.S. Geological Survey Scientific Investigations Map 2014, 3309, Scale 1:18,000. Available online: <https://pubs.er.usgs.gov/publication/sim3309> (accessed on 26 September 2021). [CrossRef]
421. Wilson, S.A.; Howard, A.D.; Moore, J.M.; Grant, J.A. Geomorphic and stratigraphic analysis of Crater Terby and layered deposits north of Hellas basin, Mars. *J. Geophys. Res. Planets* **2007**, *112*, E08009:1–E08009:39. [CrossRef]
422. Oehler, D.Z.; Allen, C.C. Evidence for pervasive mud volcanism in Acidalia Planitia, Mars. *Icarus* **2010**, *208*, 636–657. [CrossRef]
423. Wheatley, D.F.; Chan, M.A.; Okubo, C.H. Clastic pipes and mud volcanism across Mars: Terrestrial analog evidence of past Martian groundwater and subsurface fluid mobilization. *Icarus* **2019**, *328*, 141–151. [CrossRef]
424. Migoń, P.; Kasprzak, M. (Eds.) *Sandstone Landscapes: Diversity, Ecology, and Conservation, Proceedings of the 3rd International Conference on Sandstone Landscapes*; University of Wrocław: Wrocław, Poland, 2012; ISBN 978-836-267-329-2.
425. Migoń, P.; Viles, H.A. Sandstone geomorphology. *Z. Geomorphol. Suppl.* **2015**, *59*, 1–2. [CrossRef]
426. Migoń, P.; Różycka, M.; Jancewicz, K.; Duszyński, F. Evolution of sandstone mesas—Following landform decay until death. *Prog. Phys. Geogr.* **2018**, *42*, 1–19. [CrossRef]
427. Migoń, P. Sandstone geomorphology—Recent advances. *Geomorphology* **2021**, *373*, 107484:1–107484:16. [CrossRef]
428. Le Deit, L.; Hauber, E.; Fueten, F.; Pondrelli, M.; Rossi, A.P.; Jaumann, R. Sequence of infilling events in Gale crater, Mars: Results from morphology, stratigraphy, and mineralogy. *J. Geophys. Res. Planets* **2013**, *118*, 2439–2473. [CrossRef]
429. Schieber, J. Reinterpretation of the Martian Eberswalde delta in light of new HiRISE images. In Proceedings of the 38th Lunar and Planetary Science Conference, Houston, TX, USA, 12–16 March 2007; Abstract Number 1982. Lunar and Planetary Institute: Houston, TX, USA, 2007. Available online: <https://hdl.handle.net/20.500.11753/1086> (accessed on 26 September 2021).
430. Lohman, S.W. The geologic story of Arches National Park. *U.S. Geol. Surv. Bull.* **1975**, *1393*, 1–113. [CrossRef]
431. Le Deit, L.; Mangold, N.; Forni, O.; Cousin, A.; Lasue, J.; Schröder, S.; Wiens, R.C.; Sumner, D.; Fabre, C.; Stack, K.M.; et al. The potassic sedimentary rocks in Gale crater, Mars, as seen by ChemCam on board Curiosity. *J. Geophys. Res. Planets* **2016**, *121*, 784–804. [CrossRef]
432. Banham, S.G.; Gupta, S.; Bryk, A.B.; Rubin, D.M.; Edgett, K.S.; Dietrich, W.E.; Caravaca, G.; Edgar, L.A.; Bedford, C.C.; Vasavada, A.R. Reconstruction of aeolian palaeoenvironments and past climate events at the Greenheugh pediment, Aeolis Mons, Mars. In Proceedings of the 52nd Lunar and Planetary Science Conference, Virtual Meeting, 15–19 March 2021; Abstract Number 2300. Lunar and Planetary Institute: Houston, TX, USA, 2021. Available online: <https://www.hou.usra.edu/meetings/lpsc2021/pdf/2300.pdf> (accessed on 26 September 2021).
433. Arvidson, R.E.; Seelos, F.P., IV; Deal, K.S.; Koeppen, W.D.; Snider, N.O.; Kieniewicz, J.M.; Hynek, B.M.; Mellon, M.T.; Garvin, J.B. Mantled and exhumed terrains in Terra Meridiani, Mars. *J. Geophys. Res. Planets* **2003**, *108*, 8073:1–8073:20. [CrossRef]
434. Rapin, W.; Dromart, G.; Rubin, D.; Le Deit, L.; Mangold, N.; Edgar, L.A.; Gasnault, O.; Herkenhoff, K.; Le Mouélic, S.; Anderson, R.B.; et al. Alternating wet and dry depositional environments recorded in the stratigraphy of Mount Sharp at Gale crater, Mars. *Geology* **2021**, *49*, 842–846. [CrossRef]
435. Dromart, G.; Le Deit, L.; Rapin, W.; Gasnault, O.; Le Mouélic, S.; Quantin-Nataf, C.; Mangold, N.; Rubin, D.; Lasue, J.; Maurice, S.; et al. Deposition and erosion of a light-toned yardang-forming unit of Mt Sharp, Gale crater, Mars. *Earth Planet. Sci. Lett.* **2021**, *554*, 116681:1–116681:13. [CrossRef]
436. Mangold, N.; Thompson, L.M.; Forni, O.; Fabre, C.; Le Deit, L.; Wiens, R.C.; Williams, A.J.; Williams, R.M.; Anderson, R.B.; Blaney, D.L.; et al. Composition of conglomerates analyzed by the Curiosity rover: Implications for Gale crater crust and sediment sources. *J. Geophys. Res. Planets* **2016**, *121*, 353–387. [CrossRef]
437. Johnson, S.Y. Significance of loessite in the Maroon Formation (Middle Pennsylvanian to Lower Permian), Eagle Basin, northwest Colorado. *J. Sed. Pet.* **1989**, *59*, 782–791. [CrossRef]
438. Soreghan, G.S.; Elmore, R.D.; Lewchuk, M.T. Sedimentologic-magnetic record of western Pangean climate in upper Paleozoic loessite (lower Cutler beds, Utah). *Geol. Soc. Am. Bull.* **2002**, *114*, 1019–1035. [CrossRef]
439. Smalley, I.; Marshall, J.; Fitzsimmons, K.; Whalley, W.B.; Ngambi, S. Desert loess: A selection of relevant topics. *Geologos* **2019**, *25*, 91–102. [CrossRef]
440. Bridges, N.T.; Muhs, D.R. Duststones on Mars: Source, transport, deposition, and erosion. In *Sedimentary Geology of Mars*; Grotzinger, J.P., Milliken, R.E., Eds.; SEPM Special Publication: Tulsa, OK, USA, 2012; Volume 102, pp. 169–182. ISBN 978-156-576-313-5. [CrossRef]
441. Tsoar, H.; Pye, K. Dust transport and the question of desert loess formation. *Sedimentology* **1987**, *34*, 139–153. [CrossRef]
442. Edgett, K.S.; Christensen, P.R. The particle size of Martian aeolian dunes. *J. Geophys. Res. Planets* **1991**, *96*, 22765–22776. [CrossRef]
443. Edgar, L.A.; Grotzinger, J.P.; Bell, J.F., III; Hurowitz, J.A. Hypotheses for the origin of fine-grained sedimentary rocks at Santa Maria crater, Meridiani Planum. *Icarus* **2014**, *234*, 36–44. [CrossRef]
444. Sun, V.Z.; Stack, K.M.; Kah, L.C.; Thompson, L.; Fischer, W.; Williams, A.J.; Johnson, S.S.; Wiens, R.C.; Kronyak, R.E.; Nachon, M.; et al. Late-stage diagenetic concretions in the Murray formation, Gale crater, Mars. *Icarus* **2019**, *321*, 866–890. [CrossRef]

445. Stack, K.; Arvidson, R.E.; Bennett, K.A.; Bryk, A.B.; Edgett, K.S.; Fedo, C.; Fox, V.K.; Fraeman, A.; House, C.H.; Rabinovitch, J.; et al. In-situ investigation of periodic bedrock ridges in the Glen Torridon area with the MSL Curiosity rover, Gale crater, Mars. In Proceedings of the American Geophysical Union Fall Meeting 2019, San Francisco, CA, USA, 9–13 December 2019. Abstract Number P33B-02.
446. Milliken, R.E.; Grotzinger, J.P.; Thomson, B.J. Paleoclimate of Mars as captured by the stratigraphic record in Gale crater. *Geophys. Res. Lett.* **2010**, *37*, L04201:1–L04201:6. [[CrossRef](#)]
447. Frydenvang, J.; Mangold, N.; Wiens, R.C.; Fraeman, A.A.; Edgar, L.A.; Fedo, C.M.; L'Haridon, J.; Bedford, C.C.; Gupta, S.; Grotzinger, J.P.; et al. The chemostratigraphy of the Murray formation and role of diagenesis at Vera Rubin ridge in Gale crater, Mars, as observed by the ChemCam instrument. *J. Geophys. Res. Planets* **2020**, *125*, e2019JE006320:1–e2019JE006320:21. [[CrossRef](#)]
448. Pain, C.F.; Ollier, C.D. Inversion of relief—A component of landscape evolution. *Geomorphology* **1995**, *12*, 151–165. [[CrossRef](#)]
449. McLennan, S.M.; Bell, J.F., III; Calvin, W.M.; Christensen, P.R.; Clarke, B.C.; de Souza, P.A.; Farmer, J.; Farrand, W.H.; Fike, D.A.; Gellert, R.; et al. Provenance and diagenesis of the evaporite-bearing Burns formation, Meridiani Planum, Mars. *Earth Planet. Sci. Lett.* **2005**, *240*, 95–121. [[CrossRef](#)]
450. Osterloo, M.M.; Anderson, F.S.; Hamilton, V.E.; Hynek, B.M. Geologic context of proposed chloride-bearing materials on Mars. *J. Geophys. Res. Planets* **2010**, *115*, E10012:1–E10012:29. [[CrossRef](#)]
451. Beck, A.W.; Murchie, S.L.; Viviano, C.E. A search for early- to mid-Noachian chloride-rich deposits on Mars. *Icarus* **2020**, *338*, 113552:1–113552:4. [[CrossRef](#)]
452. Ehlmann, B.L.; Mustard, J.F.; Murchie, S.L.; Poulet, F.; Bishop, J.L.; Brown, A.J.; Calvin, W.M.; Clark, R.N.; Des Marais, D.J.; Milliken, R.E.; et al. Orbital identification of carbonate-bearing rocks on Mars. *Science* **2008**, *322*, 1828–1832. [[CrossRef](#)]
453. Wray, J.J.; Murchie, S.L.; Bishop, J.L.; Ehlmann, B.L.; Milliken, R.E.; Wilhelm, M.B.; Seelos, K.D.; Chojnacki, M. Orbital evidence for more widespread carbonate-bearing rocks on Mars. *J. Geophys. Res. Planets* **2016**, *121*, 652–677. [[CrossRef](#)]
454. Bridges, J.C.; Hicks, L.J.; Treiman, A.H. Carbonates on Mars. In *Volatiles in the Martian Crust*; Filiberto, J., Schwenzer, S.P., Eds.; Elsevier: Amsterdam, The Netherlands, 2019; pp. 89–118, ISBN 978-012-804-191-8. [[CrossRef](#)]
455. Morris, R.V.; Ruff, S.W.; Gellert, R.; Ming, D.W.; Arvidson, R.E.; Clark, B.C.; Golden, D.C.; Siebach, K.; Klingelhöfer, G.; Schröder, C.; et al. Identification of carbonate-rich outcrops on Mars by the Spirit rover. *Science* **2010**, *329*, 421–424. [[CrossRef](#)]
456. Glotch, T.D.; Bandfield, J.L.; Tornabene, L.L.; Jensen, H.B.; Seelos, F.P. Distribution and formation of chlorides and phyllosilicates in Terra Sirenum, Mars. *Geophys. Res. Lett.* **2010**, *37*, L16202:1–L16202:5. [[CrossRef](#)]
457. Hynek, B.M.; Osterloo, M.K.; Kierein-Young, K.S. Late-stage formation of Martian chloride salts through ponding and evaporation. *Geology* **2015**, *43*, 787–790. [[CrossRef](#)]
458. Daswani, M.M.; Kite, E.S. Paleohydrology on Mars constrained by mass balance and mineralogy of pre-Amazonian sodium chloride lakes. *J. Geophys. Res. Planets* **2017**, *122*, 1802–1823. [[CrossRef](#)]
459. El-Maarry, M.R.; Pommerol, A.; Thomas, N. Analysis of polygonal cracking patterns in chloride-bearing terrains on Mars: Indicators of ancient playa settings. *J. Geophys. Res. Planets* **2013**, *118*, 2263–2278. [[CrossRef](#)]
460. Glotch, T.D.; Bandfield, J.L.; Wolff, M.J.; Arnold, J.A.; Che, C. Constraints on the composition and particle size of chloride salt-bearing deposits on Mars. *J. Geophys. Res. Planets* **2016**, *121*, 454–471. [[CrossRef](#)]
461. Ye, B.; Huang, J.; Michalski, J.; Xiao, L. Geomorphologic characteristics of polygonal features on chloride-bearing deposits on Mars: Implications for Martian hydrology and astrobiology. *J. Earth Sci.* **2019**, *30*, 1049–1058. [[CrossRef](#)]
462. Fisher, Q.J.; Casey, M.; Clennell, M.B.; Knipe, R.J. Mechanical compaction of deeply buried sandstones of the North Sea. *Mar. Pet. Geol.* **1999**, *16*, 605–618. [[CrossRef](#)]
463. Morad, S.; Ketzer, J.M.; de Ros, L.F. Spatial and temporal distribution of diagenetic alterations in siliciclastic rocks: Implications for mass transfer in sedimentary basins. *Sedimentology* **2000**, *47*, 95–120. [[CrossRef](#)]
464. Milliken, K.L.; Day-Stirrat, R.J. Cementation in mudrocks: Brief review with examples from cratonic basin mudrocks. In *Critical Assessment of Shale Resource Plays*; Chatellier, J., Jarvie, D., Eds.; AAPG: Tulsa, OK, USA, 2013; Volume 103, pp. 133–150. ISBN 978-089-181-904-2.
465. Bjørlykke, K. Relationships between depositional environments, burial history and rock properties: Some principal aspects of diagenetic process in sedimentary basins. *Sediment. Geol.* **2014**, *301*, 1–14. [[CrossRef](#)]
466. Marsaglia, K.M.; Browne, G.H.; George, S.C.; Kemp, D.B.; Jaeger, J.M.; Carson, D.; Richaud, M.; IODP Expedition 317 Scientific Party. The transformation of sediment into rock: Insights from IODP Site U1352, Canterbury Basin, New Zealand. *J. Sed. Res.* **2017**, *87*, 272–287. [[CrossRef](#)]
467. Sharp, J.M., Jr.; Galloway, W.E.; Land, L.S.; McBride, E.F.; Blanchard, P.D.; Bodner, D.P.; Dutton, S.P.; Farr, M.R.; Gold, P.B.; Jackson, T.J.; et al. Diagenetic processes in northwestern Gulf of Mexico sediments. In *Diagenesis II, Developments in Sedimentology 43*; Chilingarian, G.V., Wolf, K.H., Eds.; Elsevier: Amsterdam, The Netherlands, 1988; pp. 43–113, ISBN 978-044-442-922-3. [[CrossRef](#)]
468. Mangold, N.; Schmidt, M.E.; Fisk, M.R.; Forni, O.; McLennan, S.M.; Ming, D.W.; Sautter, V.; Sumner, D.; Williams, A.J.; Clegg, S.M.; et al. Classification scheme for sedimentary and igneous rocks in Gale crater, Mars. *Icarus* **2017**, *284*, 1–17. [[CrossRef](#)]
469. Brooke, B. The distribution of carbonate eolianite. *Earth Sci. Rev.* **2001**, *55*, 135–164. [[CrossRef](#)]
470. McLaren, S.J. Aeolianite. In *Geochemical Sediments and Landscapes*; Nash, D.J., McLaren, S.J., Eds.; Wiley-Blackwell: Oxford, UK, 2007; pp. 144–172, ISBN 978-047-071-291-7. [[CrossRef](#)]
471. Viles, H.A.; Pentecost, A. Tufa and travertine. In *Geochemical Sediments and Landscapes*; Nash, D.J., McLaren, S.J., Eds.; Wiley-Blackwell: Oxford, UK, 2007; pp. 173–199, ISBN 978-047-071-291-7. [[CrossRef](#)]

472. Chivas, A.R. Terrestrial evaporites. In *Geochemical Sediments and Landscapes*; Nash, D.J., McLaren, S.J., Eds.; Wiley-Blackwell: Oxford, UK, 2007; pp. 330–364, ISBN 978-047-071-291-7. [[CrossRef](#)]
473. Cino, C.D.; Dehouck, E.; McLennan, S.M. Geochemical constraints on the presence of clay minerals in the Burns formation, Meridiani Planum, Mars. *Icarus* **2017**, *281*, 137–150. [[CrossRef](#)]
474. Golombek, M.P.; Grant, J.A.; Crumpler, L.S.; Greeley, R.; Arvidson, R.E.; Bell, J.F., III; Weitz, C.M.; Sullivan, R.; Christensen, P.R.; Soderblom, L.A.; et al. Erosion rates at the Mars Exploration Rover landing sites and long-term climate change on Mars. *J. Geophys. Res. Planets* **2006**, *111*, E12S10:1–E12S10:14. [[CrossRef](#)]
475. McEwen, A.S.; Banks, M.E.; Baugh, N.; Becker, K.; Boyd, A.; Bergstrom, J.W.; Beyer, R.A.; Bortolini, E.; Bridges, N.T.; Byrne, S.; et al. The High Resolution Imaging Science Experiment (HiRISE) during MRO's Primary Science Phase (PSP). *Icarus* **2010**, *205*, 2–37. [[CrossRef](#)]
476. McLennan, S.M.; Grotzinger, J.P.; Hurowitz, J.A.; Tosca, N.J. The sedimentary cycle on early Mars. *Annu. Rev. Earth Planet. Sci.* **2019**, *47*, 91–118. [[CrossRef](#)]
477. Sharp, R.P. Surface processes modifying Martian craters. *Icarus* **1968**, *8*, 472–480. [[CrossRef](#)]
478. Chapman, C.R.; Pollack, J.B.; Sagan, C. An analysis of the Mariner-4 cratering statistics. *Astron. J.* **1969**, *74*, 1039–1051. [[CrossRef](#)]
479. Parsley, R.L. *Sedimentary Features on the Surface of Mars as Seen from Mariner 6 and 7 Photographs*; NASA Contractor Report CR-2194; U.S. Government Printing Office; National Aeronautics and Space Administration: Washington, DC, USA, 1973.
480. Bandfield, J.L.; Edwards, C.S.; Montgomery, D.R.; Brand, B.D. The dual nature of the Martian crust: Young lavas and old clastic materials. *Icarus* **2013**, *222*, 188–199. [[CrossRef](#)]
481. Carter, J.; Loizeau, D.; Mangold, N.; Poulet, F.; Bibring, J.-P. Widespread surface weathering on early Mars: A case for a warmer and wetter climate. *Icarus* **2015**, *248*, 373–382. [[CrossRef](#)]
482. Robas García, C.; Nieto Masot, A.; Schnable, S. Morfologías fluvio-glaciares del cráter Gale y sus análogos terrestres, como evidencias del clima frío y húmedo del Marte primitivo. In *Tecnologías de la Información Geográfica en el Análisis Espacial*; Nieto Masot, A., Ed.; Universidad de Extremadura: Badajoz, Spain, 2016; pp. 269–283, ISBN 978-846-176-760-1.
483. Christensen, P.R. Regional dust deposits on Mars: Physical properties, age, and history. *J. Geophys. Res. Solid Earth* **1986**, *91*, 3533–3545. [[CrossRef](#)]
484. Soderblom, L.A.; Kreidler, T.J.; Masursky, H. Latitudinal distribution of a debris mantle on the Martian surface. *J. Geophys. Res.* **1973**, *78*, 4117–4122. [[CrossRef](#)]
485. Mustard, J.F.; Cooper, C.D.; Rifkin, M.K. Evidence for recent climate change on Mars from the identification of youthful near-surface ground ice. *Nature* **2001**, *412*, 411–414. [[CrossRef](#)] [[PubMed](#)]
486. Herkenhoff, K.E.; Murray, B.C. High-resolution topography and albedo of the south polar layered deposits on Mars. *J. Geophys. Res. Solid Earth* **1990**, *95*, 14511–14529. [[CrossRef](#)]
487. Malin, M.C.; Caplinger, M.A.; Davis, S.D. Observational evidence for an active surface reservoir of solid carbon dioxide on Mars. *Science* **2001**, *294*, 2146–2148. [[CrossRef](#)]
488. Rogers, A.D.; Aharonson, O.; Bandfield, J.L. Geologic context of in situ rocky exposures in Mare Serpentis, Mars: Implications for crust and regolith evolution in the cratered highlands. *Icarus* **2009**, *200*, 446–462. [[CrossRef](#)]
489. Rogers, A.D.; Ferguson, R.L. Regional-scale stratigraphy of surface units in Tyrhena and Iapygia Terrae, Mars: Insights into highland crustal evolution and alteration history. *J. Geophys. Res. Planets* **2011**, *116*, E08005:1–E08005:24. [[CrossRef](#)]
490. Edwards, C.S.; Bandfield, J.L.; Christensen, P.R.; Rogers, A.D. The formation of infilled craters on Mars: Evidence for widespread impact induced decompression of the early Martian mantle? *Icarus* **2014**, *228*, 149–166. [[CrossRef](#)]
491. Mangold, N.; Ansan, V.; Masson, P.; Vincendon, C. Estimate of aeolian dust thickness in Arabia Terra, Mars: Implications of a thick mantle (>20 m) for hydrogen detection. *Géomorphologie* **2009**, *15*, 23–42. [[CrossRef](#)]
492. Hynek, B.M.; Phillips, R.J. Evidence for extensive denudation of the Martian highlands. *Geology* **2001**, *29*, 407–410. [[CrossRef](#)]
493. Edgett, K.S.; Malin, M.C. Martian sedimentary rock stratigraphy: Outcrops and interbedded craters of northwest Sinus Meridiani and southwest Arabia Terra. *Geophys. Res. Lett.* **2002**, *29*, 2179–2179:4. [[CrossRef](#)]
494. Bennett, K.A.; Bell, J.F., III. A global survey of Martian central mounds: Central mounds as remnants of previously more extensive large-scale sedimentary deposits. *Icarus* **2016**, *264*, 331–341. [[CrossRef](#)]
495. Moore, J.M. Nature of the mantling deposit in the heavily cratered terrain of northeastern Arabia, Mars. *J. Geophys. Res. Solid Earth* **1990**, *95*, 14279–14289. [[CrossRef](#)]
496. Fassett, C.I.; Head, J.W., III. Layered mantling deposits in northeast Arabia Terra, Mars: Noachian-Hesperian sedimentation, erosion, and terrain inversion. *J. Geophys. Res. Planets* **2007**, *112*, E08002:1–E08002:19. [[CrossRef](#)]
497. Loizeau, D.; Werner, S.C.; Mangold, N.; Bibring, J.-P.; Vago, J.L. Chronology of deposition and alteration in the Mawrth Vallis region, Mars. *Planet. Space Sci.* **2012**, *72*, 31–43. [[CrossRef](#)]
498. McCauley, J.F. Geologic Map of the Coprates Quadrangle of Mars. U.S. Geological Survey Miscellaneous Investigations Series Map 1978, I-897, Scale 1:5,000,000. Available online: <https://pubs.er.usgs.gov/publication/i897> (accessed on 26 September 2021). [[CrossRef](#)]
499. Witbeck, N.E.; Tanaka, K.L.; Scott, D.H. Geologic Map of the Valles Marineris Region, Mars (East Half and West Half). U.S. Geological Survey Miscellaneous Investigations Series Map 1991, I-2010, Scale 1:2,000,000. Available online: <https://pubs.er.usgs.gov/publication/i2010> (accessed on 26 September 2021). [[CrossRef](#)]

500. Rotto, S.; Tanaka, K.L. Geologic/Geomorphologic Map of the Chryse Planitia Region of Mars. U.S. Geological Survey Miscellaneous Investigations Series Map 1995, I-2441, Scale 1:5,000,000. Available online: <https://pubs.er.usgs.gov/publication/i2441> (accessed on 26 September 2021). [CrossRef]
501. Rodríguez, J.A.P.; Sasaki, S.; Dohm, J.M.; Tanaka, K.L.; Strom, B.; Kargel, J.; Kuzmin, R.; Miyamoto, H.; Spray, J.G.; Fairén, A.G.; et al. Control of impact crater fracture systems on subsurface hydrology, ground subsidence, and collapse, Mars. *J. Geophys. Res. Planets* **2005**, *110*, E06003:1–E06003:22. [CrossRef]
502. Singh, P.; Sarkar, R.; Porwal, A. Origin of theater-headed valleys in the Valles Marineris region, Mars. *Icarus* **2021**, *368*, 114599:1–114599:16. [CrossRef]
503. Carr, M.H.; Masursky, H.; Saunders, R.S. A generalized geologic map of Mars. *J. Geophys. Res.* **1973**, *78*, 4031–4036. [CrossRef]
504. Flahaut, J.; Quantin, C.; Clenet, H.; Allemand, P.; Mustard, J.F.; Thomas, P. Pristine Noachian crust and key geologic transitions in the lower walls of Valles Marineris: Insights into early igneous processes on Mars. *Icarus* **2012**, *221*, 420–435. [CrossRef]
505. Lucchitta, B.K. Morphology of chasma walls, Mars. *J. Res. U.S. Geol. Surv.* **1978**, *6*, 651–662. [CrossRef]
506. Davis, J.M.; Grindrod, P.M.; Banham, S.G.; Warner, N.H.; Conway, S.J.; Boazman, S.J.; Gupta, S. A record of syn-tectonic sedimentation revealed by perched alluvial fan deposits in Valles Marineris, Mars. *Geology* **2021**, *49*. [CrossRef]
507. Flahaut, J.; Mustard, J.F.; Quantin, C.; Clenet, H.; Allemand, P.; Thomas, P. Dikes of distinct composition intruded into Noachian-aged crust exposed in the walls of Valles Marineris. *Geophys. Res. Lett.* **2011**, *38*, L15202:1–L15202:7. [CrossRef]
508. Brustel, C.; Flahaut, J.; Hauber, E.; Fueten, F.; Quantin, C.; Stesky, R.; Davies, G.R. Valles Marineris tectonic and volcanic history inferred from dikes in eastern Coprates Chasma. *J. Geophys. Res. Planets* **2017**, *122*, 1353–1371. [CrossRef]
509. Keszthelyi, L.; Jaeger, W.; McEwen, A.; Tornabene, L.; Beyer, R.A.; Dundas, C.; Milazzo, M. High Resolution Imaging Science Experiment (HiRISE) images of volcanic terrains from the first 6 months of the Mars Reconnaissance Orbiter Primary Science Phase. *J. Geophys. Res. Planets* **2008**, *113*, E04005:1–E04005:25. [CrossRef]
510. Keszthelyi, L.; McEwen, A. Comparison of flood lavas on Earth and Mars. In *The Geology of Mars: Evidence from Earth Based Analogues*; Chapman, M., Ed.; Cambridge University Press: Cambridge, UK, 2007; pp. 126–150, ISBN 978-051-153-601-4. [CrossRef]
511. Williams, J.-P.; Paige, D.A.; Manning, C.E. Layering in the wall rock of Valles Marineris: Intrusive and extrusive magmatism. *Geophys. Res. Lett.* **2003**, *30*, 1623:1–1623:4. [CrossRef]
512. Lucchitta, B.K.; McEwen, A.S.; Clow, G.D.; Geissler, P.E.; Singer, R.B.; Schutz, R.A.; Squyres, S.W. The canyon system on Mars. In *Mars*; Kieffer, H.H., Jakosky, B.M., Snyder, C.W., Matthews, M.S., Eds.; University of Arizona Press: Tucson, AZ, USA, 1992; pp. 453–492, ISBN 978-081-651-257-7.
513. Lucchitta, B.K.; Isbell, N.K.; Howington-Kraus, A. Topography of Valles Marineris: Implications for erosional and structural history. *J. Geophys. Res. Planets* **1994**, *99*, 3783–3798. [CrossRef]
514. Schultz, R.A. Multiple-process origin of Valles Marineris basins and troughs, Mars. *Planet. Space Sci.* **1998**, *46*, 827–834. [CrossRef]
515. Chapman, M.G. Layered, massive and thin sediments on Mars: Possible Late Noachian to Late Amazonian tephra? In *Volcano-Ice Interaction on Earth and Mars*; Smellie, J.L., Chapman, M.G., Eds.; Geological Society, London, Special Publications: London, UK, 2002; Volume 202, pp. 273–293. [CrossRef]
516. Fueten, F.; Flahaut, J.; Le Deit, L.; Stesky, R.; Hauber, E.; Gwinner, K. Interior layered deposits within a perched basin, southern Coprates Chasma, Mars: Evidence for their formation, alteration, and erosion. *J. Geophys. Res. Planets* **2011**, *116*, E02003:1–E02003:18. [CrossRef]
517. Fueten, F.; Novakovic, N.; Stesky, R.; Flahaut, J.; Hauber, E.; Rossi, A.P. The evolution of Juventae Chasma, Valles Marineris, Mars: Progressive collapse and sedimentation. *J. Geophys. Res. Planets* **2017**, *122*, 2223–2249. [CrossRef]
518. Andrews-Hanna, J.C. The formation of Valles Marineris: 3. Trough formation through super-isostasy, stress, sedimentation, and subsidence. *J. Geophys. Res. Planets* **2012**, *117*, E06002:1–E06002:20. [CrossRef]
519. Montgomery, D.R.; Gillespie, A. Formation of Martian outflow channels by catastrophic dewatering of evaporite deposits. *Geology* **2005**, *33*, 625–628. [CrossRef]
520. Catling, D.C.; Wood, S.E.; Leovy, C.; Montgomery, D.R.; Greenberg, H.M.; Glein, C.R.; Moore, J.M. Light-toned layered deposits in Juventae Chasma, Mars. *Icarus* **2006**, *181*, 26–51. [CrossRef]
521. Fueten, F.; Racher, H.; Stesky, R.; MacKinnon, P.; Hauber, E.; McGuire, P.C.; Zegers, T.; Gwinner, K. Structural analysis of interior layered deposits in northern Coprates Chasma, Mars. *Earth Planet. Sci. Lett.* **2010**, *294*, 343–356. [CrossRef]
522. Nedell, S.S.; Squyres, S.W.; Andersen, D.W. Origin and evolution of the layered deposits in the Valles Marineris, Mars. *Icarus* **1987**, *70*, 409–441. [CrossRef]
523. Treiman, A.H.; Fuks, K.H.; Murchie, S. Diagenetic layers in the upper walls of Valles Marineris, Mars: Evidence for drastic climate change since the mid-Hesperian. *J. Geophys. Res. Planets* **1995**, *100*, 26339–26344. [CrossRef]
524. Ward, A.W. Yardangs on Mars: Evidence of recent wind erosion. *J. Geophys. Res. Solid Earth* **1979**, *84*, 8147–8166. [CrossRef]
525. Mutch, T.A.; Arvidson, R.E.; Head, J.W., III; Jones, K.L.; Saunders, R.S. Physiographic provinces. In *The Geology of Mars*; Princeton University Press: Princeton, NJ, USA, 1976; pp. 56–91, ISBN 978-069-108-173-1.
526. Harrison, S.K.; Balme, M.R.; Hagermann, A.; Murray, J.B.; Muller, J.-P. Mapping Medusae Fossae Formation materials in the southern highlands of Mars. *Icarus* **2010**, *209*, 405–415. [CrossRef]
527. Dunning, I.T. Mapping the Previous Extent of the Medusae Fossae Formation. Master's Thesis, State University of New York at Buffalo, New York, NY, USA, 2018.

528. Kerber, L.; Head, J.W. The age of the Medusae Fossae Formation: Evidence of Hesperian emplacement from crater morphology, stratigraphy, and ancient lava contacts. *Icarus* **2010**, *206*, 669–684. [CrossRef]
529. Kerber, L.; Dickson, J.L.; Head, J.W.; Grosfils, E.B. Polygonal ridge networks on Mars: Diversity of morphologies and the special case of the eastern Medusae Fossae Formation. *Icarus* **2017**, *281*, 200–219. [CrossRef]
530. Morgan, G.A.; Campbell, B.A.; Carter, L.M.; Plaut, J.J. Evidence for the episodic erosion of the Medusae Fossae Formation preserved within the youngest volcanic province on Mars. *Geophys. Res. Lett.* **2015**, *42*, 7336–7342. [CrossRef]
531. Stacey, K.N. Interactions between Athabasca Valles Flood Lavas and the Medusae Fossae Formation (Mars): Implications for Lava Emplacement Mechanisms and the Triggering of Steam Explosions. Master's Thesis, University of Texas at Dallas, Richardson, TX, USA, 2019. Available online: <https://hdl.handle.net/10735.1/8687> (accessed on 26 September 2021).
532. Hughes, C.M.; Cardenas, B.T.; Goudge, T.A.; Mohrig, D. Deltaic deposits indicative of a paleo-coastline at Aeolis Dorsa, Mars. *Icarus* **2019**, *317*, 442–453. [CrossRef]
533. Jacobsen, R.E.; Burr, D.M. Dichotomies in the fluvial and alluvial fan deposits of the Aeolis Dorsa, Mars: Implications for weathered sediment and paleoclimate. *Geosphere* **2017**, *13*, 2154–2168. [CrossRef]
534. Smith, D.E.; Zuber, M.T.; Frey, H.V.; Garvin, J.B.; Head, J.W.; Muhleman, D.O.; Pettengill, G.H.; Phillips, R.J.; Solomon, S.C.; Zwally, H.J.; et al. Mars Orbiter Laser Altimeter: Experiment summary and the first year of global mapping of Mars. *J. Geophys. Res. Planets* **2001**, *106*, 23689–23722. [CrossRef]
535. Burr, D.M.; Enga, M.-T.; Williams, R.M.E.; Zimbelman, J.R.; Brennand, T.A. Pervasive aqueous paleoflow features in the Aeolis/Zephyria Plana region, Mars. *Icarus* **2009**, *200*, 52–76. [CrossRef]
536. Putzig, N.E.; Mellon, M.T. Apparent thermal inertia and the surface heterogeneity of Mars. *Icarus* **2007**, *191*, 68–94. [CrossRef]
537. Kerber, L.; Head, J.W. A progression of induration in Medusae Fossae Formation transverse aeolian ridges: Evidence for ancient aeolian bedforms and extensive reworking. *Earth Surf. Process. Landf.* **2012**, *37*, 422–433. [CrossRef]
538. Boyd, A.S. Sand Deposit Mapping and Aeolian Morphologies as Clues for Identifying Origins of Dark Sand in Aeolis Dorsa. Master's Thesis, University of Tennessee, Knoxville, TN, USA, 2018. Available online: https://trace.tennessee.edu/utk_gradthes/5182 (accessed on 26 September 2021).
539. Tanaka, K.L. The stratigraphy of Mars. *J. Geophys. Res. Solid Earth* **1986**, *91*, E139–E158. [CrossRef]
540. Tanaka, K.L.; Skinner, J.A., Jr.; Dohm, J.M.; Irwin, R.P., III; Kolb, E.J.; Fortezzo, C.M.; Platz, T.; Michael, G.G.; Hare, T.M. Geologic Map of Mars. U.S. Geological Survey Scientific Investigations Map 2014, 3292, Scale 1:20,000,000. Available online: <https://pubs.er.usgs.gov/publication/sim3292> (accessed on 26 September 2021). [CrossRef]
541. Harrison, S.K.; Balme, M.R.; Hagermann, A.; Murray, J.B.; Muller, J.-P.; Wilson, A. A branching, positive relief network in the middle member of the Medusae Fossae Formation, equatorial Mars—Evidence for sapping? *Planet. Space Sci.* **2013**, *85*, 142–163. [CrossRef]
542. Tanaka, K.L. Dust and ice deposition in the Martian geologic record. *Icarus* **2000**, *144*, 254–266. [CrossRef]
543. Mouginis-Mark, P.J.; Zimbelman, J.R. Rafted pumice: A new model for the formation of the Medusae Fossae Formation, Mars. *Icarus* **2020**, *343*, 113684:1–113684:5. [CrossRef]
544. Parker, T.J. A comparison of the Martian Medusae Fossae formation with terrestrial carbonate platforms. In Proceedings of the 22nd Lunar and Planetary Science Conference, Houston, TX, USA, 18–22 March 1991; Lunar and Planetary Institute: Houston, TX, USA, 1991; pp. 1029–1030.
545. Schultz, P.H.; Lutz, A.B. Polar wandering of Mars. *Icarus* **1988**, *73*, 91–141. [CrossRef]
546. Carter, L.M.; Campbell, B.A.; Watters, T.R.; Phillips, R.J.; Putzig, N.E.; Safaeinili, A.; Plaut, J.J.; Okubo, C.H.; Egan, A.F.; Seu, R.; et al. Shallow radar (SHARAD) sounding observations of the Medusae Fossae Formation, Mars. *Icarus* **2009**, *199*, 295–302. [CrossRef]
547. Orosei, R.; Rossi, A.P.; Cantini, F.; Caprarelli, G.; Carter, L.M.; Papiano, I.; Cartacci, M.; Cicchetti, A.; Noschese, R. Radar sounding of Lucus Planum, Mars, by MARSIS. *J. Geophys. Res. Planets* **2017**, *122*, 1405–1418. [CrossRef]
548. Francis, P.W.; Wood, C.A. Absence of silicic volcanism on Mars: Implications for crustal composition and volatile abundance. *J. Geophys. Res. Solid Earth* **1982**, *87*, 9881–9889. [CrossRef]
549. Rubin, D.M.; Carter, C.L. *Cross-Bedding, Bedforms, and Paleocurrents*, 2nd ed.; Society for Sedimentary Geology (SEPM): Tulsa, OK, USA, 2006; ISBN 978-156-576-101-8. [CrossRef]
550. Wells, G.L.; Zimbelman, J.R. Extraterrestrial arid surface processes. In *Arid Zone Geomorphology*, 1st ed.; Thomas, D.S.G., Ed.; Belhaven: London, UK, 1989; pp. 335–358, ISBN 978-185-293-020-2.
551. Lucchitta, B.K.; Ferguson, H.M.; Summers, C. Sedimentary deposits in the northern lowland plains, Mars. *J. Geophys. Res. Solid Earth* **1986**, *91*, E166–E174. [CrossRef]
552. Jöns, H.-P. Das Relief des Mars' Versuch einer zusammenfassenden Übersicht. *Geol. Rundsch.* **1990**, *79*, 131–164. [CrossRef]
553. Tanaka, K.L. Sedimentary history and mass flow structures of Chryse and Acidalia Planitiae, Mars. *J. Geophys. Res. Planets* **1997**, *102*, 4131–4149. [CrossRef]
554. Mouginot, J.; Pommerol, A.; Beck, P.; Kofman, W.; Clifford, S.M. Dielectric map of the Martian northern hemisphere and the nature of plains filling materials. *Geophys. Res. Lett.* **2012**, *39*, L02202:1–L02202:5. [CrossRef]
555. Parker, T.J.; Gorsline, D.S.; Saunders, R.S.; Pieri, D.C.; Schneeberger, D.M. Coastal geomorphology of the Martian northern plains. *J. Geophys. Res. Planets* **1993**, *98*, 11061–11078. [CrossRef]

556. Carr, M.H.; Head, J.W., III. Oceans on Mars: An assessment of the observational evidence and possible fate. *J. Geophys. Res. Planets* **2003**, *108*, 5042:1–5042:28. [CrossRef]
557. Carr, M.H.; Head, J.W., III. Mars: Formation and fate of a frozen Hesperian ocean. *Icarus* **2019**, *319*, 433–443. [CrossRef]
558. Ivanov, M.A.; Hiesinger, H. The Acidalia Mensa region on Mars: A key element to test the Mars ocean hypothesis. *Icarus* **2020**, *349*, 113874:1–113874:18. [CrossRef]
559. Parker, T.J.; Bills, B.G. Mars northern plains ocean. In *Mars Geological Enigmas: From the Late Noachian Epoch to the Present Day*; Soare, R.J., Williams, J.-P., Conway, S.J., Oehler, D.Z., Eds.; Elsevier: Amsterdam, The Netherlands, 2021; pp. 41–59. ISBN 978-012-820-245-6. [CrossRef]
560. Dapremont, A.M.; Wray, J.J. Insights into Mars mud volcanism using visible and near-infrared spectroscopy. *Icarus* **2021**, *359*, 114299:1–114299:13. [CrossRef]
561. Oehler, D.Z.; Allen, C.C. Giant polygons and mounds in the lowlands of Mars: Signatures of an ancient ocean? *Astrobiology* **2012**, *12*, 601–615. [CrossRef] [PubMed]
562. Salvatore, M.R.; Christensen, P.R. On the origin of the Vastitas Borealis Formation in Chryse and Acidalia Planitiae, Mars. *J. Geophys. Res. Planets* **2014**, *119*, 2437–2456. [CrossRef]
563. Ivanov, M.A.; Hiesinger, H.; Erkeling, G.; Reiss, D. Evidence for large reservoirs of water/mud in Utopia and Acidalia Planitiae on Mars. *Icarus* **2015**, *248*, 383–391. [CrossRef]
564. McGill, G.E.; Hills, L.S. Origin of giant Martian polygons. *J. Geophys. Res. Planets* **1992**, *97*, 2633–2647. [CrossRef]
565. Buczkowski, D.L.; Seelos, K.D.; Cooke, M.L. Giant polygons and circular graben in western Utopia basin, Mars: Exploring possible formation mechanisms. *J. Geophys. Res. Planets* **2012**, *117*, E08010:1–E08010:18. [CrossRef]
566. Tanaka, K.L.; Skinner, J.A.; Hare, T.M. Geologic Map of the Northern Plains of Mars. U.S. Geological Survey Scientific Investigations Map 2005, 2888, Scale 1:15,000,000. Available online: <https://pubs.er.usgs.gov/publication/sim2888> (accessed on 26 September 2021). [CrossRef]
567. Salvatore, M.R.; Christensen, P.R. Evidence for widespread aqueous sedimentation in the northern plains of Mars. *Geology* **2014**, *42*, 423–426. [CrossRef]
568. Gross, C.; Carter, J.; Sowe, M.; Bishop, J.L. Uplifted sediments in the northern plains of Mars? In Proceedings of the 8th International Conference on Mars 8, Pasadena, CA, USA, 14–18 July 2014; Abstract Number 1116. Lunar and Planetary Institute: Houston, TX, USA, 2014. Available online: <https://hdl.handle.net/20.500.11753/1536> (accessed on 26 September 2021).
569. Johansen, L.A. Vesiculation and lithification behavior of saline muds in near vacuum. In *Reports of Planetary Geology Program—1981*; Holt, H.E., Ed.; NASA Technical Memorandum, 84211; U.S. Government Printing Office; National Aeronautics and Space Administration: Washington, DC, USA, 1981; pp. 277–279.
570. Sharp, P.R.; Malin, M.C. Surface geology from Viking landers on Mars: A second look. *Geol. Soc. Am. Bull.* **1984**, *94*, 1398–1412. [CrossRef]
571. Boynton, W.V.; Feldman, W.C.; Squyres, S.W.; Prettyman, T.H.; Brückner, J.; Evans, L.G.; Reedy, R.C.; Starr, R.; Arnold, J.R.; Drake, D.M.; et al. Distribution of hydrogen in the near surface of Mars: Evidence for subsurface ice deposits. *Science* **2002**, *297*, 81–85. [CrossRef]
572. Byrne, S.; Dundas, C.M.; Kennedy, M.R.; Mellon, M.T.; McEwen, A.S.; Cull, S.C.; Daubar, I.J.; Shean, D.E.; Seelos, K.D.; Murchie, S.L.; et al. Distribution of mid-latitude ground ice on Mars from new impact craters. *Science* **2009**, *325*, 1674–1676. [CrossRef]
573. Cull, S.; Arvidson, R.E.; Mellon, M.T.; Skemer, P.; Shaw, A.; Morris, R.V. Compositions of subsurface ices at the Mars Phoenix landing site. *Geophys. Res. Lett.* **2010**, *37*, L24203:1–L24203:4. [CrossRef]
574. Squyres, S.W. Martian fretted terrain: Flow of erosional debris. *Icarus* **1978**, *34*, 600–613. [CrossRef]
575. Levy, J.S.; Head, J.W.; Marchant, D.R. Lineated valley fill and lobate debris apron stratigraphy in Nilosyrtis Mensae, Mars: Evidence for phases of glacial modification of the dichotomy boundary. *J. Geophys. Res. Planets* **2007**, *112*, E08004:1–E08004:19. [CrossRef]
576. Morgan, G.A.; Head, J.W., III; Marchant, D.R. Lineated valley fill (LVF) and lobate debris aprons (LDA) in the Deuteronilus Mensae northern dichotomy boundary region, Mars: Constraints on the extent, age and episodicity of Amazonian glacial events. *Icarus* **2009**, *202*, 22–38. [CrossRef]
577. van Gesselt, S.; Hauber, E.; Neukum, G. Lineated valley fill at the Martian dichotomy boundary: Nature and history of degradation. *J. Geophys. Res. Planets* **2010**, *115*, E08003:1–E08003:15. [CrossRef]
578. Bandfield, J.L.; Amador, E.S. Extensive aqueous deposits at the base of the dichotomy boundary in Nilosyrtis Mensae, Mars. *Icarus* **2016**, *275*, 29–44. [CrossRef]